From Wind Climate to Wind Turbine Loads

efficient and accurate decision support and reliability analysis

Slot, René Meklenborg Miltersen

Publication date:
2019

Document Version
Publisher's PDF, also known as Version of record

FROM WIND CLIMATE TO WIND TURBINE LOADS

EFFICIENT AND ACCURATE DECISION SUPPORT AND RELIABILITY ANALYSIS

BY
RENÉ MEKLENBORG MILTERSEN SLOT

DISSERTATION SUBMITTED 2019

AALBORG UNIVERSITY
DENMARK

FROM WIND CLIMATE TO WIND TURBINE LOADS

EFFICIENT AND ACCURATE DECISION SUPPORT AND RELIABILITY ANALYSIS

by

René Meklenborg Miltersen Slot

AALBORG UNIVERSITY
DENMARK

Dissertation submitted 26-08-2019

Dissertation submitted: 26.08.2019

PhD supervisor: Prof. John Dalsgaard Sørensen,
Aalborg University

Assistant PhD supervisors: PhD Lasse Svenningsen,
EMD International A/S

MSc Morten Lybech Thøgersen,
EMD International A/S

PhD committee: Associate Professor Peter Frigaard (chairman)
Aalborg University

Professor Po-Wen Cheng
Universität Stuttgart

Head of section Katherine Dykes
Technical University of Denmark

PhD Series: Faculty of Engineering and Science, Aalborg University

Department: Department of Civil Engineering

ISSN (online): 2446-1636
ISBN (online): 978-87-7210-483-6

Published by:
Aalborg University Press
Langagervej 2
DK – 9220 Aalborg Ø
Phone: +45 99407140
aauf@forlag.aau.dk
forlag.aau.dk

Printed in Denmark by Rosendahls, 2019

PREFACE

This dissertation marks the conclusion of the industrial PhD project "From wind climate to wind turbine loads" and thereby embodies a fruitful collaboration between Aalborg University and EMD International A/S. The work was conducted from 1 July 2016 to 14 July 2019 with three months spent as a visiting PhD student at ETH Zürich in the spring 2018. Two weeks were spent on parental leave after the birth of my second child.

The thesis is submitted to the Doctoral School of Engineering and Science as a collection of five scientific papers in partial fulfillment to obtain the PhD degree. The main body includes a joint introduction and highlights the main results of the papers, which share the same topic of 'efficient and accurate decision support and reliability analysis'. The following papers are included:

- **Paper 1:** R. M. M. Slot, L. Svenningsen, J. D. Sørensen, and M. L. Thøgersen, "Importance of Shear in Site Assessment of Wind Turbine Fatigue Loads," *J. Sol. Energy Eng.*, vol. 140, no. 4, p. 041012, 2018, doi:10.1115/1.4039748.

- **Paper 2:** R. M. M. Slot, J. D. Sørensen, L. Svenningsen, W. Moser, and M. L. Thøgersen, "Effective Turbulence and its Implications in Wind Turbine Fatigue Assessment," *Submitted to: Wind Energy (Accepted for publication)*.

- **Paper 3:** R. Slot, J. Schwarte, L. Svenningsen, J. Sørensen, and M. Thøgersen, "Directional fatigue accumulation in wind turbine steel towers," *J. Phys. Conf. Ser.*, vol. 1102, no. 1, 2018, doi:10.1088/1742-6596/1102/1/012017.

- **Paper 4:** René M. M. Slot, J. D. Sørensen, B. Sudret, L. Svenningsen, and M. L. Thøgersen, "Surrogate Model Uncertainty in Wind Turbine Reliability Assessment," *Submitted to: Renewable Energy (Under peer-review)*.

- **Paper 5:** René M. M. Slot, L. Svenningsen, J. D. Sørensen, and M. L. Thøgersen, "Consistent direct-drive version of the NREL 5MW turbine," *Proceeding to WindEurope 2018*.

SUMMARY

Wind energy plays a critical role in reaching the climate goals set out by the Paris Agreement. To keep wind turbines a main pillar of sustainable energy, improved decision support is required to fully exploit the best wind resources avaliable. This thesis aims to improve accuracy and efficiency in onshore wind turbine site suitability evaluations. It quantifies how critical and uncertain assumptions on wind climate measurements propagate to uncertainties in the estimated fatigue loads on wind turbine components and affect their structural reliability.

The IEC 61400-1 design standard accounts for variability in turbulence for fatigue loads by a wind speed dependent 90% quantile of the observed turbulence including wake contributions. However, for wind shear the overall mean value is considered, accounting neither for the wind speed dependence of shear nor for the significant shear variability around the mean. Using wind data from 99 real sites, this thesis shows how this leads to inconsistent fatigue load assessment of wind turbine blades. Instead, a 60% quantile of wind shear conditioned on wind speed is proposed, which reduces the inconsistency across real sites by a factor of approximately two.

The effective turbulence approximation is widely used to significantly reduce the required aeroelastic simulations in site-suitability assessment. The approximation is slightly conservative and leads to fatigue load predictions within 4% on average when compared to full sector-wise simulations. An inevitable consequence of the effective turbulence is that directional information of turbulence is lost, which is a simplification for components below the yaw bearing. This leads to fatigue load over-predictions of 14% on average across the 99 available sites. A simple method is proposed to avoid this over-prediction and thereby significantly reduce material consumption of steel towers.

Traditional engineering methods for wind turbine structural evaluations are based on deterministic design approaches. This is a necessity to limit the computational requirement and the design efforts for the engineers. Deterministic methods are designed to ensure a low probability of structural failure, but this probability of failure cannot be quantified or divided into individual contributions from climate modelling, model uncertainties or material uncertainties. In this thesis, a fast and efficient probabilistic framework is developed by utilizing a Kriging surrogate model to approximate fatigue loads. The framework quantifies the relative importance of the site-specific climate conditions, from the model uncertainties as well as the uncertainty related to the strength and material models. Analyses of the relevant uncertainties lead to insight into the relative importance of different wind farm planning decisions such as mast equipment and height. This improved knowledge provides a sound basis for rational decision-making by identifying the most important uncertainties that can be reduced to increase structural reliability of wind turbines.

RESUME

Vindenergi spiller en meget vigtig rolle for at nå klimamålene, der er vedtaget i Paris Aftalen. For at fastholde vindmøller som en af de afgørende brikker i fremtidens vedvarende energi, er det nødvendigt at der tilbydes forbedret beslutningsstøtte, sådan at hver enkelt mølle udnyttes mere optimalt. Denne afhandlings mål er at forbedre nøjagtigheden og øge effektiviteten af beslutningssøtte vedrørende placeringen af møller på land. Det kvantificeres, hvordan usikkerheder fra vigtige antagelser og beslutninger omkring vindmålinger propagerer til usikkerheder på vindmøllelaster, og påvirker vindmøllers strukturelle pålidelighed.

IEC 61400-1 design standarden tager højde for variabiliteten af turbulens i lastberegninger ved at benytte en karakteristisk 90% fraktil som funktion af vindhastighed. For vindgradienten bruges en middelværdi, hvorved hverken varians eller korrelationen med vindhastighed tages i betragning for denne parameter. Ud fra vind data fra 99 instrumenterede master, viser denne afhandling at den simple model for vindgradienten, der benyttes i dag, medfører inkonsistent strukturel pålidelighed af vindmøllevinger. I stedet foreslåes der, at en 60% fraktil afhængig af vindhastiged benyttes, hvorved inkonsistensen på tværs af de tilgængelige master halveres.

Den effektive turbulens approksimation bruges ofte for markant at reducere mængden af aeroelastiske simuleringer, der er krævet for at eftervise vindmøllers strukturelle integritet. Approksimationen er konservativ og fører til overestimering af laster, dog inden for 4%. En uundgåelig konsekvens af den effektive turbulens er, at retningsinformation går tabt. Dette er en simplificring for vindmølle komponenter, der er under krøjesystemet. Her vises det, hvordan det fører til signifikant overestimering af tårnlaster på 14% i gennemsnit. En simpel metode forelåes til at nudgå overestimeringen, og derved spare stål i fremtidens vindmølletårne.

Traditionelle ingenør-metoder til at eftervise vindmøllers strukturelle pålidelighed er baseret på deterministisk design. Det er en nødvendighed for at holde beregningernes omfang på et realistisk niveau i praksis. Deterministiske metoder er udviklet til at sikre en lav svigtsandsynlighed, men det kan ikke kvantificeres, hvorvidt svigtsandsynligheden domineres af vindklima usikkerheder, styrke usikkerheder eller model usikkerheder. I denne afhandling udvikles der hurtige og nøjagtige metoder til at estimere svigtsansynligheden af vindmøller, samt kvantificering af sensitiviteter for de enkelte usikkerhedsbidrag til den totale usikkerhed og strukturel pålidelighed. Denne form for forbedret beslutningsstøtte giver et solidt grundlag for rationel beslutningstagen, ved at identificere de vigtigste usikkerheder, sådan at disse kan reduceres først.

ACKNOWLEDGEMENTS

The work presented in this thesis has been carried out in close collaboration with my three supervisors: Lasse Svenningsen, John D. Sørensen and Morten L. Thøgersen. I want to thank Lasse for sharing his insight and immense knowledge on meteorology and for teaching me good scientific practice when processing real data. I thank John for helping me interpret the intentions of the IEC 61400-1 standard, and for being able to answer all my questions regarding structural reliability. Morten, I thank for his ability to stay objective and for his useful reviews of the research paper that embodies this project together with this thesis. During the three years of this project, I have never gone in vain for supervision, guidance and motivation to keep seaching for the answers.

I also want to thank Wolfgang Moser (Innogy) and Jörg Schwarte (Nordex) for commiting to this project as third parties. Their invaluable insight into design of wind turbines in the industry has been vital in adjusting the scope of this project. I thank Jason Jonkman (NREL) for always following up on my emails with ellaborate answers when I had questions related to aeroelastic simulation in FAST – and thanks to Thorkild Sørensen (EMD) who helped me run, literally, millions of aeroelastic simulations throughout the project.

During my project, I visited professor Dr. Bruno Sudret's Chair of Risk Safety and Uncertainty Quantification at ETH Zürich. I want to thank him and everybody in the Chair for their great hospitality, and for helping me in more matters than I can reasonably state here. While I stayed abroad, Gitte took care of both our children, and I am forever grateful that she gave her consent, without any hesitation, for this adventure – even though our second child had just seen the world for the first time. I thank Paul Hannah (EMD) and Vivi Søndergaard (AAU) for proof reading this thesis and Lynge Andersen for helping me with the figures. Finally, I also thank all of my collegues at EMD International A/S and Aalborg University for their input to the project, but most of all for making it a joy to go to work every single day.

The data used in this thesis was provided by KNMI, ICDC, CliSAP/KlimaCampus, University of Hamburg, DTU, Vattenfall and VENTUS INGENIERÍA. I am thankful for their significant and generous contributions. The project has been funded in collaboration between EMD International A/S, Aalborg University and Innovation Fund Denmark case number 5189-00022B. The financial support is greatly appreciated.

TABLE OF CONTENTS

CHAPTER 1. INTRODUCTION

"In theory, there is no difference between theory and practice; but in practice, there is"

Walter J. Savitch ([1], p. 366).

Research on wind turbine technology is conducted at an increasing rate. This has resulted in a significant body of literature with innovative solutions to increase the productivity of wind turbines and optimize their material consumption. However, due to the stochastic nature of wind and the complex dynamics inherent in wind turbines, state-of-the-art results often rely on time-consuming methods and comprehensive theoretical concepts. Over time, this has created a vacuum between academia and the industry which has led to both novel and important findings seeing little use outside of the universities.

The following research is greatly inspired by my own ambition to bridge this increasing gap and unify the significant effort on creating a green and sustainable future. I therefore encourage the reader to keep the concise words of Walter J. Savitch in mind on this journey from 'wind climate to wind turbine loads'.

1.1. A BRIEF HISTORY OF WIND TURBINES

Using wind as a resource to generate electricity began in the summer of 1887 with a vertical axis wind turbine constructed by Professor James Blyth [2], and a few months after, a horizontal axis wind turbine was created by Mr. Charles F. Brush [3]. Four years later, in 1891, the first Danish wind turbine was erected by the physicist, meteorologist and wind energy pioneer Poul la Cour [4]. His turbine also utilized a horizontal axis, but it was designed to operate with four blades thereby standing in great contrast to Charles' machine that had a total of 144 blades. This incredible difference originated in Poul la Cour's landmark discovery that the extracted energy scales with the rotor swept area rather than just the area covered by the blades (which was commonly believed at this point in time). La Cour continued making electricity from wind throughout his life and eventually discovered the vital importance of 'lift' and aerodynamics, thus providing one of the most critical steps towards the success of modern wind turbines.

After wind energy's first appearance in the late 1880s, it remained a niche for almost a hundred years until the oil embargo crisis in 1973. The resulting massive increase of oil prices and consciousness of limited resources gave rise to government funded projects to unlock the full potential of wind energy [5]. This gave birth to the American Wind Energy Association (AWEA) in 1974 [6], and few years later in 1982, the European Wind Energy Association (EWEA) emerged [7]. Together, the

increased funding and new initiatives resulted in full scale prototypes of both horizontal and vertical axis wind turbines. From this, the design concept of a three-bladed horizontal-axis wind turbine proved to be remarkably successful [8]. While vertical-axis wind turbines are still being developed and show promising features for large-scale floating offshore wind power [9], [10] the upwind three-bladed horizontal axis design is by far dominating the commercial turbine market today [11].

1.2. IMPORTANCE OF WIND ENERGY TODAY

Reducing greenhouse gas emission is of imminent importance to world society and has been ratified internationally by the Paris Agreement [12]. The agreement sets out a legally binding deal to avoid dangerous climate change by limiting global warming to 2°C compared to pre-industrial times. The long-term goal is to reduce greenhouse gas emission substantially by 80-95% at 2050. To reach this ambitious goal at least 40% the emission is to be cut by 2030 with no less than 32% of total energy consumption being from renewable energy sources [13]. In 2018 a major step was taken in that direction with 95% of all new power installation in the EU being renewable. Wind power is of special importance in this context by accounting for 49% of the total power capacity installations which is more than any other form of power generation [14]. Figure 1 illustrates the growth in EU wind energy capacity since 2008. The set-back in new installations in 2018 is due to the introduction of new national auction-based approaches of subsidizing wind farms, resulting in a slow-down. However, 2018 marked a record year in terms of final investment decisions with 4.2GW offshore and 12.5GW onshore achieving financial close [14], confirming that wind energy is still a growing sector with a vital role in realizing the Paris Agreement.

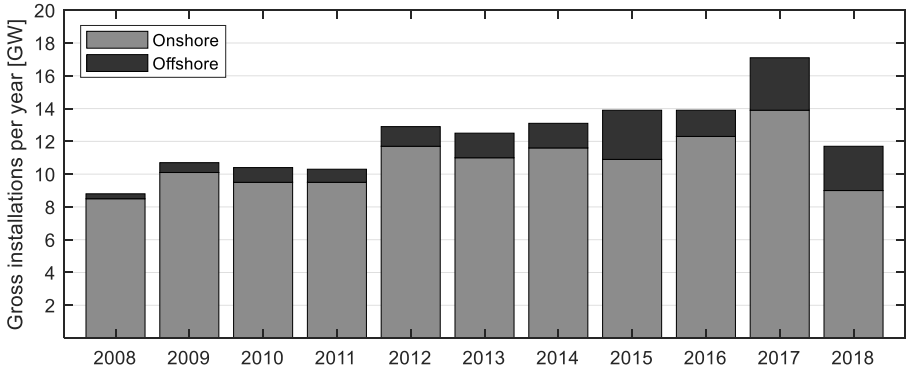

Figure 1: Growth in wind energy capacity in the EU from 2008-2018 divided into onshore and offshore wind energy [14].

Since 2016, wind energy is the second largest form of power generation capacity in the EU and is likely to become the largest in 2019. Wind farms already generate

enough power to meet 14% of the EU's electricity demand, and in Denmark the national goal of covering 50% of its electricity demand by renewable sources in 2030 is almost met with 41% covered by wind in 2018 [14]. However, a report by the Danish Energy Agency states that this share is expected to be reduced to 39.8% by 2030 without any new initiatives, mainly because of the expected increase in energy consumption together with an expected decline in renewable energy deployment [15]. It is therefore clear that, even for one of the world leaders in wind energy, there are still big challenges to resolve before meeting the 2030 target. This stresses the importance of continuing research and development of wind energy technology, both to reduce the environmental impact and to keep it economically attractive compared to non-renewable energy sources.

1.3. BACKGROUND AND MOTIVATION FOR THIS PROJECT

Onshore wind turbines dominate wind energy production which is also indicated in Figure 1. The main reason is the reduced foundation, installation and O&M costs compared to offshore turbines which makes onshore wind energy cheaper [16]. Analyses by IRENA show that the global weighted-average levelized cost of energy (LCOE) of onshore wind projects commissioned in 2018 was USD 0.056/kWh compare to USD 0.127/kWh for offshore [17]. It is further estimated that 77% of onshore wind energy commissioned in 2020 will be less expensive than the least-cost fossil fuel alternative. This rapid development of onshore wind energy has been partly driven by the research and development of wind turbines which has resulted in a significant increase of the rotor diameter throughout the years. The motivation for increasing the rotor size is straight-forward as the potential wind energy a turbine can harvest grows linearly with the swept rotor area and thereby scales with the rotor diameter squared. Thus, bigger rotors equal a higher nominal power output.

To keep onshore wind energy in a leading position the most intuitive solution is to keep increasing the rotor size. However, as onshore wind turbines have increased dramatically in size they have become associated with negative environmental implications (noise, visual, and wildlife impacts) and without careful planning their social acceptance is often doubtful [18]. In addition, the economy of increasing the rotor size beyond today's standards is questioned in [19] due to increased initial cost of wind turbines. Therefore, efforts must be made to utilize each turbine more efficiently. In the summarising words of Veldkamp, ([20], p. xiii): "*For wind to make a really substantial contribution to world energy supply, it is therefore imperative that the cost of wind energy is brought down even further, which means that wind turbines must be designed to be exactly as strong as necessary, but no stronger*.".

The rapid increase of the size of wind turbines, and fierce competition between manufacturers, has already brought their design closer to the limit since conservative (heavy) designs are no longer feasible. This has resulted in cleaner wind energy from a life-cycle perspective and a reduction of the LCOE of wind energy. However, as

safety margins are reduced it becomes an increasingly important and difficult task to document that modern wind turbines are not compromising structural reliability regulations. Not only would such violations be uneconomical from a societal point of view due to the non-optimal use of materials, but it would also result in higher failure rates of wind turbines which could further weaken their social acceptance. If people perceive them as unsafe structures, it could potentially slow down the development of new onshore wind energy projects and in turn damage the entire industry.

Improving the productivity of turbines while securing structural integrity requires increasingly effective and more accurate decision support for site suitability-assessment. Both in wind farm planning to help wind farm owners choose the most economically feasible wind turbine class for a prospect site and park layout, but also in lifetime extension assessments of existing turbines. This accurately captures the motivation for this industrial PhD project: To improve decision support for site-suitability assessment of wind turbines to reach towards an optimal use of materials from a societal point of view.

1.4. SCOPE AND OBJECTIVES OF THIS THESIS

The title *"From wind climate to wind turbine loads"* defines the scope of this thesis on the interface between wind climate and wind turbine loads. At this interface, an observed wind climate for a turbine position is translated into estimates of loads on the wind turbine components. These load estimates determine if design loads are exceeded for the turbine model in question – i.e. if the model is 'suitable' or 'not suitable' for the site and park configuration. Such decisions of turbine suitability are important when projecting a feasible wind farm, where site suitability analyses form the decision basis for selecting appropriate candidate turbine models and making initial wind farm layouts for optimal use of available land, land lease/purchase agreements and permits.

Decisions critical to success and feasibility of a wind farm project, such as turbine size (rotor and hub height) and turbine positions, must be made at the early project stages where project developers have no access to load calculations as no agreement has yet been made with a turbine manufacturer. This prohibits that the absolute loads on commercial wind turbines can be replicated, but by utilizing relative information it is still possible to make rational decisions. Loads on a representative reference wind turbine can be established for a certain wind turbine design class, and then compared to the loads obtained at a specific site. If the ratio of these loads is in favour of the design (i.e. if the site loads are lower than the design loads), this indicates that a similar turbine from a manufacturer will also be suitable for the prospect site and wind farm layout. The following list shows important requirements for the decision support:

- Provide estimates of approximate but accurate loads, with no access to the specific aeroelastic model.
- Ensure that simplifications in input data (characteristic wind climate) do not lead to poor decisions.
- Ensure that the decision support accounts sufficiently for relevant uncertainties and their sensitivities.

These principal requirements match closely the content of the two following chapters in this thesis where the goal is:

- To advance existing deterministic decision support and identify the weakest links of the IEC 61400-1 characteristic wind climate description and propose improvements.
- To develop a framework for probabilistic decision support, intended for practical implementation, that considers relevant wind climate uncertainties and quantify their effect on structural reliability.

The main objective of this PhD project is thus to contribute to improving the accuracy and efficiency in the process of evaluating wind turbine suitability by reference to loads for a site and park configuration in practice. The project is delimited to fatigue loads during normal operation of onshore wind turbines to provide the first important step towards a full decision support framework that covers both fatigue and ultimate loads in the future.

1.5. STATE OF THE ART OF SITE-SUITABILTY ASSESSMENT

This section seeks to explain the most important concepts and present the state-of-the-art research that constitutes the foundation of this thesis. First, the design basis of wind turbines according to the IEC 61400-1 standard is covered. This is followed by an introduction to wind turbine load effect assessment by aeroelastic simulation and surrogate models. Then an overview of reference wind turbines and a description of wind in the context of fatigue loads is presented. Finally, the development in probabilistic design of wind turbines is highlighted which forms the basis for next generation decision support in practice. There is a comprehensive amount of theory behind these related topics which is not described in detail here, and instead some recommended references are provided.

1.5.1. DESIGN BASIS AND CURRENT STATUS OF STANDARDS

Most modern wind turbines are designed according to the minimum requirements defined by the International Electrotechnical Commission (IEC) standard 61400-1 [21]. This standard specifies the design requirements for type certification as shown in Table 1 which allows for series production, and thereby extensive optimization, of wind turbines.

Table 1. Wind turbine design classes in IEC 61400-1 ed. 4 [22].

Wind turbine class		I	II	III	S
U_{ave} [m/s]		10.0	8.5	7.5	Values specified by the designer
U_{ref} [m/s]		50.0	42.5	37.5	
$U_{ref,T}$ [m/s] (tropical)		57.0	57.0	57.0	
A+	I_{ref} [-]		0.18		
A	I_{ref} [-]		0.16		
B	I_{ref} [-]		0.14		
C	I_{ref} [-]		0.12		

The values correspond to hub height:

U_{ave}	Average annual 10 min. mean wind speed.
U_{ref}	Reference 10 min. mean wind speed.
I_{ref}	Reference value for turbulence intensity at 15m/s

Wind turbine design comprises a wide range of engineering disciplines including civil engineering, mechanical engineering, and electrical engineering. However, in the early development of wind turbine standardization in the 1980's they were deemed 'civil engineering structures' [23]. The overall guidelines are therefore based on the traditional civil engineering approach of dividing the design life into separate individual design load cases (DLCs). Each DLC couples an expected state of the wind turbine during its lifetime (transport, normal operation, fault, etc.) with an external condition (extreme wind speed, normal turbulence, extreme turbulence, etc.). The DLCs are divided by two groups; ultimate limit state analysis (ULS) and fatigue limit state analysis (FLS). Both are equally important to secure safe operations of wind turbines over the course of their lifetime of typically 20 years[1]. However, the FLS often becomes decisive due to the highly dynamic response of wind turbines in a turbulent environment, and it also plays a vital role for end of lifetime decisions. The latter is immediately clear from the lifetime extension guidelines provided by the DNV GL [24] and UL [25] standards.

The fatigue limit state is divided by design situations during normal power production, fault conditions, parked and idling conditions, and start-up and shut-down procedures, as summarized in Table 2. Fault conditions and start-up/shut-down procedures are heavily wind turbine and controller specific and may therefore not be accurately assessed by reference wind turbines. This thesis therefore concentrates on normal

[1] A third 'serviceability limit state (SLS)' related to deformations (e.g. tilt angle of the foundation) is also considered but it is not explicitly mentioned in the IEC 61400-1 standard.

operation during power production (DLC 1.2) which also covers the majority of the turbine's lifetime[2].

Table 2: Design load cases in FLS [22].

Design load case	Wind turbine state	External condition	Wind speed range
DLC 1.2	Power production	NTM	$U_{in} < U < U_{out}$
DLC 2.4	Power production plus fault	NTM	$U_{in} < U < U_{out}$
DLC 3.1	Start-up	NWP	$U_{in} < U < U_{out}$
DLC 4.1	Normal shut-down	NWP	$U_{in} < U < U_{out}$
DLC 6.4	Standing still or idling	NTM	$U < U_{ref}$

NTM: Normal turbulence model.

NWP: Normal wind profile.

U_{in} : Cut-in wind speed.

U_{out} : Cut-out wind speed.

The IEC standard[3] was recently released in a fourth edition [22]. This new edition introduces some significant changes and improvements towards more accurate site-suitability assessment with reference to loads. The three most important changes for DLC 1.2 are listed below:

- A Weibull distribution is recommended for the NTM.
- Annex K is introduced with guidelines to calibration of structural safety factors.
- The 'Dynamic Wake Meandering (DWM)' model is introduced.

Changing the NTM from a lognormal to a Weibull distribution directly addresses the large discrepancy between the turbulence distribution standard deviation adopted by the lognormal NTM and real observations. In Chapter 3 it is shown how this change of the NTM may lead to lighter designs of turbines in a probabilistic design approach.

An important step towards probabilistic design of turbines in the industry is the new Annex K of the IEC standard. This increased transparency of the assumptions behind the partial safety factors opens for reliability assessment of wind turbines without requiring access and knowledge of the background documents. In Chapter 3 a more detailed description of the new information in annex K is provided and it is shown

[2] For the wind turbine design classes in Table 1 normal operation encompass approximately 90% of the lifetime.

[3] To ease readability the IEC 61400-1 standard is referred to as the 'IEC standard'. When relevant, the edition (either third or fourth) is clearly mentioned and a reference is provided.

how it can be used for probabilistic design and decision support in a fast and accurate framework for reliability assessment.

Finally, the fourth edition recommends the DWM model. It combines the main wake effects in terms of the wind speed deficit, the increased turbulence intensity, and the meandering of the wake downstream. This has significant advantages in optimization of wind farm layouts by providing a consistent framework for both power production and load assessment. The main downside of the model is the relatively high computational cost compared to the 'Frandsen wake added turbulence model'. The majority of the work leading to this thesis was done before the fourth edition of the IEC standard was released, and therefore the 'Frandsen wake added turbulence model' has been considered when calculating wake added turbulence.

1.5.2. SITE-SUITABILITY ASSESSMENT OF WIND TURBINES

The IEC standard specifies how to assess if a particular wind turbine model is suitable for a specific wind climate and park layout based on the partial safety factor method [22], [26]. For each new wind power project, the site-specific ambient wind climate and wind farm layout are different, so the structural integrity of wind turbines must be verified under these unique conditions. This may be documented in one of two ways [22]:

- By a 'site-suitability assessment with reference to wind climate', or
- By a 'site-suitability assessment with reference to loads'.

In both cases the following wind climate parameters are required to assess DLC 1.2:

- 10 min. mean wind speed distribution (U) (Weibull distributed)
- 10 min. wind speed standard deviation (σ_U) (90% quantile)
- 10 min. wind shear exponent (α) (mean value)
- Air density (ρ) (mean value)
- Flow inclination (φ) (maximum value)

Each of these parameters, except air density, shall be estimated for directional sectors (θ) of 30° or less to account for variations in the surrounding terrain. The characteristic wind speed standard deviation, commonly referred to as 'turbulence'[4], shall be estimated for wind speed bins of 2m/s or less. The wind shear defines the vertical variation of wind speed and is modelled by a power law. The characteristic value of the wind shear power law exponent (α_c) is defined as the mean value in each sector. The characteristic air density (ρ_c) is to be taken as the average value at the turbine position for wind speed above rated, and finally the characteristic flow inclination

[4] Another typical way to express the wind speed variation is in terms of the 10 min. wind speed coefficient of variation (referred to as 'turbulence intensity (TI)').

(φ_c) can be modelled by the maximum inclination of a fitted plane around the turbine position [22].

For each of the design classes in Table 1 a reference wind climate is defined. Here the shape parameter of the wind speed Weibull distribution is 2.0 and the scale parameter is determined from U_{ave}. Turbulence is modelled as function of wind speed by I_{ref} and the mean wind shear[5] should be taken as 0.2. The average air density is assumed to be 1.225kg/m^3, and finally, flow inclination should be assumed the worst case between -8° and +8°.

In a 'site-suitability assessment with reference to wind climate', the site-specific characteristic wind climate parameters including influence from wakes are checked against the IEC standard's reference wind climate for the relevant design class. For example, the site-specific wind speed probability density at hub height shall be less than or equal to the design class wind speed probability density between $0.2U_{ref}$ and $0.4U_{ref}$. Similar checks are defined for all wind climate parameters and each must be verified to ensure structural integrity of the considered wind turbine. In reality, at least one of the parameters (almost) always exceed the checks due to the natural variation in the wind climate combined with the strong need to exploit wind turbines to the limit to have profitable wind farm projects. In this case, it is possible that the margin in one wind climate parameter cancels out the exceedance of another. To analyse this in the right perspective, structural integrity must be documented by a 'site-suitability assessment with reference to loads'.

1.5.3. WIND TURBINE LOAD ASSESSMENT

Wind turbines are complex dynamic systems exposed to stochastic aerodynamic loading from the wind and quasi-static cyclic loading from the revolution of the rotor. To predict the response of the load-bearing components, current state-of-the-art is to use aero(servo)elastic codes that solves the differential equation of motion by a forward time-marching approach. Essentially, all aeroelastic codes are composed of two main modules: An aerodynamic model that maps the incoming wind field to forces on the blades, and a structural model to couple the dynamic response of the entire turbine. Most modern codes compute the aerodynamic forces by the 'blade element momentum' theory [27] with various engineering corrections (e.g. Prandtl's tip loss correction [28]) [29]. To calculate the dynamic response different formulations are considered across modern codes such as multi-body dynamics, finite element methods or modal approaches. Each formulation has pros and cons in terms of speed and accuracy [30].

[5] The wind shear power law exponent is referred to as 'wind shear' to ease readability.

As mentioned, wind turbines have increased dramatically in size over time. This has made it an increasingly difficult task to provide accurate aeroelastic codes. While bigger wind turbines have lowered the LCOE of wind energy, it has also introduced significant aeroelastic effects by the interaction of the stochastic aerodynamic loads and large elastic deflections. A recent review of aeroelasticity of wind turbine blades was provided by Wang et al. [31]. Other notable references which gives a broad insight into the development of state-of-the-art of aeroelasticity of wind turbines over the last decades includes [32] and [33].

Aeroelastic simulation is a key requirement for site-suitability assessment by reference to loads. However it is computationally expensive and especially in probabilistic design of wind turbines it becomes uneconomic to use direct simulation [20], [34]. To overcome this problem various methods have been proposed to simplify wind turbine load assessment using surrogate models, also referred to as meta-models, response surfaces, emulators or proxies. This technique aims at approximating the output of expensive-to-evaluate models by a data-driven bottom-up approach. The concept is illustrated in Figure 2.

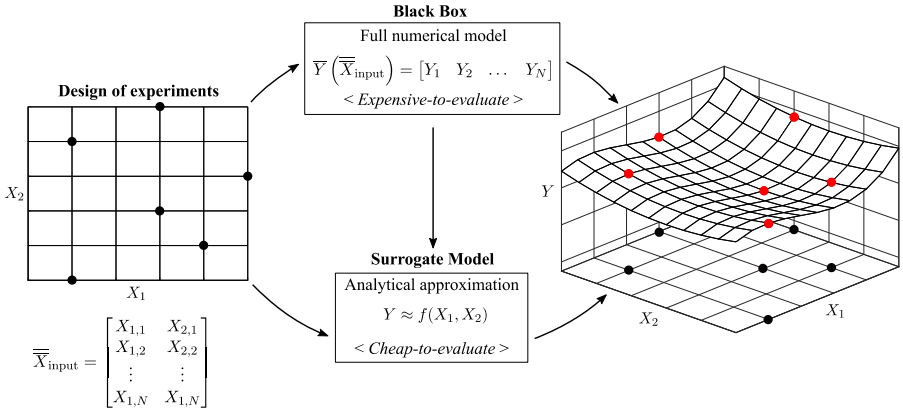

Figure 2: Concept of surrogate models illustrated for a 2D design space.

Specifically, for wind turbine loads a collection of input points (wind climate combinations) is arranged in an experimental design and the output loads are estimated by direct simulation. The aeroelastic code is then subsequently treated as a 'black box' which is approximated by another model that is much cheaper to evaluate. If a well-calibrated surrogate model is considered the loss in accuracy is made up for by the vast increase in computational speed. The technique has therefore allowed researchers to study probabilistic methods and refined reliability-based design optimization schemes, e.g. [19] and [35]–[39]. This is the essence of surrogate models as postulated by George E. P. Box in his famous quote, ([40], p. 424): "*Essentially, all models are wrong, but some are useful*."

In [41] a simple first order multivariate regression model was considered. This is similar to the product approximation used in [20] where it was compared to a first order Taylor expansion. In [42] a large range of wind speeds from 3m/s to 25m/s was considered using Taylor expansion and compared to a quadratic regression model calibrated on top of a central composite experimental design. The latter was superior when predicting wind turbine fatigue loads. However, to capture the controller imposed higher order effects on fatigue loads several quadratic response surfaces had to be established at discrete wind speeds. This drawback may be avoided by using more advanced surrogate techniques such as artificial neural networks, polynomial chaos expansion, or Kriging. A clear advantage of these techniques, compared to simpler regression methods, is the possibility to capture arbitrary functions. This was recently shown for onshore turbines using PCE and Kriging in [43] and for offshore turbines using artificial neural networks in [44].

1.5.4. REFERENCE WIND TURBINES

A basic requirement to use any aeroelastic code and train surrogate models is a mathematical description of the considered wind turbine (mass, stiffness and damping). Typically, the exact models of commercial wind turbines (CWTs) are confidential property of the manufacturers. For research purposes representative generic reference wind turbines (RWTs) are therefore utilized instead. This is mainly justified by the fact that most modern CWTs have a similar architecture; They have three blades, face upwind, operate at variable speed, and use full span collective pitch and torque control to limit rotor speed and regulate power. Most CWTs are also designed with "soft" towers with a natural frequency between the one- and three-per-revolution excitation frequencies, 1P and 3P, and the eigenfrequencies of the blades in flap-wise bending are typically above 3P. It therefore follows that modern wind turbines will respond in a similar way to relative changes of the basic wind climate parameters: wind speed, turbulence, wind shear, air density and flow inclination. In turn, the relative change in response between different environmental conditions can be well represented by RWTs with similar dynamic properties and control strategies [45].

Multiple RWTs have been developed with different rotor spans and nominal power output. Some important examples are the 1.5MW windPACT turbine [46], the 5MW reference turbine by NREL [47], and the 10MW turbine by DTU [48]. To fill the gap between the 5MW and 10MW turbines an 8MW reference turbine was developed as part of the LEANWIND project [49]. The RWTs mentioned all represent the 'typical architecture' of CWTs noted earlier, and their cut-in wind speed, rated wind speed and cut-out wind speed are approximately 3m/s, 12m/s and 25m/s respectively, which represent optimal values for modern turbines from an economical point of view [20].

Special attention is given here to the 5MW RWT. While its definition is now an official document by NREL [47] it was originally developed in 2007 by Jason

Jonkman [50]. Overall, it is a composite of conceptual models used in the WindPACT, RECOFF, and DOWEC projects with the specifications of the Repower 5M machine used as final target [47]. This specific reference turbine has now been the main workhorse in academia for more than 10 years, and is therefore also used throughout this thesis, as it provides a sound basis for comparison of results between new research and previous published work. It was also used as basis for the 10MW RWT by DTU where the overall structural definition, except for the blades, was obtained by upscaling the 5MW RWT using classical similarity rules [48]. The 8MW RWT was primarily based on available data for the Vestas V164 8MW turbine. However, when data was not available, the specifications of the turbine were based on scaling between the 5MW RWT and 10MW RWT [49]. This creates a direct link between the available next-generation representative RWTs and the 5MW RWT. On the one hand, this bears witness to the great work on developing a representative multi-megawatt RWT for the wind energy community by Jonkman [50]. On the other hand, it raises the question whether enough attention has been given towards developing new representative generic turbines to accurately capture the increasing diversity of commercial turbines.

All the mentioned RWTs operate with a gearbox to increase rotational speed of the main shaft to match their high-speed electrical generators. However, due to high maintenance costs of gearboxes [51]–[54] the concept of direct-drive, where the rotor is directly coupled to low-speed electrical generators, has seen an increasing attention [55]. This creates a need for representative direct-drive RWTs to study and understand the difference between the two concepts from a structural response point of view. For offshore application [56] describes a conversion of the 5MW RWT from gearbox to direct-drive. The need for generic direct-drive generic turbines is also acknowledged by the "IEA Wind Task 37 – Systems Engineering" [57], with the aim of developing a direct-drive version of the 10MW RWT. To extend the portfolio of publicly available RWTs this thesis describes a one-to-one conversion of the important 5MW RWT to a direct-drive configuration for onshore application in Paper 5. It is intended as an open access reference turbine for comparative studies using the freely available aeroelastic code FAST [58].

The available collection of RWTs represents modern turbines in the sense that they utilize pitch control and have a nominal power in the megawatt range. This has enabled academia to study the possibilities and implications of next-generation wind turbines in the past 10-15 years. However, with the increasing age of the world's wind fleet, requests for end of life decision support are now emerging in the industry [59]. Here, an important engineering task is to revisit the design basis of older turbines to check if any remaining useful fatigue lifetime exists [59]. To increase the accuracy of such re-evaluations it is essential to have access to RWTs that accurately represent older turbines (e.g. stall regulated and with nominal power in the kilowatt range). To this author's best knowledge, no such turbines are publicly available, and it is therefore recommended for future development within the topic of RWTs.

1.5.5. WIND CLIMATE PARAMETERS

Simulating load effects of onshore wind turbines requires a wind field to represent the aerodynamic excitation. Modelling representative wind fields is complex and requires reconstruction of three-dimensional wind velocity vectors that are stochastic and correlated in both time and space as carefully outlined in [60] and [61]. For simplicity, turbulence is typically modelled as a zero-mean stationary Gaussian random process imposed on a time-invariant mean wind speed field and corrected vertically by the wind shear exponent. Two turbulence spectral models are recommended by the IEC standard to model the tempo-spatial coherence; the Kaimal spectral and exponential coherence model [62] and the Mann uniform shear model [63]. In reality, the wind speed and turbulence are not stationary and the typical 10 min. wind statistics therefore have to be de-trended [21]. Trends in the wind speeds, either increasing or decreasing, will increase the measured variance [20]. Numerous authors have developed methods to de-trend (or de-spike) data, e.g. [64]–[66], and a recent benchmark of a broad range of different methods is provided in [67].

The IEC standards' wind climate characterization of using five parameters along with a (fixed) turbulence coherence model is a simplification. More parameters are needed to fully describe a wind field. In a recent study the sensitivity between fatigue loads and eighteen onshore environmental parameters were investigated [68], showing that wind speed, wind shear and turbulence are the governing parameters in fatigue assessment. This agrees with another recent study published in [43] where nine parameters were considered. Of secondary to negligible importance was the anisotropy factor of the Mann turbulence model, wind veer, mean inflow angle (both vertical and horizontal), and air density. These findings comply with a long list of previous authors who also studied the influence of wind climate on fatigue loads, e.g. [35], [43] and [69]–[72]. In summary, it is broadly acknowledged that turbulence and wind speed are the principal drivers of fatigue loads on the main load-bearing components of modern wind turbines. This is followed by the influence of wind shear, but specifically for the blade flap-wise response. This result is not surprising. Fatigue damage is induced by stress cycles and therefore mainly driven by the absolute wind speed variation which depends strongly on the mean wind speed. The same argument can be used for wind shear in the context of the flap-wise response, as each blade will experience cyclic loading when rotating through the sheared wind field. By contrast, the non-blade load bearing components are excited by the integrated thrust force across the entire rotor thereby significantly reducing the quasi-stationary harmonic response [70].

1.5.6. ATMOSPHERIC STABILITY

The primary wind climate parameters (wind speed, turbulence and wind shear) are connected via atmospheric stability [73]. In general, atmospheric stability is governed by the thermally induced buoyancy forces in the atmospheric boundary layer (ABL)

and is classified as stable, neutral, or unstable. In neutral ABLs mechanical effects dominate which is governed by the up-stream terrain and surface roughness. Unstable ABLs are convective and increase turbulence but reduce wind shear compared to the background mechanical level. By contrast, stable ABLs lead to stratified flow thereby reducing turbulence and increasing wind shear. While this is a brief explanation of a complex phenomenon, it captures the essence that wind shear and turbulence may be expected to be inversely correlated. For a more detailed explanation of atmospheric stability see e.g. [74] and [75].

In Figure 3 the variation of atmospheric stability for increasing wind speed is illustrated based on data from a meteorological mast at Høvsøre in Denmark. This mast is frequently used for academic purposes due to the accessibility and quality of the data and a description of the site can be found in [76]. What is important to notice is the higher variation of stability at lower wind speeds which is representative for most sites. A larger variation of turbulence intensity and wind shear is therefore expected at lower wind speeds.

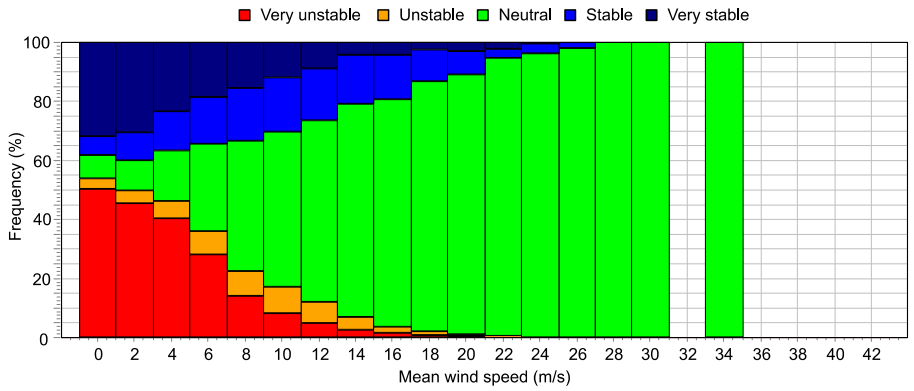

Figure 3: Atmospheric stability as function of wind speed divided into 5 classes. Notice that the atmospheric stability becomes increasingly dominated by neutral conditions at medium to high wind speeds.

The effect of atmospheric stability on wind turbine fatigue loads was investigated in e.g. [71], [77] and [78] showing that an accurate model of wind shear is important to assess fatigue loads. This is not yet acknowledged by the IEC standard where it is modelled as a mean value, thereby neglecting its natural variation and correlation with turbulence. To address this problem [70] proposed a novel standardized wind shear model for the IEC design classes. The model is partly based on the results published in [79] and aims to capture the main effects of atmospheric stability by modelling wind shear conditioned on both turbulence and wind speed. In Chapter 3 this model will be used for probabilistic analysis of the turbine design classes, where the current wind shear description in the IEC standard is insufficient. However, despite its utility

in the context of reliability assessment of wind turbines the model is not included in the fourth edition of the IEC standard [22].

The consequence of the IEC standard's significant simplifications of the wind climate on site-specific wind turbine fatigue load estimates was studied using two test cases and published in [72]. They also concluded that a more detailed shear description is needed to capture blade fatigue loads and suggested the use of a 75% quantile as function of wind speed and direction to partly account for atmospheric stability. In this thesis a follow up study is presented with a significantly improved statistical base of almost a hundred masts, and a simple yet accurate characteristic wind shear model is suggested for the IEC standard. The model captures the influence of site-specific wind shear variation on blade fatigue load effects by a wind speed dependent 60% quantile of wind shear conditioned on direction.

A different approach to account for atmospheric stability in load assessments was suggested in [80] by introducing a 'fatigue equivalent stability'. However, although the proposed model is promising and provides accurate results, a main drawback is that it relies on the Monin-Obukhov Length (MOL). This makes it less useful in practice as the well-established standard methods to estimate MOL require measurements that are typically not available (temperature gradients or 3D covariance measurements). In [81] a novel method is presented to derive the MOL based on wind shear, turbulence and wind speed measurements. This could potentially open for improved stability classifications by MOL estimates in practice, but the method still needs further validation.

1.5.7. WAKE EFFECTS INSIDE WIND FARMS

Modern wind turbines are typically installed in dense clusters (i.e. wind farms) to benefit from the best wind resources available and to reduce cost of land-lease or ownership, maintenance, and infrastructure. In these wind farms each turbine interacts with the wind. Their main purpose is to extract kinetic energy and convert it to mechanical energy thereby effectively reducing the mean wind speed in the downstream wake (wake deficit). In addition, the blades directly affect the passing wind field by reaction forces and vortex shredding which increases turbulence intensity and creates a shear layer around the wake. This is intuitively clear from the famous picture of Horns Rev 1 offshore wind farm, shown in Figure 4, where rare atmospheric conditions allowed cloud formation in the wake field [82]. The photo shows that wakes are a complex phenomenon, and that the wind fields exposed to the wake affected turbines are significantly different than the ambient wind fields hitting the front row. Consequently, the resulting dynamic loads that are experienced by wake affected turbines are significantly different than for solitary turbines [83]. This stresses that accurate wake models are essential to reliably predict fatigue loads and loss of energy production which has also motivated a considerable amount of research on wake effects on wind turbine loads and power output since the beginning of modern

wind turbine development in the 1970s. Some of the earliest experimental and analytical studies of wakes are presented already in [84] and [85] and a comprehensive and recent theoretical background to wakes is presented in [86].

Figure 4: Photo of Horns Rev 1 owned by Vattenfall. Photographer Christian Steiness. The photo was taken 12 February 2008 at around 10:10 CET.

Today, complex high order flow models that solve the Navier-Stokes equation (under certain assumptions) allow wakes to be studied in detail by computer simulations. Some relevant examples are the actuator disc model, the actuator line model, vortex models, and large eddy simulation techniques. All of these approaches show good agreement with experimental data [87]–[90], but the computational times make them infeasible in practice. Thus, their main use is restricted to academic purposes to understand the fundamental behaviour of wakes and calibrate and validate simpler models for practical use [90].

A significant effort has been made to develop semi-empirical engineering simplifications to model the wind speed deficit in wakes. These models are traditionally based on conservation of momentum and mass following the important work of Albert Betz[6] [91]. Three well known and important examples of practical

[6] Albert Betz also introduced the famous 'Betz limit' stating that wind turbines may extract no more than 59.3% of the kinetic energy in the wind.

wake deficit models are: the ‘Larsen model [92], [93]’, the ‘Frandsen model [94]’, and the ‘N.O. Jensen model [95]’. However, with focus on the wake deficit only, all three models are primarily useful to assess power output and not fatigue loads. A typical approach to account for wakes in fatigue load assessments in the industry is to use the ‘Frandsen wake added turbulence model [23]’. This allows the wake added turbulence to be considered together with ambient measurements thereby making it beneficial in site-suitability analyses. A recent study of the accuracy of the ‘Frandsen wake added turbulence model’ to predict fatigue damage is published in [96]. Based on measured data from a large wind farm they show that the model is a reasonable approximation, although conservative in near-wake situations.

The current engineering wake models share two main drawbacks. They do not model the meandering of wakes due to large scale turbulence, and they are designed to handle a single aspect of wake operation; either the wind speed deficit for power production or the increased turbulence intensity for load calculations. As mentioned, this is addressed in the fourth edition of the IEC standard by adopting the ‘Dynamic Wake Meandering (DWM)’ model which consistently combines models for the wake meandering, the wake deficit, and the increased turbulence intensity. The framework was first introduced to the wind energy community in [97] with the scope to capture the most important physics of wakes, but at the same keep the computational demand low enough to be used for design of wind farms in practice. Numerous improvements and validations of the DWM model by high-fidelity flow simulations and full scale measurements have been made after its first appearance, e.g. [98]–[103]. Also, in [104] a ‘stand-alone’ version of the DWM was developed and validated to use for power production without requiring the coupling to aeroelastic simulation. A recent study in [105] compared the current wake models used by the industry with the DWM model. By reference to measured data from two onshore wind farms it was shown that it leads to more accurate fatigue assessments than the ‘Frandsen wake added turbulence model’, while both methods seem to be conservative.

The main disadvantage of the DWM model is that it requires more computational effort compared to the Frandsen wake added turbulence model. This is especially pronounced as the Frandsen wake added turbulence model is typically combined with the ‘effective turbulence’ approximation (which was also developed by Frandsen [23]). This approximation allows engineers to integrate out the directional variation of turbulence due to wake and ambient effects resulting in a ‘fatigue equivalent’ omnidirectional value. This significantly reduces the simulations required to assess fatigue loads, and it is therefore widely used in practice. However, with the new alternative recommendation in the IEC standard of using the DWM model, it is very relevant to assess the accuracy of the effective turbulence approximation. In Paper 2 a comprehensive study of its implications is presented. An overall conclusion is that it is very conservative when estimating tower loads due to the loss of directional information. This issue is addressed further in Paper 3 [106] where a simplified method for directional fatigue load assessment of steel towers is derived and validated.

1.5.8. PROBABILISTIC ASSESSMENT OF WIND TURBINE SUITABILITY

The deterministic (semi-probabilistic) site-suitability assessment defined in the IEC standard accounts for the uncertainty in strength and load effect parameters by using characteristic values and partial safety factors. This simplified calculation procedure is a necessity to reduce the simulation effort required to document structural integrity of wind turbines in practice; however, it may lead to inconsistent reliability across sites as shown in e.g. [72], [107]. To optimize material consumption of wind turbines, and thereby both their environmental fingerprint and the LCOE of wind energy, the next generation of decision support should focus on probabilistic methods. This will allow the aleatory (physical) and epistemic (measurement, statistical, model) uncertainties related to each wind climate parameter to be considered, and the relative importance of the individual contributions to the total uncertainty and structural reliability may be quantified.

Probabilistic design of wind turbines is based on the traditional civil engineering methods developed for structural reliability assessment. This topic is standard textbook material and has been covered extensively in [108]. A significant amount of work has been made to define robust probabilistic models for wind turbines. For extreme loads both [109] and [110] represent some important milestones and in [111] a novel framework for probabilistic modelling of the fatigue life of wind turbine drivetrains is developed. Still, in the context of fatigue load assessment, the single most important contribution during the last two decades is probably the work of Veldkamp [20]. His PhD thesis combined the most notable work on reliability and code calibration released prior to his project and tied up the loose ends. It has therefore provided a comprehensive basis for succeeding research in the field of probabilistic design of wind turbines and is still relevant today.

The main challenge of probabilistic design in FLS is that fatigue damage accumulates, and therefore fatigue loads have to be integrated across the entire joint distribution of the wind climate parameters [112]. This encompasses tens of thousands of aeroelastic simulations and is therefore intractable in practice without using highly efficient integration schemes. With focus on floating offshore wind turbines the recent study in [113] suggested Monte-Carlo simulation to integrate fatigue loads, which removes the ‘curse of dimensionality’ of typical grid-based approaches, thus reducing the simulation effort to a practical level. The success of this method was partly achieved by carefully sampling the input combinations of environmental conditions using a quasi-random sequence to improve convergence. In [114] and [115] a similar approach was pursued with focus on offshore substructures. Also here, a Monte-Carlo integration scheme is proposed with emphasis towards optimizing the sampling technique to obtain fast convergence.

To significantly alleviate the simulation effort when studying probabilistic methods and reliability-based design optimization in academia, a common approach is use surrogate models. In [112] and [113] Kriging was used for reliability analysis of

offshore wind turbines in ULS and FLS, respectively. Focussing on blades [19] proposed a reliability-based design optimization using multiple Kriging surrogate models. Also recently, [36] used the basic properties of polynomial chaos expansion to propagate uncertainty from wind climate assessments to the output of aeroelastic simulation in terms of both fatigue loads and power output.

Looking through the literature on probabilistic design, the overall scope is to identify and include the most important uncertainty contributions, both aleatory and epistemic [19], [20], [35], [37], [43], [44], [116]–[119]. A general feature throughout these publications is that some sort of surrogate model is used to approximate loads; yet, no publication has been dedicated to study and quantify the model uncertainty that is introduced by the surrogate model itself. This is the topic in Paper 4. Here the model uncertainty of Kriging and polynomial chaos expansion is quantified for the important 5MW RWT. It shows that the model uncertainty may be neglected in FLS, but it requires a careful arrangement of the experimental design, and it depends on the type of surrogate model considered (regression or interpolation).

In [119] and [35] probabilistic design of wind turbines was put directly into the context of site-suitability decision support. Both publications show that it has a great potential and that accounting for uncertainties on the wind climate assessment may reverse a decision of a turbine being ‘suitable’ to being ‘not suitable’ (or vice versa). However, in [119] the methods used are not clearly described and it is therefore difficult to replicate the approach. Meanwhile, the methodology used in [35] is clearly outlined, but due to its complexity it is not feasible in practice without further simplification. This is partly the motivation for the work described in Chapter 3. Here a framework is developed for the next generation of decision support by a probabilistic design approach to assess structural reliability, with clear emphasis on practical implementation, but without compromising accuracy. However, the method requires a substantial computational effort compared to a deterministic design approach. Hence, both methodologies are useful to establish fast and efficient decision support and reliability analysis.

CHAPTER 2. DETERMINISTIC DECISION SUPPORT

"Simplicity is the outcome of technical subtlety. It is the goal, not the starting point"

Maurice Saatchi ([120], p.1)

This chapter introduces a simple and efficient framework for deterministic site-suitability assessment with reference to fatigue loads during normal operation based on the current recommendations of the IEC standard. The framework is developed with focus on delivering fast and consistent results for a broad range of commercial turbines, but by using publicly available RWTs. This property makes it applicable at all stages of wind energy projects including the early planning where no specific manufacturer is attached to the project yet. The methods are developed with attention towards using surrogate models to map wind climates into wind turbine loads without a significant loss in accuracy.

The framework is tied to the IEC standard and its overall accuracy can therefore not surpass that of the IEC standard's simplifications on site-specific wind climate assessment. These simplifications are studied in detail and the weakest links in the context of the proposed framework are identified. Based on measured wind data from 99 real sites it is shown that the current characteristic wind climate adopted by the IEC standard leads to an unnecessarily inconsistent structural reliability across sites particularly for wind turbine blades. The available data is then used to develop a novel and improved characteristic wind shear model that partly accounts for atmospheric stability to advance blade fatigue load assessments. This is followed by a quantification of the accuracy and implications of the widely used 'effective turbulence' approximation, which shows that it significantly overestimates tower fatigue loads by removing directional information. A novel and practical method to account for directions in fatigue assessment of towers is, therefore, developed. Finally, this chapter is closed with a summary and recommendations on deterministic design in the present context of efficient and accurate decision support.

2.1. DETERMINISTIC SITE-SUITABILITY ASSESSMENT

The single most important concept to establish an efficient framework for deterministic site-suitability assessment[7] is that of 'damage equivalent loads'. A clear definition of this concept is therefore outlined and then used to define the deterministic

[7] To ease readability 'site-suitability with reference to fatigue loads during normal operation' is referred to as 'site-suitability assessment' in the remainder of this thesis.

'*load index*' which reduces site-suitability assessment to a single scalar metric well-suited for early decision support.

2.1.1. DAMAGE EQUIVALENT LOADS

In wind turbine design the fatigue strength of materials is typically modelled by the macroscopic SN-approach which relates a given load effect range (S) to a number of cycles (N) before failure occurs. This is shown in Eq. (1) where m and K are constants determined by experiments.

$$N(S) = K\,S^{-m} \tag{1}$$

In double logarithmic representation the failure line (i.e. SN-curve) is assumed linear and the slope is determined by m (commonly referred to as the 'Wöhler exponent'). Both m and K can be found in standardized codes on materials, e.g. EN 1993-1-9 for steel [121].

Wind turbine load effects are estimated by simulating their response in the time domain using aeroelastic codes. This produces load effect time histories which are reduced to a spectrum of load effect ranges (S_i) and a corresponding number of cycles (n_i) following standard counting procedures [122]. A broad range of counting schemes have been suggested, but in general 'Rainflow Counting' is preferred when predicting fatigue failure [123]. To combine fatigue damage from the varying amplitude load cycles Miner's rule [124] of linear damage accumulation is applied as outlined in Eq. (2). The failure criterion is defined by $D \geq 1$.

$$D = \sum_i \frac{n_i}{N(S_i)} \tag{2}$$

Instead of using Eq. (2) to assess and compare fatigue damage in site-suitability assessment the IEC standard allows a direct comparison of fatigue load effects. However, it is difficult to make a one-to-one comparison of two different spectra. The fatigue load effect is, therefore, often represented by a single equivalent fatigue load effect range (S_{eq}) corresponding to an arbitrarily selected equivalent number of cycles (N_{eq}). This is shown in Eq. (3).

$$D = \frac{N_{eq}}{N(S_{eq})} \tag{3}$$

Since the fatigue strength is described by a linear SN-curve S_{eq} can be isolated as outlined in Eq. (4).

$$S_{eq} = \left(\frac{1}{N_{eq}} \sum_i n_i S_i^m\right)^{\frac{1}{m}} \tag{4}$$

For a given wind climate each aeroelastic simulation corresponds to a single realization of the stochastic wind field process over a finite time period (T_{sim}). S_{eq} is,

therefore, a random variable with respect to the macroscopic input wind climate parameters. To reduce the statistical uncertainty, common practice is to use several different seeds (n_{seed}). It follows from Eq. (4) that if the same simulation length is applied for all seeds then the output $S_{eq,j}$, $j = 1 \dots n_{seed}$, may be combined as the generalized mean of order m (also referred to as power mean or Hölder mean). This leads to the definition of the T_{sim} representative 'damage equivalent load (DEL)' used in this thesis shown in Eq. (5). It is assumed that $S_{eq,j}$ are independent and identically distributed (i.i.d) variables inferring that DEL converges almost surely to the expected value of S_{eq} when $n_{seed} \to \infty$. Thus, if a long time period is considered[8], for example the entire lifetime of the turbine, then the DEL is deterministic $\left(\mathbb{E}\left[S_{eq}\right]\right)$. This is also assumed in the remainder of this thesis, which is partly justified by using no less than 20 seeds to calculate DELs, where each seed corresponds to an effective[9] simulation length of 10 min.

$$DEL \stackrel{\text{def}}{=} \left(\frac{1}{n_{seed}} \sum_{j=1}^{n_{seed}} S_{eq,j}^{m} \right)^{\frac{1}{m}} \text{ where } \lim_{n_{seed} \to \infty} DEL = \mathbb{E}\left[S_{eq}\right] \tag{5}$$

It follows from their definition that DELs from different wind climates can be combined to an equivalent load effect (F) representative of T_{sim} as the weighted generalized mean value of order m. This is outlined in Eq. (6) where $r_k, k = 1 \dots n_{DEL}$, models the weight of each considered DEL.

$$F = \left(\sum_{k=1}^{n_{DEL}} r_k DEL_k^m \right)^{\frac{1}{m}} \tag{6}$$

There has been much debate over the validity of using DELs in wind turbine fatigue assessments, see e.g. [20]. The two main issues are that SN-curves from experiments are typically non-linear and may depend on mean stresses, and that Miner's rule was derived by testing aluminum alloys [124]. Its accuracy for other materials, especially modern composites used in blades, is therefore doubtful. The main reason why DELs are still widely used is straight-forward (albeit not very scientific): because they are simple. The DEL framework makes site-suitability assessment with reference to loads a much faster routine compared to alternatives such as using Goodman diagrams [125] or crack growth models based on fracture mechanics [126]. Another important reason is that DELs are allowed by the IEC standard, thus, their lack of accuracy is partly considered through the recommended safety factors [112]. Finally, it is also relevant

[8] A long time period has to be considered to justify that 'infinite' seeds are needed to estimate $\mathbb{E}[S_{eq}]$, which can be interpreted as simulating an 'infinite' time-series.

[9] Effective refers to that transient start-up behaviour has been removed from the simulations by omitting the first 2 min. of the simulated time-series.

to mention that DELs reduce the load effect spectrum to a single scalar which in turn can be approximated by surrogate techniques, e.g. [36], [42] and [43].

2.1.2. THE DETERMINISTIC LOAD INDEX

Site-suitability assessment of wind turbines requires a verification of the structural integrity under the site-specific wind conditions [22]. The typical scenario is that DELs represent internal cross-sectional load effects (bending moments, torsional moments, shear forces, etc.) and that K is defined for stress-ranges (as in EN 1993-1-9 for steel details [121]). In this case a deterministic design equation (G) may be written where the resistance is modelled in terms of Miners failure criterion and the load effect in terms of accumulated fatigue damage over the turbine's lifetime (T_L), see Eq. (7). Subscript c indicates that characteristic values are considered and γ_m, γ_n and γ_f are the partial safety factors for strength, consequence, and loads, respectively. Finally, z is the design parameter relating the characteristic one-year equivalent fatigue load effect (F_G) to stresses (e.g. by Euler-Bernoulli or Timoshenko beam theory).

$$G(z, T_L, F_G) = 1 - \frac{N_{eq} T_L}{K_c} \left(\gamma_m \gamma_n \gamma_f \frac{F_G\left(f_\theta, f_U, U, \sigma_{U,c}, \alpha_c, \rho_c, \varphi_c\right)}{z} \right)^m \geq 0 \tag{7}$$

The fatigue load[10] is assessed by weighting the DELs with respect to their probability of occurrence modelled by the probability density functions of wind speed (f_U) and direction (f_θ), as outlined in Eq. (8). Note that the DELs are not modelled as function of direction which is a common simplification for components below the yaw bearing. The effect of this simplification is investigated in section 2.3.

$$\begin{aligned} &F_G\left(f_\theta, f_U, U, \sigma_{U,c}, \alpha_c, \rho_c, \varphi_c\right) \\ &= \left(\frac{T_{ref}}{T_{sim}} \int_\theta f_\theta(\theta) \int_{U_{in}}^{U_{out}} f_U(U|\theta) DEL(U, \sigma_{U,c}, \alpha_c, \rho_c, \varphi_c)^m \, d\theta dU \right)^{\frac{1}{m}} \end{aligned} \tag{8}$$

To type certify a turbine for a certain design class manufacturers must document its structural integrity by showing that $G \geq 0$ under the corresponding design class reference wind climate[11]. In this process they fix the design of the turbine, thus, in a site-suitability assessment z, K_c and m may be treated as constants. Since F_G is the only wind climate dependent parameter in G, and because the accumulated fatigue damage is monotonic with respect to F_G, the equality in Eq. (9) applies. To ease notation two important subscripts are introduced, namely $site$ and IEC, to indicate that site-specific and IEC design class specific input is considered, respectively. Based on this the deterministic *'load index* (I_F)' is defined as shown in Eq. (10).

[10] To ease readability the 'one-year equivalent fatigue load effect' is just referred to as 'fatigue load' in the remainder of this thesis.

[11] This check represents one of many. Before a wind turbine can get a type certificate all DLCs are considered, and the structural integrity must be documented for each.

$$F_{G,site} \leq F_{G,IEC} \Leftrightarrow G_{site}(z, T_L, F_{G,site}) \geq G_{IEC}(z, T_L, F_{G,IEC}) \quad (9)$$

$$I_F \stackrel{\text{def}}{=} \frac{F_{G,site}}{F_{G,IEC}} \quad (10)$$

It follows from its definition that the considered turbine is 'suitable' if $I_F \leq 1$ and 'not suitable' if $I_F > 1$. In addition, the design margin (M_I) may be assessed by I_F as shown in Eq. (11).

$$M_I = 1 - I_F \quad (11)$$

2.1.3. PROPERTIES OF THE DETERMINISTIC LOAD INDEX

There are essentially two very important properties of the *load index* that should be highlighted:

- ***Property 1****:* The *load index* partly cancels out multiplicative errors.
- ***Property 2****:* Decisions by the *load index* are invariant to additive loads.

Property 1 is conceptually demonstrated in Figure 5. Here it is assumed that a RWT is used to estimate the *load index* of a CWT which is smaller, but with a similar architecture. This introduces a large error on the absolute loads (ϵ_{abs}), but in the ideal case the relative fatigue load increase (R) is equal when moving from a site-specific climate to the design class climate. In turn, I_F is unaffected by using a RWT. In reality some additional error (ϵ_Δ) will inevitably be introduced as the two turbines are not exactly the same. This error may reasonably be assumed to depend on the 'step length' taken in the wind climate, which is effectively regulated by the design classes. Generally, one would choose the design class where I_F is closest to 1.0 from below (Recall that wind turbine owners want the cheapest turbine that is exactly as strong as necessary, but no stronger). Property 1 also justifies the use of surrogate models to approximate I_F instead of using direct simulation. Since the same RWT can be used to represent a broad range of CWTs it is worth investing relatively many simulations in training the surrogate model. In this case the error is surrogate model dependent and, therefore, partly cancels out.

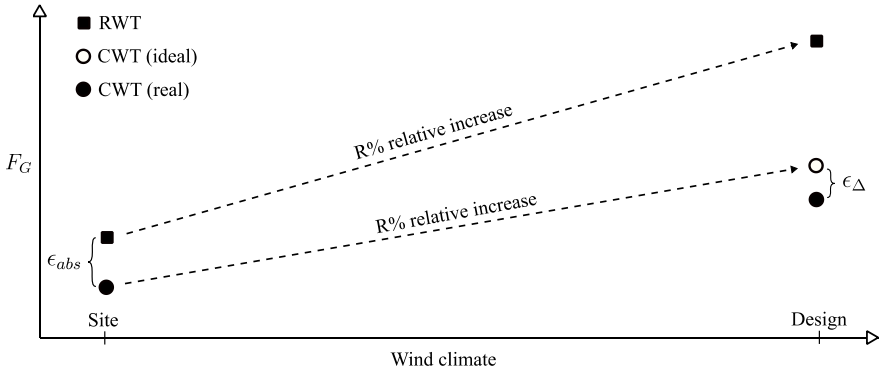

Figure 5: Conceptual illustration of the load index property 1.

To demonstrate property 2, consider some arbitrary fatigue load F_Δ. This may be combined with the fatigue load from normal operation by assigning unity weight to each load contribution. This is outlined in Eq. (12) where F_{FLS} is the total fatigue load to consider in FLS.

$$F_{FLS}(m; F_G, F_\Delta) = (F_G^m + F_\Delta^m)^{\frac{1}{m}} \tag{12}$$

If F_Δ is assumed wind climate independent, and if the same load is expected in both the design phase of the turbine and at the site, it follows that:

$$\text{sgn}(M_I) = \text{sgn}\left(1 - \frac{F_{FLS}(m; F_{G,site}, F_\Delta)}{F_{FLS}(m; F_{G,IEC}, F_\Delta)}\right) \tag{13}$$

where sgn is the signum function. This validates that the provided decision support in terms of 'suitable' or 'not suitable' can be representative for more DLCs than just normal operation, even though they are not explicitly considered. In particular, start-ups (DLC 3.1) and shut-downs (DLC 4.1) may reasonably be approximated by F_Δ since these states are coupled to the normal wind profile without turbulence [22]. This result is important since these DLCs are heavily influenced by the exact control strategy used for start-up and shut-down routines and they can therefore only be estimated tentatively by RWTs. In contrast, the *load index* could with relative ease be extended to accurately include DLC 6.4 (stand still or idling) by using RWTs but this is outside the scope of this thesis.

Its noted that it follows from Eq. (13) that the design margin estimated by the *load index*, M_I, is non-conservative as the magnitude of M_I is over-predicted. However, F_{FLS} rapidly approaches the maximum value of the individual contributions as m increases, see Figure 6. Given that normal operation is typically the largest contributor to fatigue damage, and that Wöhler exponents in the range of 4-12 are considered, this indicates that M_I is not significantly incorrectly estimated.

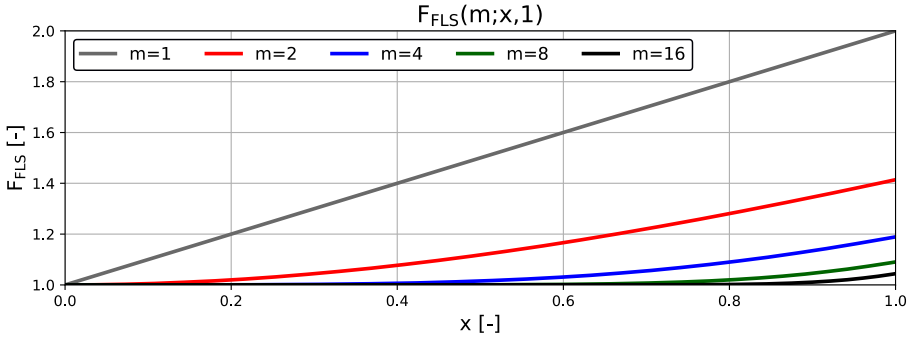

Figure 6: Relative importance of adding a constant to the weighted generalized mean for increasing Wöhler exponents.

A main question that remains is whether the decision support provided by the *load index* is accurate. It is clear from its definition that its accuracy is tied to the characteristic description of the ambient wind climate. Hence, a closer look at the current characteristic wind climate models defined by the IEC standard is required. This is the focus in the remainder of this chapter where the accuracy of the current wind climate description is analysed for the three sensors listed in Table 3. The components are chosen to represent three typical materials used in wind turbine design, while also demonstrating the overall path of wind loads from acting on the blades until being reacted by the foundation.

Table 3: Selected components and sensors.

Component	Wöhler exponent	Description
Blades	10 (Fibre composite)	Blade root bending moment
Drivetrain	6 (Cast steel)	Low speed shaft torque moment
Tower	4 (Welded steel)	Tower bottom fore-aft bending moment

2.2. AMBIENT CHARACTERISTIC WIND CLIMATE

To study the ambient characteristic wind climate the first step is to clearly define what it is supposed to model. This is directly coupled to the calibration of design codes (such as the IEC standard) which can be broken down into three levels of rational decision-making as shown in Figure 7, using the definitions in ISO 2394:2015 [26].

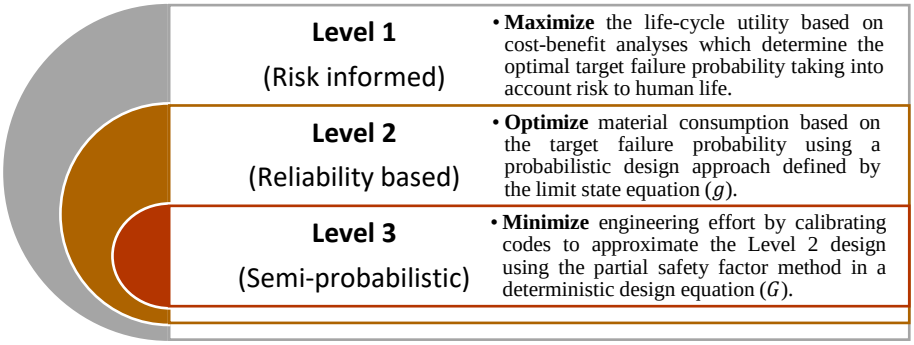

Figure 7: Code-based design calibration to implicitly account for risk and safety by a deterministic (semi-probabilistic) approach.

2.2.1. PURPOSE OF THE CHARACTERISTIC WIND CLIMATE

Figure 7 indicates how the characteristic wind climate used in Level 3 is closely related to the probabilistic limit state equation (LSE) used in Level 2. The design in Eq. (7) is based on the LSE from the IEC background document for calibration of partial safety factors [112] shown in Eq. (14) for a linear SN-curve. Bold font indicates stochastic variables where $\boldsymbol{\Delta}$ and $\boldsymbol{K}$ models the uncertainty related to the resistance in terms of Miner's rule and SN-curves, and $\boldsymbol{X}_{load}$ and $\boldsymbol{X}_{SCF}$ accounts for uncertainty on stresses in terms of wind load effects and stress concentration factors, respectively. For more details see e.g. [35], [112], [118]. The LSE divides the sample space into a 'failure region' and a 'safe region' such that the probability of failure (p_f) with respect to g may be assessed by Eq. (15).

$$g(z, T_L, F_g) = \boldsymbol{\Delta} - \frac{N_{eq} T_L}{\boldsymbol{K}} \left(\boldsymbol{X}_{load} \boldsymbol{X}_{SCF} \frac{F_g(f_\theta, f_w, \bar{W})}{z} \right)^m \tag{14}$$

$$p_f(z, T_L, F_g) = P\big(g(z, T_L, F_g) \leq 0\big) \tag{15}$$

The fatigue load in the limit state equation (F_g) is assessed by weighting DELs with respect to the measured[12] joint wind climate distribution (f_w) given direction. This is outlined in Eqs. (16) and (17) where $F_{g,\theta}$ is the sector-wise integrated fatigue load across the wind climate parameters, $\bar{W} = [U, \sigma_U, \alpha, \rho, \varphi]$. To ease notation the integration across wind speed is not explicitly stated from U_{in} to U_{out}.

$$F_g(f_\theta, f_w, \bar{W}) = \left(\frac{T_{ref}}{T_{sim}} \int_\theta f_\theta(\theta) F_{g,\theta}^m(f_w, \bar{W}) d\theta \right)^{\frac{1}{m}} \tag{16}$$

[12] The variation of the fatigue load due to uncertainty in wind climate assessment is assumed to be covered by $\boldsymbol{X}_{load}$.

$$\text{Where} \quad F_{g,\theta}^{m}(f_w, \bar{W}) = \int_{\bar{W} \in \mathbb{R}^5} f_w(\bar{W}|\theta) DEL(\bar{W})^m d\bar{W} \tag{17}$$

By comparing G and g (Eqs. (7) and (14), respectively) the purpose of the characteristic wind climate becomes clear; namely to account for the variability of the individual wind climate parameters and their covariance such that $F_{G,site} \approx F_{g,site}$. In a practical setup the natural variability of a given wind climate parameter can be considered by using characteristic quantiles to account for both its mean value and standard deviation. To account for atmospheric stability effects, and resulting covariance between the wind climate parameters, they can be conditioned on each other (resembling the Rosenblatt transformation of f_w). Finally, to account for the effect of the surrounding terrain and local speed-up factors (orography) the characteristic parameters can be conditioned on direction. This would encompass a consistent failure probability across sites[13], which in turn may be calibrated to meet the target failure probability from Level 1 by partial safety factors. In this context it is noted that the third edition of the IEC standard [21] recommends the partial safety factor for fatigue loads as a constant value of $\gamma_f = 1.0$ which is also implicitly assumed by the *load index* via Eq. (9). This is updated in the new annex K of the fourth edition IEC standard [22] where the partial safety factor for fatigue loads is now specified from 1.0 to 1.2 to consider that $\boldsymbol{X}_{load}$ is site-specific (e.g. due to varying quality of wind measurements from site to site). However, in case $\boldsymbol{X}_{load}$ is expected to be a decisive factor for the site-suitability assessment, it is recommended to follow the probabilistic framework outlined in Chapter 3.

2.2.2. ACCURACY OF THE CHARACTERISTIC WIND CLIMATE

To assess the accuracy of the characteristic wind climate recommended by the IEC standard F_G is assumed a mathematical model with the aim to approximate F_g. The accuracy at a specific site is then quantified by the ratio (ΔF_c) defined in Eq. (18), where $F_{g,site}$ is assessed by combining DELs across each 10 min. measurement of wind speed, turbulence, and wind shear to fully account for their variability and atmospheric stability effects (see Paper 1 for further details). The input variables are explicitly shown to clearly indicate the difference between the two fatigue load assessments

$$\Delta F_c = \frac{F_{G,site}\left(f_{\theta,site}, f_{U,site}, U, \sigma_{U,c}, \alpha_c, \rho_c, \varphi_c\right)}{F_{g,site}\left(f_{\theta,site}, f_{w,site}, \bar{W}\right)} \tag{18}$$

The result of this comparison is shown in Figure 8 across the 99 available sites (a detailed description of the data can be found in Paper 1). It is seen that the tower

[13] When designing a component to the limit the ratio F_G/z in G is constant across all sites. Assuming $F_G = F_g$, then F_g/z is also constant, which in turn provides a fully consistent reliability level if the remaining variables in g are unchanged.

and drivetrain fatigue loads are captured consistently across the sites but also with a significant bias. This bias may be intended by the code writing committees and is often referred to as 'hidden safety'. Noting the relatively small partial safety factor recommended by the IEC standard for wind turbine fatigue loads it seems likely that the hidden safety seen in Figure 8 is on purpose; but, in that case there is clearly an issue for the blade flap-wise bending which is very inconsistently evaluated, and for seventeen sites (17%) the hidden safety is not conservative. To optimize material consumption and improve the accuracy of the *load index*, it is therefore necessary to fine-tune the current characteristic wind climate description to capture blade fatigue loads.

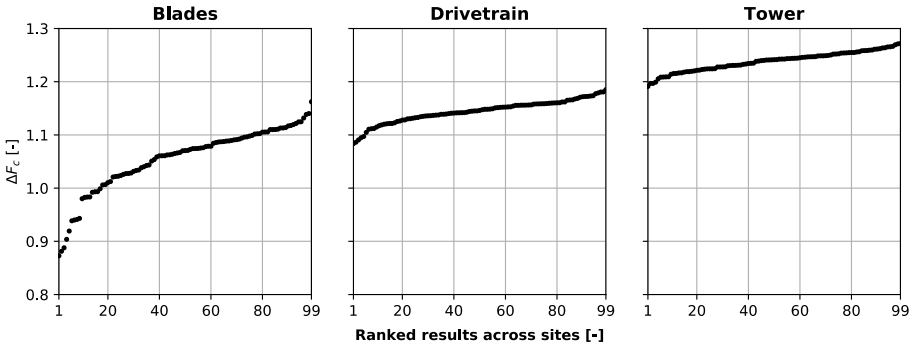

Figure 8: ΔF_c calculated for 99 sites based on 10 min. measurements of wind speed, turbulence, and wind shear. The results are ranked to clearly show the inconsistency of the blade fatigue load evaluations across sites.

2.2.3. OPTIMIZATION OF THE CHARACTERISTIC WIND CLIMATE

Considering Figure 8 it seems reasonable to model ΔF_c as a random variable (denoted $\boldsymbol{X}_c$) when it is considered across all sites. The mean value ($\mu_{\boldsymbol{X}_c}$) and standard deviation ($\sigma_{\boldsymbol{X}_c}$) of $\boldsymbol{X}_c$ then signify the average hidden safety and inconsistency of the considered characteristic wind climate, respectively. Two main objectives to optimize the characteristic wind climate description are then to minimize $\sigma_{\boldsymbol{X}_c}$ while keeping $\mu_{\boldsymbol{X}_c}$ approximately equal across components whose partial safety factors are the same. A third, and equally important, objective of the characteristic wind climate is to ensure a short lower tail of $\boldsymbol{X}_c$ as to avoid a non-conservative hidden safety.

For the stated optimization problem two constraints are considered. First, the characteristic wind climate should encompass a tractable number of simulations. Without this constraint the characteristic wind climate may as well be defined as the full joint wind climate used in F_g which is clearly not feasible for a code-based design approach. Secondly, the characteristic wind climate description should be based on reliable input. A very complex characteristic wind climate description may be theoretically correct such that highly accurate results are expected; however, if the

model relies on input that in practice is poorly approximated, or based on rules of thumb, the consequent error propagation may lead to worse decisions than using a simpler description based on well-defined and measured input. In other words, the 'GIGO' concept[14] applies and should be kept in mind when proposing models that are intended for code-based design. With this, the last constraint on the optimization problem is introduced. Namely that an improved characteristic wind climate description should be based on the already well-established wind climate parameters: wind direction, wind speed, turbulence, wind shear, air density and flow inclination.

2.2.4. IMPORTANCE OF WIND SHEAR

Having the optimization objectives and constraints in mind F_G and F_g are compared to determine which characteristic wind climate parameter that is most important to update (Eqs. (8) and (16), respectively). First it is seen that both wind speed and direction are explicitly handled in both equations. Focus is therefore on the remaining four parameters of turbulence, wind shear, air density and flow inclination. Typically, air density and flow inclination are estimated by simple approximative methods to compensate for the lack of measurements, and potentially these methods could be improved. However, state-of-the-art research on fatigue loads shows that their importance is negligible compared to turbulence and wind shear [68], [70], [72]. This is also intuitively clear by Figure 9 which shows the sensitivity between fatigue loads and each of the considered wind climate parameters. Thus, a significant effort could be made to improve the assessment of air density and flow inclination, but it would most likely be irrelevant in practice. This leaves turbulence and wind shear as the remaining parameters of interest.

Turbulence is already modelled as a quantile value dependent on both wind speed and direction to account for its variability and correlation with wind speed. By contrast, wind shear is modelled by its mean value thereby neither accounting for its natural variability, nor its negative correlation with turbulence via atmospheric stability. Recalling that blades are the only components affected by wind shear this explains the results in Figure 8, and it is therefore left as the most important wind climate parameter to study in this present context. Moreover, Figure 9 indicates that the characteristic wind shear model may be optimized to improve consistency across sites for blades without shifting the hidden safety of the remaining components. This is a preferred route which avoids a recalibration of the currently recommended partial safety factors in the IEC standard.

[14] The 'GIGO' concept is often credited to George Fuechsel who used it to remind his students that 'Garbage In, Garbage Out'.

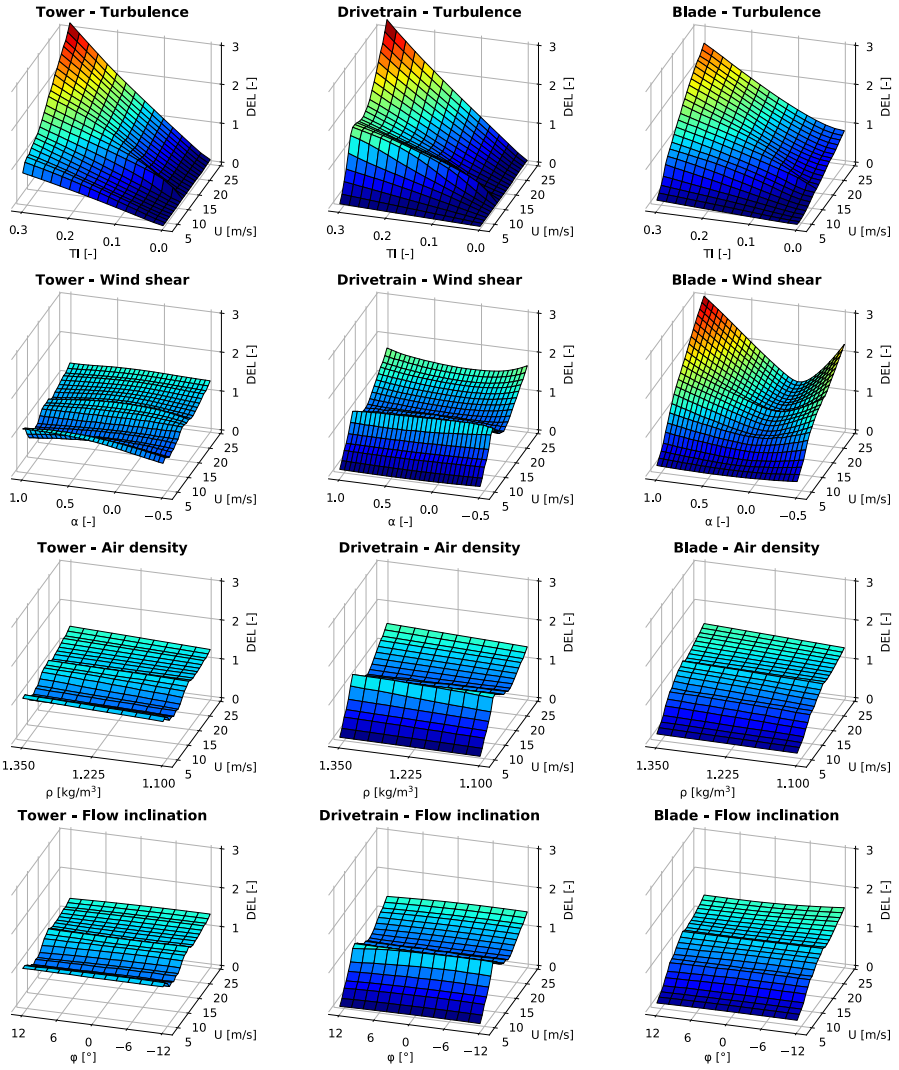

Figure 9: Fatigue load variation with the main wind climate parameters for the considered sensors. Each DEL is assessed using 100 seeds to minimize statistical uncertainty.

2.2.5. IMPROVED WIND SHEAR MODEL FOR SITE ASSESSMENT

Paper 1 presents the study of the characteristic wind shear model showing that the current characteristic wind climate leads to $\sigma_{\boldsymbol{X}_c} \approx 0.06$ for the blades (the results shown in Figure 8). In comparison $\sigma_{\boldsymbol{X}_c} \approx 0.02$ for both the tower and the shaft. To minimize the variation across sites for the blades, a novel model is proposed where the characteristic wind shear is modelled by a 60% quantile to account for natural

variability (assuming a normal distribution), while being dependent on both wind speed and direction (like turbulence) to partly account for atmospheric stability. The chosen quantile (q) minimizes $\sigma_{\boldsymbol{X}_c}$ for blades in the interval from $0.50 \leq q \leq 0.95$ while keeping the minimum value of ΔF_c across the sites above 1.0, see Paper 1 for details. The latter effectively raises the lower tail of $\boldsymbol{X}_c$ to avoid non-conservative hidden safety which may result in significant violations of structural integrity. The proposed model reduces the inconsistency of blade fatigue assessments across the sites by factor of approximately two, see Table 4, thus making it in line with that of the other components. This improvement is obtained without affecting the tower and drivetrain which is emphasized by Figure 10. It is noted that the proposed shear model is consistent with the current characteristic turbulence, which makes it easy to implement in practice.

Table 4: Comparison of the current and the proposed characteristic shear.

Variable	Model	Blades	Drivetrain	Tower
$\sigma_{\boldsymbol{X}_c}$	Current [-]	0.060	0.021	0.018
	Proposed [-]	0.034	0.021	0.018
$\mu_{\boldsymbol{X}_c}$	Current [-]	1.05	1.14	1.24
	Proposed [-]	1.07	1.14	1.24

Current model: Mean wind shear as function of direction.

Proposed model: 60% quantile of wind shear as function of wind speed and direction.

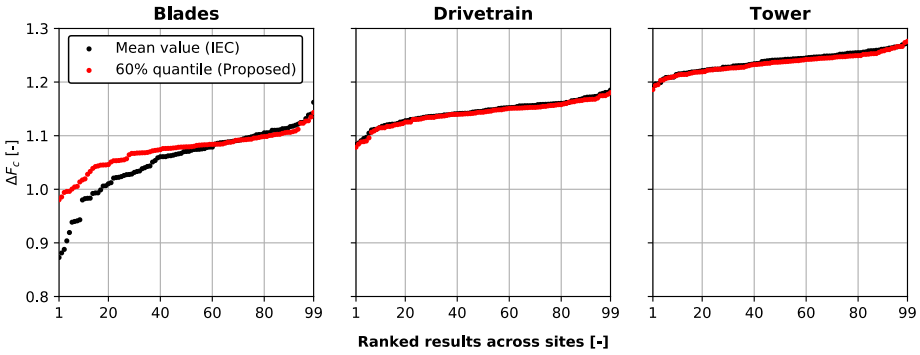

Figure 10: Comparison of the current and the proposed characteristic wind climate models across 99 real sites.

2.3. EFFECTIVE TURBULENCE AND WAKES

Until now a solitary wind turbine affected by the ambient characteristic wind climate has been considered. This does not reflect the reality of most turbines that are installed in wind farms where wakes are present and cannot be neglected in fatigue load assessments. A typical approach is to use the 'Frandsen wake added turbulence model' outlined in Eq. (19) where $\sigma_{U,T}$ is the total characteristic turbulence, RD is the distance to the upwind turbine in rotor diameters, and C_T is the thrust coefficient [22].

$$\sigma_{U,T}(\theta,U) = \sqrt{\sigma_{U,c}^2(U,\theta) + \sigma_{U,wake}^2(U,\theta)}$$
$$\text{where } \sigma_{U,wake}(U,\theta) = \left(\frac{U}{1.5 + \frac{0.8RD(\theta)}{\sqrt{C_T(U)}}}\right) \tag{19}$$

To reduce the number of aeroelastic simulations required in fatigue assessments the IEC standard allows engineers to combine the wake model with the 'effective turbulence approximation'. The approximation, first introduced by Frandsen [23], was intended as a simple turbulence model applicable for structural fatigue analysis of wind turbine farms during normal operation[15]. The model integrates out the directional variation of turbulence conditioned on mean wind speed as shown in Eq. (20) where $\sigma_{U,eff}$ is the effective turbulence [21].

$$\sigma_{U,eff}(U) = \left(\int_0^{2\pi} f_\theta(\theta|U)\sigma_{U,T}(\theta,U)^m d\theta\right)^{\frac{1}{m}} \tag{20}$$

If the effective turbulence is considered alongside the IEC standard's characteristic wind climate then fatigue loads may be assessed as shown in Eq. (21).

$$F_{G,eff}(f_U, U, \sigma_{U,eff}, \alpha_c, \rho_c, \varphi_c)$$
$$= \left(\frac{T_{ref}}{T_{sim}}\int_{U_{in}}^{U_{out}} f_U(U) DEL(U, \sigma_{U,\text{eff}}, \alpha_c, \rho_c, \varphi_c)^m \, dU\right)^{\frac{1}{m}} \tag{21}$$

The effective turbulence is a widely used concept. In the case of wakes it quickly becomes useful as they are typically not perfectly aligned with the defined sectors. Then the effective turbulence can be used, either to integrate the wake added turbulence across the defined sectors, or to calculate a fatigue equivalent omnidirectional turbulence. Here it is assumed that the effective turbulence is used to its full potential of defining an omnidirectional turbulence, which is also the original

[15] The effective turbulence does not intend to represent the actual turbulence exposed to the turbines but may be interpreted as a "fatigue equivalent turbulence".

intention of Frandsen [23] and in the IEC standard. This specific case is of distinct interest here, since it prohibits the use of the proposed characteristic wind shear model which has to be conditioned on both wind speed and direction to partly account for atmospheric stability. Implicitly, the proposed model therefore encompasses more simulations than current practice, but the benefit of this increased investment is also twofold: it removes the implications of the effective turbulence and it improves consistency of structural reliability across sites. While the previous section demonstrated the increased consistency, it is unclear what the benefit is of removing the implications of the effective turbulence. The results published in [20], [127] and [128] suggest that the effective turbulence is conservative, but a quantification for a broad range of real sites is still missing in the literature. To make such quantification a closer look at the effective turbulence formulation is needed to explore its underlying assumptions.

2.3.1. KEY ASSUMPTIONS OF THE EFFECTIVE TURBULENCE

By comparing F_G and $F_{G,eff}$ (Eqs. (8) and (21), respectively) it is seen that the main assumption of the effective turbulence is that DELs are proportional to turbulence intensity (i.e. proportional to turbulence at fixed wind speeds):

$$\text{for fixed } U\text{: } DEL \propto \sigma_U \tag{22}$$

This important relationship may be derived by considering the structural response resulting from turbulence as a narrow-band stationary Gaussian stochastic process. In that case the 'narrow-band approximation [129]' to assess fatigue damage in the frequency domain shows that [130]:

$$DEL \propto \sigma_y \tag{23}$$

where σ_y is the standard deviation of the load effect response process. Further, by assuming a stationary wind turbine component (or just a chimney) whose structural response is dominated by the first mode of vibration, and by neglecting second order effects from the turbulence on total wind pressure, it can be shown that [8], [23]:

$$\text{for fixed } U\text{: } \sigma_y \propto \sigma_U \tag{24}$$

This leads to the following four key assumptions of the effective turbulence:

1. The response of wind turbine components is a narrow-band Gaussian process.
2. The standard deviation of the process is proportional to turbulence intensity.
3. Fatigue strength of materials can be modelled by a linear SN-cuve.
4. Fatigue damage accumulates independent of wind direction.

Assumptions 1 and 2 are directly related to the proportionality between DEL and turbulence intensity. Assumption 3 is introduced through the DEL framework which results in the effective turbulence formulation relying on a single Wöhler exponent.

Finally, assumption 4 is a consequence of removing directional information which implies that fatigue damage accumulates independent of direction, which is a general simplification for load bearing sub-structures below the yaw bearing (i.e. tower and foundation).

Paper 2 investigates the implications of the effective turbulence in terms of its accuracy (effect of assumptions 1 and 2) and its consequences (effect of assumptions 3 and 4). In the following the main results are summarized and linked to the *load index*. For further details on the calculations and additional explanation of the results see Paper 2.

2.3.2. ACCURACY OF ASSUMPTIONS 1 AND 2

If effective turbulence is considered its accuracy propagates directly to the *load index* as it only applies to the site-specific loads and not the design loads[16]. In brief, the accuracy is quantified by the fatigue load ratio defined in Eq. (25) across the 99 available sites.

$$\Delta F_{eff} = \frac{F_{G,eff,site}\left(f_{U,site}, U, \sigma_{U,eff}, \alpha_c, \rho_c, \varphi_c\right)}{F_{G,site}\left(f_{\theta,site}, f_{U,site}, U, \sigma_{U,T}, \alpha_c, \rho_c, \varphi_c\right)} \tag{25}$$

$F_{G,eff,site}$ is obtained by Eq. (21) using site-specific omnidirectional turbulence estimated by the Wöhler exponents in Table 3. To reflect the increased variability of turbulence with directions in wind farms, wakes are considered according to Eq. (19) by assuming a rectangular grid layout of turbines with a distance between rows of 5 rotor diameters in the predominant wind direction, and 3 rotor diameters perpendicular to that.

The results of this analysis are shown in Figure 11. As suggested in previous literature the effective turbulence is generally conservative. On average across sites it over-predicts fatigue loads on the tower with 1% and the drivetrain and blades with 4%. So, considering its simplicity, and underlying assumptions, the effective turbulence is surprisingly accurate; however, when the average 4% reduction in blade fatigue loads is considered alongside the increased consistency of structural reliability by the proposed characteristic wind shear model it becomes very relevant to utilize sector-wise simulations. In particular, because a surrogate model can be used to calculate the *load index*, which makes the difference in calculation cost between sector-wise and omnidirectional fatigue load assessments a matter of seconds.

[16] The design class wind climates are per definition omni-directional.

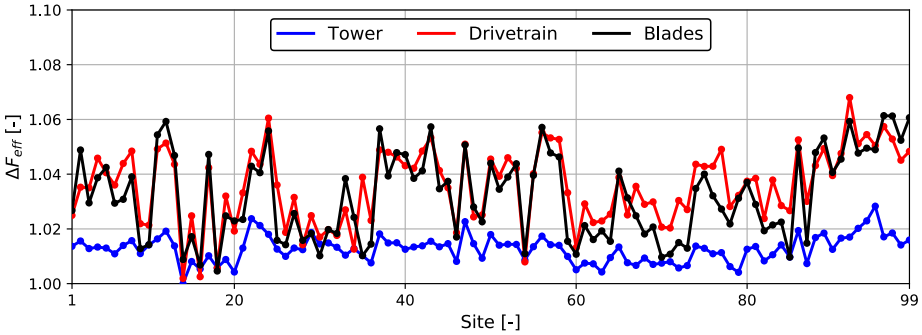

Figure 11: Accuracy of the effective turbulence approximation across 99 real sites.

2.3.3. CONSEQUENCE OF ASSUMPTION 3

The third assumption of the effective turbulence is coupled to the DEL framework and therefore applies to the *load index* on both site-specific and design loads. Its effect is analysed for a steel tower by calculating its required moment of resistance using a linearized SN-curve and the bi-linear SN-curve for welded steel defined EN 1993-1-9 in terms of stress ranges ($\Delta\sigma$), see Figure 12 [121]. The consequence of the assumption is quantified by the moment of resistance ratio (ΔW) shown in Eq. (26), where W_l and W_b is obtained by the linearized and bi-linear SN-curves, respectively.

$$\Delta W = \frac{W_{b,site}\left(f_{\theta,site}, f_{U,site}, U, \sigma_{U,T}, \alpha_c, \rho_c, \varphi_c, m_1, m_2\right)}{W_{l,site}\left(f_{\theta,site}, f_{U,site}, U, \sigma_{U,T}, \alpha_c, \rho_c, \varphi_c, m_3\right)} \tag{26}$$

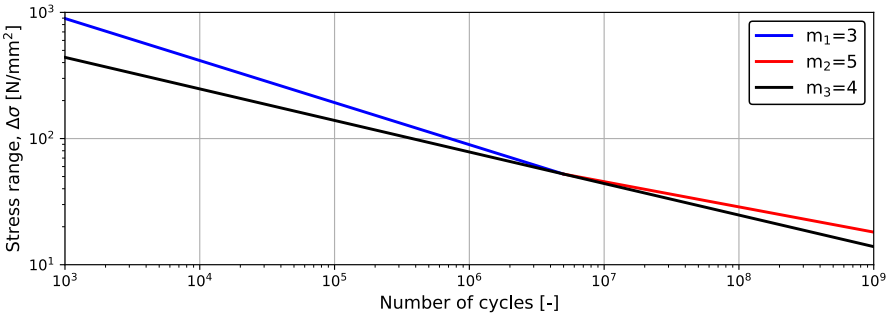

Figure 12: Bi-linear SN-curve from DS/EN 1993-1-9 and the considered conservative linearization shown for detail category 71. Changing the detail category has no influence on the presented results.

The result of this analysis is shown in Figure 13. A particularly important observation is that ΔW is almost equal across sites with a mean value of 0.92 and a standard deviation of 0.004. This indicates that the reduction in moment of resistance is turbine design specific and not driven by the wind climate. It is therefore of interest when

estimating absolute loads, but for the *load index* the reduction partly cancels out by its first property.

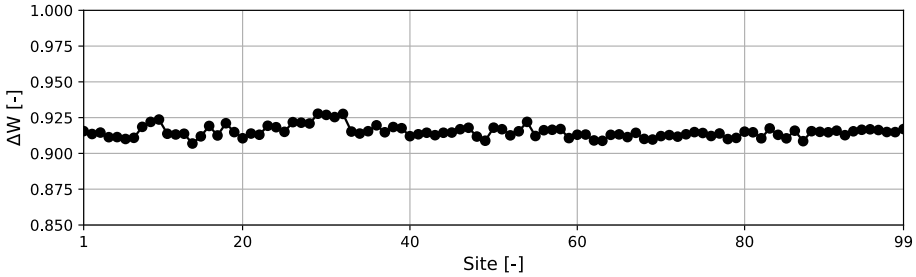

Figure 13: Consequence of assumption 3 in terms of the required moment of resistance ratio shown across the 99 available sites.

2.3.4. CONSEQUENCE OF ASSUMPTION 4

The loss of directional information makes the effective turbulence conservative for wind turbine towers [20]. However, as mentioned it is common in both industry and academia to combine tower fore-aft and side-side loads independent of direction, also when effective turbulence is not considered. This is likely because the tower load effects, by default, are defined in coordinate-systems relative to the wind direction in aeroelastic codes, e.g. [131], [132]. Accounting for direction therefore requires additional post-processing of the output. One approach is to calculate load effect time-series at fixed points along the tower circumference (M_{p_j}) taking into account the simultaneous effect of both fore-aft (M_y) and side-side (M_x) moments at each time-step (t_s). This is outlined in Eq. (27) and conceptually visualized in Figure 14 where 36 equidistant points along the circumference are considered starting with the first point (p_1) at North (**N**).

$$M_{p_j}(t_s, \theta) = M_x(t_s) \sin\Big(\alpha_j(\theta)\Big) + M_y(t_s) \cos\Big(\alpha_j(\theta)\Big) \tag{27}$$

DELs for the projected moment timeseries are then combined to point-wise fatigue loads, see Papers 2 and 3 for details, and the maximum fatigue load ($F_{G,pmax}$) is decisive when designing the tower.

The consequence of neglecting direction is quantified by comparing fatigue loads as shown in Eq. (28) where $F_{G,pmax,site}$ is the site-specific fatigue load obtained by the described directional approach.

$$\Delta F_{pmax} = \frac{F_{G,eff,site}\big(f_{U,site}, U, \sigma_{U,eff}, \alpha_c, \rho_c, \varphi_c\big)}{F_{G,pmax,site}\big(\theta, f_{\theta,site}, f_{U,site}, U, \sigma_{U,T}, \alpha_c, \rho_c, \varphi_c\big)} \tag{28}$$

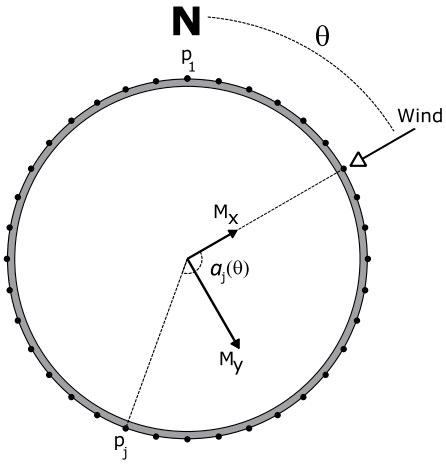

Figure 14: Cross-section of the tower bottom (no door is considered).

The result of this analysis across all 99 sites is shown in Figure 15 where the average over-prediction across sites is ~14%. This over-prediction propagate one-to-one to the *load index* since the design climates are defined without any specification of a directional distribution.

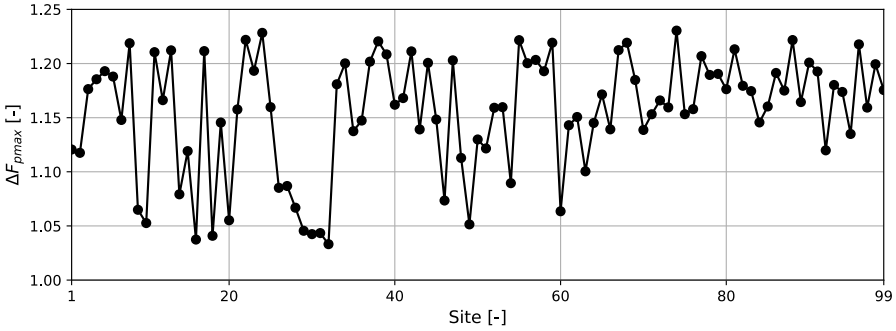

Figure 15: Overestimation of damage equivalent loads across 99 sites by considering omnidirectional fatigue assessment compared to directional simulation. The large spread in the results is because of the varying wind roses from site to site.

2.3.5. SIMPLIFIED DIRECTIONAL LOAD ASSESSMENT OF TOWERS

It is possible to include $F_{G,pmax,site}$ when assessing the *load index* but it is also laborious. It requires additional post-processing of the simulation output directly in the time-domain and it introduces a new artificial sensor for each considered point along the circumference (36 in the shown example). Therefore, even though the proposed method is theoretically correct, it is time-consuming and impractical.

To address this issue three simplified methods are proposed in Paper 3. The methods, from one to three, are increasingly accurate but also rely on an increasing simulation effort. The most precise approximation ($F_{G,twr}$) relies on sector-wise simulations as outlined in Eqs. (29) and (30) which makes it well-suited alongside the suggested wind shear model. Here $F_{G,y,site}$ and $F_{G,x,site}$ are the site-specific fore-aft and side-side fatigue load effects, respectively, both determined by the traditional approach without considering directions, and $F_{dir,site,j}$ is the approximated load at point j on the tower circumference. The accuracy of the method is checked across the 99 available sites by Eq. (31).

$$F_{G,pmax,site} \cong F_{G,twr,site} = \max_j\left(F_{dir,site,j}\right) \tag{29}$$

Where $F_{dir,site,j}$

$$= \left(\int_\theta f_{\theta,site}(\theta) \left(\sqrt{\left|\cos\left(\alpha_j(\theta)\right) F_{G,y,site}\right|^2 + \left|\sin\left(\alpha_j(\theta)\right) F_{G,x,site}\right|^2} \right)^m \right)^{\frac{1}{m}} \tag{30}$$

$$\Delta F_{dir,site} = \frac{F_{G,twr,site}\left(\theta, f_{\theta,site}, f_{U,site}, U, \sigma_{U,T}, \alpha_c, \rho_c, \varphi_c\right)}{F_{G,pmax,site}\left(\theta, f_{\theta,site}, f_{U,site}, U, \sigma_{U,T}, \alpha_c, \rho_c, \varphi_c\right)} \tag{31}$$

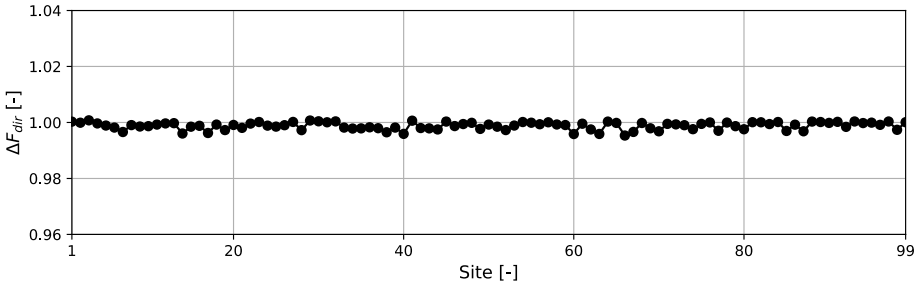

Figure 16: Accuracy of the proposed simplified method to account for directional fatigue accumulation in wind turbine steel towers across the 99 available sites.

The results are shown in Figure 16 where the average value across sites is 1.00 with a standard deviation of 0.001, thereby documenting the accuracy of the method. Note that this method still requires post-processing of the tower fatigue loads, but it has been moved from the time-domain directly to DELs and no artificial sensors are introduced. Thus, it is straight-forward to include it in the *load index* and thereby significantly optimize material consumption of steel towers in practice.

2.4. SUMMARY AND RECOMMENDATIONS

The deterministic *load index* provides a simple yet accurate framework for efficient and robust decision support by utilizing publicly available RWTs and surrogate models to establish a fast route from wind climate to wind turbine loads. Once the surrogate model is established, which is a one-time effort per RWT, it can be used to

calculate the *load index* within seconds on a standard desktop PC. This opens up possibilities for interactive optimization with consideration of fatigue loads. As an example, it would be possible to use the *load index* in the early optimization of wind farm layouts, where power output is typically the key metric for decision support [133]–[138].

The accuracy of the *load index* depends on the description of the characteristic wind climate. By analysing 99 real sites it was shown that the current model for wind shear (mean value) results in inconsistent fatigue load assessments of blades. To improve this, a new characteristic wind shear model is therefore recommended using a 60% quantile dependent on both wind speed and direction. This improved model may significantly benefit both wind turbine owners and manufacturers by providing a more consistent reliability level of blades, and thereby a more optimal use of materials from an economical perspective.

To significantly reduce computational effort in site-suitability assessments current practice is to use the effective turbulence approximation to integrate out directional variation of turbulence. This results in significant over-predictions of tower fatigue loads (14% on average across sites), when compared to directional fatigue load accumulation. It is therefore expected that a significant number of towers are designed with a too conservative (and unknown) design margin. To avoid this in future design, the practical method proposed in section 2.3 is recommended to assess the directional fatigue load based on simple post-processing of the traditional ‘fore-aft’ and ‘side-side’ fatigue loads. This may significantly benefit the wind industry, by providing lighter tower designs, and thereby lower the LCOE and the environmental fingerprint of wind turbines when the entire lifecycle is considered.

CHAPTER 3. PROBABILISTIC DECISION SUPPORT

"While in theory randomness is an intrinsic property, in practice, randomness is incomplete information"

Nassim Nicholas Tabel ([139], p. 198)

The deterministic *load index* will be almost equal across sites with similar measured characteristic wind climates, even if there is a significant difference in the quality of the measurement campaigns. This does not reflect reality where a 'better' measurement campaign will encompass a higher structural reliability of the turbine (more 'complete' information of the loads is provided). Therefore, this chapter presents a probabilistic framework for site-suitability assessment, which explicitly accounts for the quality of the wind climate assessment. The epistemic measurement uncertainty is highlighted here since it may be assessed already in the initial stages of wind farm planning, and it is possible to reduce it before final decisions are made. Hence, the clear benefit of this framework is that wind farm developers who carefully plan and execute their measurement campaign are rewarded for the effort.

The downside of the probabilistic framework is that it requires more models, data and computations than the deterministic framework. Both to assess the structural reliability, and to propagate uncertainty from wind climate to wind turbine loads. To keep calculations at a practical limit, a closed form solution to the probability of failure is derived by transforming the limit state equation. Then a generic approach is presented to determine the integrated fatigue load across the joint wind climate distribution using Monte-Carlo simulation. The uncertainty of wind climate assessments is then propagated to wind turbine loads using polynomial chaos, which is further simplified by a first order Taylor expansion. To emphasize the potential benefit of the increased investment associated to probabilistic design it is compared to the deterministic method. This shows that it is important to account for wind climate uncertainties when turbines are placed in environments close to their design limit.

Finally, to close this chapter, a brief outlook to lifetime analysis is provided. It will be shown how both the deterministic and probabilistic frameworks can be utilized to calculate useful fatigue lifetime of wind turbines, without requiring any additional computational or engineering effort. This partly addresses the increasing requests for decision support by wind farm owners where the turbines are now getting close to, or exceeding, their intended design lifetime.

3.1. PROBABILISTIC SITE-SUITABILITY ASSESSMENT

The most important aspect of probabilistic site-suitability assessment is to calculate the structural reliability of the considered wind turbine. This section presents a practical approach to this matter by transforming the limit state equation, which results in a closed form solution of the probability of failure. Based on this, the probabilistic *'beta index'* is defined, which reduces probabilistic decision support to a single scalar metric (equivalent to the *load index*).

3.1.1. LIMIT STATE EQUATION

To explicitly include wind climate uncertainties, the limit state equation (LSE) is redefined in this chapter as outlined in Eq. (32) where t models time in years. Compared to the LSE defined in Chapter 2, $\boldsymbol{X}_{load}$ is here divided into three separate contributions: $\boldsymbol{X}_{aero}$ related to aeroelastic simulation (lift, drag, finite seeds, etc.), $\boldsymbol{X}_{proxy}$ related to using a surrogate model to approximate DELs and $\boldsymbol{X}_{exp}$ to account for the quality of the wind climate assessment (exposure). Note that $\boldsymbol{X}_{exp}$ depends on the uncertainties related to each wind climate parameter (modelled by the vector $\bar{\boldsymbol{X}}_w$) which is covered in detail in section 3.3.

$$g(z,t,F_g,\boldsymbol{X}_{exp}) = \boldsymbol{\Delta} - \frac{N_{eq}t}{\boldsymbol{K}}\left(\boldsymbol{X}_{aero}\boldsymbol{X}_{proxy}\boldsymbol{X}_{SCF}\boldsymbol{X}_{exp}(\bar{\boldsymbol{X}}_w)\frac{F_g(f_\theta,f_w,\bar{W})}{z}\right)^m \tag{32}$$

Each of the considered uncertainties are in the following modelled according to Table 5 based partly on references [21], [34], [112], [118] and [140]. Typically, the statistical moments of the uncertainties are defined in intervals as the exact values are different between manufacturers and depend on their investments in experimental data and model calibration (aeroelastic codes, finite element models, etc.). Here, 'medium' values are defined which is assumed to be representative for real applications. In the following it is also expected that only F_G and $\boldsymbol{X}_{exp}$ changes between the design class and the site-specific wind climate – i.e. it is assumed that manufacturers have not reduced the turbine specific uncertainties in the time between it is designed and when it is erected at a specific site.

Table 5: Uncertainty models.

Variable	Mean value [-]	Standard deviation [-]			Distribution	Description
		m=4	m=6	m=10		
$\boldsymbol{\Delta}$	1.0	0.30	0.40	0.50	Lognormal	Miner's rule
$\log \boldsymbol{K}$	$\mu_{\log K}$*	0.20	0.15	0.25	Normal	SN-curve
$\boldsymbol{X}_{aero}$	1.0	0.10	0.10	0.10	Lognormal**	Aeroelastic simulation
$\boldsymbol{X}_{SCF}$	1.0	0.10	0.15	0.15	Lognormal	Stress concentration factor
$\boldsymbol{X}_{proxy}$	1.0		0.00*		Lognormal	Surrogate model
$\boldsymbol{X}_{exp}$	1.0	Depends on the quality of the measurement campaign			Lognormal***	Wind climate assessment

*The mean value of $\log \boldsymbol{K}$ depends on the considered SN-curve which is detail-specific (e.g. divided by detail categories in EN 1993-1-9 [121]).

**The surrogate model uncertainty is highly dependent on the computational effort invested in training it, see Paper 4. Here a Kriging model with 'high' accuracy is considered.

***$\boldsymbol{X}_{exp}$ and $\boldsymbol{X}_{aero}$ are implicitly assumed lognormal distributed in the IEC background document where $\boldsymbol{X}_{load} = \boldsymbol{X}_{aero}\boldsymbol{X}_{exp}$ is modelled by a lognormal distribution [112].

3.1.2. TRANSFORMATION OF THE LIMIT STATE EQUATION

Recall that the LSE divides the sample space into a 'safe region' and a 'failure region' such that the probability of failure can be obtained as the probability $P(g \leq 0)$. This is invariant to a logarithmic transformation as shown in Eqs. (33) and (34) where $\sigma_{\boldsymbol{X}_{exp}}$ is the standard deviation of $\boldsymbol{X}_{exp}$. Note that this $g \rightarrow g_{ln}$ transformation is allowed as both terms in g are positive, and $\ln x$ is a strictly increasing function for $x > 0$.

$$g_{ln}\left(z, t, F_g, \boldsymbol{X}_{exp}\right) = \ln(\boldsymbol{\Delta}) - \ln\left(\frac{N_{eq}t}{\boldsymbol{K}}\left(\boldsymbol{X}_{aero}\boldsymbol{X}_{proxy}\boldsymbol{X}_{SCF}\boldsymbol{X}_{exp}(\overline{\boldsymbol{X}}_w)\frac{F_g(f_\theta, f_w, \overline{W})}{z}\right)^m\right) \quad (33)$$

$$p_{f,ln}\left(z, t, F_g, \sigma_{\boldsymbol{X}_{exp}}\right) = P\left(g_{ln}\left(z, t, F_g, \boldsymbol{X}_{exp}\right) \leq 0\right) = P\left(g\left(z, t, F_g, \boldsymbol{X}_{exp}\right) \leq 0\right) \quad (34)$$

Since all stochastic variables in g_{ln} are lognormally distributed ($\log K$ being normal infers that K is lognormal in base 10), it can be cast as a sum of normal variables. This is outlined in Eq. (35) where subscript N indicates the normal distributed variables associated to the lognormal variables. Table 6 summarizes the full expansion of the transformed limit state equation.

$$g_{ln}\left(z, t, F_g, \boldsymbol{X}_{exp}\right) = a_0\left(z, t, F_g\right) + \sum_i a_i \boldsymbol{X}_{N,i} \text{ where } \boldsymbol{X}_{N,i} = \ln(\boldsymbol{X}_i) \quad (35)$$

Table 6: Transformed LSE coefficients.

i	a_i	X_i
0	$-\ln(N_{eq}t) + m\left(\ln z - \ln\left(F_g(f_\theta, f_w, \overline{W})\right)\right)$	-
1	1	$\boldsymbol{\Delta}$
2	ln (10)*	$\boldsymbol{K}$
3	$-m$	$\boldsymbol{X}_{aero}$
4	$-m$	$\boldsymbol{X}_{SCF}$
5	$-m$	$\boldsymbol{X}_{proxy}$
6	$-m$	$\boldsymbol{X}_{exp}$

*This follows from changing the logarithmic base from 10 to e

It follows from the basic properties of normal distributed variables that the mean value and standard deviation of g_{ln} can be obtained by Eqs. (36) and (37), where $\mu_{\boldsymbol{X}_i}$ and $\sigma_{\boldsymbol{X}_i}$ model the mean and standard deviations outlined in Table 5.

$$\mu_{g_{ln}}\left(t, z, F_g, \sigma_{\boldsymbol{X}_{exp}}\right) = a_0(z, t, F_g) + \sum_i a_i \mu_{\boldsymbol{X}_{N,i}} \quad \text{where} \quad \mu_{\boldsymbol{X}_{N,i}} = \ln\left(\frac{\mu_{\boldsymbol{X}_i}}{\sqrt{1 + \frac{\sigma_{\boldsymbol{X}_i}^2}{\mu_{\boldsymbol{X}_i}^2}}}\right) \tag{36}$$

$$\sigma_{g_{ln}}\left(\sigma_{\boldsymbol{X}_{exp}}\right) = \sqrt{\sum_i a_i^2 \sigma_{\boldsymbol{X}_{N,i}}^2} \quad \text{where} \quad \sigma_{X_{N,i}} = \sqrt{\ln\left(1 + \frac{\sigma_{\boldsymbol{X}_i}^2}{\mu_{\boldsymbol{X}_i}^2}\right)} \tag{37}$$

Consequently, the probability of failure related to g_{ln} can be estimated in closed form by Eq. (38) where Φ is the standard normal cumulative distribution function, and β is the Hasofer & Lind [141] reliability index defined by Eq. (39)[17].

$$p_{f,ln}\left(z, t, F_g, \sigma_{\boldsymbol{X}_{exp}}\right) = \Phi\left(-\beta_{ln}\left(z, t, F_g, \sigma_{\boldsymbol{X}_{exp}}\right)\right) \tag{38}$$

$$\text{where } \beta_{ln}(z, t, F_g, \sigma_{\boldsymbol{X}_{exp}}) = \frac{\mu_{g_{ln}}\left(z, t, F_g, \sigma_{\boldsymbol{X}_{exp}}\right)}{\sigma_{g_{ln}}\left(\sigma_{\boldsymbol{X}_{exp}}\right)} \tag{39}$$

The advantage of this closed form solution is two-fold. Firstly, it avoids approximation errors associated to first and second order reliability methods (FORM and SORM) or Monte-Carlo simulations. Secondly, it does not require the LSE to be evaluated multiple times which effectively reduce the computational effort.

It is noted that Eq. (38) defines the cumulative failure probability up to time t. Target values are often given in terms of the failure probability at the last year of service (t_L)

[17] This entire approach to estimate the probability of failure is inspired by reliability assessments in the oil and gas industry in the 1970s when calculations were done 'by hand'.

given survival of the structure (Δp_f). This conditioned failure probability, and the corresponding reliability index ($\Delta\beta$), may be obtained by Eqs. (40) and (41), respectively.

$$\Delta p_{f,ln}\left(z, t_L, F_g, \sigma_{\boldsymbol{X}_{exp}}\right) = \frac{p_{f,ln}\left(z, t_L, F_g, \sigma_{\boldsymbol{X}_{exp}}\right) - p_{f,ln}\left(z, t_L - 1, F_g, \sigma_{\boldsymbol{X}_{exp}}\right)}{1 - p_{f,ln}\left(z, t_L - 1, F_g, \sigma_{\boldsymbol{X}_{exp}}\right)} \tag{40}$$

$$\Delta\beta_{ln}\left(z, t_L, F_g, \sigma_{\boldsymbol{X}_{exp}}\right) = -\Phi^{-1}\left(\Delta p_{f,ln}\left(z, t_L, F_g, \sigma_{\boldsymbol{X}_{exp}}\right)\right) \tag{41}$$

3.1.3. THE PROBABILISTIC BETA INDEX

To estimate $\Delta\beta_{ln}$, the component specific design parameter, z, is required, which relies on detailed information of the exact commercial wind turbine (e.g. technical drawings). To circumvent this, and thereby allow RWTs to be considered, a relative approach is taken as outlined in the following.

First, the RWT is designed to the limit by calculating the required minimum design parameter for the considered design class ($z_{min,IEC}$), such that the target reliability index at the last year of service ($\Delta\beta_t$) is reached exactly. This is outlined in Eq. (42) where $\Delta\beta_t = 3.3$ is taken directly from the new Annex K in the fourth edition of the IEC standard[18] [22].

$$\Delta\beta_{ln,IEC}\left(z_{min,IEC}, t_L, F_{g,IEC}, \sigma_{\boldsymbol{X}_{exp},IEC}\right) = \Delta\beta_t = 3.3 \tag{42}$$

By using the estimated design parameter, the site-specific reliability index is then assessed as outlined in Eq. (43). Based on this, the *'beta index* (I_β)' is defined as shown in Eq. (44).

$$\Delta\beta_{ln,site}\left(z_{min,IEC}, t_L, F_{g,site}, \sigma_{\boldsymbol{X}_{exp},site}\right) \tag{43}$$

$$I_\beta \stackrel{\text{def}}{=} \frac{\Delta\beta_{ln,IEC}}{\Delta\beta_{ln,site}} \tag{44}$$

It follows that the considered turbine is 'suitable' for the site-specific wind climate and associated uncertainty if $I_\beta \leq 1$ and 'not suitable' if $I_\beta > 1$ (equivalent to the *load index*). It is noted that the mean value of $\mu_{\log \boldsymbol{K}}$ is required to assess I_β. Apparently, this

[18] This relatively low target reliability reflects that wind turbines are unmanned structures placed in safe distance from nearby population (e.g. due to noise restrictions).

is an issue when RWTs are considered, but due to the relative approach it can be selected arbitrarily[19].

Overall, the described framework provides a closed form solution to the probability of failure, and thus also to the *beta index*, which can be estimated by RWTs. However, it is still not an easy task to calculate the *beta index* in practice since F_g and $\sigma_{\boldsymbol{X}_{exp}}$ have to be assessed for both the design class and at the site-specific wind climate. This requires fatigue load integration across the entire joint wind climate distribution as discussed in Chapter 2 (where it was rejected for being too expensive for code-based design). Focus in the remainder of this chapter is, therefore, to define efficient and accurate methods to integrate fatigue loads and propagate the wind climate uncertainties to wind turbine loads, suited for practical applications.

3.2. INTEGRATED FATIGUE LOAD ASSESSMENT

The integrated fatigue load is a function of the joint wind climate distribution, f_w. Therefore, the first step is to define this distribution for real sites, such that it may be estimated by the data typically available. A proposal to extend the current IEC design classes to full joint distributions is then presented, and finally, a Monte-Carlo integration scheme to assess F_g is outlined.

3.2.1. JOINT WIND CLIMATE DISTRIBUTION

Atmospheric stability effects and orography are critical factors for fatigue loads, which should be captured by the description of the site-specific joint wind climate distribution. A forthright approach is to condition wind direction, wind speed, turbulence and wind shear on each other (in that specific order to reflect importance) as summarized in Table 7. However, this approach requires a long measurement campaign (one year is considered here) to ensure a reasonable statistical basis when estimating the wind shear distribution moments. In practice, especially in the early stages of wind farm planning, data may only be available from preliminary short-term measurement campaigns. In this case, the wind shear could be conditioned on direction and wind speed only to partly account for atmospheric stability (in line with the proposed characteristic wind shear model). The resulting loss of accuracy can subsequently be considered through the wind climate uncertainties described in the next section.

Measurements required to estimate air density (temperature, pressure) are typically not available in practice but its marginal distribution may be estimated relatively cheaply by meso-scale models. Measurements of flow inclination are also not available from typical measurement campaigns. In principle, the distribution of this

[19] By rearranging g, it can be shown that z scales linearly with $\sqrt[m]{10^{\mu_{\log K}}}$, thereby proving that $\mu_{\log K}$ can be selected arbitrarily without affecting I_β.

parameter, conditioned on direction, may be assessed by computational fluid dynamics (CFD) models. However, this is extremely computationally demanding and disproportional to the importance of the parameter, so it is proposed to model it as a fixed value depending on the site-specific topography. Later it is shown that flow inclination is unimportant in probabilistic design, and this simplification will consequently not significantly influence the results. The full description of the site-specific joint wind climate distribution is outlined in Eq. (45), and the considered statistical parameters ($\bar{M}_{site}$) are listed in Eq. (46). For a detailed description of how to obtain the statistical parameters, refer to Paper 4.

$$f_{w,site}\left(\bar{M}_{site}(\theta)\right) = f_U(U|\theta) f_{\sigma_U}(\sigma_U|U,\theta) f_\alpha(\alpha|\sigma_U,U,\theta) f_\rho(\rho) \tag{45}$$

$$\text{Where } \bar{M}_{site}(\theta) = \left[A_{U,\theta}, k_{U,\theta}, \mu_{\sigma_U,\theta}, \sigma_{\sigma_U,\theta}, \mu_{\alpha,\theta}, \sigma_{\alpha,\theta}, \mu_\rho, \sigma_\rho\right] \tag{46}$$

Table 7: Site-specific joint wind climate description.

Wind climate parameter	Notation	Distribution	Statistical parameters	
Wind direction	$P_\theta(\theta)$	Discrete	-	-
Wind speed	$f_U(U\|\theta)$	Weibull	$A_{U,\theta}(\theta)$	$k_{U,\theta}(\theta)$
Turbulence	$f_{\sigma_U}(\sigma_U\|U,\theta)$	Lognormal[20]	$\mu_{\sigma_U,\theta}(U,\theta)$	$\sigma_{\sigma_U,\theta}(U,\theta)$
Wind shear	$f_\alpha(\alpha\|\sigma_U,U,\theta)$	Normal	$\mu_{\alpha,\theta}(\sigma_U,U,\theta)$	$\sigma_{\alpha,\theta}(\sigma_U,U,\theta)$
Air density	$f_\rho(\rho)$	Normal	μ_ρ	σ_ρ
Flow inclination*	φ_{fix}	Fixed	-	-

*The flow inclination is set to 0° for flat terrain, 6° for hilly terrain, and 12° for steep terrain.

3.2.2. WIND TURBINE DESIGN CLASSES

For the IEC design classes, wind speed distributions are explicitly defined, and the normal turbulence model (NTM) defines the statistical parameters of the turbulence distribution given wind speed, see Table 8. By contrast, wind shear is defined as a

[20] The new Weibull NTM is later recommended for the design classes in probabilistic design. For consistency, a Weibull distribution could also be considered at real sites, but here a lognormal distribution is considered.

scalar value of 0.2, which reflects that the mean value is required in deterministic design. It is possible to use this fixed value in probabilistic design, but it also appears to abuse the intention of its definition. Therefore, the wind shear model proposed for the IEC standard by Dimitrov et al. [70] is considered. Apparently, the model is conditioned on wind speed only, but it implicitly accounts for turbulence as the expression for the wind shear mean value is derived using the NTM. The air density of the design climates is, like wind shear, also defined as a scalar value. In the following, the defined value of 1.225kg/m^3 is assumed to model the air density mean value and the standard deviation is set to 0.05kg/m^3 (taken as the average value across the 99 available real sites). Finally, the flow inclination for the design classes is defined as the value resulting in the highest deterministic fatigue load in the interval $[-8°, +8°]$. For simplicity, this fixed value is also used for the probabilistic design. The resulting joint wind climate distribution of the design classes is outlined in Eqs. (47) and (48) for the lognormal NTM (which is used in the following).

$$f_{w,IEC}(\bar{M}_{IEC}) = f_{U,IEC}(U) f_{\sigma_U,IEC}(\sigma_U|U) f_{\alpha,IEC}(\alpha|\sigma_U, U) f_{\rho,IEC}(\rho) \tag{47}$$

$$\text{Where } \bar{M}_{IEC} = [A_{U,IEC}, k_{U,IEC}, \mu_{\sigma_U,IEC}, \sigma_{\sigma_U,IEC}, \mu_{\alpha,IEC}, \sigma_{\alpha,IEC}, \mu_{\rho,IEC}, \sigma_{\rho,IEC}] \tag{48}$$

Table 8: Design class joint wind climate description.

Wind climate parameter	Notation	Distribution	Statistical parameters	
Wind speed	$f_{U,IEC}(U)$	Weibull	$A_{U,IEC} = 2U_{ave}/\sqrt{\pi}$	$k_{U,IEC} = 2.0$
Turbulence	$f_{\sigma_U,IEC}(\sigma_U\|U)$	Lognormal*	$\mu_{\sigma_U,IEC}(U) = I_{ref}(0.75U + c_\mu)$	$\sigma_{\sigma_U,IEC}(U) = (I_{ref}\, 1.4m/s)$
		Weibull**	$A_{\sigma_U,IEC} = I_{ref}(0.75U + c_A)$	$k_{\sigma_U,IEC} = 0.27U + 1.4m/s$
Wind shear [70]	$f_{\alpha,IEC}(\alpha\|U)$	Normal	$\mu_{\alpha,IEC}(U) = 0.088(\ln U - 1)$	$\sigma_{\alpha,IEC}(U) = \frac{1}{U}$
Air density	$f_{\rho,IEC}(\rho)$	Normal	$\mu_\rho = 1.225kg/m^3$	$\sigma_\rho = 0.05kg/m^3$
Flow inclination	φ_{IEC}	Fixed	-	-

*The distribution parameters are taken from IEC 61400-1 edition 3 [21] where $c_\mu = 3.8m/s$.

**The distribution parameters are taken from IEC 61400-1 edition 4 [22] where $c_A = 3.3m/s$.

3.2.3. NUMERICAL INTEGRATION

The integrated fatigue load corresponding to the defined ambient joint wind climates is outlined in Eqs. (49) and (50). The dimension is reduced compared to Eq. (16) as φ is assumed fixed, and a summation is used across direction to clearly indicate that it is modelled by discrete sectors.

$$F_g(P_\theta, f_w, \overline{W}) = \left(\frac{T_{ref}}{T_{sim}} \sum_\theta P_\theta(\theta) F_{g,\theta}^m(f_w, \overline{W}) \right)^{\frac{1}{m}} \tag{49}$$

$$\text{Where } F_{g,\theta}^m(f_w, \overline{W}) = \int_{\overline{W} \in \mathbb{R}^4} f_w\big(\overline{M}(\theta)\big) DEL(\overline{W})^m d\overline{W} \tag{50}$$

$F_{g,\theta}^m$ may be approximated by Monte-Carlo (MC) simulation. This is outlined in Eq. (51), where N_{MC} is the number of samples considered and p_{MC} is the MC sampling probability density function.

$$F_{g,\theta}^m(f_w, \overline{W}) \approx \frac{1}{N_{MC}} \sum_{i=1}^{N_{MC}} \frac{f_w\big(\overline{W}_i | \overline{M}(\theta)\big) DEL(\overline{W}_i)^m}{p_{MC}(\overline{W}_i)} \tag{51}$$

The integration in Eq. (51) is defined across the sample space of real numbers, but in practice 'upper bounds' on the wind climate parameters has to be considered. This is important in order to ensure validity of aeroelastic simulations and to avoid extrapolation by the considered surrogate model, see Paper 4 for further details.

Other authors have also considered the MC approach to integrate fatigue loads to avoid the 'curse of dimensionality' e.g. [34], [113] and [115]. Their research clearly shows that the convergence behavior depends strongly on p_{MC}. In [34] and [43], a somewhat simple approach was considered by selecting $p_{MC} = f_w$, thereby putting clear emphasis on the wind climate distribution. However, for components with a high Wöhler exponent ($m \geq 10$), this results in very slow convergence [34], thereby strongly indicating that the influence of the DEL response has to be taken into account. A straight-forward explanation for this is that as m increases, the function DEL^m will eventually grow faster than f_w decays. A sampling strategy to account for this effect was pursued in [114] where an efficient procedure, 'Damage distribution based Monte Carlo sampling (DMCS)', was defined. The main purpose of this approach is to ensure that p_{MC} resembles the product of f_w and DEL^m (i.e. importance sampling). However, the apparent strength of the DMCS sampling procedure is also its biggest flaw in the present context. Since the algorithm depends on both f_w and the DEL response, the MC sampling strategy becomes unique for each considered sensor, at each considered turbine position. In practice, it is far more convenient if the same samples may be used across all calculations. The following is, therefore, reflected when selecting p_{MC}:

- The DEL response will vary across sensors for the same turbine.
- The DEL response will vary for the same sensor across different turbines.
- f_w is unique at each individual turbine position (and for each design class).
- f_w will vary across sectors for the same turbine position.

Having this in mind a straight-forward compromise is to sample p_{MC} uniformly[21], which in turn introduces two valuable properties. First, it reduces the expression for $F_{g,\theta}$ to Eq. (52) since the probability of drawing each sample is $1/V_{MC}$, where V_{MC} is the hypervolume of the considered input domain (see Paper 4 for details on the input domain).

$$F_{g,\theta}^{m}\left(f_{w,site},\overline{W}\right) \approx \frac{V_{MC}}{N_{MC}} \sum_{i=1}^{N_{MC}} f_{w,site}(W_i|\overline{M}_{site}) DEL(\overline{W}_i)^m \tag{52}$$

Second, and most importantly, it allows the same DEL samples to be used across all sites and design classes. They can, therefore, be pre-calculated and stored in an $N_{MC} \times N_{sens}$ matrix, where N_{sens} is the number of considered sensors, which in turn significantly speeds up calculations. This also allows any surrogate model to be considered, despite their difference in computational time. The importance of this is clear from [50] where the accuracy in terms of predicting DELs was benchmarked for a broad range of surrogate models. In conclusion, they recommended polynomial chaos expansion (regression) over Kriging (interpolation), mainly because it is much faster to predict new samples by regression. However, Paper 4 shows how Kriging obtains great accuracy per invested aeroelastic simulation directly in the context of reliability assessment in FLS. Kriging is, therefore, preferred considering that the aeroelastic simulations required to train a surrogate model are, by far, the most expensive part of the entire framework developed in this chapter.

To determine how many samples are required to evaluate the integrated fatigue load, a convergence study has been conducted. This is unambiguous and, therefore, only the conclusion of this study is outlined here. At each available site, one million samples were used to determine the 'true' converged value. Subsequently, it was found that $N_{MC} = 250.000$ samples estimate F_g within ~0.5% of the converged value. Note that this very high accuracy is required for the uncertainty propagation presented in the next section to avoid that it is significantly influenced by the MC integration itself.

3.3. UNCERTAINTY PROPAGATION FROM WIND TO LOADS

The final missing piece to calculate structural reliability by the transformed LSE is to estimate the standard deviation of $\boldsymbol{X}_{exp}$ by propagating wind climate uncertainties to loads. A straight-forward approach is to consider brute force MC simulation; it is both easy to implement and may provide highly accurate results. However, in this context it is also associated with an infeasible computational effort, thus, in practice a more efficient method is required.

[21] A simple approach is by drawing samples uniformly from a hypercube that fully encloses the input domain and then applying an acceptance-rejection algorithm.

Here two approaches are outlined. First using polynomial chaos expansion which is highly accurate and can be applied in the general case, and then using a first order Taylor expansion which excels by its simplicity (often referred to as 'Gaussian uncertainty propagation'). However, the first objective is to define a simple yet representative model for the wind climate uncertainty.

3.3.1. WIND CLIMATE UNCERTAINTY

Toft et al. [35] recently covered the aleatory and epistemic uncertainties related to wind climate assessments in the context of fatigue reliability analysis. They identified the following main uncertainty contributions that should be considered:

- Measurement and statistical uncertainty related to the short-term measurements.
- Model uncertainty from long-term corrections by e.g. measure-correlate-predict.
- Model uncertainty related to speed-up factors from micro-scale flow models.
- Physical and statistical uncertainty related to terrain and roughness data.

Generally, the uncertainties can be modelled by treating the statistical moments of f_w as stochastic variables. This is utilized in the following to define simple uncertainty models for each wind climate parameter, where the aleatory and epistemic uncertainties are combined. For a detailed description of the physical, model, measurement and statistical uncertainties, refer to [35].

The uncertainty on wind speed is assumed to be included as multiplicative terms on the Weibull scale ($\boldsymbol{X}_A$) and shape ($\boldsymbol{X}_k$) parameters as shown in Eq. (53).

$$\begin{aligned} \boldsymbol{A}_U(\theta) &= \boldsymbol{X}_A A_U(\theta) \\ \boldsymbol{k}_U(\theta) &= \boldsymbol{X}_k k_U(\theta) \end{aligned} \tag{53}$$

The uncertainty on the turbulence distribution is modeled as multiplicative terms on its mean value ($\boldsymbol{X}_{\mu_{\sigma_U}}$) and standard deviation ($\boldsymbol{X}_{\sigma_{\sigma_U}}$) as shown in Eq. (54). Note that a higher uncertainty is considered for the standard deviation compared to the mean value, so as to reflect that the two orders of statistical moments are determined by the same number of samples[22].

$$\begin{aligned} \boldsymbol{\mu}_{\sigma_U}(U,\theta) &= \boldsymbol{X}_{\mu_{\sigma_U}} \mu_{\sigma_U}(U,\theta) \\ \boldsymbol{\sigma}_{\sigma_U}(U,\theta) &= \boldsymbol{X}_{\sigma_{\sigma_U}} \sigma_{\sigma_U}(U,\theta) \end{aligned} \tag{54}$$

The uncertainty related to the measured wind shear distribution is considered as an additive term on the mean value ($\boldsymbol{X}_{\boldsymbol{\alpha}}$) as shown in Eq. (55).

[22] This was not considered in [35] where the turbulence standard deviation was modelled as function of wind speed only to enhance the statistical basis (number of measurements).

$$\boldsymbol{\mu}_{\alpha}(U,\theta,\sigma_U) = \boldsymbol{X}_{\alpha} + \mu_{\alpha}(U,\theta,\sigma_U) \tag{55}$$

The uncertainty related to the meso-scale modelled air density distribution is included as a multiplicative term on the mean value as shown in Eq. (56), and finally, the uncertainty on the fixed flow inclination is modelled as an additive term as shown in Eq. (57).

$$\boldsymbol{\mu}_{\rho} = \boldsymbol{X}_{\rho}\mu_{\rho} \tag{56}$$

$$\boldsymbol{\varphi}_{max} = \boldsymbol{X}_{\boldsymbol{\varphi}} + \varphi_{max} \tag{57}$$

The considered uncertainties are summarized in Table 9 and gathered in the vector $\bar{\boldsymbol{X}}_w$ defined by Eq. (58). For further reference three uncertainty classes are introduced; namely 'low', 'medium' and 'high' which are based on the recommended intervals in [35].

$$\bar{\boldsymbol{X}}_w = \left[\boldsymbol{X}_A, \boldsymbol{X}_k, \boldsymbol{X}_{\mu,\sigma_U}, \boldsymbol{X}_{\sigma,\sigma_U}, \boldsymbol{X}_{\alpha}, \boldsymbol{X}_{\rho}, \boldsymbol{X}_{\varphi}\right] \tag{58}$$

Table 9: Wind climate uncertainty models.

Variable	Distribution	Mean value	Standard deviation		
			low	medium	high
$\boldsymbol{X}_A$	Lognormal	1.0	2%	5%	10%
$\boldsymbol{X}_k$	Lognormal	1.0	2%	5%	10%
$\boldsymbol{X}_{\mu,\sigma_U}$	Lognormal	1.0	5%	10%	20%
$\boldsymbol{X}_{\sigma,\sigma_U}$	Lognormal	1.0	6%	12%	25%
$\boldsymbol{X}_{\alpha}$	Normal	0.0	0.02	0.04	0.06
$\boldsymbol{X}_{\rho}$	Normal	1.0	0.5%	1%	3%
$\boldsymbol{X}_{\varphi}$	Normal	0.0	2°	4°	6°

The presented wind climate uncertainty model is related to site-specific wind climate assessments, but it is straightfoward to apply it to the defined IEC design class distributions. However, it is not directly specified in the IEC standard [22], nor in its background document for partial safety factors [112], what uncertainty that has been assumed for the design class wind climates. Here, 'medium' uncertainties are chosen based on the viewpoint that: "If a wind turbine is designed to the limit for a given wind turbine design class, and the corresponding design class wind climate is measured at a given site using an average measurement campaign (typical equipment, measurement period, met-mast position, etc.), then the design should characterize the target reliability index exactly*"* – i.e. it is assumed that the IEC standard is calibrated with 'average' data in mind.

Finally, it is noted that the uncertainties are assumed fully uncorrelated in this thesis. This is a crude simplification as, for example, the statistical uncertainty contributions related to $\boldsymbol{X}_A$ and $\boldsymbol{X}_k$ will be correlated (the same samples are used to assess both). The implication of this has not been investigated further, and is as such open for continued research. As will be shown later, it is of particular importance to study any potential correlation between the turbulence uncertainties ($\boldsymbol{X}_{\mu,\sigma_U}$ and $\boldsymbol{X}_{\sigma,\sigma_U}$) as these are the main contributors to the standard deviation of $\boldsymbol{X}_{exp}$.

3.3.2. UNCERTAINTY PROPAGATION BY MONTE CARLO SIMULATION

Consider now Eq. (59) where $\boldsymbol{Y}_F$ is a stochastic variable to model the uncertainty on the integrated fatigue load (output) after propagating the wind climate uncertainties (input).

$$\boldsymbol{Y}_F(f_\theta, f_w(\bar{\boldsymbol{X}}_w, \bar{M}), \bar{W}) = \boldsymbol{X}_{exp}(\bar{\boldsymbol{X}}_w) F_g\big(f_\theta, f_w(\bar{M}), \bar{W}\big) \tag{59}$$

Recall that $\boldsymbol{X}_{exp}$ is modelled lognormal and assumed unbiased (mean value of 1.0) which directly implies that $\boldsymbol{Y}_F$ is also lognormal and that $\mu_{\boldsymbol{Y}_F} = F_g$. An advantage of this is that $CV_{\boldsymbol{Y}_F} = CV_{\boldsymbol{X}_{exp}} \Longrightarrow \sigma_{\boldsymbol{X}_{exp}} = \sigma_{\boldsymbol{Y}_F}/\mu_{\boldsymbol{Y}_F}$ where CV denotes coefficient of variation. The stated assumptions are in line with the IEC standard background document [112] and, as will be shown later, they are not a significant source of error.

It is straight-forward to approximate the mean value and standard deviation of $\boldsymbol{Y}_F$ by MC simulation as outlined in Eqs. (60) to (62), where $\bar{x}_{w,i} = [x_{A,i}, x_{k,i}, \dots, x_{\varphi,i}]$, $i = 1 \dots n_{MC}$, denotes realizations of $\bar{\boldsymbol{X}}_w$ and $y_{F,i}$ is the corresponding realized output.

$$y_{F,i} = F_g\big(f_\theta, f_w(\bar{x}_{w,i}, \bar{M}), \bar{W}\big) \tag{60}$$

$$\mu_{\boldsymbol{Y}_F,MC} \approx \frac{1}{n_{MC}}\left(\sum_{i=1}^{n_{MC}} y_{F,i}\right) \tag{61}$$

$$\sigma_{\boldsymbol{Y}_F,MC} \approx \sqrt{\frac{1}{n_{MC}-1}\sum_{i=1}^{n_{MC}}\big(y_{F,i} - \mu_{\boldsymbol{Y}_F}\big)^2} \tag{62}$$

As discussed earlier, each realization of $\boldsymbol{Y}_F$ requires fatigue load integration by at least 250,000 DEL values. Thus, even with the proposed strategy of using a pre-populated $N_{MC} \times N_{sens}$ 'surrogate matrix', the MC approach to propagate uncertainty quickly becomes impractical. So, the method is mainly useful to validate cheaper alternatives as shown in the following where polynomial chaos and Taylor expansion is applied in order to significantly reduce the required realizations of $\boldsymbol{Y}_F$.

3.3.3. POLYNOMIAL CHAOS EXPANSION

The Wiener-Askey generalized polynomial chaos expansion (PCE) is utilized here [142], following its implementation in the general purpose uncertainty quantification framework UQLab [143]. In the current context, the PC expansion can be written as shown in Eq. (63), where Ψ_j are multivariate polynomials orthonormal to $\overline{\boldsymbol{X}}_w \in \mathbb{R}^D$, c_j are the corresponding expansion coefficients, and j is a multi-index of the components used to construct Ψ_j. For more a more detailed explanation of PCE, see [144].

$$for\ a\ fixed\ site\text{:}\ \boldsymbol{Y}_F(\overline{\boldsymbol{X}}_w) = \sum_{j \in \mathbb{N}^D} c_j\, \Psi_j(\overline{\boldsymbol{X}}_w) \tag{63}$$

Note that in real applications, the expansion has to be truncated, e.g. using the hybrid least angle regression algorithm described in [145] (see also UQLab [146]).

Due to the orthonormality of the polynomial basis, the expansion coefficients contain information of the mean value and standard deviation of $\boldsymbol{Y}_F$ as shown in Eqs. (64) and (65), respectively.

$$\mu_{\boldsymbol{Y}_F,PCE} \approx c_0 \tag{64}$$

$$\sigma_{\boldsymbol{Y}_F,PCE} \approx \sqrt{\sum_{j \in \mathbb{N}^D \setminus \{0\}} c_j} \tag{65}$$

The PCE approach is validated by reference to MC simulation in Table 10 for design class 2B and a representative site assuming 'medium' wind climate uncertainties. In the direct MC simulation, 10,000 realizations of $\boldsymbol{Y}_F$ are considered and the PCE is trained using the first 50 samples only[23]. The results are also visualized for the tower in Figure 17 to emphasize that PCE converges significantly faster than the MC simulation. Notice also that $F_g(\overline{M}) \cong \mu_{\boldsymbol{Y}_F}$ and that $\boldsymbol{Y}_F$ is lognormal distributed, thereby validating the assumptions related to Eq. (61). However, the clear lognormal shape can be tracked back to the distribution shape of $\boldsymbol{X}_{\mu,\sigma_U}$, so if other distributions are considered, the effect of this must be checked.

[23] Polynomials up to the tenth degree are considered when training the PCE using the 'leave-one-out' error as selection criterion to avoid over-fitting.

Table 10: Validation of PCE by MC simulation.

Wind climate	Method	$F_g(\overline{M})$	$\mu_{\boldsymbol{Y}_F}$			$\sigma_{\boldsymbol{X}_{exp}}$		
		All	**T**	**D**	**B**	**T**	**D**	**B**
2B	MC	1.00	0.998	1.000	1.002	0.077	0.080	0.077
	PCE		0.998	1.000	1.002	0.077	0.080	0.077
Real site	MC	1.00	1.001	1.000	1.001	0.071	0.070	0.068
	PCE		1.001	1.000	1.001	0.071	0.069	0.068

The following abbreviations are used: (**T**)ower, (**D**)rivetrain and (**B**)lades

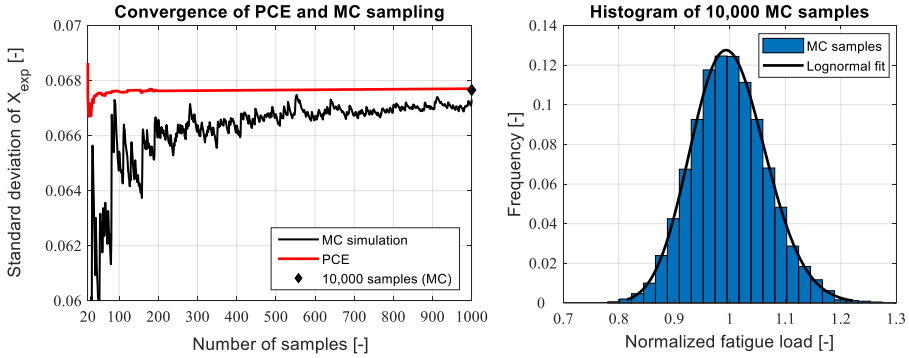

Figure 17: ***Left:*** *Convergence of $\sigma_{\boldsymbol{X}_{exp}}$ for the tower using PCE and MC simulation. The diamond indicates the value obtained after 10,000 realizations.* ***Right:*** *Histogram of $\boldsymbol{Y}_F$ based on 10,000 MC samples.*

3.3.4. SIMPLIFIED UNCERTAINTY PROPAGATION

A simple and cheap approach to approximate the mean value and standard deviation of $\boldsymbol{Y}_F$ is via a first order Taylor series expansion as outlined in Eqs. (66) and (67). By estimating the partial derivatives using a step-length in each considered wind climate uncertainty ($\overline{\boldsymbol{X}}_{w,i}$) equal to, for example, half their standard devation ($\sigma_{\overline{\boldsymbol{X}}_{w,i}}$), this approach reduces the required evalutions of $\boldsymbol{Y}_F$ to $N_{eval} = 1 + \text{len}(\overline{\boldsymbol{X}}_w) = 8$.

$$\mu_{\boldsymbol{Y}_F,app} \approx F_g(f_\theta, f_w(\overline{M}), \overline{W}) \tag{66}$$

$$\sigma^2_{\boldsymbol{Y}_F,app} \approx \sum_{i=1}^{N_X} \left(\frac{\partial F_g}{\partial \overline{\boldsymbol{X}}_{w,i}} \right)^2 \sigma^2_{\overline{\boldsymbol{X}}_{w,i}} \tag{67}$$

Figure 18 illustrates the comparison between PCE and the Taylor expansion across all 99 sites for the blades assuming 'low', 'medium' and 'high' uncertainties, respectively (the blades are chosen to present the component in which the results deviate the most). The results show that the Taylor expansion provides very accurate results. However, this may be significantly influenced by the assumed wind climate uncertainties that, as mentioned, are modelled fully uncorrelated. While correlation terms can be added to Eq. (67) without increasing N_{eval} [147], the underlying assumption of linearity (i.e. that a first order Taylor expansion is sufficient) would have to be verified.

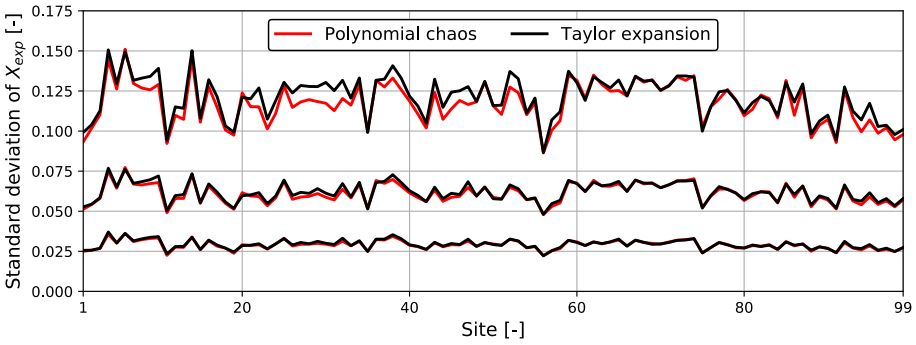

Figure 18: Comparison of PCE and the first order Taylor expansion approximation. The comparison is made across all sites for 'low' wind climate uncertainty (lower graphs), 'medium' wind climate uncertainty (middle graphs) and 'high' wind climate uncertainty (upper graphs).

3.3.5. RELIABILITY SENSITIVY INDICES

Recall that the ultimate purpose of propagating the wind climate uncertainties is to calculate and compare reliability indices by the *beta index*. Therefore, it is critical to interpret $\boldsymbol{X}_{exp}$, and, in turn, the effect of all the wind climate uncertainties combined, in this perspective. A typical metric in this context is the 'reliability sensitivity factor (α_s)' [108]. Due to the transformation of the LSE, it can be obtained analytically as shown in Eq. (68). Table 11 shows a calculation of α_s for each uncertainty model included in the LSE for design class 2B, when designing to the limit (i.e. by using $z_{min,IEC}$ such that $\beta_{IEC} = 3.3$).

$$\alpha_{s,\boldsymbol{X}_i} = \frac{-a_i \sigma_{\boldsymbol{X}_{N,i}}}{\sqrt{\sum_i a_i^2 \sigma_{\boldsymbol{X}_{N,i}}^2}} \tag{68}$$

Table 11: Comparison of reliability sensitivity factors for design class 2B.

Component	Reliability index	Reliability sensitivity factors					
		$\alpha_{s,\Delta}$	$\alpha_{s,\log K}$	$\alpha_{s,X_{SCF}}$	$\alpha_{s,X_{aero}}$	$\alpha_{s,X_{exp}}$	$\alpha_{s,X_{proxy}}$
Tower [-]		-0.34	-0.54	0.47	0.47	0.39	
Drivetrain [-]	3.30	-0.30	-0.27	0.70	0.47	0.36	0.00*
Blades [-]		-0.23	-0.28	0.71	0.48	0.36	

*The surrogate model uncertainty is neglected as a highly accurate kriging model is used, see Paper 4 for details.

As shown, it is important to consider wind climate uncertainties, but they are not dominating. This result is of interest to manufacturers who have the possibility to reduce all the epistemic uncertainties, for example, by investing in fatigue strength tests, or by improving their mathematical models (aeroelastic codes, beam theories, finite element models, etc.). However, wind farm owners' capabilities in this context are limited to improving the measurement campaign, thus, special emphasis should still be given to $\boldsymbol{X}_{exp}$.

3.3.6. SOBOL SENSITVITY INDICES

To reduce the standard deviation of $\boldsymbol{X}_{exp}$, and in turn increase structural reliability, investments could potentially be made to reduce each separate uncertainty in $\bar{\boldsymbol{X}}_w$. Hence, a vital part of efficient decision support is to provide information about which uncertainty that is most important so the 'lowest hanging fruit' can be identified. For example, if the wind shear uncertainty is 'important', it indicates that it would be beneficial to install an additional cup-anemometer at a new height to improve its assessment (and vice versa). To quantify this and establish the basis for rational decision-making, Sobol sensitivity indices ($S_{\boldsymbol{X}}$) [148] can be used. In simple terms, the Sobol sensitivity indices quantify how much of the output variance of $\boldsymbol{X}_{exp}$ that is explained by the variance of each individual uncertainty in $\bar{\boldsymbol{X}}_w$. It turns out that both PCE and the Taylor expansion have a direct advantage in this context as the first order Sobol sensitivity indices can be obtained analytically without requiring additional realization of $\boldsymbol{Y}_F$. For PCE, the Sobol indices are encoded in the expansion coefficients[24] (similar to the mean and standard deviation), see [149] for details, and

[24] All orders of the Sobol indices are encoded in the expansion coefficient, but here the first order indices are considered. If correlation between the wind climate uncertainties is modelled, the total Sobol indices could be considered instead.

for the Taylor expansion the first order Sobol indices may be approximated by Eq. (69).

$$S_{\bar{\boldsymbol{X}}_{w,i}} \approx \left(\frac{\frac{\partial F_g}{\partial \bar{\boldsymbol{X}}_{w,i}} \sigma_{\bar{\boldsymbol{X}}_{w,i}}}{\sigma_{\boldsymbol{Y}_F,app}} \right)^2 \tag{69}$$

Table 12 summarizes the mean and standard deviations of the Sobol indices across all available sites, assuming 'medium' wind climate uncertainties. This shows that turbulence is by far the most dominant parameter on average; except for the blades where shear and the wind speed parameters are also significant. This is not surprising and reflects the results in Chapter 2. Another important observation is that both $\boldsymbol{X}_\rho$ and $\boldsymbol{X}_\varphi$ are insignificant at real sites, thereby indicating that both can be omitted. In turn, this reduces N_{eval} to six for the Taylor expansion which is a factor of ~10 lower compared to PCE and a factor of ~2000 compared to the MC simulation. Moreover, it also strongly suggests that the recommended simplifications for air density (marginal distribution) and flow inclination (fixed value) will have negligible effect on probabilistic site assessment of wind turbines. This conclusion is confirmed by calculating the first order Sobol sensitivity indices for design class 2B as shown in Table 13 (the results are representative for all design classes).

Comparing the Sobol indices across sites with those obtained for the design classes yields an interesting result; namely that $S_{\boldsymbol{X}_{\sigma,\sigma_U}}$ changes from being neglectable to having the second highest impact, respectively. This indicates that the turbulence standard deviation of the lognormal NTM in the third edition of the IEC standard is too low compared to real sites, and in turn the turbulence mean value is too extreme in order to compensate for this (to keep the characteristic 90% quantile representative). Since turbulence is the most important parameter when assessing $\boldsymbol{X}_{exp}$, it is necessary to have a closer look at the NTM.

Table 12: Sobol indices across all available sites.

Component	Statistic	$S_{\boldsymbol{X}_A}$	$S_{\boldsymbol{X}_k}$	$S_{\boldsymbol{X}_{\mu,\sigma_U}}$	$S_{\boldsymbol{X}_{\sigma,\sigma_U}}$	$S_{\boldsymbol{X}_\alpha}$	$S_{\boldsymbol{X}_\rho}$	$S_{\boldsymbol{X}_\varphi}$
Tower [-]	Mean	0.07	0.00	0.66	0.25	0.00	0.01	0.01
	Std.	0.06	0.00	0.10	0.13	0.00	0.00	0.00
Drivetrain [-]	Mean	0.08	0.00	0.48	0.43	0.00	0.00	0.01
	Std.	0.06	0.00	0.20	0.23	0.00	0.00	0.01
Blades [-]	Mean	0.23	0.04	0.27	0.23	0.20	0.01	0.02
	Std.	0.11	0.03	0.15	0.25	0.14	0.00	0.01

Table 13: Sobol indices for design class 2B.

Component	S_{X_A}	S_{X_k}	$S_{X_{\mu,\sigma_U}}$	$S_{X_{\sigma,\sigma_U}}$	S_{X_α}	S_{X_ρ}	S_{X_φ}
Tower [-]	0.02	0.00	0.97	0.00	0.00	0.00	0.01
Drivetrain [-]	0.01	0.00	0.98	0.01	0.00	0.00	0.00
Blades [-]	0.08	0.02	0.70	0.00	0.17	0.01	0.01

3.4. THE NORMAL TURBULENCE MODEL

So far, the lognormal NTM (denoted L-NTM in this section) [21] has been considered, but as shown it may underestimate the turbulence distribution standard deviation compared to real sites. This has been addressed by the new Weibull NTM (denoted W-NTM in this section) [22] as illustrated in Figure 19 for design class 2B. The 90% quantile of turbulence ($\sigma_{U,90\%}$) is also specified in the figure to emphasize that it is unchanged, given that Eq. (70) is recommended in both the third and fourth editions of the IEC standard [21], [22]. Thus, it has no influence on the deterministic *load index* which turbulence model is considered for the IEC design climates.

$$\sigma_{U,90\%,IEC} = I_{ref}(0.14U + 5.6m/s) \tag{70}$$

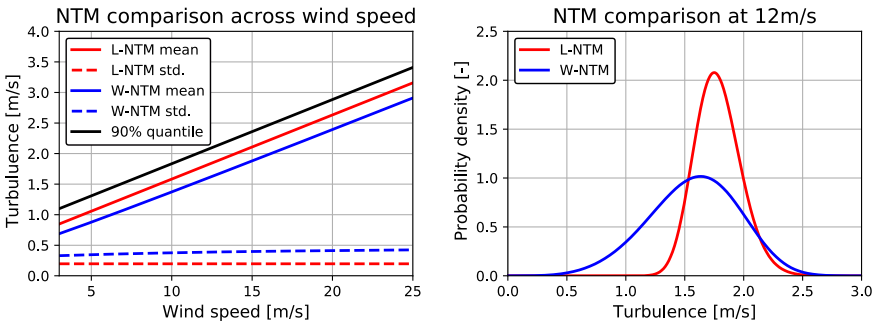

Figure 19: Comparison of the L-NTM and W-NTM. Notice that the W-NTM has a significantly higher probability mass at lower turbulence compared to the L-NTM (shown here at 12m/s but this is general across wind speeds).

3.4.1. COMPARISON AND A RECOMMENDATION

To compare the W-NTM and the L-NTM, the Sobol sensitivity indices have been recalculated for design class 2B. The results are summarised in Table 14, where the importance of $S_{X_{\sigma,\sigma_U}}$ has increased, thereby implying that the W-NTM provides a better representation of real sites in probabilistic design of wind turbines.

Table 14: Sobol indices for design class 2B when W-NTM is considered.

Component	S_{X_A}	S_{X_A}	$S_{X_{\mu,\sigma_U}}$	$S_{X_{\sigma,\sigma_U}}$	S_{X_α}	S_{X_ρ}	S_{X_φ}
Tower [-]	0.03	0.00	0.91	0.05	0.00	0.00	0.01
Drivetrain [-]	0.01	0.00	0.90	0.09	0.00	0.00	0.00
Blades [-]	0.09	0.02	0.62	0.05	0.20	0.01	0.01

Looking at Figure 19, and given the importance of turbulence, it is expected that the effect of using the W-NTM will have a significant impact on the total reliability index. In general, it may be expected that μ_{Y_F} will be lower for the W-NTM as more probability mass occurs at lower turbulence (see also Figure 9). This has been quantified in Table 15 where the design parameter (z_L) is calibrated to meet the target reliability for each component using the L-NTM. Subsequently, z_L is used together with the W-LTM which, as shown, increases the reliability index across all three components (the numbers are representative for all design classes). A direct implication of this result is that manufacturers who use the L-NTM in probabilistic design will end up with more expensive (heavier) design class turbines on average, compared to manufacturers who use the W-NTM[25]. It is thus expected that the W-NTM will be adopted by the industry for probabilistic design of wind turbines. Consequently, it is also recommended to use it to assess the *beta index* to avoid non-conservative site assessments[26].

Table 15: Comparison of reliability indices for the L-NTM and W-NTM.

Design class	NTM	Design parameter	Reliability index		
			Tower [-]	Drivetrain [-]	Blades [-]
2B	Lognormal	z_L	3.30	3.30	3.30
	Weibull	z_L	3.58	3.48	3.40

3.4.2. TURBULENCE DISTRIBUTION AT REAL SITES

A reasonable question arises as to whether turbulence at real sites is lognormal or Weibull distributed. Previous literature has most often considered a lognormal

[25] It is outside the scope of this thesis (and also outside of this author's knowledge) whether this is actually intended by the IEC committee.

[26] If the L-NTM is considered, $z_{min,IEC}$ increases compared to the W-NTM which increases $\beta_{ln,site}$. In turn, I_β decreases which leads to non-conservative decisions.

distribution and the motivation for this seems to be the NTM. So, it is likely that a Weibull distribution will become the 'standard assumption', also for real sites, in probabilistic design of wind turbines. However, the turbulence distribution may significantly influence the structural reliability, and it is therefore critical that it reflects real data to provide accurate estimations of F_g.

Out of the 99 sites made available for this project, three sites included a measurement campaign of five years or longer. At these sites, all turbulence data from the predominant sector has been considered, and the Kolmogorov-Smirnoff (KS) statistic has been calculated at each wind speed bin with 100 data points or more. Figure 20 shows the result of this analysis. Both distributions seem to be 'better' depending on the wind speed considered. The Weibull assumption is preferred at low to medium wind speeds while the lognormal assumption is superior at medium to high wind speeds (the Cramér-Von Mises statistic also supports this). This result indicates that one of two things needs to be considered to fully capture turbulence at real sites in probabilistic design: either a more flexible distribution should be applied to capture all wind speeds or the turbulence distribution family should be conditioned on atmospheric stability. However, both options will add complexity and thus require more data than typically available. A simplified approach could be to condition the turbulence distribution family on wind speed instead of atmospheric stability – e.g. by using a Weibull distribution below some predetermined fixed wind speed and a lognormal distribution above. However, this topic is not covered further in this thesis as more data is needed to derive a general recommendation. Until a better model is developed, it seems appropriate to consider both distributions for probabilistic design as they are equally good (or equally bad).

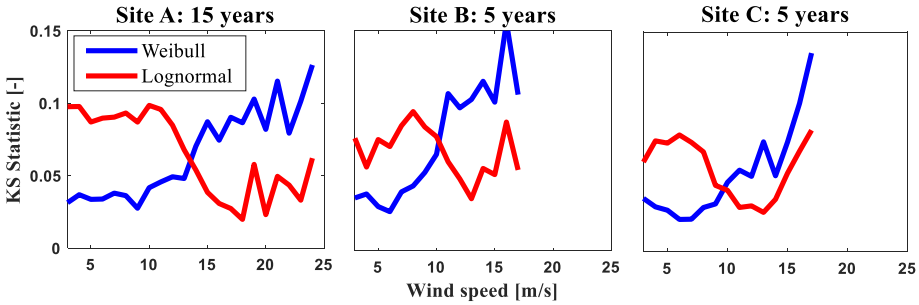

Figure 20: Comparison of a lognormal and a Weibull distribution to model turbulence at real sites based on multiple years of data. Only wind speed bins with at least 100 data points are considered.

3.4.3. CHARACTERISTIC TURBULENCE APPROXIMATION

A typical approach to assess the characteristic 90% quantile of turbulence at real sites is to assume a normal distribution, see Eq. (71)[27].

$$\sigma_{U,c} \approx \mu_{\sigma_U} + 1.28\sigma_{\sigma_U} \tag{71}$$

The error associated to this assumption, quantified by ϵ_{σ_U} in Eq. (72), depends on the underlying 'real' distribution. For both a Weibull and lognormal distribution, ϵ_{σ_U} can be calculated as a function of the turbulence distribution coefficient of variation (CV_σ), as shown in Figure 21. The result indicates that Eq. (71) is a reasonable simplification in a deterministic code-based design approach, unaffected by whether a Weibull or lognormal distribution is assumed.

$$\epsilon_{\sigma_U} = \frac{\sigma_{U,c}}{\sigma_{U,90\%,site}} \tag{72}$$

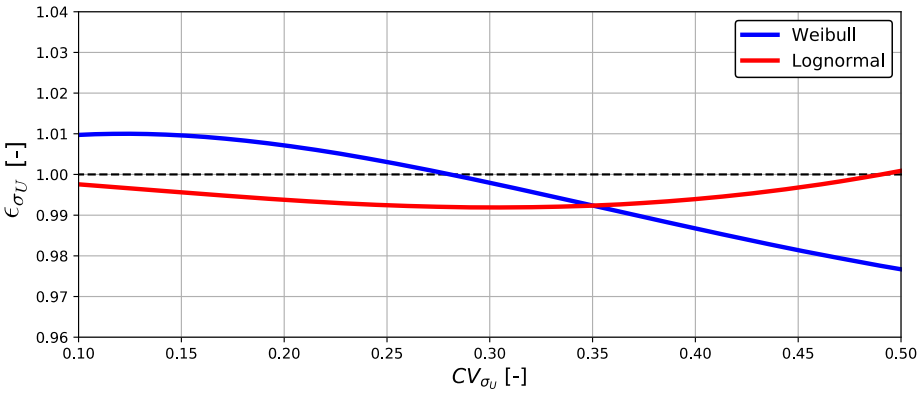

Figure 21: Error associated to assuming a normal distribution when estimating the characteristic turbulence quantified for a Weibull and a lognormal distribution.

3.5. SUMMARY AND COMPARISON TO THE LOAD INDEX

By comparing site-specific reliability indices with the target specified in the fourth edition of the IEC standard [22], the *beta index* provides a sound basis for the next generation of probabilistic decision support using specific turbines or RWTs. The developed framework to integrate fatigue loads and propagate uncertainties ensures that the index can be calculated in practice, once a surrogate model has been trained.

[27] The IEC standard recommends this assumption. In the fourth edition, it is explicitly stated that is an approximation.

A direct benefit of the developed framework is that sensitivity indices (both Sobol indices and reliability sensitivity indices) may be obtained analytically with no additional computational cost. In turn, these sensitivities form the basis for rational decision-making by enabling engineers to recognise and improve the uncertainties that matter the most.

3.5.1. COMPARISON OF THE LOAD INDEX AND THE BETA INDEX

Compared to the deterministic *load index* it is expensive, and requires more data, to conduct site-suitability assessment by probabilistic methods. However, by accounting explicitly for wind climate uncertainties, the assessment also becomes more accurate, and wind farm owners who invest in their measurement campaigns are directly rewarded. This is demonstrated by the results in Table 16, in which the deterministic and probabilistic decision support metrics are compared. Here it is assumed that the design class 2B wind climate [22] is measured exactly at three sites: one using top notch and well-calibrated equipment ('low' wind climate uncertainty), one using average equipment ('medium' wind climate uncertainty) and the last representing a short-term campaign using outdated equipment ('high' wind climate uncertainty). This shows that it is important to consider probabilistic decision support to validate structural integrity of turbines placed in environments close to their limit. A recommended approach is, therefore, to use the *load index* as a constraint in initial layout optimization when the turbine positions are repositioned frequently. Once an optimal layout is decided, the *beta index* can be calculated for the turbines closest to their design limit. If the *beta index* exceeds 1.0 this suggests that investments in better data are required, and the Sobol sensitivities may identify on which particular climate parameters to focus. This route of including loads in the initial stages of wind farm planning may potentially alleviate wind farm owners of unnecessary curtailment and thereby increase the benefit of each turbine in a park configuration.

Table 16: Comparison of the *load index* and the *beta index*.

Site-suitability assessment method	**Component**	**Wind climate uncertainty**		
		Low	Medium	High
Probabilistic, I_β [-]	Tower	0.97	1.0	1.09
	Drivetrain	0.98	1.0	1.06
	Blades	0.98	1.0	1.05
Deterministic, I_F [-]	Tower		1.0	
	Drivetrain			
	Blades			

3.5.2. A BRIEF OUTLOOK TO LIFETIME EXTENSION

Finally, to close this chapter a brief outlook to lifetime extension decision support is provided. Consider first the case where uncertainties are not taken into account. Through some manipulation of the design equation in Eq. (7) it can be shown that the useful fatigue life time (T_{fat}) can be obtained by Eq. (73), where I_F^{-m} can be interpreted as a 'fatigue lifetime factor'.

$$T_{fat} = T_L I_F^{-m} \tag{73}$$

I_F^{-m} is demonstrated in Figure 22 to emphasize the significant effect of raising to the power of m. Hence, the predicted lifetime should be interpreted with this in mind.

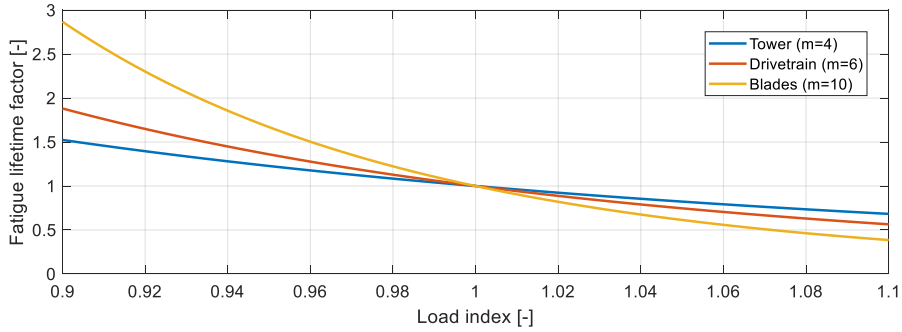

Figure 22: Fatigue lifetime predicted by the load index for the tower, drivetrain and blades.

Consider now the case where the *load index* 1.0 but uncertainties are taken into account, and recall that the limit state equation, and in turn the reliability index, is defined as function of time. Since the LSE can be evaluated analytically it involves no computational cost, nor engineering effort, to calculate the fatigue lifetime of the turbine as outlined in Eq. (74).

$$\Delta\beta_{ln,site}\left(z_{min,IEC}, t_{use}, F_{g,site}, \sigma_{\mathbf{X}_{exp},site}\right) = \Delta\beta_t = 3.3 \tag{74}$$

This is demonstrated in Figure 23 where $\Delta\beta_{ln,site}$ is plotted as function of time for the tower using the same example as considered in Table 16. The useful lifetime of the turbine in terms of Miner's sum can then simply be checked as the intersection with the target reliability index (marked by crosses).

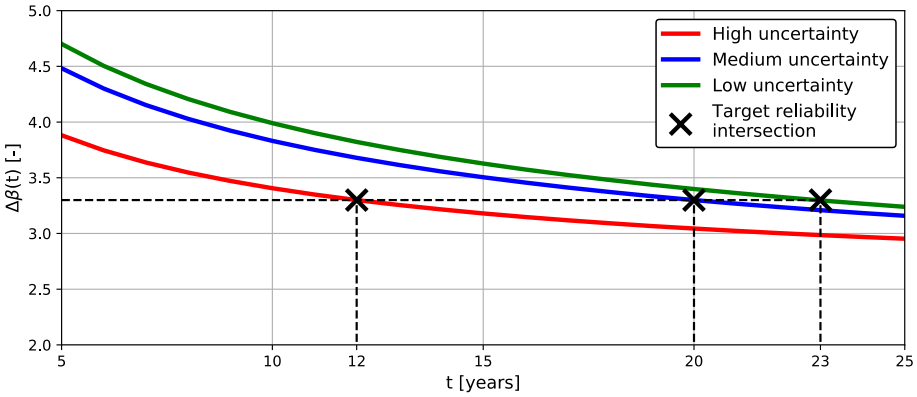

Figure 23: Probabilistic fatigue lifetime analysis of a wind turbine tower by checking the time when the structural reliability intersects the target reliability (marked with crosses).

Before closing this topic, and thereby also this thesis, it is remarked that lifetime extension has other aspects and requirements than estimating T_{fat} (which is somewhat 'theoretical'). In practice, the decision to lifetime extend relies on a set of legal, technical and economic factors. For a recent, and very well written, overview of state-of-the-art of lifetime extension this author refers to [59].

CHAPTER 4. CONCLUSIONS

This thesis has presented two frameworks for site-suitability assessment with reference to fatigue loads during normal operation. The first framework, characterised by the deterministic '*load index'*, aims to supply fast and accurate decision support in early wind farm planning. The second framework, characterised by the probabilistic '*beta index*', constitutes the foundation for the next generation of reliability-based decision support in practice. Both frameworks can be calculated by specific or reference wind turbines and are tailored to provide accurate results when surrogate models are considered. To improve deterministic site-suitability decisions, the wind climate simplifications adopted by the IEC 61400-1 design standard were analysed using wind data from 99 real sites. The main findings are published in Papers 1 and 2 in which the following main conclusions are drawn:

- To improve consistency of blade fatigue load assessments, it is proposed to model wind shear by a 60% quantile conditioned on wind speed and direction.
- The effective turbulence approximation is conservative and over-predicts fatigue loads by 1-4% on average compared to full sector-wise simulations.
- Neglecting the influence of direction on fatigue damage accumulation in steel towers leads to over-predictions of fatigue loads by 14% on average.

Paper 3 presents a simplified method accounting for direction to reduce steel consumption of towers. The method is developed directly within the DEL framework, thereby preventing added post-processing of aeroelastic simulations in the time-domain.

The elementary procedures to calculating the probabilistic *beta index* are published in Paper 4 in which two main conclusions are highlighted:

- Kriging (interpolation) is more accurate than polynomial chaos expansion (regression) when predicting lifetime fatigue loads in a reliability assessment.
- The model uncertainty of Kriging is negligible, but to avoid bias at least 400 DEL samples are needed in the experimental design, using 75 seeds to estimate each.

A highly accurate Kriging model was used in this thesis to propagate wind climate uncertainties to fatigue loads and calculate sensitivities. This revealed that wind climate uncertainties are important in reliability assessments, but they are not dominant compared to uncertainties on material fatigue strength and stress analysis. Using the developed probabilistic framework, the influence of the Weibull NTM was studied and compared to the lognormal NTM. An interesting and important conclusion is that:

- The Weibull NTM results in lighter turbines on average than the lognormal NTM for probabilistic design of wind turbines.

Several important factors for fatigue assessment of onshore wind turbines were not covered in detail here, and some of the presented results request further research. The 'Frandsen wake added turbulence model' was considered throughout all wake calculations; however, it is recommended that the DWM model is implemented in future decision support tools. This requires further simplification of the DWM model to reduce its computational time in practice.

In order to reduce computational effort when estimating the *beta index*, a first order Taylor expansion is proposed to propagate uncertainties from wind climate to loads. It shows accurate results but may be significantly influenced by the assumption made in this thesis that the wind climate uncertainties are uncorrelated. Therefore, it is necessary to analyse and quantify the correlation between the wind climate uncertainties and to study its effect on the total uncertainty on fatigue loads. In particular, it is important to establish the correlation between the dominant uncertainties on the turbulence distribution parameters.

This thesis tried to find evidence that a Weibull distribution provides a better fit to turbulence data than a lognormal distribution at real sites. However, no clear conclusion could be drawn, but it seems to depend on atmospheric stability which distribution is 'better'. It is thus recommended to investigate this matter further in order to provide a simple approach to accurately capture turbulence distributions at real sites in probabilistic design.

Finally, the 5MW RWT by NREL was used in this thesis. Other wind turbine design configurations should be considered in the future to evaluate if the results presented cover the full diversity of modern commercial wind turbines. To provide an important step in that direction, Paper 5 presents a fully consistent conversion of the 5MW reference wind turbine from gearbox to direct drive. The developed turbine is public and intended for comparative studies between the two drivetrain configurations from a structural response point of view.

REFERENCES

[1] W. J. Savitch, *Pascal, an introduction to the art and science of programming*. Benjamin/Cummings Pub. Co, 1984.

[2] J. Blyth, “On the application of wind power to the generation and storage of electricity,” *Proc. Philos. Soc. Glas.*, pp. 1–2, 1888.

[3] “Mr. Brush’s Windmill Dynamo,” *Sci. Am.*, vol. 63, no. 25, pp. 389–389, 1890.

[4] H. C. Hansen, *Poul la Cour - Grundtvigianer, opfinder og folkeoplyser*. Samfundslitteratur, 1985.

[5] H. B. Mortensen, “The Valuation History of Dansih Wind Power. PhD Thesis,” Aalborg University, 2018.

[6] The American Wind Energy Association, “History of AWEA.” [Online]. Available:https://www.awea.org/wind-101/history-of-wind/1970s. [Accessed: 13-Jul-2019].

[7] The European Wind Energy Association, “History of EWEA.” [Online]. Available: http://www.ewea.org/history/. [Accessed: 13-Jul-2019].

[8] T. Burton, D. Sharpe, N. Jenkins, and E. Bossanyi, *WIND ENERGY HANDBOOK*. West Sussex, PO19 UD, England: John Wiley & Sons, Ltd, 2001.

[9] P. Jamieson, *Innovation in Wind Turbine Design*, 2nd ed. West Sussex, PO19 8SQ, UK For: John Wiley & Sons Ltd, 2018.

[10] L. Liu, Y. Guo, H. Zhao, and Y. Tang, “Motions of a 5 MW floating VAWT evaluated by numerical simulations and model tests,” *Ocean Eng.*, vol. 144, pp. 21–34, 2017, doi:10.1016/j.oceaneng.2017.08.004.

[11] I. Yahyaoui and A. S. Cantero, *Modeling and Characterization of a Wind Turbine Emulator*. Elsevier Inc., 2018.

[12] UNFCCC, “Paris Agreement - Status of Ratification.” [Online]. Available: https://unfccc.int/process/the-paris-agreement/status-of-ratification [Accessed 2019-06-18]. [Accessed: 05-Jun-2019].

[13] European Comission, “EU climate action,” 2019. [Online]. Available: https://ec.europa.eu/clima/citizens/eu_en [Accessed 2019-06-18]. [Accessed:

05-Jun-2019].

[14] I. Komusanac, D. Fraile, and G. Brindley, “Wind energy in Europe in 2018 - Trends and statistics,” 2019.

[15] Danish Energy Agency, “Denmark’s Energy and Climate Outlook 2018,” 2018.

[16] C. Kost, S. Shammugam, V. Jülch, H.-T. Nguyen, and T. Schlegl, “Levelized Cost of Electricity Renewable Energy Technologies,” Freiburg, 2018.

[17] IRENA, “Renewable Power Generation Costs in 2018,” Abu Dhabi, 2019.

[18] E. Kondili and J. K. Kaldellis, “Environmental-Social Benefits/Impacts of Wind Power,” in *Comprehensive Renewable Energy*, vol. 2, Elsevier Ltd., 2012, pp. 503–540.

[19] W. Hu, K. K. Choi, and H. Cho, “Reliability-based design optimization of wind turbine blades for fatigue life under dynamic wind load uncertainty,” *Struct. Multidiscip. Optim.*, vol. 54, no. 4, pp. 953–970, Oct. 2016, doi:10.1007/s00158-016-1462-x.

[20] D. Veldkamp, “Chances in Wind Energy. PhD Thesis,” Delft University, 2006.

[21] IEC., “International Standard IEC 61400-1 ed. 3, ‘Wind Turbines - Part 1 Design Requirements’.” 2010.

[22] IEC., “International Standard IEC 61400-1 ed. 4, ‘Wind Turbines - Part 1 Design Requirements’.” 2019.

[23] S. T. Frandsen, *Turbulence and turbulence- generated structural loading in wind turbine clusters.*, vol. R-1188, no. January. Technical University of Denmark, 2007.

[24] DNVGL-ST-0262, “DNV GL. Lifetime extension of wind turbines.” 2016.

[25] UL-4143, “UL. Outline of investigation for wind turbine generator life time extension (LTE).” 2016.

[26] ISO., “International Standard ISO 2394:2015, ‘General principles on reliability for structures.’” 2015.

[27] H. Glauert, “Airplane Propellers,” in *Aerodynamic Theory*, Berlin,

Heidelberg: Springer Berlin Heidelberg, 1935, pp. 169–360.

[28] L. Prandtl and A. Betz, *Vier Abhandlungen zur Hydrodynamik und Aerodynamik*. Göttingen: Göttinger Nachr, 1927.

[29] J. N. Sørensen, "Blade-Element/Momentum Theory," Springer, 2016, pp. 99–121.

[30] M. B. Ageze, Y. Hu, and H. Wu, "Wind Turbine Aeroelastic Modeling: Basics and Cutting Edge Trends," *Int. J. Aerosp. Eng.*, vol. 2017, pp. 1–15, Mar. 2017, doi:10.1155/2017/5263897.

[31] L. Wang, X. Liu, and A. Kolios, "State of the art in the aeroelasticity of wind turbine blades: Aeroelastic modelling," *Renew. Sustain. Energy Rev.*, vol. 64, pp. 195–210, 2016, doi:10.1016/j.rser.2016.06.007.

[32] F. Rasmussen *et al.*, "Present Status of Aeroelasticity of Wind Turbines," *Wind Energy*, vol. 228, pp. 213–228, 2003, doi:10.1002/we.98.

[33] P. Zhang and S. Huang, "Review of aeroelasticity for wind turbine: Current status , research focus and future perspectives," *Front. Energy*, vol. 5, no. 4, pp. 419–434, 2011, doi:10.1007/s11708-011-0166-6.

[34] P. A. Graf, G. Stewart, M. Lackner, K. Dykes, and P. Veers, "High-throughput computation and the applicability of Monte Carlo integration in fatigue load estimation of floating offshore wind turbines," *Wind Energy*, vol. 19, pp. 861–872, 2016, doi:110.1002/we.1870.

[35] H. S. Toft, L. Svenningsen, J. D. Sørensen, W. Moser, and M. L. Thøgersen, "Uncertainty in wind climate parameters and their influence on wind turbine fatigue loads," *Renew. Energy*, vol. 90, pp. 352–361, 2016, doi:10.1016/j.renene.2016.01.010.

[36] J. P. Murcia *et al.*, "Uncertainty propagation through an aeroelastic wind turbine model using polynomial surrogates," *Renew. Energy*, vol. 119, pp. 910–922, 2017, doi:10.1016/j.renene.2017.07.070.

[37] Q. Huchet, C. Mattrand, P. Beaurepaire, N. Relun, and N. Gayton, "Cost effective strategy using Kriging surrogates to compute fatigue at multiple locations of a structure: Application to offshore wind turbine certification," *MATEC Web Conf.*, vol. 165, 2018, doi:10.1051/matecconf/201816517001.

[38] D. Zwick and M. Muskulus, "Simplified fatigue load assessment in offshore wind turbine structural analysis," *Wind Energy*, vol. 19, pp. 265–278, 2016,

doi:10.1002/we.

[39] B. K. Sun, J. H. Y. Yoon, and H. L. Jun, “Reliability analysis of laterally loaded piles for an offshore wind turbine support structure using response surface methodology,” *Wind Struct.*, vol. 21, no. 6, pp. 597–607, 2015, doi:10.12989/was.2015.21.6.597.

[40] G. E. P. Box, *Empirical Model Building and Response Surfaces*, 1st ed. New York, NY: Wiley & Sons, 1987.

[41] F. Mouzakis, E. Morfiadakis, and P. Dellaportas, “Fatigue loading parameter identification of a wind turbine operating in complex terrain,” *J. Wind Eng. Ind. Aerodyn.*, vol. 82, pp. 69–88, Aug. 1999, doi:10.1016/S0167-6105(98)00211-6.

[42] H. S. Toft, L. Svenningsen, W. Moser, J. D. Sørensen, and M. L. Thøgersen, “Assessment of wind turbine structural integrity using response surface methodology,” *Eng. Struct.*, vol. 106, pp. 471–483, 2016, doi:10.1016/j.engstruct.2015.10.043.

[43] N. Dimitrov, M. Kelly, A. Vignaroli, and J. Berg, “From wind to loads: wind turbine site-specific load estimation using databases with high-fidelity load simulations,” *Wind Energy Sci.*, vol. 3, pp. 767–790, 2018, doi:10.5194/wes-2018-18.

[44] K. Müller, M. Dazer, and P. W. Cheng, “Damage Assessment of Floating Offshore Wind Turbines Using Response Surface Modeling,” *Energy Procedia*, vol. 137, pp. 119–133, 2017, doi:10.1016/j.egypro.2017.10.339.

[45] D. Malcolm, K. Lybarger, and G. Randall, “Advances in Wind Turbine Site Assessment,” *49th AIAA Aerosp. Sci. Meet. Incl. New Horizons Forum Aerosp. Expo.*, no. January, pp. 2–7, Jan. 2011, doi:10.2514/6.2011-456.

[46] D. J. Malcolm and A. C. Hansen, “WindPACT Turbine Rotor Design Study WindPACT Turbine Rotor Design Study,” National Renewable Energy Laboratory, NREL/SR-500-32495, 2006.

[47] J. M. Jonkman, S. Butterfield, W. Musial, and G. Scott, “Definition of a 5-MW reference wind turbine for offshore system development,” National Renewable Energy Laboratory, NREL/TP-500-38060, 2009.

[48] C. Bak *et al.*, “Description of the DTU 10 MW Reference Wind Turbine,” DTU, DTU Wind Energy Report-I-009, 2013.

[49] C. Desmond, J. Murphy, L. Blonk, and W. Haans, “Description of an 8 MW reference wind turbine,” *J. Phys. Conf. Ser.*, vol. 753, 2016, doi:10.1088/1742-6596/753/9/092013.

[50] J. M. Jonkman, “Dynamics Modeling and Loads Analysis of an Offshore Floating Wind Turbine,” National Renewable Energy Laboratory, NREL/TP-500-41958, 2007.

[51] Z. An, Y. Zhang, and Z. Wang, “Reliability Copula Model for Wind Turbine Gearbox,” *J. Shanghai Jiao Tong Univ.*, vol. 20, no. 3, pp. 312–316, 2015, doi:10.1007/s12204-015-1628-5.

[52] S. Koukoura, J. Carroll, A. Mcdonald, and S. Weiss, “Wind turbine gearbox planet bearing failure prediction using vibration data,” *J. Phys. Conf. Ser.*, vol. 1104, 2018, doi:10.1088/1742-6596/1104/1/012016.

[53] M. D. Reder, E. Gonzalez, and J. J. Melero, “Wind Turbine Failures - Tackling current Problems in Failure Data Analysis,” in *Journal of Physics: Conference Series*, 2016, vol. 753.

[54] S. Sheng, “Report on Wind Turbine Subsystem Reliability - A Survey of Various Databases,” National Renewable Energy Laboratory, NREL/PR-5000-59111, 2013.

[55] J. Carroll, A. Mcdonald, I. Dinwoodie, D. Mcmillan, M. Revie, and I. Lazakis, “Availability , operation and maintenance costs of offshore wind turbines with different drive train configurations,” *Wind Energy*, vol. 20, pp. 361–378, 2017, doi:10.1002/we.

[56] L. Sethuraman, Y. Xing, Z. Gao, V. Venugopal, M. Mueller, and T. Moan, “A 5MW direct-drive generator for floating spar-buoy wind turbine: Development and analysis of a fully coupled Mechanical model,” *Proc. Inst. Mech. Eng. Part A J. Power Energy*, vol. 228, no. 7, pp. 718–741, 2014, doi:10.1177/0957650914537262.

[57] IEA, “Wind Task 37 Systems Engineering.” [Online]. Available: https://windbench.net/iea37 [Accessed 2019-06-18].

[58] J. Jonkman, “FAST An aeroelastic computer-aided engineering (CAE) tool for horizontal axis wind turbines,” 2015. [Online]. Available: https://nwtc.nrel.gov/FAST [Accessed 2019-06-18]. [Accessed: 03-Apr-2017].

[59] L. Ziegler, E. Gonzales, T. Rubert, U. Smolka, and J. J. Melero, “Lifetime

extension of onshore wind tubines: A review covering Germany, Spain, Denmark and the UK," *Renew. Sustain. Energy Rev.*, vol. 82, pp. 1261–1271, 2018, doi:10.1016/j.rser.2017.09.100.

[60] J. Mann, "Wind field simulation," *Probabilistic Eng. Mech.*, vol. 13, no. 4, pp. 269–282, 1998, doi:10.1016/S0266-8920(97)00036-2.

[61] P. S. Veers, "Three-Dimensional Wind Simulation," Sandia National Laboratories, Applied Mechanics Divison IV, SAND88-0152 UC-261, 1988.

[62] J. C. Kaimal, J. C. Wyngaard, and O. R. Coté, "Spectral characteristics of surface-layer turbulence," *Q. J. R. Meteorol. Soc.*, vol. 89, no. 418, pp. 563–589, 1972, doi:10.1002/qj.49709841707.

[63] J. Mann, "The spatial structure of neutral atmospheric surface-layer turbulence," *J. Fluid Mech.*, vol. 273, pp. 141–168, 1994, doi:10.1017/S0022112094001886.

[64] J. Højstrup, "A Statistical Data Screening Procedure," *Meas. Sci. Technol.*, vol. 4, pp. 153–157, 1993.

[65] G. C. Larsen and K. S. Hansen, "De-trending of wind speed variance based on first-order and second-order statistical moments only," *Wind Energy*, vol. 17, no. 12, pp. 1905–1924, Dec. 2014, doi:10.1002/we.1676.

[66] F. V. Brock, "A Nonlinear Filter to Remove Impulse Noise from Meteorological Data," *J. Atmos. Ocean. Technol.*, vol. 3, no. 1, pp. 51–58, Mar. 1986, doi:10.1175/1520-0426(1986)003<0051:ANFTRI>2.0.CO;2.

[67] D. Starkenburg *et al.*, "Assessment of Despiking Methods for Turbulence Data in Micrometeorology," *J. Atmos. Ocean. Technol.*, vol. 33, no. 9, pp. 2001–2013, 2016, doi:10.1175/JTECH-D-15-0154.1.

[68] A. Robertson, L. Sethuraman, J. M. Jonkman, and J. Quick, "Assessment of Wind Parameter Sensitivity on Ultimate and Fatigue Wind Turbine Loads: Preprint," National Renewable Energy Laboratory, NREL/CP-5000-70445, 2018.

[69] B. Ernst and J. R. Seume, "Investigation of Site-Specific Wind Field Parameters and Their Effect on Loads of Offshore Wind Turbines," *energies*, vol. 5, no. 10, pp. 3835–3855, 2012, doi:10.3390/en5103835.

[70] N. Dimitrov, A. Natarajan, and M. Kelly, "Model of wind shear conditional on turbulence and its impact on wind turbine loads," *Wind Energy*, vol. 18,

no. 11, pp. 1917–1931, Nov. 2015, doi:10.1002/we.1797.

[71] A. Sathe, J. Mann, T. Barlas, W. A. A. M. Bierbooms, and G. J. W. van Bussel, “Influence of atmospheric stability on wind turbine loads,” *Wind Energy*, vol. 16, no. 7, pp. 1013–1032, 2013, doi:10.1002/we.1528.

[72] H. Stensgaard Toft, L. Svenningsen, W. Moser, J. Dalsgaard Sørensen, and M. Lybech Thøgersen, “Wind Climate Parameters for Wind Turbine Fatigue Load Assessment,” *J. Sol. Energy Eng.*, vol. 138, no. 3, 2016, doi:10.1115/1.4033111.

[73] S. Wharton and J. K. Lundquist, “Assessing atmospheric stability and its impacts on rotor-disk wind characteristics at an onshore,” vol. 15, pp. 525–546, 2012, doi:10.1002/we.

[74] R. B. Stull, *An Introduction to Boundary Layer Meteorology*, 1st ed. Springer Netherlands, 1988.

[75] X. Lee, *Fundamentals of Boundary-Layer Meteorology*, 1st ed. Springer International Publishing, 2018.

[76] A. Peña, R. Floors, and S.-E. Gryning, “The Høvsøre tall wind profile experiment– a description of wind profile observations in the atmospheric boundary layer.” [Online]. Available: http://veaonline.risoe.dk/tallwind/cases/Hovsore_tall_wind_profile.pdf. [Accessed: 08-Jul-2019].

[77] M. C. Holtslag, W. A. A. M. Bierbooms, and G. J. W. van Bussel, “Estimating atmospheric stability from observations and correcting wind shear models accordingly,” *J. Phys. Conf. Ser.*, vol. 555, pp. 1–10, 2014, doi:10.1088/1742-6596/555/1/012052.

[78] K. S. Hansen, G. C. Larsen, and S. Ott, “Dependence of offshore wind turbine fatigue loads on atmospheric stratification,” *J. Phys. Conf. Ser.*, vol. 524, pp. 1–13, 2014, doi:10.1088/1742-6596/524/1/012165.

[79] M. Kelly, G. Larsen, N. K. Dimitrov, and A. Natarajan, “Probabilistic Meteorological Characterization for Turbine Loads,” *J. Phys. Conf. Ser.*, vol. 524, p. 012076, 2014, doi:10.1088/1742-6596/524/1/012076.

[80] M. C. Holtslag, W. A. A. M. Bierbooms, and G. J. W. van Bussel, “Definition of the equivalent atmospheric stability for wind turbine fatigue load assessment,” *J. Phys. Conf. Ser.*, vol. 524, pp. 1–10, Jun. 2014, doi:10.1088/1742-6596/524/1/012110.

[81] L. Svenningsen, R. M. M. Slot, and M. L. Thøgersen, “A novel method to quantify atmospheric stability,” *J. Phys. Conf. Ser.*, vol. 1102, 2018, doi:10.1088/1742-6596/1102/1/012009.

[82] C. B. Hasager, L. Rasmussen, A. Peña, L. E. Jensen, and P. Réthoré, “Wind Farm Wake: The Horns Rev Photo Case,” *energies*, vol. 6, pp. 696–716, 2013, doi:10.3390/en6020696.

[83] S. Lee, M. Churchfield, P. Moriarty, J. M. Jonkman, and J. Michalakes, “Atmospheric and wake turbulence impacts on wind turbine fatigue loading,” National Renewable Energy Laboratory, NREL/CP-5000-53567, 2012.

[84] P. Vermeulen, “An experimental analysis of wind turbine wakes,” in *Proceedings Third International Symposium on Wind Energy Systems*, 1980, pp. 431–450.

[85] P. Lissaman, “Energy effectiveness of arbitrary arrays of wind turbines,” *J. Energy*, vol. 3, no. 6, pp. 1–7, 1979.

[86] T. Göçmen, P. van der Laan, P.-E. Réthoré, A. P. Diaz, G. C. Larsen, and S. Ott, “Wind turbine wake models developed at the technical university of Denmark: A review,” *Renew. Sustain. Energy Rev.*, vol. 60, pp. 752–769, Jul. 2016, doi:10.1016/j.rser.2016.01.113.

[87] R. Mikkelsen, “Actuator disc methods applied to wind turbines. PhD Thesis,” Technical University of Denmark, DTU, 2003.

[88] N. Troldborg, “Actuator Line Modeling of Wind Turbine Wakes. PhD Thesis,” Technical University of Denmark, DTU, 2008.

[89] S. G. Voutsinas, “Vortex methods in aeronautics: how to make things work,” *Int. J. Comut. Fluid Dyn.*, vol. 20, no. 1, pp. 3–18, 2006, doi:10.1080/10618560600566059.

[90] N. Sedaghatizadeh, M. Arjomandi, R. Kelso, B. Cazzolato, and M. Ghayeshm, “Modelling of wind turbine wake using large eddy simulation,” *Renew. Energy*, vol. 115, pp. 1166–1176, 2018, doi:10.1016/j.renene.2017.09.017.

[91] A. Betz, *Introduction to the Theory of Flow Machines*, 1st ed. PERGAMON PRESS, 1966.

[92] G. C. Larsen, “A Simple Wake Calculation Procedure,” Risø National Laboratory, Risø-M-2760, 1988.

[93] G. C. Larsen, “A simple stationary semi-analytical wake model,” Risø National Laboratory, Risø-R-1713(EN), 2009.

[94] S. Frandsen *et al.*, “Analytical modelling of wind speed deficit in large offshore wind farms,” *Wind Energy*, vol. 9, no. 1–2, pp. 39–53, Jan. 2006, doi:10.1002/we.189.

[95] N. O. Jensen, “A Note on Wind Generator Interaction,” Risø National Laboratory (Internal tecnical report), 1983.

[96] P. Argyle, S. Watson, C. Mantovon, I. Jones, and M. Smith, “Modelling turbulence intensity within a large offshore wind farm,” *Wind Energy*, vol. 21, pp. 1329–1343, 2018, doi:10.1002/we.2257.

[97] H. A. Madsen, K. Thomsen, and G. C. Larsen, “A new method for prediction of detailed wake loads,” in *IEA Joint Action of Wind Turbines 16th Symposium*, 2003, pp. 171–188.

[98] G. C. Larsen, H. A. Madsen, K. Thomsen, and T. J. Larsen, “Wake Meandering: A Pragmatic Approach,” *Wind Energy*, vol. 11, pp. 377–395, 2008, doi:10.1002/we.267.

[99] H. A. Madsen, C. G. Larsen, T. J. Larsen, N. Troldborg, and R. Mikkelsen, “Calibration and Validation of the Dynamic Wake Meandering Model for Implementation in an Aeroelastic Code,” *J. Sol. Energy Eng.*, vol. 132, no. 4, pp. 1–14, 2010, doi:10.1115/1.4002555.

[100] T. J. Larsen, H. A. Madsen, G. C. Larsen, and K. S. Hansen, “Validation of the dynamic wake meander model for loads and power production in the Egmond aan Zee wind farm,” *Wind Energy*, vol. 16, no. October 2012, pp. 605–624, 2013, doi:10.1002/we.

[101] R. Keck, D. Veldkamp, H. A. Madsen, and G. C. Larsen, “Implementation of a mixing length turbulence formulation into the dynamic wake meandering model,” *J. Sol. Energy Eng.*, vol. 134, no. 2, p. 13, 2011, doi:10.1115/1.4006038.

[102] R. Keck, M. De Maré, M. Churchfield, S. Lee, G. C. Larsen, and H. A. Madsen, “Two improvements to the dynamic wake meandering model: including the effects of atmospheric shear on wake turbulence and incorporating turbulence build-up in a row of wind turbines,” *Wind Energy*, vol. 18, no. 1, pp. 111–132, 2013.

[103] R.-E. Keck, “A consistent turbulence formulation for the dynamic wake

meandering model in the atmospheric boundary layer," Technical University of Denmark, 2013.

[104] R. Keck, "Validation of the standalone implementation of the dynamic wake meandering model for power production," no. June 2014, pp. 1579–1591, 2015, doi:10.1002/we.

[105] I. Reinwardt, N. Gerke, P. Dalhoff, D. Steudel, and W. Moser, "Validation of wind turbine wake models with focus on the dynamic wake meandering model," *J. Phys. Conf. Ser.*, vol. 1037, pp. 1–11, 2018, doi:10.1088/1742-6596/1037/7/072028.

[106] R. Slot, J. Schwarte, L. Svenningsen, J. Sørensen, and M. Thøgersen, "Directional fatigue accumulation in wind turbine steel towers," *J. Phys. Conf. Ser.*, vol. 1102, no. 1, pp. 1–10, Oct. 2018, doi:10.1088/1742-6596/1102/1/012017.

[107] R. M. M. Slot, L. Svenningsen, J. D. Sørensen, and M. L. Thøgersen, "Importance of Shear in Site Assessment of Wind Turbine Fatigue Loads," *J. Sol. Energy Eng.*, vol. 140, no. 4, p. 041012, Apr. 2018, doi:10.1115/1.4039748.

[108] O. Ditlevsen and H. O. Madsen, *Structural Reliability Methods*, Internet e. 1st edition published by Wiley & Sons (1996), 2007.

[109] H. S. Toft, "Probabilistic Design of Wind Turbines," PhD thesis, Aalborg Unviersity, 2010.

[110] I. Abdallah, "Wind Energy PhD Report 2015," PhD thesis, Technical University of Denmark, 2015.

[111] H. M. Rafsanjani, "Probabilistic Modeling of Wind Turbine Drivetrain Components," PhD thesis, Aalborg University, 2016.

[112] 61400-1 IEC, "Safety Factors - IEC 61400-1 ed. 4 - background document." 2014.

[113] K. Müller and P. W. Cheng, "Application of a Monte Carlo procedure for probabilistic fatigue design of floating offshore wind turbines," *Wind Energy Sci.*, vol. 3, no. 1, pp. 149–162, Mar. 2018, doi:10.5194/wes-3-149-2018.

[114] C. Hübler, C. G. Gebhardt, and R. Rolfes, "Methodologies for fatigue assessment of offshore wind turbines considering scattering environmental conditions and the uncertainty due to finite sampling," *Wind Energy*, vol. 21,

no. 11, pp. 1092–1105, Nov. 2018, doi:10.1002/we.2216.

[115] C. Hübler *et al.*, "Validation of Improved Sampling Concepts for Offshore Wind Turbine Fatigue Design," *Energies*, vol. 12, no. 4, p. 603, Feb. 2019, doi:10.3390/en12040603.

[116] A. Morató, S. Sriramula, and N. Krishnan, "Kriging models for aero-elastic simulations and reliability analysis of offshore wind turbine support structures," *Ships Offshore Struct.*, vol. 0, no. 0, pp. 1–14, 2018, doi:10.1080/17445302.2018.1522738.

[117] R. Teixeira, A. O'Connor, M. Nogal, N. Krishnan, and J. Nichols, "Analysis of the design of experiments of offshore wind turbine fatigue reliability design with Kriging surfaces," *Procedia Struct. Integr.*, vol. 5, pp. 951–958, 2017, doi:10.1016/j.prostr.2017.07.132.

[118] J. D. Sørensen, S. Frandsen, and N. J. Tarp-Johansen, "Effective turbulence models and fatigue reliability in wind farms," *Probabilistic Eng. Mech.*, vol. 23, no. 4, pp. 531–538, Oct. 2008, doi:10.1016/j.probengmech.2008.01.009.

[119] E. de las Heras, R. Gutiérrez, E. Azagra, and J. Sørensen, "Assessment of Wind Turbine for Site-Specific Conditions Using Probabilistic Methods," *Proceedings.Ewea.Org*, vol. 2, no. February, pp. 1–10, 2013.

[120] Steve Armstrong, "Maurice Saatchi on his 'brutal simplicity of thought,'" *www.theguardian.com*, p. 1, 2010.

[121] E. Standard, "EUROPEAN STANDARD EUROPÄISCHE NORM Eurocode 3 : Design of steel structures - Part 1-9 : Fatigue," pp. 1–34, 2005.

[122] ASTM, "ASTM No. E1049-85, 'Standard Practice for Cycle Counting in Fatigue Analysis'." ASTM International, 2011.

[123] N. E. Dowling, "Fatigue failure predictions for complicated stress-strain histories," Urbana, Illinois, 1971.

[124] M. A. Miner, "Cumulative damage in fatigue," *J. Appl. Mech.*, vol. 12, pp. 159–164, 1945.

[125] H. J. Sutherland and J. F. Mandell, "Optimized Constant-Life Diagram for the Analysis of Fiberglass Composites Used in Wind Turbine Blades," *J. Sol. Energy Eng.*, vol. 127, no. 4, p. 563, 2005, doi:10.1115/1.2047589.

[126] A. Beržonskis and J. D. Sørensen, "Reliability Analysis of Fatigue Fracture

of Wind Turbine Drivetrain Components," *Energy Procedia*, vol. 94, no. January, pp. 146–154, Sep. 2016, doi:10.1016/j.egypro.2016.09.209.

[127] S. S. Henriksen, D. J. Malcolm, and J. Thomson, "Effective Turbulence in Wind Turbine Site Suitability Assessment," in *European Wind Energy Conference and Exhibition 2012, EWEC 2012. 2.*, 2012, pp. 959–966.

[128] S. T. Frandsen, "Turbulence and turbulence- generated structural loading in wind turbine clusters," Technical University of Denmark, 2007.

[129] J. W. Miles, "On Structural Fatigue Under Random Loading," *J. Aeronaut. Sci.*, vol. 21, no. 11, pp. 753–762, Nov. 1954, doi:10.2514/8.3199.

[130] I. Rychlik, "On the 'narrow-band' approximation for expected fatigue damage," *Probabilistic Eng. Mech.*, vol. 8, no. 1, pp. 1–4, Jan. 1993, doi:10.1016/0266-8920(93)90024-P.

[131] J. Jonkman and M. Buhl, "FAST User's Guide," 2005, doi:10.2172/15020796.

[132] T. J. Larsen, "How to HAWC2, the user's manual," Risø National Laboratory, Risø-R-1597(ver. 4-5)(EN), 2014.

[133] Y. Eroğlu and S. U. Seçkiner, "Wind farm layout optimization using particle filtering approach," *Renew. Energy*, vol. 58, pp. 95–107, Oct. 2013, doi:10.1016/j.renene.2013.02.019.

[134] Y. Eroğlu and S. U. Seçkiner, "Design of wind farm layout using ant colony algorithm," *Renew. Energy*, vol. 44, pp. 53–62, Aug. 2012, doi:10.1016/j.renene.2011.12.013.

[135] P. Hou, W. Hu, M. Soltani, and Z. Chen, "Optimized Placement of Wind Turbines in Large-Scale Offshore Wind Farm Using Particle Swarm Optimization Algorithm," *IEEE Trans. Sustain. Energy*, vol. 6, no. 4, pp. 1272–1282, Oct. 2015, doi:10.1109/TSTE.2015.2429912.

[136] S. A. MirHassani and A. Yarahmadi, "Wind farm layout optimization under uncertainty," *Renew. Energy*, vol. 107, pp. 288–297, Jul. 2017, doi:10.1016/j.renene.2017.01.063.

[137] L. Parada, C. Herrera, P. Flores, and V. Parada, "Wind farm layout optimization using a Gaussian-based wake model," *Renew. Energy*, vol. 107, pp. 531–541, Jul. 2017, doi:10.1016/j.renene.2017.02.017.

[138] D. Wilson *et al.*, “Evolutionary computation for wind farm layout optimization,” *Renew. Energy*, vol. 126, pp. 681–691, Oct. 2018, doi:10.1016/j.renene.2018.03.052.

[139] N. N. Taleb, *The black swan : the impact of the highly improbable*. Allen Lane, 2007.

[140] I. Abdallah, A. Natarajan, and J. D. Sørensen, “Impact of uncertainty in airfoil characteristics on wind turbine extreme loads,” *Renew. Energy*, vol. 75, pp. 283–300, Mar. 2015, doi:10.1016/j.renene.2014.10.009.

[141] H. AM and N. Lind, “An Exact and Invariant First Order Reliability Format,” *J. Eng. Mech.*, vol. 100, 1974.

[142] D. Xiu and G. E. Karniadakis, “The Wiener--Askey Polynomial Chaos for Stochastic Differential Equations,” *SIAM J. Sci. Comput.*, vol. 24, no. 2, pp. 619–644, Jan. 2002, doi:10.1137/S1064827501387826.

[143] S. Marelli and B. Sudret, “UQLab: A Framework for Uncertainty Quantification in Matlab,” in *Vulnerability, Uncertainty, and Risk*, 2014, pp. 2554–2563.

[144] B. Sudret, “Polynomial chaos expansions and stochastic finite element methods,” in *Risk and Reliability in Geotechnical Engineering*, K. K. Phoon and J. Ching, Eds. Taylor and Francis, 2015, pp. 265–300.

[145] G. Blatman and B. Sudret, “Adaptive sparse polynomial chaos expansion based on least angle regression,” *J. Comput. Phys.*, vol. 230, pp. 2345–2367, 2011, doi:10.1016/j.jcp.2010.12.021.

[146] S. Marelli and B. Sudret, “UQLab user manual - Polynomial Chaos Expansions,” Report UQLab-V1.0-105, ETH Zurich, 2017.

[147] T. V Anderson, “Efficient, Accurate, and Non-Gaussian Error Propagation Through Nonlinear, Closed-Form, Analytical System Models,” Master’s thesis, Brigham Young University, 2011.

[148] I. M. Sobol’, “Sensitivity Estimates for Nonlinear Mathematical Models,” *Math. Model. Comput. Exp.*, vol. 1, pp. 407–414, 1993.

[149] B. Sudret, “Global sensitivity analysis using polynomial chaos expansions,” *Reliab. Eng. Syst. Saf.*, vol. 93, no. 7, pp. 964–979, Jul. 2008, doi:10.1016/j.ress.2007.04.002.

SCIENTIFIC PAPERS

- **Paper 1:** R. M. M. Slot, L. Svenningsen, J. D. Sørensen, and M. L. Thøgersen, "Importance of Shear in Site Assessment of Wind Turbine Fatigue Loads," *J. Sol. Energy Eng.*, vol. 140, no. 4, p. 041012, 2018, doi:10.1115/1.4039748.
  Original publisher: ASME Publishing. Reprinted by permission.

- **Paper 2:** R. M. M. Slot, J. D. Sørensen, L. Svenningsen, W. Moser, and M. L. Thøgersen, "Effective Turbulence and its Implications in Wind Turbine Fatigue Assessment," *Submitted to: Wind Energy (Accepted for publication)*.
  Original publisher: John Wiley & Sons Ltd. Reprinted by permission.

- **Paper 3:** R. Slot, J. Schwarte, L. Svenningsen, J. Sørensen, and M. Thøgersen, "Directional fatigue accumulation in wind turbine steel towers," *J. Phys. Conf. Ser.*, vol. 1102, no. 1, 2018, doi:10.1088/1742-6596/1102/1/012017.
  Original publisher: IOP Publishing. Open access under the terms of the Creative Commons Attribution 3.0 licence.

- **Paper 4:** René M. M. Slot, J. D. Sørensen, B. Sudret, L. Svenningsen, and M. L. Thøgersen, "Surrogate Model Uncertainty in Wind Turbine Reliability Assessment," *Submitted to: Renewable Energy (Under peer-review)*.
  Reprinted here by permission from Elsevier.

- **Paper 5:** René M. M. Slot, L. Svenningsen, J. D. Sørensen, and M. L. Thøgersen, "Consistent direct-drive version of the NREL 5MW turbine," *Proceeding to WindEurope 2018*.
  Open access under the terms of the Creative Commons Attribution 3.0 licence.

Importance of Shear in Site Assessment of Wind Turbine Fatigue Loads

René M. M. Slot
Department of Civil Engineering,
Aalborg University,
Aalborg 9220, Denmark;
EMD International,
Aalborg 9220, Denmark
e-mail: rmms@civil.aau.dk

Lasse Svenningsen
EMD International,
Aalborg 9220, Denmark

John D. Sørensen
Department of Civil Engineering,
Aalborg University,
Aalborg 9220, Denmark

Morten L. Thøgersen
EMD International,
Aalborg 9220, Denmark

Wind turbines are subjected to fatigue loading during their entire lifetime due to the fluctuating excitation from the wind. To predict the fatigue damage, the design standard IEC 61400-1 describes how to parametrize an on-site specific wind climate using the wind speed, turbulence, wind shear, air density, and flow inclination. In this framework, shear is currently modeled by its mean value, accounting for neither its natural variance nor its wind speed dependence. This very simple model may lead to inaccurate fatigue assessment of wind turbine components, whose structural response is nonlinear with shear. Here we show how this is the case for flapwise bending of blades, where the current shear model leads to inaccurate and in worst case nonconservative fatigue assessments. Based on an optimization study, we suggest modeling shear as a wind speed dependent 60% quantile. Using measurements from almost one hundred sites, we document that the suggested model leads to accurate and consistent fatigue assessments of wind turbine blades, without compromising other main components such as the tower and the shaft. The proposed shear model is intended as a replacement to the mean shear, and should be used alongside the current IEC models for the remaining climate parameters. Given the large number of investigated sites, a basis for evaluating the uncertainty related to using a simplified statistical wind climate is provided. This can be used in further research when assessing the structural reliability of wind turbines by a probabilistic or semiprobabilistic approach. [DOI: 10.1115/1.4039748]

Keywords: wind turbine loads, fatigue loads, wind shear

1 Introduction

Modern onshore wind turbines are typically designed to operate for at least 20 years according to the design standard IEC 61400-1 [1]. For a prospect site, it is therefore important to verify that the fatigue life of the wind turbine either equals or exceeds this design lifetime, also referred to as fulfilling the fatigue limit state. For this purpose, the IEC standard describes how to parametrize a site specific wind climate used for fatigue load calculations during normal operation of the turbine (design load case 1.2 (DLC 1.2)) based on the following statistics:

- Mean wind speed distribution (V) (Weibull distributed).
- Wind speed standard deviation (σ) (wind speed dependent 90% quantile).
- Vertical wind speed variation (α) (mean value).
- Air density (ρ) (average value).
- Flow inclination (φ) (maximum value).

Each of these parameters, except air density, is estimated for directional sectors (θ) of 30 deg or less, taking into account that the surrounding terrain and general wind conditions may vary significantly depending on which way the rotor is facing.

In the statistical framework of the IEC standard, the wind speed standard deviation (i.e., *turbulence*) is modeled by a wind speed-dependent 90% quantile, which can be estimated based on the turbulence mean value (σ_μ) and standard deviation (σ_σ) by the following equation:

$$\sigma_{90}(V,\theta) = \sigma_\mu(V,\theta) + 1.28\sigma_\sigma(V,\theta) \tag{1}$$

Often, turbulence is also described by the turbulence intensity (TI), which represents the wind speed coefficient of variation as shown in the below equation:

$$\mathrm{TI} = \frac{\sigma}{V} \tag{2}$$

The vertical variation of wind speed (i.e., *wind shear*) is approximated by the power law profile defined in Eq. (3), relating the wind speeds at heights z and z_r by the wind shear exponent (α)

$$V(z) = V(z_r)\left(\frac{z}{z_r}\right)^{\alpha} \tag{3}$$

For fatigue assessment, the shear exponent is modeled by its mean value across all wind speeds ($\alpha_\mu(\theta)$) thereby neglecting its wind speed dependence as well as its natural variance, which may be inaccurate for components whose structural response varies nonlinearly with wind shear. The objective of this paper is therefore to assess the accuracy of the wind shear model used in the IEC standard, and propose an improved wind shear model for assessment of site-specific fatigue loads based on wind measurements.

The characterization of a site specific wind climate was thoroughly investigated in Ref. [2] with focus on DLC1.2, and based on three different datasets it was demonstrated that modeling the shear exponent by its mean value could lead to a nonconservative fatigue load assessment of blade root flapwise bending. Instead, Stensgaard Toft et al. [2] proposed to model the shear exponent as a wind speed-dependent 75% quantile (assumed normal distributed) to effectively account for its variation, which lead to a conservative fatigue assessment of blades, without introducing an unnecessary increase in fatigue load assessment of the tower bottom for-aft moment or the low speed shaft torque.

The effect of wind shear on wind turbine fatigue loads was also investigated in Ref. [3], illustrating its importance especially when evaluating blade root flapwise moment. In their research,

[1]Corresponding author.

Contributed by the Solar Energy Division of ASME for publication in the Journal of Solar Energy Engineering: Including Wind Energy and Building Energy Conservation. Manuscript received September 24, 2017; final manuscript received March 19, 2018; published online April 9, 2018. Assoc. Editor: Yves Gagnon.

the joint distribution of turbulence and the shear exponent was utilized to develop a simple expression of the shear exponent related to the 90% quantile of turbulence following the "Normal turbulence model" [1]. This resulted in a slight reduction of the expected fatigue damage compared to the current approach in the IEC standard for sites dominated by relatively low turbulence. In Ref. [4], the site-specific wind climate parameters were investigated partly focusing on blade root fatigue loads on offshore wind turbines. In their study, the shear exponent was obtained by two methods: first, using two anemometers and second, using multiple anemometers. In general, the latter method resulted in higher shear exponents, which in turn led to higher fatigue loads, but overall, they found turbulence to be the main contributor to fatigue loads.

Further studies on wind turbine fatigue loads were also made in Ref. [5] where the influence of atmospheric stability was investigated based on four different sites, showing that turbulence affects all wind climate sensitive structural components while the wind profile mainly affects rotor and blade loads. In Ref. [6], the effect of atmospheric stability was further investigated, suggesting an equivalent atmospheric stability to obtain accurate fatigue load assessments with the need of fewer aeroelastic simulations, compared to accounting for stability using different stability classes.

In Ref. [7], measurements at four tall masts combined with surface layer and similarity theory were used to connect wind shear to stability and turbulence intensity, in relation to wind turbine fatigue loads. Their research led to a condensed model of turbulence given wind shear, applicable for heights above the atmospheric surface layer.

In this paper, a wind shear model that accurately captures site-specific fatigue loads for onshore wind turbines in DLC 1.2 is sought. For this purpose, a wind speed-dependent quantile of the shear exponent is proposed to effectively account for its natural variation. The model assumes that the shear exponent is normal distributed, and is intended to be applied alongside the current description of the remaining site climate parameters used in the IEC standard (wind speed dependent 90% quantile of turbulence, average air density, and maximum flow inclination). To assess the accuracy of the proposed model, the fatigue damage obtained by the on-site wind climate parametrization is compared to that obtained by direct simulation of the 10 min joint time series measurements of wind speed, turbulence, and wind shear. The method is similar to that of Ref. [2], but in comparison, this work includes wind measurements from almost a hundred international sites with varying site characteristics. This setup provides a solid statistical basis, which is used in an optimization study to recommend a shear exponent quantile that results in not only a safe but also consistent assessment of fatigue damage across different sites. Furthermore, the large statistical basis is used to quantify the uncertainty related to using a statistical wind climate description, which can be used in further development of structural reliability models of wind turbines by a probabilistic or semiprobabilistic approach.

2 Wind Measurements

The basis for this study is high quality 10 min measurements of mean wind speed, turbulence, and mean wind direction from 99 meteorological masts located across the world. The sites have a wide geographical spread, see Fig. 1, and represent varying orography, with and without nearby forest, see Table 1. At all masts, measurements are recorded for at least 1 year to account for the significant seasonal variation of wind shear, e.g., reported in Ref. [8]. In addition, all masts have a top anemometer installed at a height of at least 70 m, which is assumed to represent hub height of modern turbines, and therefore no extrapolation of wind speeds is performed.

To evaluate the shear exponent at each 10 min time-step, wind speed measurements at three heights or more are arranged in a $\log(z)$–$\log(V)$ plot, and the shear exponent is determined based on linear regression using the method of least squares. The used heights depend on the instrumentation of the masts and vary between sites from 20 m up to 244 m, where the most typical heights are close to 40 m, 60 m, 80 m, and 100 m. To enable a robust analysis of rotor representative wind shear in accordance with Ref. [9], only sites with a separation between the top and bottom anemometer of at least 40 m are considered, assuming this distance covers one-third of the rotor diameter of typical modern turbines.

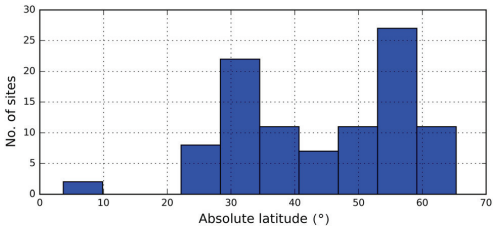

Fig. 1 Absolute latitude distribution of all considered sites

Table 1 Site characteristics of all considered sites

Number of sites with site characteristics		Orography: Flat	Hilly	Steep
Forestry	None	36	14	12
	Partly	4	2	4
	Dominant	11	7	9

For all sites, the flow inclination is unknown and information needed to calculate air density is not available in the data. To overcome this lack of information, the flow inclination has been fixed to 0.0 deg for sites with flat terrain and 8.0 deg for complex sites with hilly or steep terrain, while the air density is fixed to 1.225 kg/m^3 for all sites. This may seem like a rather crude simplification, but given the very low sensitivity between the two parameters and fatigue loads, shown in Fig. 2, it is expected to have very little influence on the results presented in this paper. To verify the expectation, approximately 30 sites have been analyzed using mesoscale modeled air density, and on an average, a relative difference of less than 1% was observed in the fatigue damage compared to using a fixed value, which is practically negligible compared to the overall uncertainty of the applied fatigue damage models described in Sec. 3.

All wind measurements included in this paper are either from wind power projects or from meteorological research masts and have therefore been available as initially screened data with a recovery rate between 75% and 100% with the most sites (>75) having a recovery rate above 90%. However, all data are available in a 10 min resolution, and the turbulence is derived based on the assumption of stationarity of the wind speed process over this interval. This is a simplification where a possibly time variant mean wind speed is replaced by its average over the considered 10 min, which is then used as basis for calculating the turbulence [10]. As the results in this paper rely on the fatigue damage calculated directly on the time series, the assumption of stationarity of the wind speed process becomes critical as it may lead to erroneous extreme values of the 10 min turbulence if the wind speed has a trend, either increasing or decreasing over the time interval. Similarly, the shear exponent is prone to noise as it accentuate errors from wind speed measurements at multiple heights, and a few erroneous extreme shear exponent values may significantly influence the fatigue damage calculations. Therefore, additional screening is needed, focusing on removing or replacing unrealistic

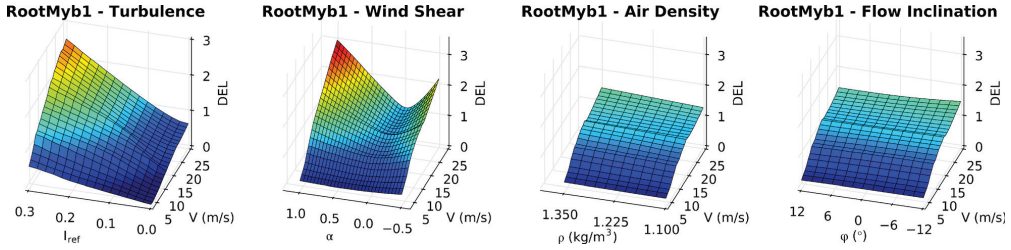

Fig. 2 Variation of damage equivalent loads for blade root flapwise bending for each wind climate parameter as function of wind speed. The loads are normalized with turbine class IIB design loads for comparison.

and erroneous extreme turbulence and shear exponent values. For this purpose, a general screening procedure has been applied to all sites, using the nonlinear median filter algorithm with threshold logic carefully outlined in Ref. [11]. This algorithm is chosen based on its superior performance in Ref. [12], where numerous despike algorithms are benchmarked based on their performance on high frequency data in micrometeorology. A detailed description of the data screening procedure is presented in the Appendix. The additional screening removes 0–12% of the measurements at each site, and the final recovery rate of the screened measurements compared to a full year is between 72% and 97%, with most sites above 85%.

3 Fatigue Load Assessment

The fatigue load calculations in this paper are based on simulations of the NREL 5.0 MW reference wind turbine with the standard collective pitch controller [13]. The turbine has a hub height of 90.0 m, a rotor diameter of 126.0 m, and cut in and cut out wind speeds at 3.0 m/s and 25.0 m/s, respectively. To determine the structural response of the reference turbine, the aeroelastic software FAST is used [14], and the wind field imposed on the rotor is generated by TurbSim [15], using the Kaimal spectrum [1]. All simulations in FAST are configured to represent normal operation of the wind turbine corresponding to DLC1.2, and the loads are evaluated at the load sensors described in Table 2.

The results from FAST are given as load time series, which are reduced by Rainflow counting to load ranges and a corresponding amount of cycles [16]. The fatigue damage is estimated by linear SN-curves using the Wöhler exponents in Table 2 and in order to combine damage from different load ranges, linear damage accumulation by Miner's rule is performed. This enables the fatigue damage to be expressed in terms of damage equivalent loads (DELs), calculated for a specific wind climate by the below equation:

$$\mathrm{DEL}\left(V_j, \sigma_j, \alpha_j, \rho_j, \varphi_j\right) = \sqrt[m]{\frac{1}{N_{\mathrm{eq}}} \sum_i n_i (\Delta F_i)^m} \tag{4}$$

In the equation, n_i represents the number of cycles with load range ΔF_i at wind climate j, m is the Wöhler exponent for the considered material, and N_{eq} is a predefined equivalent number of cycles, set to 10^7. DELs from different wind climates can be combined using Eq. (5) with w representing the relative weight of each considered wind climate, which is evaluated directly from the measurements as the amount of data with joint wind climate j over the total amount of data

$$F_{\mathrm{DEL}} = \sqrt[m]{\sum_j w\left(V_j, \sigma_j, \alpha_j, \rho_j, \varphi_j\right) \cdot \mathrm{DEL}\left(V_j, \sigma_j, \alpha_j, \rho_j, \varphi_j\right)^m} \tag{5}$$

3.1 Fatigue Load Variation With Wind Climate Parameters.

As a first step toward understanding how fatigue loads vary with each wind climate parameter, simulations are performed based on wind turbine design class IIB described in Ref. [1], varying one wind climate parameter at a time as function of wind speed, as shown for blade root flapwise bending in Fig. 2. Note that to be in compliance with how turbulence is defined for wind turbine class IIB, the reference turbulence intensity (I_{ref}) is used, which relates the turbulence and wind speed by the "Normal turbulence model." By looking along the wind speed axis in Fig. 2, it is seen that the blade root flapwise moment has a nonlinear response with wind speed, and looking along the parameter axes, it is clear that air density and flow inclination have almost no influence on the fatigue damage compared to wind shear and turbulence. The remaining sensors in Table 2 show similar sensitivity toward turbulence, air density, and flow inclination, while the response to wind shear varies significantly across the sensors, which is shown in Fig. 3. Overall, it is seen that blade root flapwise moment is affected most by wind shear compared to the other sensors. This is also expected as the magnitude of the shear exponent directly influences the distribution of wind velocities along the rotating blades, whereas the fatigue loads on the remaining sensors are influenced by the integrated thrust force across the entire rotor, which shows less harmonic variation [3]. However, it is important to note that the wind turbine used in Ref. [3] and also the one used in this study use collective pitch control. It is expected that if cyclic pitch control is considered instead, the blade root fatigue load sensitivity toward wind shear would be less pronounced [17]. The expected impact of the control strategy on the final results is discussed further in Sec. 5.

From Fig. 2, it is clear that the wind shear sensitivity in the fatigue load response of the blades for the simulated turbine is very wind speed dependent; hence, a wind shear model used for fatigue load calculations needs to reflect this observation. Therefore, two models are investigated in this paper, namely, a wind speed dependent 60% and 75% quantile of the shear exponent,

Table 2 Selected wind turbine load sensors

Sensor	Description	Wöhler exponent	Unit
RootMyb1	Blade root flapwise bending moment	10	kNm
TwrBsMyt	Tower bottom for-aft bending moment	4	kNm
YawBrMyp	Yaw bearing tilt	4	kNm
LSSGagMxa	Low speed shaft torque	6	kNm

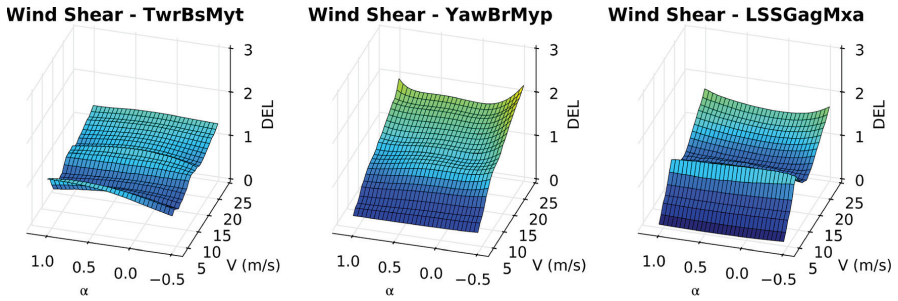

Fig. 3 Variation of damage equivalent loads for varying wind shear as function of wind speed for selected sensors in Table 2. The loads are normalized with turbine class IIB design loads for comparison.

along with the wind shear model currently used in the IEC standard for comparison.

3.2 Accuracy Assessment of Wind Shear Models. The accuracy of the fatigue damage obtained by the wind shear models is evaluated by comparison to the fatigue damage obtained by direct simulation of the 10 min measurements. This is referred to as the *fatigue damage ratio* (FDR), which is calculated following Eq. (6), where $\alpha_Q(V,\theta)$ in the numerator indicates that a wind speed-dependent quantile (Q) of the shear exponent is used and $\sigma_{90}(V,\theta)$ indicates the wind speed dependent 90% quantile of turbulence. Note that the 90% quantile of turbulence is estimated based on measurements using Eq. (1), and the shear exponent quantile is likewise estimated from measurements, assuming that it is normal distributed within each sector and wind speed bin. In the denominator, wind speed, turbulence, and the shear exponent are modeled as function of time (t) indicating that each 10 min measurement in the screened data is used to accumulate the fatigue damage requiring up to 52,560 DEL evaluations to cover an entire year. The weight of each measurement is taken relative to the total amount of samples in the screened data, and similarly, the weight of the directional wind speed bins in the numerator ($V(\theta)$) is found directly from the screened data. For example, the weight of a wind speed of 5 m/s in a given sector is found as the amount of data between 4.5 m/s and 5.5 m/s divided by the total amount of screened data. This weighting method is chosen as it ensures that the total weight used in both the numerator and denominator is equal, thereby avoiding that approximation error from fitting a Weibull distribution to the wind speeds influences the results. Finally, the air density and flow inclination are treated as constants in both the numerator and denominator, following the discussion in Sec. 2

$$\mathrm{FDR}_1 = \frac{F_{\mathrm{DEL}}(V(\theta),\sigma_{90}(V,\theta),\alpha_Q(V,\theta),\rho,\varphi)}{F_{\mathrm{DEL}}(V(t),\sigma(t),\alpha(t),\rho,\varphi)} \tag{6}$$

From the FDR, it is easily determined whether the statistical representation of the wind climate leads to underprediction of fatigue loads (FDR < 1.0), and because the FDR is a normalized measure of the accuracy, it is also directly comparable between different sites and load sensors.

The results from Eq. (6) reflect the accuracy of the overall wind climate characterization, accounting for the models used for both turbulence and wind shear. To isolate the effect of wind shear, the FDR is also calculated as outlined in Eq. (7), where the wind speed-dependent 90% quantile of turbulence is substituted into the 10 min measurements. The substitution is done by identifying the wind speed and direction at each measurement, and then replacing the actual turbulence value ($\sigma(t)$) with the 90% turbulence quantile for the corresponding speed and direction from the statistical model ($\sigma_{90}(V,\theta)$)

$$\mathrm{FDR}_2 = \frac{F_{\mathrm{DEL}}(V(\theta),\sigma_{90}(V,\theta),\alpha_Q(V,\theta),\rho,\varphi)}{F_{\mathrm{DEL}}(V(t),\sigma_{90}(V,\theta),\alpha(t),\rho,\varphi)} \tag{7}$$

Note that for both Eqs. (6) and (7), FDRs can be obtained for the IEC wind shear model by replacing $\alpha_Q(V,\theta)$ in the numerator with $\alpha_\mu(\theta)$.

The analyses are conceptually visualized in Fig. 4 in terms of the degree of wind shear and turbulence simplification, respectively, showing the proposed model along with the current wind shear and turbulence models used in the IEC standard. The figure clearly shows that FDR_2 isolates the effect of wind shear (horizontal comparison), while FDR_1 includes both the wind shear and turbulence model (diagonal comparison).

In general, the fatigue damage obtained by simulating the actual 10 min wind measurements requires up to 52,560 simulations to cover an entire year if only one seed is used to generate the turbulence. This is extremely computationally expensive, so in order to reduce the computational time considerably, the response surface methodology (RSM) described in detail in Ref. [18], and used for a similar purpose in Ref. [2], is adopted. Overall, the method uses presimulated fatigue loads to fit a regression model parametrized in the wind climate parameters. The presimulated fatigue loads are arranged in a central composite design, which enables the regression model to account for both second-order and interaction terms. To capture the higher order nonlinearity between fatigue loads and wind speeds, a response surface is established at each wind speed bin of 1 m/s, and to simulate the DELs at the design points 100 turbulence seeds are used to minimize the statistical

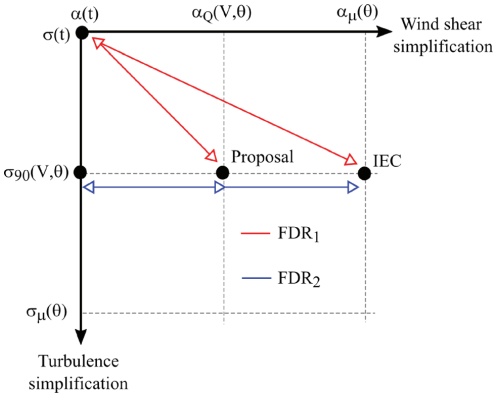

Fig. 4 Visualization of FDRs used to assess the accuracy of the wind shear models

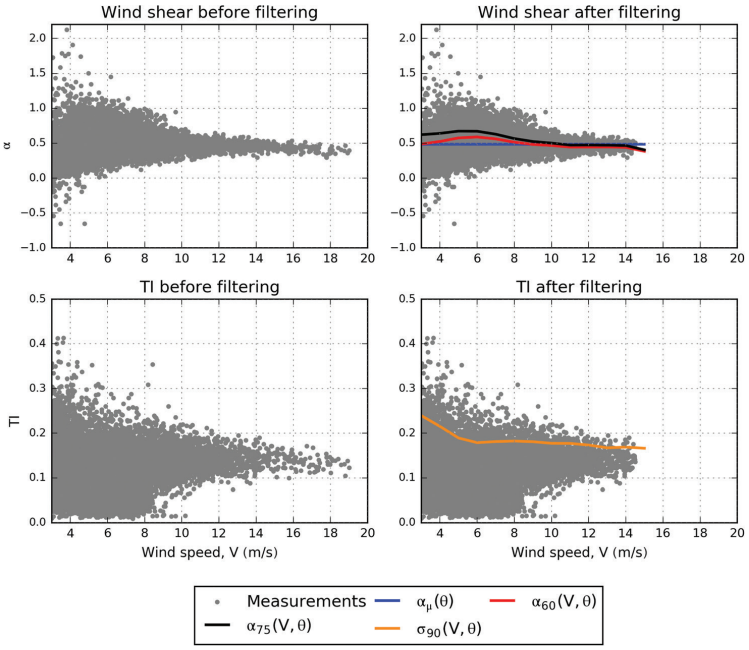

Fig. 5 Wind measurements from Karlsruhe before and after screening including statistical parameters used for the analysis

uncertainty. This results in 57,500 simulations to establish response surfaces for all wind speeds from cut in to cut out which roughly correspond to simulating DELs for an entire year at a single site. The accuracy of the RSM has been evaluated by calculating FDR values at 10% of the sites using both RSM and direct simulation in FAST. This showed an accuracy of the RSM for the investigated sensors listed in Table 2 within 2% for the blades, 4% for the tower, and 1% for the yaw bearing and the low speed shaft. It is noted that the sites used to check the accuracy represent FDRs from lowest to highest throughout the 99 investigated sites.

4 Case Study, Karlsruhe

In this section, the methodology described in Sec. 3 is applied to a case study of the 200 m tall Karlsruhe Boundary Layer Measurement Tower, located in Germany [19]. At first, the data are briefly presented and then FDRs are calculated by Eqs. (6) and (7) using wind speed-dependent 60% ($\alpha_{60}(V,\theta)$) and 75% ($\alpha_{75}(V,\theta)$) shear exponent quantiles. Finally, the FDRs are also calculated using the current IEC wind shear model ($\alpha_\mu(\theta)$) for comparison.

In total, 10 years of measurements of mean wind speed, turbulence, and wind direction at heights ranging from 2 m to 200 m were made available from the Karlsruhe Meteorological Mast for the purpose of this study. The measurements at 100 m are considered representative of wind turbine hub height, and the shear exponent is determined using wind speeds at 40 m, 50 m, 60 m, 80 m, 100 m, 130 m, and 160 m thus fully representing the rotor swept area. In the following, the first year of measurements is considered and in Fig. 5, the result of the screening procedure is shown for all data in the main wind direction along with the considered wind shear models. For the shown data, the screening procedure has a recovery rate of 94% with most of the removed data being from wind speeds above 15 m/s as those wind speed bins has less than 50 data points, which would lead to poor estimates of the turbulence and shear exponent quantiles used in the analyses.

In Table 3, FDRs for the considered wind shear models are presented, showing that the choice of wind shear model has negligible impact on the fatigue loads for this particular site since the three models obtain similar results. This is mainly because the shear

Table 3 Fatigue damage ratios based on various wind shear models

	FDR_1			FDR_2		
Load sensor	$\alpha_\mu(\theta)$	$\alpha_{60}(V,\theta)$	$\alpha_{75}(V,\theta)$	$\alpha_\mu(\theta)$	$\alpha_{60}(V,\theta)$	$\alpha_{75}(V,\theta)$
RootMyb1	1.09	1.07	1.09	1.02	1.01	1.02
TwrBsMyt	1.24	1.24	1.23	1.01	1.01	1.00
YawBrMyp	1.19	1.18	1.17	1.00	1.00	0.99
LSSGagMxa	1.15	1.15	1.15	1.01	1.01	1.00

Note: The color code used in the table is made to easily differentiate between the IEC wind shear model (blue) and the proposed models using a 60% quantile (red) and 75% quantile (black). This color code is used in the remainder of the paper.

exponent has very small variation for wind speeds above 10 m/s. However, it is important to note that using a wind speed-dependent 60% quantile in fact reduces the FDRs slightly, which is explained in Fig. 5 where the wind speed-dependent 60% quantile is lower than the mean value at higher wind speeds, as the wind speed-independent mean value is governed by the high density of measurements at lower wind speeds.

The effect of turbulence (seen as the difference between FDR_1 and FDR_2) is contrary to wind shear very pronounced and for all sensors the characteristic 90% quantile of turbulence leads to conservative results. Especially, the tower bottom for-aft moment is increased when the characteristic 90% quantile of turbulence is included with almost 25% overprediction of the DEL compared to the direct time series fatigue accumulation.

5 Wind Shear in Fatigue Damage Assessment

In this section, all available data sets are analyzed following the procedure described in the previous case study. Based on the results, an optimization study is made where shear exponent quantiles ranging from 50% to 95% are considered to make a qualified recommendation of the wind shear model which, within the framework of this paper, performs best in terms of being sufficiently conservative for all sites while in addition, and very importantly, ensuring a consistent fatigue load evaluation across the sites. Then, it is investigated whether the results are heavily influenced by including only 1 year of data at each site, thereby neglecting the year-to-year variation of the wind climate parameters, and finally, it is examined if it is necessary to make the proposed wind shear model dependent on terrain complexity and forestry.

5.1 Fatigue Damage Ratios Across All Sites. The results of analyzing all 99 sites are shown in Fig. 6, where each dot represents the FDR of a single site analyzed using either the current wind shear model in the IEC standard (blue dots), a wind speed-dependent 60% shear exponent quantile (red dots), or a wind speed-dependent 75% shear exponent quantile (black dots). In order to understand the case study results listed in Table 3 clearly, these are marked with crosses using the same color code. Note that the results for each wind shear model are ranked from lowest to highest to easily identify the sites with nonconservative assessments, and to emphasize the consistency across the sites.

Looking at Fig. 6(*a*), it is clear that blade root flapwise moment is very sensitive to wind shear, consistent with findings in previous studies [2,3], and also shown in Fig. 2. By comparing Figs. 6(*a*) and 6(*e*), it is seen that the current turbulence model increases the FDR of the blades considerably but still 17 sites obtain a FDR_1 below 1.0 when the mean value of the shear exponent is used. This can be prevented by using a wind speed-dependent 75% quantile, as proposed in Ref. [2], which raises the minimum FDR_1 to 0.99. However, the downside is that the most conservative site assessments also see an increase in FDR_1, which may lead to unnecessary material consumption. Instead, using a wind speed-dependent 60% quantile has the advantage that the upper tail of FDR_1 follows the IEC model, while the lower part of the tail is raised significantly. Still, this leaves five sites with a slightly nonconservative assessment, but within 2%, which is hardly significant as the accuracy of using RSM for blade root flapwise fatigue load assessment is also 2% as discussed in Sec. 3.

By comparing FDR_1 (Figs. 6(*a*)–6(*d*)) and FDR_2 (Figs. 6(*e*)–6(*h*)), it is observed that wind shear has a negligible effect on tower bottom moment, yaw bearing tilt, and shaft torque compared to the conservatism obtained through the turbulence model used in the IEC standard. This observation complies with the previous finding in Refs. [2] and [3] and is explained by the low sensitivity between fatigue loads on these components and wind shear, as shown in Fig. 3.

For all investigated sensors, a change in shape of the results is observed, when the turbulence model is fully accounted for by going from FDR_2 to FDR_1. Especially, the upper tail of blade root flapwise moment changes from being almost equal for the mean value and wind speed-dependent 75% quantile (Fig. 6(*e*)), to being almost equal for the mean value and the wind

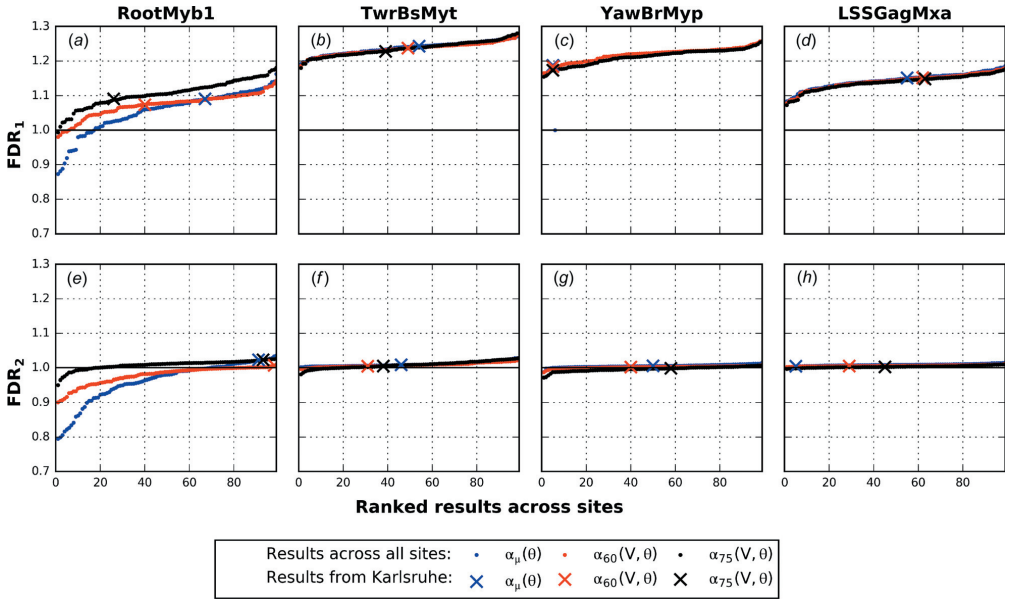

Fig. 6 Fatigue damage ratio for varying wind shear models across all studied sites. The results are ranked to emphasize the consistency in fatigue damage assessment across sites, and the results from the case study are marked with crosses.

Table 4 Descriptive statistics of FDR_1 across sites for varying wind shear models

	$\alpha_\mu(\theta)$			$\alpha_{60}(V,\theta)$			$\alpha_{75}(V,\theta)$		
Sensor	$FDR_{1,min}$	$FDR_{1,mean}$	$FDR_{1,SD}$	$FDR_{1,min.}$	$FDR_{1,mean}$	$FDR_{1,SD}$	$FDR_{1,min.}$	$FDR_{1,mean}$	$FDR_{1,SD}$
RootMyb1	0.87	1.05	0.060	0.98	1.07	0.034	0.99	1.11	0.038
TwrBsMyt	1.19	1.24	0.018	1.19	1.24	0.018	1.18	1.24	0.021
YawBrMyp	1.17	1.22	0.019	1.16	1.22	0.020	1.15	1.21	0.022
LSSGagMxa	1.08	1.14	0.021	1.08	1.14	0.021	1.07	1.14	0.021

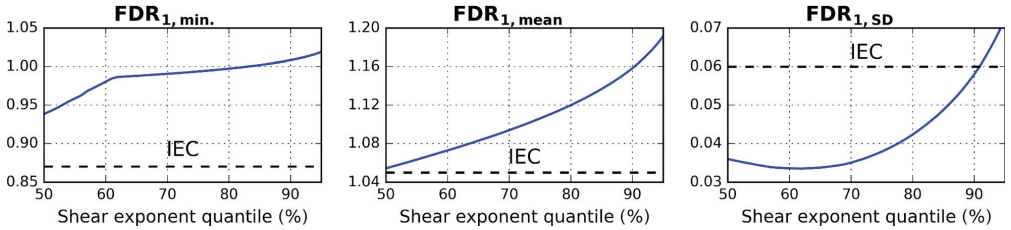

Fig. 7 Basic descriptive statistics of FDR_1 for blade root flapwise moment as function of shear exponent quantile. The results using the current IEC 61400-1 wind shear model are shown for comparison as dashed lines.

speed-dependent 60% quantile (Fig. 6(*a*)). Consequently, the recommendations in this paper are bound to the currently used turbulence model and may differ significantly if another quantile of turbulence is used instead, which could be relevant to lower the relatively high FDR_1 values obtained for all shown sensors except the blades. A possible approach of getting FDR values closer to 1.0 for the nonblade sensors could be to model the turbulence using different quantiles depending on the considered component, e.g., a 75% quantile instead of 90%. However, this is beyond the scope of this paper where the main focus is to develop an accurate and consistent wind shear model.

5.2 Optimizing Wind Shear Model. In general, an optimized wind shear model should have a minimum FDR_1 ($FDR_{1,min}$) value just above one to ensure a conservative design. At the same time, the mean value ($FDR_{1,mean}$) should be as close to one as possible to avoid unnecessary material consumption on average, and the standard deviation ($FDR_{1,SD}$) across sites should be as low as possible to obtain a consistent site-specific fatigue assessment.

In Table 4, the FDR_1 results for all considered sensors shown in Figs. 6(*a*)–6(*d*) are summarized using the mentioned descriptive statistics. Note that only blade root flapwise bending shows sensitivity to how wind shear is modeled, which is also seen in Fig. 6, and therefore only these sensors will be considered further in the optimization study.

Figure 7 illustrates the descriptive statistics of the blade root flapwise moment calculated as function of the quantile used in the proposed wind shear model, along with the IEC model for comparison. The results show that if a minimum value above 1.0 is required, a very high shear exponent quantile of approximately 85% is needed, due to the change of slope in the minimum value at the 62% quantile. Meanwhile, the mean value increases almost linearly with the used quantile up to 80%, while the standard deviation is relatively low up to the 75% quantile with minimum at 62%.

Based on these observations, it is recommended to use a 60% quantile in the proposed wind shear model as it is a reasonable compromise between optimizing all three parameters. However, the recommendation is based on the assumption that the safety factor for fatigue loads does not include bias and uncertainty related to the current wind shear model. If this is not the case, it is important to note that the recommended model will require a recalibration of the safety factors, where the mean value of the model uncertainty for blade root moment is slightly increased (from 1.05 to 1.07) while the standard deviation is greatly reduced (from 0.060 to 0.034). Finally, following the discussion on collective versus cyclic pitch control in Sec. 3, it is noted that the results in Ref. [17] indicate that utilizing individual blade pitch control reduces the sensitivity between blade root loads and wind shear by approximately 20% compared to collective pitch control (when evaluating DELs at a shear exponent of 0.2 and 0.3). However, they conclude that if a turbine with collective pitch control is deemed to exceed the IEC design conditions, then the same will also apply to a corresponding turbine that utilizes individual blade pitch control. Therefore, it is expected that the proposed model is applicable for both control strategies, even though this has not been verified by simulating a turbine with cyclic pitch control in the present study.

5.3 Year-to-Year Variation. All results presented in the preceding are calculated based on 1 year of data; hence, year-to-year variation of the 10 min mean wind speed distribution, wind shear, and turbulence is not accounted for. To investigate whether this significantly influences the FDR_1 variation of the blade root flapwise moment observed across the analyzed sites, five longer measurement campaigns are studied in further detail in this section, evaluating the year-to-year variation by treating each measured year individually.

In Fig. 8, the results of analyzing each of the 10 years of measurements available from the Karlsruhe Boundary Layer Measurement Tower are visualized. The results show some degree of variation; however, the magnitude is clearly lower than the variation seen across sites in Fig. 6(*a*), which is emphasized by using the same scale on the *y*-axis.

Similarly, the remaining four sites have been analyzed and Table 5 summarizes the year-to-year standard deviation of FDR_1 as function of each considered wind shear model, in general showing a much smaller year-to-year variation than the variation observed across sites. Another important observation of the results is that the year-to-year variation is reduced by accounting for wind speed dependence of wind shear. This generally improves

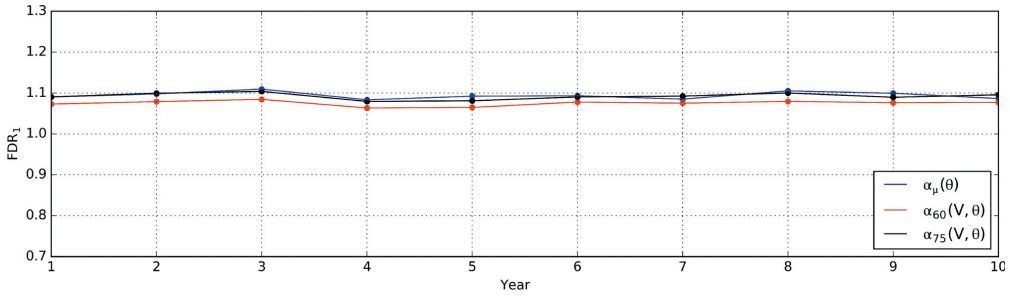

Fig. 8 FDR_1 for varying wind shear models for 10 years of measurements at Karlsruhe. The scale of the *y*-axis represents that of Fig. 6 for easy comparison.

Table 5 Year-to-year standard deviation of FDR_1 for blade root flapwise moment at five different sites with 5 years of measurements or more. Karlsruhe is marked with an asterisk.

Site	No. years	$FDR_{1,SD}(\alpha_\mu(\theta))$	$FDR_{1,SD}(\alpha_{60}(V,\theta))$	$FDR_{1,SD}(\alpha_{75}(V,\theta))$
1	16	0.016	0.008	0.011
2*	10	0.008	0.006	0.007
3	6	0.009	0.004	0.004
4	5	0.017	0.006	0.007
5	5	0.008	0.004	0.003

Table 6 Descriptive statistics of FDR_1 for blade root loads based on site characteristics

	$\alpha_\mu(\theta)$			$\alpha_{60}(V,\theta)$			$\alpha_{75}(V,\theta)$		
Sites	$FDR_{1,min.}$	$FDR_{1,mean}$	$FDR_{1,SD}$	$FDR_{1,min.}$	$FDR_{1,mean}$	$FDR_{1,SD}$	$FDR_{1,min.}$	$FDR_{1,mean}$	$FDR_{1,SD}$
All (99)	0.87	1.05	0.060	0.98	1.07	0.034	0.99	1.11	0.038
Complex (37)	0.94	1.06	0.046	0.99	1.06	0.035	0.99	1.09	0.040
Forested (48)	0.94	1.07	0.047	0.99	1.08	0.031	1.02	1.11	0.037

the accuracy and robustness of a fatigue damage assessment based on a single or few years of data, further emphasizing the potential advantage of using the proposed wind shear model for fatigue damage assessment in DLC 1.2.

5.4 Site Characteristics. The presented wind shear model is optimized using descriptive statistics across all 99 sites, without explicit consideration of the terrain complexity and forestry of the sites. This leads to a general wind shear model, which can be used for any site; however, it is important to investigate whether this is an oversimplification, i.e., if the recommended wind shear model would differ significantly if the sites are grouped by their orography and forestry. In Table 6, the result of computing the descriptive statistics for the varying site characteristics is shown, where complex terrain includes "Hilly" and "Steep" orography, and forested sites include "Partly" and "Dominant" forestry, as defined in Table 1. For easy reference, the results from analyzing all 99 sites are shown again.

Overall, the results show that it is unnecessary to increase the complexity of the recommended wind shear model by differentiation between the site characteristics. The main conclusion that a 60% wind speed-dependent shear exponent quantile leads to safer and more consistent results remains the same for both complex and forested sites. Note that the minimum value, mean value, and standard deviation found for the complex terrain and forested sites are within 0.01 compared to that obtained throughout all sites when the recommended wind shear model is used.

6 Conclusion

Wind turbine fatigue loads vary nonlinearly with wind shear during normal operation, in particular for blade root flapwise bending. This variation is not accounted for in the design standard IEC 61400-1 ed. 3 when assessing site specific fatigue loads, where the shear exponent is currently modeled by its directional mean value across all wind speeds. In this paper, the accuracy of the current wind shear model was investigated for 99 international sites based on simulations of a multimegawatt wind turbine with collective pitch control using the aeroelastic software FAST. To assess the accuracy the target fatigue load to be reached by a statistical wind climate, was calculated by direct accumulation of fatigue loads for each 10 min measurement of mean wind speed, turbulence, and wind shear using a highly accurate response surface methodology.

The results show that using the wind speed-independent mean shear exponent leads to inconsistent fatigue damage assessment of blade root flapwise moment across the analyzed sites, ranging from 13% under-prediction to 16% over-prediction compared to the target fatigue damage. Out of the 99 investigated sites, approximately one sixth showed fatigue loads lower than target when

using the IEC wind shear model, which indicates that those sites would potentially be nonconservatively assessed.

To improve the accuracy when assessing blade root flapwise fatigue loads during normal operation, it was proposed to model wind shear using a wind speed-dependent 60% quantile of the shear exponent, which can be used regardless of terrain complexity or nearby forest. This significantly improved the consistency of fatigue assessments across the investigated sites, by reducing the standard deviation of the fatigue damage ratios across the sites almost by a factor of 2 from 0.060 to 0.034. Additionally, only five sites were slightly nonconservatively assessed, with the worst case being a fatigue damage ratio of 0.98, which is hardly significant given the overall uncertainties present throughout the load evaluations. By improving the consistency in fatigue assessments across sites, the proposed wind shear model may contribute to a more consistent structural integrity of wind turbines. This may enhance decision support when determining a wind turbine size for a prospect site, while also helping manufacturers to avoid unnecessary material consumption, which overall leads to a reduction in the cost of wind energy.

As the shear exponent is most often increased by using a 60% quantile as function of wind speed compared to the current IEC model, it was shown that it does not lead to nonconservative fatigue load assessment of the yaw bearing tilt, where higher wind shear counteracts gravity loads from the rotor. In addition, the tower bottom for-aft moment and low speed shaft torque were analyzed, but these sensors showed negligible sensitivity to wind shear, compared to the high fatigue damage ratio obtained by the current turbulence model used by the IEC standard. For the tower, the fatigue damage ratios ranged from 1.19 to 1.27 and for the shaft from 1.08 to 1.19.

The results in this paper strongly suggest that it would be more accurate and therefore cost-efficient to calculate fatigue loads of onshore wind turbines during normal operation, using a wind speed-dependent 60% quantile of the shear exponent. However, it is important to note that the recommended wind shear model is very dependent on how turbulence is modeled, where the IEC standard currently use a wind speed-dependent 90% quantile. Furthermore, a change of wind shear model could have an impact on the load safety factors currently used in the IEC standard, but the information needed for a recalibration is provided in this paper, as the uncertainties related to both the current and the proposed wind shear model. Finally, all results in the present paper are based on a single multimegawatt turbine with collective pitch control, and to ensure a general applicable wind shear model more turbine designs and control strategies needs to be studied. Especially, cyclic pitch control would be important to investigate as it would change the blade fatigue load sensitivity toward wind shear.

For further research, the statistical basis, established by analyzing 99 international sites, makes it possible to include the uncertainty of using a statistical wind climate characterization in a probabilistic design approach, thereby effectively accounting for e.g., the relatively high over-prediction of tower bottom for-aft fatigue loads.

Acknowledgment

The authors of this paper wish to thank the following data providers; KNMI for providing the Cesar data, ICDC, CliSAP/KlimaCampus, University of Hamburg for providing data from the Lindenberg Boundary Layer Measurement Tower [20] and the Karlsruhe Boundary Layer Measurement Tower, DTU for granting access to data from the Høvsøre Testcenter, and last but not least Vattenfall and VENTUS INGENIERÍA for providing high quality measurements for this study. The work presented in this paper is part of the project "From wind climate to wind turbine loads—Efficient and accurate decision support and risk analysis" cofunded between Innovation Fund Denmark, AAU and EMD. Their financial support is much appreciated.

Appendix: Data Screening Procedure

This section presents a detailed description of the data screening procedure applied to all investigated sites. First a step-by-step description is given followed by a thorough explanation of each step:

(1) Exactly 1 year of data is extracted from the considered dataset.
(2) All missing data are filled with an arbitrary distinct value, in this case 1000.
(3) For all anemometers, the standard deviation of the 10 min mean wind speed measurements (σ_V) is evaluated in a 1 h moving window, removing the entire window and additionally 90 min on each side if $\sigma_V < 0.05$ m/s.
(4) All data created in step 2 is removed.
(5) All gaps in the dataset are filled by linear interpolation between the median of the nine neighboring samples on each side of the gap.
(6) Shear exponent and turbulence measurements are despiked by detecting and correcting extreme outliers in the time domain. The despike procedure follows the nonlinear median filter with threshold logic and replacement as carefully outlined in Ref. [11], using the following filter specifications:
    (6.1) Shear exponents are despiked by a fifth-order filter with a fixed bin size of 0.066 to determine the threshold logic.
    (6.2) Turbulence is despiked by a sixth-order filter with a fixed bin size of 0.025 m/s to determine the threshold logic.
(7) All data generated in step 5 are removed.
(8) The first and last measurements unable to be evaluated by the despike procedure are omitted.
(9) Measurements of shear exponents above 3.0 and measurements of turbulence intensity above 0.75 are removed.
(10) Data in 1 m/s wind speed and 30 deg sector bins with less than 50 samples are omitted.

The first step of the screening procedure is defined to reduce the seasonal bias in the final results by including exactly a 1 year measurement period. Steps 2 to 4 are designed to detect malfunction of anemometers at any height, based on the available wind speed measurements. The actual detection happens in step 3; however to be able to redetect malfunctions, which are removed in the initial screening, steps 2 and 4 are introduced. In general, this is necessary as the initial screening often overlooks the removal of bad data close to a malfunction, e.g., slow down and speed up before and after an icing event.

Step 5 is introduced to make the chosen despike algorithm robust by ensuring that measurements are always defined in the entire moving windows, except at the very beginning and end of the entire data series. The linear interpolation is based on the median of the closest samples at each side of a gap to enable detection of spikes at the vicinity of gaps.

In step 6, turbulence and shear exponents are despiked with replacement in the time domain, and afterward it is verified that no more than 1% of either of the signals is flagged as spikes, as higher detection would indicate either a bad dataset or a too sensitive filter. The filter specifications for turbulence and shear exponents have been determined based on visual inspection of the data at all sites before and after filtering, choosing the specifications that effectively capture erroneous spikes with the least over detection.

The seventh and eighth step ensure that all artificial data, and data that could not be effectively detected by the despike algorithm, are removed. Step 9 introduces absolute limits to remove unrealistic high extreme values of turbulence and shear exponents in an absolute sense, where the despike algorithm has a relative focus for a given time window and is not able to detect every single outlier throughout all studied sites. Finally, the last step ensures a sufficient statistical basis for estimating the mean and standard deviation of turbulence and the shear exponent.

Overall, the data processing procedure is calibrated to detect and correct all erroneous spikes in the data as one very bad measurement is enough to skew the results significantly, when

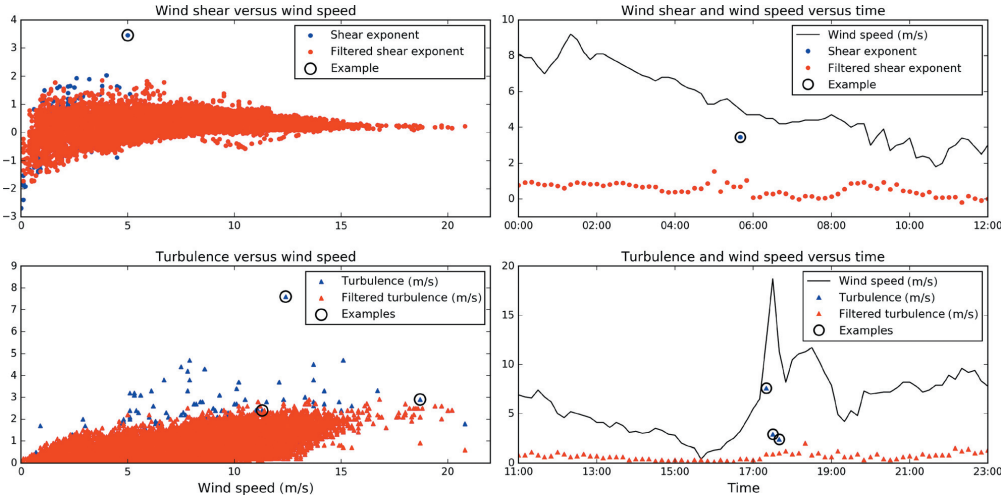

Fig. 9 Shear exponent and turbulence before and after applying the despike algorithm. The upper plots show the shear exponent and the lower plots the turbulence. To the left are shown scatter plots and selected spikes are encased with black circles and shown in the time domain to the right. Notice that the spikes are replaced and not discarded.

calculating fatigue damage directly from the 10 min measurements. In Fig. 9 the performance of the despike algorithm is shown for a site with a relatively poor initial screening before it was made available for this work compared to most sites. The upper figures show the shear exponent before and after despiking and the lower figures show the turbulence. To the left are shown scatter plots of all data and to the right a few selected spikes (encased by black circles) are shown in the time domain. Notice how the turbulence spikes occur at an event where the wind speed has a sharp increase followed by a sharp decrease where a trend is very likely over the 10 min periods. The spike with a turbulence value of ~7 m/s is easy to detect in the scatter plot, whereas the two following spikes are apparent in the time-domain only.

References

[1] IEC, 2005, "Wind Turbines—Part 1: Design Requirements," International Electrotechnical Commission, Geneva, Switzerland, Standard No. IEC 61400-1.

[2] Stensgaard Toft, H., Svenningsen, L., Moser, W., Dalsgaard Sørensen, J., and Lybech Thøgersen, M., 2016, "Wind Climate Parameters for Wind Turbine Fatigue Load Assessment," ASME J. Sol. Energy Eng., **138**(3), p. 031010.

[3] Dimitrov, N., Natarajan, A., and Kelly, M., 2015, "Model of Wind Shear Conditional on Turbulence and Its Impact on Wind Turbine Loads," Wind Energy, **18**(11), pp. 1917–1931.

[4] Ernst, B., and Seume, J. R., 2012, "Investigation of Site-Specific Wind Field Parameters and Their Effect on Loads of Offshore Wind Turbines," Energies, **5**(10), pp. 3835–3855.

[5] Sathe, A., Mann, J., Barlas, T., Bierbooms, W. A. A. M., and van Bussel, G. J. W., 2013, "Influence of Atmospheric Stability on Wind Turbine Loads," Wind Energy, **16**(7), pp. 1013–1032.

[6] Holtslag, M. C., Bierbooms, W. A. A. M., and van Bussel, G. J. W., 2014, "Definition of the Equivalent Atmospheric Stability for Wind Turbine Fatigue Load Assessment," J. Phys. Conf. Ser., **524**, p. 12110.

[7] Kelly, M., Larsen, G., Dimitrov, N. K., and Natarajan, A., 2014, "Probabilistic Meteorological Characterization for Turbine Loads," J. Phys. Conf. Ser., **524**, p. 12076.

[8] Kubik, M. L., Coker, P. J., Barlow, J. F., and Hunt, C., 2013, "A Study Into the Accuracy of Using Meteorological Wind Data to Estimate Turbine Generation Output," Renew. Energy, **51**, pp. 153–158.

[9] IEC, 2016, "Wind Turbines—Part 1: Design Requirements," International Electrotechnical Commission, Geneva, Switzerland, Standard No. IEC CDV 61400-1.

[10] Larsen, G. C., and Hansen, K. S., 2014, "De-Trending of Wind Speed Variance Based on First-Order and Second-Order Statistical Moments Only," Wind Energy, **17**(12), pp. 1905–1924.

[11] Brock, F. V., 1986, "A Nonlinear Filter to Remove Impulse Noise From Meteorological Data," J. Atmos. Oceanic Technol., **3**(1), pp. 51–58.

[12] Starkenburg, D., Metzger, S., Fochesatto, G. J., Alfieri, J. G., Gens, R., Prakash, A., and Cristóbal, J., 2016, "Assessment of Despiking Methods for Turbulence Data in Micrometeorology," J. Atmos. Oceanic Technol., **33**(9), pp. 2001–2013.

[13] Jonkman, J., Butterfield, S., Musial, W., and Scott, G., 2009, "Definition of a 5-MW Reference Wind Turbine for Offshore System Development," National Renewable Energy Laboratory, Golden, CO, Report No. NREL/TP-500-38060.

[14] Jonkman, J., 2015, "FAST An Aeroelastic Computer-Aided Engineering (CAE) Tool for Horizontal Axis Wind Turbines," National Renewable Energy Laboratory, Golden, CO, accessed Apr. 3, 2017, https://nwtc.nrel.gov/FAST

[15] Jonkman, B., and Kelley, N., 2016, "TurbSim A Stochastic, Full-Field, Turbulence Simulator Primarialy for Use With InflowWind/AeroDyn-Based Simulation Tools," National Renewable Energy Laboratory, Golden, CO, accessed Apr. 3, 2017, https://nwtc.nrel.gov/TurbSim

[16] ASTM, 2011, "Standard Practice for Cycle Counting in Fatigue Analysis," American Society for Testing and Materials, West Conshohocken, PA, Standard No. E1049-85.

[17] Malcolm, D., Lybarger, K., and Randall, G., 2011, "Advances in Wind Turbine Site Assessment," AIAA Paper No. 2011-456.

[18] Toft, H. S., Svenningsen, L., Moser, W., Sørensen, J. D., and Thøgersen, M. L., 2016, "Assessment of Wind Turbine Structural Integrity Using Response Surface Methodology," Eng. Struct., **106**, pp. 471–483.

[19] Kohler, M., Metzger, J., and Kalthoff, N., 2017, "Trends in Temperature and Wind Speed From 40 Years of Observations at a 200-M High Meteorological Tower in Southwest Germany," Int. J. Climatol., **38**(1), pp. 23–34.

[20] Beyrich, F., and Adam, W. K., 2007, "Site and Data Report for the Lindenberg Reference Site in CEOP—Phase I," Berichte des Deutschen Wetterdienstes, p. 55.

Effective Turbulence and its Implications in Wind Turbine Fatigue Assessment

René M. M. Slot[1,2], John D. Sørensen[1], Lasse Svenningsen[2], Wolfgang Moser[3] and Morten L. Thøgersen[2]

[1]Department of Civil Engineering, University of Aalborg, Aalborg, 9220, Denmark
[2]EMD International A/S, Aalborg, 9220, Denmark
[3]Nordex Energy GmbH, Turbine Engineering, Langenhauser Chaussee 600, 22419 Hamburg, Germany

Correspondence to: René M. M. Slot (rmms@civil.aau.dk)

Abstract. The effective turbulence approximation is widely used in the wind energy industry for site-specific fatigue assessment of wind turbines with reference to loads. It significantly reduces the amount of aero-elastic simulations required to document structural integrity by integrating out the directional variation of turbulence. Deriving the effective turbulence involves assumptions related to load effect histories, structural dynamics, and material fatigue strength. These assumptions may lead to low accuracy of fatigue load assessments by the effective turbulence compared to full directional simulations. This paper quantifies the implications of the effective turbulence for a multi-megawatt wind turbine during normal operation. Analyses based on wind measurements from almost one hundred international sites documents that the effective turbulence provides accurate results compared to full sector-wise simulations, but only when linear SN-curves are assumed. For a more advanced steel tower design approach using a bilinear SN-curve, a reduction of the cross-sectional design parameters by almost 10% is achieved. Additional 10% reduction can be obtained if fatigue damage is estimated utilizing the wind direction information. By applying a probabilistic approach, it is shown that this reduction in the design parameter of the steel tower, does not compromise the structural integrity when the current IEC 61400-1 standard is followed. The results presented may improve decision making in site-specific fatigue assessments of wind turbines and prevent over-conservative design, which results from the use of the effective turbulence, and thereby reduce the cost of wind energy.

Key words: Wind turbine, Fatigue loads, Effective turbulence, Structural reliability

1. Introduction

To lower the cost of wind energy it is important to choose the most cost-efficient wind turbine class that fits a given site with its given wind climate and chosen wind farm layout. A main tool for decision support is to use aero-elastic computer codes to simulate the response of a candidate turbine model and check if the loads on major components are below their design limits. Aero-elastic codes are computationally expensive, and it is therefore important to define a simple representative description of the site-specific wind climate for load estimates, without requiring excessive simulations. For this purpose the Design Standard IEC 61400-1 ed. 3[1] defines an "Effective turbulence" approximation[2] that integrates the directional variation of turbulence due to wake and ambient effects adjusted with the Wöhler exponent,

resulting in a fatigue equivalent omnidirectional value. Due to its simplicity, the approximation has been widely used in the wind industry for nearly two decades; yet, no thorough investigation of its implications for a broad range of real sites has been published.

Henriksen et al.[3] investigated the accuracy of the effective turbulence approximation in fatigue assessment using wind data from two existing wind farms. The study showed that the effective turbulence is conservative, with the highest difference compared to full sector-wise calculations at the site with the lowest ambient turbulence. This agrees with Frandsen[2] who showed that the effective turbulence would be conservative for real wind climates where the response of the turbine consists of a stochastic part (from turbulence) and a deterministic part (driven by wind shear or gravity). Based on a few experiments, he concluded that the approximation is more conservative the more equally the stochastic and deterministic parts are weighted. This was later confirmed analytically by Veldkamp[4] but neither Frandsen[2] nor Veldkamp[4] quantified the conservatism for a broad range of real wind turbine sites.

In Sørensen et al.[5], the consequence of using the effective turbulence was analysed to show the importance of modelling SN-curves with a bilinear model. By calculating the failure probability of welded steel, cast steel, and fiber-reinforced details, they demonstrated that combining the effective turbulence with bilinear SN-curves may be a viable approach to reduce cross-sectional design parameters. This conclusion is important as to avoid over-conservative wind turbine designs, but the study was based on limited data, hence, a further validation is needed to ensure that this is also the case for real wind climates with varying ambient conditions.

Removing directional variation of turbulence implies that fatigue damage in wind turbine components accumulate independent of the wind direction. This was discussed by Veldkamp[4], stating that the rule of thumb in the industry (at that time) was to assume a consequence of ~10% overprediction of fatigue damage in the tower; However, he did not connect it directly to the effective turbulence and no thorough study has been published to verify this rule of thumb.

The effect of wake induced turbulence was studied by Thomsen et al.[6] with the purpose of identifying and including the most important wake parameters for load calculations. Based on the ”Vindeby experiment” they analysed the importance of windspeed deficit, turbulence intensity, horizontal shear and the turbulence length scale in the Mann turbulence model[7]. For fatigue loads the turbulence intensity and turbulence length scale were most important, which stresses the need for accurate turbulence models.

It is broadly acknowledged that turbulence is a main driver of fatigue loads.[8–12] Dimitrov et al.[8] developed a model of wind shear dependent on turbulence to account for atmospheric stability. Fatigue load calculations with the defined model showed that wind shear was mainly important for blade flap-wise loads, whereas turbulence dominated other components. In Sathe et al.[10] atmospheric stability was modelled directly using the Monin-Obukhov length. By modelling diabatic conditions instead of neutral conditions a reduction of up to 17% was achieved for the tower base loads which compares to the consequence of integrating directional variation of turbulence indicated by Veldkamp[4].

The original intend of effective turbulence was handling wakes in a practical framework for code-based design[2]. However, its derivation does not rely on the presence of wakes and the characteristic ambient turbulence is based primarily on the validity of the approximation[4]. As

will be shown later, the effective turbulence depends on four key assumptions, which implicitly introduce a hidden design margin (conservatism) that designing engineers may not be aware of. It is therefore important to quantify this conservatism as it could reverse the decision of a turbine being 'not suitable' for a given site and park layout to being 'suitable', only at the expense of additional sector-wise simulations. Hence, the scope of this paper is to quantify the implications of the effective turbulence in site-specific fatigue assessment of onshore wind turbines during normal operation (design load case 1.2). A modern multi-megawatt reference wind turbine is considered, and all analyses are based on real wind measurements from 99 international sites, providing a solid statistical basis of varying site-specific ambient wind climates. This improved understanding of the implications of the effective turbulence may significantly enhance decision making in the wind industry when addressing whether directional simulations are worth the computational and engineering investment compared to the expected reduction in material consumption.

2. Wind data and theory of effective turbulence

In this section a description of the available wind data is presented followed by an outline of the theory and underlying key assumptions of the effective turbulence approximation.

2.1. Wind data and characteristic wind climate

High quality measurements of 10min. mean windspeed (U), mean wind direction (θ), turbulence (σ_U), and wind shear (α) from a total of 99 meteorological masts are used in this study. Measurements of flow inclination (φ) and air density (ρ) were unavailable at most sites, and for the sake of consistency they are fixed to 0.0° and $1.225\mathrm{kg/m^3}$, respectively, at all sites. This is a simplification, but the parameters have very limited influence on fatigue loads compared to turbulence and wind shear.[8,13,14] The measurements included in this study cover exactly one year, and the mast locations represent diverse site conditions from flat to steep terrain with and without forestry nearby. All the measurements are from wind power projects or meteorological research masts and were therefore carefully screened prior to this study. Still, to enhance consistency of the datasets, a supplementary cleaning procedure has been applied. This database was also used in Slot et al.,[13] which includes a more detailed description of the data and the supplementary cleaning procedure. Based on the cleaned data sets, the characteristic wind climate statistics for design load case 1.2 are derived according to the IEC standard[a] and an overview is presented in Table 1.

The site-specific characteristic wind shear (α_c) is obtained from the wind measurements as the mean value and the windspeed and direction distributions are taken directly from the data. The measurements of turbulence are used to assess the characteristic windspeed-dependent 90% quantile of turbulence ($\sigma_{U,c}$) based on the turbulence mean value ($\sigma_{U,\mu}$) and standard deviation ($\sigma_{U,\sigma}$) following Eq. (1).[1]

$$\sigma_{U,c}(U,\theta) = \sigma_{U,\mu}(U,\theta) + 1.28\sigma_{U,\sigma}(U,\theta) \quad (1)$$

[a] To ease readability the Design Standard IEC 61400-1 ed. 3[1] is referred to as the "IEC standard".

Table 1. Characteristic wind climate parameters.

Description	Measured	Characteristic value	Notation
Wind direction	Yes	Sector-wise frequency in 30° bins	f_θ
Windspeed	Yes	Windspeed frequency in 1m/s bins	f_U
Turbulence	Yes*	Windspeed and sector-dependent 90% quantile including wakes	$\sigma_{U,\mathrm{T}}$
Wind shear	Yes	Mean value	α_c
Air density	No	Fixed value ($1.225\ \mathrm{kg/m^3}$)	ρ_c
Flow inclination	No	Fixed value ($0.0°$)	φ_c

*Only the ambient turbulence is measured.

To ease notation in the remainder of this paper all characteristic non-turbulence climate parameters are grouped in the vector $\overline{C_\mathrm{c}}$ as defined in Eq. (2)

$$\overline{C_\mathrm{c}} = [f_\theta, f_U, \alpha_\mathrm{c}, \rho_\mathrm{c}, \varphi_\mathrm{c}] \tag{2}$$

2.2. Wake added turbulence

Directional variation of turbulence is amplified by wake effects inside wind farms. To reflect this, artificial wake-added turbulence is introduced at all masts by assuming neighboring turbines in a rectangular grid layout, where turbines are placed 5 rotor diameters upwind and downwind in the main wind direction (the direction with the highest probability density) and 3 rotor diameters perpendicular to that. The total turbulence ($\sigma_{U,\mathrm{T}}$) from ambient and wake contributions is combined by Eq. (3)[1] where C_T is the thrust coefficient and RD is the distance to the upwind turbine in rotor diameters. To follow the IEC standard only wakes from the nearest neighboring turbines are considered and the windspeed deficit in wakes is neglected[b].

$$\sigma_{U,\mathrm{T}}(U,\theta) = \sqrt{\frac{U^2}{\left(1.5 + \frac{0.8\mathrm{RD}}{\sqrt{C_\mathrm{T}(U)}}\right)^2} + \sigma_{U,\mathrm{c}}(U,\theta)^2} \tag{3}$$

To limit the amount of directional calculations included in this paper wake influence is assumed to cover exactly one sector of 30° regardless of distance. This simplification is slightly conservative but in-line with Frandsen's original work assuming a fixed wake influence of 22° (Frandsen[2], p. 56) and it serves the purpose of introducing a stronger directional variation of turbulence. As will be shown next, the effective turbulence may be derived without consideration of the wake expansion (or wakes at all), and the purpose here is

[b] Due to this simplification the results in this paper will not be directly comparable to results obtained by the dynamic wake meandering model.

not to assess the accuracy of Frandsen's "wake added turbulence" model in Eq. (3), which was studied recently by other authors[15,16].

2.3. Theory and key assumptions of the effective turbulence

The effective turbulence approximation was first introduced by Frandsen[2]. It integrates out the turbulence variation with direction conditioned on windspeed as shown in Eq. (4),[1] where m is the Wöhler exponent related to material fatigue strength.

$$\sigma_{U,\mathrm{eff}}(U,m) = \left(\int_0^{2\pi} \sigma_{U,\mathrm{T}}^m(U,\theta) f_\theta(\theta|U) d\theta \right)^{\frac{1}{m}} \tag{4}$$

Effective turbulence reduces the amount of simulations required considerably, since standard calculations typically divide the ambient turbulence into twelve sectors covering 30° each. Most turbines are also placed in farm layouts where wakes are not perfectly aligned with the sectors, thereby demanding additional simulations to account for turbulence variation within each wake-affected sector.

The effective turbulence approximation relies on the concept of "damage equivalent loads" (DEL). This implies that fatigue strength is modelled by a linear relationship between load effect ranges (S) and number of cycles to failure (N) on a logarithmic scale (i.e. linear SN-curve) and that fatigue damage is accumulated linearly by Miner's rule[1]. The total DEL of a wind turbine component (F_{DEL}) between the cut-in windspeed (U_{in}) and cut-out windspeed (U_{out}) can be combined by Eq. (5).

$$\begin{aligned} &F_{\mathrm{DEL}}\left(\overline{C}_{\mathrm{c}}, \sigma_{U,\mathrm{T}}(U,\theta), m\right) \\ &= \left(\int_{U_{\mathrm{in}}}^{U_{\mathrm{out}}} f_U(U) \int_0^{2\pi} f_\theta(\theta|U) \mathrm{DEL}\left(U, \sigma_{U,\mathrm{T}}(U,\theta), \alpha_{\mathrm{c}}, \rho_{\mathrm{c}}, \varphi_{\mathrm{c}}, m\right)^m d\theta dU \right)^{\frac{1}{m}} \end{aligned} \tag{5}$$

If fatigue loads are evaluated by the "narrow-band approximation" in the frequency domain,[17,18] and assuming that the standard deviation of the component-specific load effect time series is proportional to turbulence, the following important relationship can be derived:

$$\text{for fixed } U\text{: } \mathrm{DEL} \propto \sigma_U \tag{6}$$

Inserting this into the inner integral across directions in Eq. (5) leads directly to Eq. (4). Consequently, the effective turbulence approximation introduces the following four key assumptions in site-specific fatigue assessment:

I. The load effect of any wind turbine component is a narrow-band stochastic process.
II. The standard deviation of the response process is proportional to turbulence at a fixed windspeed.
III. The fatigue strength of wind turbine components can be described by a linear SN-curve.
IV. The considered component is always facing the wind directly regardless of wind direction.

The assumed narrow-band stochastic process may be centered around, for example, the first structural eigenfrequency of the considered component or the frequency of rotor revolution. The proportionality in the second assumption is basically derived by linearizing the wind load on a vertical cylinder, assuming that the structural response is well described by its first mode of vibration[2]. The third assumption is from the framework of damage equivalent loads, and finally the fourth assumption is a direct consequence of removing directional dependency of turbulence.

It is noted that assumptions III and IV are common simplifications in wind turbine design, regardless of whether effective turbulence is used or not. However, based on sector-wise simulations it is straight-forward (and impractical) to use non-linear SN-curves instead of the DEL framework. The same applies for directional fatigue accumulation in wind turbine towers. By contrast, once effective turbulence has been adopted, and 'omnidirectional simulations' have been carried out, it is no longer an option to use bi-linear SN-curves or directional fatigue accumulation. At least not without violating the basic assumptions behind the effective turbulence.

To study the implications of all four key assumptions, the remainder of this article is structured as follows: In Section 3 the accuracy of assumptions I and II is quantified by comparing fatigue loads from omnidirectional and sector-wise simulations, respectively. In Section 4 the consequence of assumptions III and IV is investigated with focus on a steel tower design by using bilinear SN-curves, and by utilizing wind direction information to accumulate fatigue damage point-wise along the tower circumference. In Section 5 a summary and discussion of the results is presented, which shows that the proposed directional method of fatigue accumulation results in significant reductions in the tower cross-sectional design parameter. This motivates a validation of the structural integrity of the proposed design which is presented in Section 6. Finally, the conclusions of this work are presented in Section 7.

Throughout this paper the term accuracy is always used specifically when addressing assumptions I and II and the term consequence is used for assumptions III and IV. This is on purpose to distinguish that Eq. (6) may (or may not) be accurate, whereas assumptions III and IV are inevitable consequences of the effective turbulence approximation.

3. Quantification of the accuracy of assumptions I and II

In this section the considered wind turbine and aero-elastic simulation procedure are described. This is followed by a quantification of the accuracy of assumptions I and II across the 99 available sites.

3.1. Wind turbine simulation and preliminary accuracy estimation

Fatigue loads are based on normal operation of the 5MW reference turbine model by NREL[19] simulated in the aero-elastic code FAST.[20] For each wind climate combination 20 seeds are used to generate turbulent wind fields in TurbSim[21] based on the Kaimal spectrum[1]. All simulations have an effective length of 10min. and load effect ranges and cycles are derived by Rainflow counting[22].

To limit the amount of results presented, only the four main components (sensors) listed in Table 2 are considered using typical Wöhler exponents.[4,5,23–26]

Table 2. Wind turbine sensors.

Sensor	Description	Wöhler exponent	Unit
TwrBsMyt	Tower bottom fore-aft bending moment	4	kNm
YawBrMyp	Yaw bearing tilt	4	kNm
LSSGagMxa	Low speed shaft torque	6	kNm
RootMyb1	Blade root flap-wise bending moment	10	kNm

An initial accuracy of the effective turbulence is estimated for each sensor by checking if there is a linear relationship between σ_U and DEL as assumed in Eq. (6). The result of this analysis is presented in Figure 1, showing that all components have a close to linear relationship at most windspeeds. This indicate that the effective turbulence will lead to accurate fatigue assessments. Turbulence intensity, TI (i.e. the windspeed coefficient of variation) is considered as it allows more realistic turbulence ranges to be shown[c].

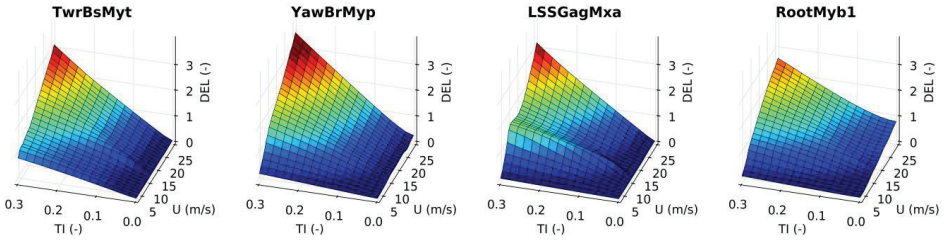

Figure 1: DELs calculated as function of windspeed and turbulence intensity for the four considered wind turbine components. The DELs are estimated using 100 seeds to minimize statistical uncertainty. For comparison, the loads are normalized with design class IIB loads.

Note that the results are turbine-specific, and different control strategies or structural properties could change the relationships shown significantly (e.g. if the controller reacts to high turbulence to reduce fatigue loads).

3.2. Methods to quantify the accuracy of assumptions I and II

Assumptions I and II combined lead to the proportionality in Eq. (6) which directly defines the effective turbulence formulation in Eq. (4). A direct way of quantifying the accuracy of these assumptions is therefore to compare sector-wise and omnidirectional fatigue assessments.

This is shown in Eq. (7) where $F_{\mathrm{DEL,eff}}$ is the site-specific fatigue load by simulating the effective turbulence and $F_{\mathrm{DEL,sect}}$ is the site-specific fatigue load by sector-wise simulations.

$$\Delta\mathrm{DEL}_{\mathrm{comp}} = \frac{F_{\mathrm{DEL,eff}}\left(\overline{C}_{\mathrm{c}}, \sigma_{U,\mathrm{eff}}(U, m_{\mathrm{s}}), m_{\mathrm{s}}\right)}{F_{\mathrm{DEL,sect}}\left(\overline{C}_{\mathrm{c}}, \sigma_{U,\mathrm{T}}(U, \theta), m_{\mathrm{s}}\right)} \tag{7}$$

[c] This has no impact on the results as DEL $\propto \sigma_U$ is equivalent to DEL $\propto$ TI when U is fixed.

The fatigue loads are obtained by Eqs. (8) and (9) where m_s is the component-specific Wöhler exponent listed in Table 2, and $\sigma_{U,\mathrm{eff}}$ is estimated according to the IEC standard by Eq. (10).

$$F_{\mathrm{DEL,sect}}\left(\overline{C}_{\mathrm{c}}, \sigma_{U,\mathrm{T}}(U,\theta), m_{\mathrm{s}}\right) = \left(\int_0^{2\pi} f_\theta(\theta) \int_{U_{\mathrm{in}}}^{U_{\mathrm{out}}} f_U(U|\theta)\mathrm{DEL}\left(U, \sigma_{U,\mathrm{T}}(U,\theta), \alpha_{\mathrm{c}}, \rho_{\mathrm{c}}, \varphi_{\mathrm{c}}, m_s\right)^{m_s} dU d\theta\right)^{\frac{1}{m_s}} \quad (8)$$

$$F_{\mathrm{DEL,eff}}\left(\overline{C}_{\mathrm{c}}, \sigma_{U,\mathrm{eff}}(U,m_{\mathrm{s}}), m_{\mathrm{s}}\right) = \left(\int_{U_{\mathrm{in}}}^{U_{\mathrm{out}}} f_U(U)\mathrm{DEL}\left(U, \sigma_{U,\mathrm{eff}}(U,m_s), \alpha_{\mathrm{c}}, \rho_{\mathrm{c}}, \varphi_{\mathrm{c}}, m_s\right)^{m_s} dU\right)^{\frac{1}{m_s}} \quad (9)$$

$$\sigma_{U,\mathrm{eff}}(U,m_s) = \left(\int_0^{2\pi} \sigma_{U,\mathrm{T}}^{m_s}(U,\theta) f_\theta(\theta|U) d\theta\right)^{\frac{1}{m_s}} \quad (10)$$

The viability of using the highest effective turbulence is also investigated as outlined in Eq. (11). This approach is appealing to the wind industry to reduce the required amount of simulations. The resulting conservatism ($\Delta\mathrm{DEL}_{\mathrm{m10}}$) is quantified by Eq. (12).

$$F_{\mathrm{DEL},m10}\left(\overline{C}_{\mathrm{c}}, \sigma_{U,\mathrm{eff}}(U,m=10), m_{\mathrm{s}}\right) = \left(\int_{U_{\mathrm{in}}}^{U_{\mathrm{out}}} f_U(U)\mathrm{DEL}\left(U, \sigma_{U,\mathrm{eff}}(U,m=10), \alpha_{\mathrm{c}}, \rho_{\mathrm{c}}, \varphi_{\mathrm{c}}, m_s\right)^{m_s} dU\right)^{\frac{1}{m_s}} \quad (11)$$

$$\Delta\mathrm{DEL}_{m10} = \frac{F_{\mathrm{DEL},m10}\left(\overline{C}_{\mathrm{c}}, \sigma_{U,\mathrm{eff}}(U,m=10), m_{\mathrm{s}}\right)}{F_{\mathrm{DEL,sect}}\left(\overline{C}_{\mathrm{c}}, \sigma_{U,\mathrm{T}}(U,\theta), m_{\mathrm{s}}\right)} \quad (12)$$

3.3. Accuracy of assumptions I and II

Figure 2 presents the results of using the highest effective turbulence across all available sites, showing that this method should be used with caution as it overestimates fatigue damage with up to 23% in the tower and yaw bearing. By contrast, a very high accuracy (within 7%) is obtained if component-specific effective turbulence is used, see Figure 3.

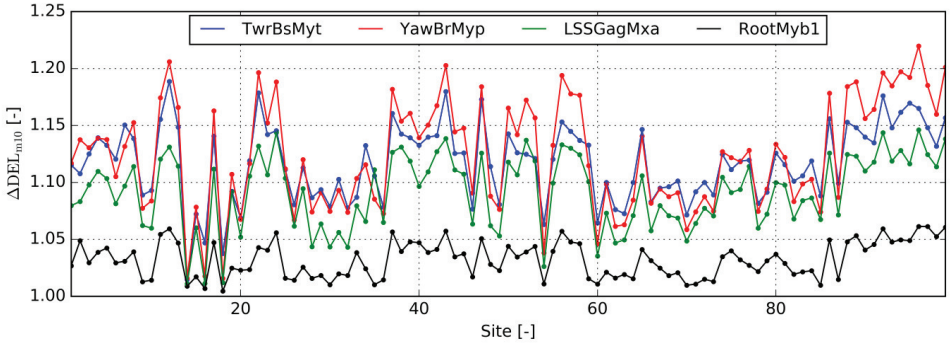

Figure 2: Accuracy of the effective turbulence across all 99 sites when the blade- specific effective turbulence is used for all components.

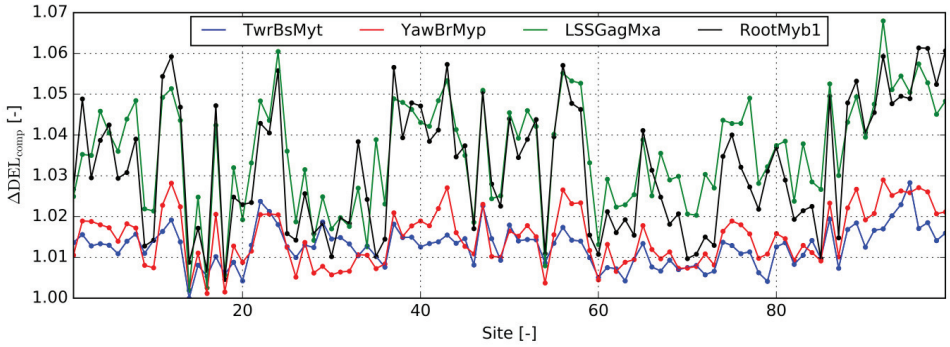

Figure 3: Accuracy of the effective turbulence across all 99 sites when component-specific effective turbulence is used. Notice that the y-scale is changed compared with Figure 2.

The least conservative predictions are obtained for the components with the lowest Wöhler exponents, consistent with the findings in Henriksen et al.[3] It is therefore enticing to conclude, as they did, that the effective turbulence is more accurate for lower Wöhler exponents. This is confirmed by calculating ΔDEL_{comp} for varying Wöhler exponents. The results are summarized in Table 3 by the mean value and standard deviation (std.) across all sites. The following is observed:

- Effective turbulence is more accurate for lower Wöhler exponents.
- The effective turbulence approximation always seems to be conservative.
- Effective turbulence is most conservative for the main shaft.

A straightforward explanation why the accuracy increases for lower Wöhler exponents is that the associated error is raised to a lower exponent. However, this does not explain why the error is increasing more for the blades compared to the tower and yaw bearing. A possible reason is that blades are significantly more sensitive to wind shear compared to other components[8,13]. Assuming that wind shear results in fewer but larger load cycles than turbulence it follows from the results of Frandsen[2] and Veldkamp[4] that higher Wöhler

exponents leads to increasingly conservative results as the deterministic load effect from wind shear is weighted higher.

Table 3. Accuracy of the effective turbulence for varying Wöhler exponents.

Assumed Wöhler exponent	TwrBsMyt [%]		YawBrMyp [%]		LSSGagMxa [%]		RootMyb1 [%]	
	Mean	Std.	Mean	Std.	Mean	Std.	Mean	Std.
3	100.96	0.33	101.27	0.57	101.51	0.74	101.55	0.78
4	101.27	0.48	101.48	0.68	102.43	1.05	102.15	1.11
5	101.57	0.64	101.62	0.74	103.08	1.24	102.59	1.34
6	101.79	0.73	101.71	0.76	103.56	1.36	102.89	1.48
10	102.09	0.75	101.86	0.86	104.46	1.62	103.21	1.56

To clarify the conservatism across all sensors the following line of arguments related to assumption I is considered: Tovo[27] showed analytically that estimating fatigue damage by the "narrow-band approximation" is equal to linear fatigue accumulation in the time domain using a level crossing counting (LCC) scheme[22]. Normally though, Rainflow counting (RC) is preferred as Dowling[28] found it superior when comparing predicted and real fatigue lives. Combining this with the work of Rychlik,[17] showing analytically that the fatigue damage obtained by LCC is an upper bound to RC, it is clear that assumption I is inherently conservative. In addition, the narrow-band approximation is generally considered conservative for wide-banded processes,[18] suggesting that the effective turbulence will be conservative, even when assumption I is not fully satisfied. This also explains why the effective turbulence is most conservative for the main shaft as demonstrated in the following.

By simulating the wind turbine for one hour using design wind climate IIB[1] the first bandwidth parameter (α_1), which tends to 1.0 for narrow-banded processes, is estimated for all considered components. The parameter is defined by Eq. (13) where λ_n represent the nth moment of the power spectral density (PSD) about its origin. The PSD of all components is computed by "Welch's method[29]".

$$\alpha_1 = \frac{\lambda_1}{\sqrt{\lambda_0 \lambda_2}} \tag{13}$$

The result of this analysis is summarized in Table 4, showing that the load response process is more wide-banded for the main shaft than the remaining components. It is important to note that the component-specific bandwidth is very dependent on the considered turbine and its control strategy. The 5MW reference turbine operates at variable rotor speed and generator torque below rated windspeed, which explains the wide-banded response of the shaft. The results presented in Table 4 are therefore not representative for the sensors in general, but it explains the results in Table 3.

Table 4. First bandwidth parameter for each considered sensor at three windspeed.

Windspeed	TwrBsMyt	YawBrMyp	LSSGagMxa	RootMyb1
6.0m/s	0.6	0.7	0.1	0.5
11.4m/s (Rated)	0.3	0.6	0.2	0.6
16.0m/s	0.4	0.6	0.6	0.7

4. Quantification of the consequence of assumptions III and IV

In this section the consequences of assumptions III and IV are quantified across all 99 available sites. Only the steel tower is considered in this study; partly due to Sørensen et al.[5] pointing out that welded steel details show much higher sensitivity to assumption III compared to cast steel, and partly because assumption IV is only relevant for components below the yaw bearing.

4.1. Fatigue damage assessment of the steel tower

Damage equivalent loads are defined for linear SN-curves and the consequence of assumption III can therefore not be quantified by the method outlined in Section 3. Instead, a representative bilinear SN-curve with Wöhler exponents 3 (m_1) and 5 (m_2) is defined based on DS/EN 1993-1-9[30] in terms of stress ranges ($\Delta\sigma$). This is outlined in Eq. (14) where the slope change occurs at stress range $\Delta\sigma_{\mathrm{D}}$ corresponding to $N_{\mathrm{D}} = 5 \cdot 10^6$ cycles.

$$\begin{aligned} N(\Delta\sigma) &= K_{\mathrm{c},1} \cdot \Delta\sigma^{-m_1} \ \text{ for } \ \Delta\sigma > \Delta\sigma_{\mathrm{D}} \\ N(\Delta\sigma) &= K_{\mathrm{c},2} \cdot \Delta\sigma^{-m_2} \ \text{ for } \ \Delta\sigma \leq \Delta\sigma_{\mathrm{D}} \end{aligned} \tag{14}$$

The characteristic parameters $K_{\mathrm{c},1}$ and $K_{\mathrm{c},2}$ are estimated by Eq. (15).

$$\Delta\sigma_{\mathrm{D}} = \left(\frac{K_{\mathrm{c}}}{N_{\mathrm{D}}}\right)^{\frac{1}{m}} \tag{15}$$

To compare the results in this section with the accuracy of assumptions I and II the bilinear SN-curve is linearized with an intermediate Wöhler exponent of 4. It is assumed strictly conservative as shown in Figure 4[d].

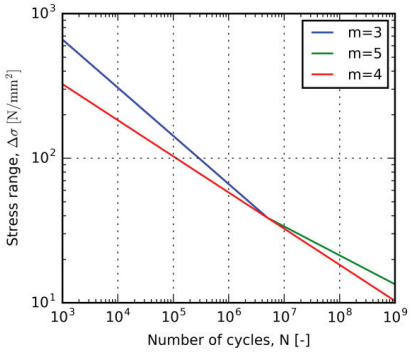

Figure 4: Bilinear SN curve from DS/EN 1991-1-9 using Wöhler exponents 3 (blue) and 5 (green) along with the linear SN curve using an intermediate Wöhler slope of 4 (red).

[d] Figure 4 shows design category 71. Changing the design category has no influence on the results presented.

The SN-curves allow the fatigue damage to be described in terms of required moment of resistances (W) given that the load effect is defined as a moment. A representative design equation (G) is defined in Eq. (16) where the tower is designed to the limit (Miners sum equal to 1.0), and W represents the constant of proportionality between moments and stresses at the tower bottom cross-section. The turbine lifetime (T_{L}) is assumed to be 20 years, ν is the number of fatigue load cycles in a year, and D is defined by Eq. (17). The characteristic parameter $K_{\mathrm{c,s}}$ is determined from Eq. (15) and f_S is the density function of load effect ranges. The vector $\bar{\gamma}$ covers the partial safety factors, γ_{n}, γ_{m}, and γ_{F}, representing the consequences of fatigue failure, strength, and loads respectively. The product of the partial safety factors is set to 1.25 as recommended by the IEC standard[1]. Note that the design equation is used to estimate W in an optimization scheme such that "strength minus load equals zero".

$$G(W) = 1 - \int_0^{2\pi} f_\theta(\theta) \int_{U_{\mathrm{in}}}^{U_{\mathrm{out}}} f_U(U|\theta) \cdot \nu \cdot T_{\mathrm{L}} \cdot D(\sigma_U, m_{\mathrm{s}}, W, \bar{\gamma})\, dU d\theta = 0 \tag{16}$$

$$D(\sigma_U, m_{\mathrm{s}}, W, \bar{\gamma}) = \int_0^{\infty} \frac{1}{K_{\mathrm{c,s}}} \left(\frac{\gamma_{\mathrm{n}}\gamma_{\mathrm{m}}\gamma_{\mathrm{F}} \cdot S}{W} \right)^{m_{\mathrm{s}}} f_{S,\mathrm{sect}}(S|U, \sigma_U, \alpha_{\mathrm{c}}, \rho_{\mathrm{c}}, \varphi_{\mathrm{c}})\, dS \tag{17}$$

4.2. Method to assess the consequences of assumption III

By evaluating the required moment of resistance using the linear SN-curve ($W_{\mathrm{l,sect}}$) and bilinear SN-curve ($W_{\mathrm{b,sect}}$) the consequence of assumption III is directly assessed by their ratio (ΔW_{sect}) as defined in Eq. (18).

$$\Delta W_{\mathrm{sect}} = \frac{W_{\mathrm{b,sect}}\left(\bar{C}_{\mathrm{c}}, \sigma_{U,\mathrm{T}}(U,\theta), m_1, m_2, \bar{\gamma}\right)}{W_{\mathrm{l,sect}}\left(\bar{C}_{\mathrm{c}}, \sigma_{U,\mathrm{T}}(U,\theta), m_{\mathrm{s}}, \bar{\gamma}\right)} \tag{18}$$

The reference moment of resistance is calculated by replacing D in the design equation with $D_{\mathrm{l,sect}}$ defined by Eq. (19), where $f_{S,\mathrm{sect}}$ is derived by sector-wise simulations.

$$\begin{aligned} &D_{\mathrm{l,sect}}\left(\sigma_{U,\mathrm{T}}(U,\theta), m_{\mathrm{s}}, W_{\mathrm{l,sect}}, \bar{\gamma}\right) \\ &= \int_0^{\infty} \frac{1}{K_{\mathrm{c,s}}} \left(\frac{\gamma_{\mathrm{n}}\gamma_{\mathrm{m}}\gamma_{\mathrm{F}} \cdot S}{W_{\mathrm{l,sect}}} \right)^{m_{\mathrm{s}}} f_{S,\mathrm{sect}}\left(S\middle|U, \sigma_{U,\mathrm{T}}(U,\theta), \alpha_{\mathrm{c}}, \rho_{\mathrm{c}}, \varphi_{\mathrm{c}}\right) dS \end{aligned} \tag{19}$$

Similarly, $W_{\mathrm{b,sect}}$ is calculated by exchanging D with $D_{\mathrm{b,sect}}$ defined by Eq. (20) where S_{D} is derived from σ_{D}.

$$\begin{aligned} &D_{\mathrm{b,sect}}\left(\sigma_{U,\mathrm{T}}(U,\theta), m_1, m_2, \mathrm{S_D}, W_{\mathrm{b,sect}}, \bar{\gamma}\right) \\ &\quad = \int_0^{S_{\mathrm{D}}} \frac{1}{K_{\mathrm{c,1}}} \left(\frac{\gamma_{\mathrm{n}}\gamma_{\mathrm{m}}\gamma_{\mathrm{F}} \cdot S}{W_{\mathrm{b,sect}}} \right)^{m_1} f_{S,\mathrm{sect}}\left(S\middle|U, \sigma_{U,\mathrm{T}}(U,\theta), \alpha_{\mathrm{c}}, \rho_{\mathrm{c}}, \varphi_{\mathrm{c}}\right) dS \\ &\quad + \int_{S_{\mathrm{D}}}^{\infty} \frac{1}{K_{\mathrm{c,2}}} \left(\frac{\gamma_{\mathrm{n}}\gamma_{\mathrm{m}}\gamma_{\mathrm{F}} \cdot S}{W_{\mathrm{b,sect}}} \right)^{m_2} f_{S,\mathrm{sect}}\left(S\middle|U, \sigma_{U,\mathrm{T}}(U,\theta), \alpha_{\mathrm{c}}, \rho_{\mathrm{c}}, \varphi_{\mathrm{c}}\right) dS \end{aligned} \tag{20}$$

To verify the important conclusion of Sørensen et al.[5] discussed in Section 1 a required moment of resistance ($W_{\mathrm{b,eff}}$) is also calculated by combining the effective turbulence and bilinear SN-curves. This is not consistent with the derivation of the effective turbulence but if it shows conservative results (i.e. if $W_{\mathrm{b,eff}} > W_{\mathrm{b,sect}}$), then it is a very effective way of optimizing material consumption, without compromising structural integrity. To calculate $W_{\mathrm{b,eff}}$ the same design equation is used where D is exchanged with $D_{\mathrm{b,eff}}$ defined by Eq. (21) using the density function of load effect ranges obtained by the component-specific effective turbulence ($f_{S,\mathrm{eff}}$).

$$\begin{aligned} &D_{\mathrm{b,eff}}\left(\sigma_{U,\mathrm{eff}}(U, m_{\mathrm{s}}), m_1, m_2, \mathrm{S_D}, W_{\mathrm{b,eff}}, \bar{\gamma}\right) \\ &= \int_0^{S_{\mathrm{D}}} \frac{1}{K_{\mathrm{c},1}} \left(\frac{\gamma_{\mathrm{n}}\gamma_{\mathrm{m}}\gamma_{\mathrm{F}} \cdot S}{W_{\mathrm{b,eff}}}\right)^{m_1} f_{S,\mathrm{eff}}\left(S \middle| U, \sigma_{U,\mathrm{eff}}(U, m_{\mathrm{s}}), \alpha_{\mathrm{c}}, \rho_{\mathrm{c}}, \varphi_{\mathrm{c}}\right) dS \\ &+ \int_{S_{\mathrm{D}}}^{\infty} \frac{1}{K_{\mathrm{c},2}} \left(\frac{\gamma_{\mathrm{n}}\gamma_{\mathrm{m}}\gamma_{\mathrm{F}} \cdot S}{W_{\mathrm{b,eff}}}\right)^{m_2} f_{S,\mathrm{eff}}\left(S \middle| U, \sigma_{U,\mathrm{eff}}(U, m_{\mathrm{s}}), \alpha_{\mathrm{c}}, \rho_{\mathrm{c}}, \varphi_{\mathrm{c}}\right) dS \end{aligned} \tag{21}$$

The accuracy of this approach (ΔW_{eff}) is quantified by Eq. (22) using the same reference as in Eq. (18).

$$\Delta W_{\mathrm{eff}} = \frac{W_{\mathrm{b,eff}}\left(\bar{C}_c, \sigma_{U,\mathrm{eff}}(U, m_{\mathrm{s}}), m_1, m_2, \bar{\gamma}\right)}{W_{\mathrm{l,sect}}\left(\bar{C}_{\mathrm{c}}, \sigma_{U,\mathrm{T}}(U, \theta), m_{\mathrm{s}}, \bar{\gamma}\right)} \tag{22}$$

4.3. Method to assess the consequences of assumption IV

To quantify the influence of varying wind direction on fatigue damage accumulation the cross-section of the tower is divided into 36 equidistant points, starting with point 1 (p_1) facing North (**N**). This is illustrated in Figure 5.

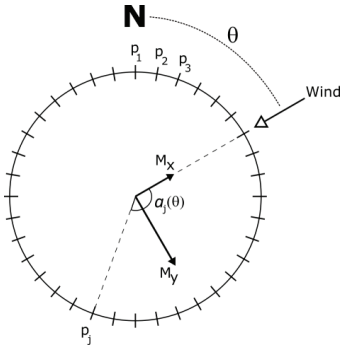

Figure 5: Sketch of the tower bottom cross section. For simplicity, the tower is assumed to be circular symmetric (no door is considered).

At each simulated time step (t_i) the tower moments are projected to each of the 36 points as outlined in Eq. (23), where M_x is the tower side-side moment, M_y is the tower fore-aft moment, M_{p_j} is the projected moment, and a_{j} is the angle with respect to wind direction.

$$M_{\mathrm{p}_j}(t_i, \theta) = M_x(t_i) \sin\Big(a_j(\theta)\Big) + M_y(t_i) \cos\Big(a_j(\theta)\Big) \tag{23}$$

The required moment of resistance at each point is then calculated via design Eq. (16) by exchanging D with $D_{\mathrm{b,p}_j}$ defined by Eq. (24), where the density function of load effect ranges is obtained explicitly at each point (f_{S,p_j}).

$$\begin{aligned} &D_{\mathrm{b,p_j}}\Big(a_j(\theta), \sigma_{U,\mathrm{T}}(U,\theta), m_1, m_2, \mathrm{S_D}, W_{\mathrm{b,p}_j}, \bar{\gamma}\Big) \\ &= \int_0^{S_\mathrm{D}} \frac{1}{K_{\mathrm{c},1}} \left(\frac{\gamma_\mathrm{n}\gamma_\mathrm{m}\gamma_\mathrm{F} \cdot S}{W_{\mathrm{b,p}_j}}\right)^{m_1} f_{S,\mathrm{p}_j}\big(S \big| a_j(\theta), U, \sigma_{U,\mathrm{T}}(U,\theta), \alpha_\mathrm{c}, \rho_\mathrm{c}, \varphi_\mathrm{c}\big)\, dS \\ &+ \int_{S_\mathrm{D}}^{\infty} \frac{1}{K_{\mathrm{c},2}} \left(\frac{\gamma_\mathrm{n}\gamma_\mathrm{m}\gamma_\mathrm{F} \cdot S}{W_{\mathrm{b,p}_j}}\right)^{m_2} f_{S,\mathrm{p}_j}\big(S \big| a_j(\theta), U, \sigma_{U,\mathrm{T}}(U,\theta), \alpha_\mathrm{c}, \rho_\mathrm{c}, \varphi_\mathrm{c}\big)\, dS \end{aligned} \tag{24}$$

In this approach the tower design is represented by the highest required moment of resistance across its circumference ($W_{\mathrm{b,pmax}}$). Subsequently, the consequence of assumption IV (ΔW_{pmax}) is assessed by Eq. (25), where a_{pmax} is the angle to the critical point. For comparison $W_{\mathrm{l,sect}}$ is used as reference.

$$\Delta W_{\mathrm{pmax}} = \frac{W_{\mathrm{b,pmax}}\big(a_{\mathrm{pmax}}(\theta), \bar{C}_\mathrm{c}, \sigma_{U,\mathrm{T}}(U,\theta), m_1, m_2, \bar{\gamma}\big)}{W_{\mathrm{l,sect}}\big(\bar{C}_\mathrm{c}, \sigma_{U,\mathrm{T}}(U,\theta), m_\mathrm{s}, \bar{\gamma}\big)} \tag{25}$$

4.4. Consequences of assumptions III and IV

In Figure 6 the consequence of assumption III is shown across all 99 available sites, where an average reduction of 8% of the moment of resistance is obtained (ΔW_{sect}). The results of using the load effect histories from the effective turbulence simulations are also shown (ΔW_{eff}), which leads to slightly higher required moment of resistances at all sites except one. This strongly suggests that it is viable, and only slightly conservative, to combine the bilinear material strength model with the effective turbulence.

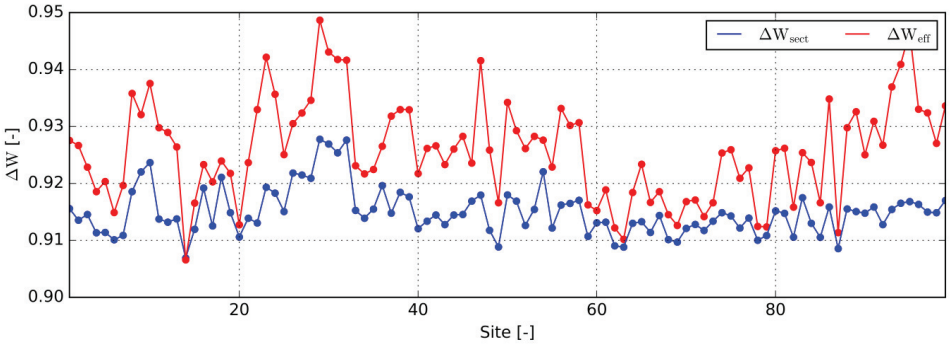

Figure 6: Consequence of using linear SN curves compared with bilinear SN curves for the steel tower assessed across the 99 available sites (ΔWsect). For comparison, the results of combining the effective turbulence and bilinear SN curves are also shown (ΔWeff). Notice that ΔWeff>ΔWsect for all sites except one.

The small conservatism does not reflect the results in Sørensen et al.[5] where a slight non-conservatism was obtained. This is explained by the choice of linearizing the bilinear SN-curve. Here, an intermediate Wöhler exponent of 4 is considered, whereas Sørensen et al.[5] used a continuation of the upper part of the bilinear SN-curve (with Wöhler exponent 3), thereby leading to a lower effective turbulence. This has been verified by linearizing the SN-curve with $m_s = 3$, which resulted in a slight non-conservatism of ~1% on average across the sites. Moreover, a linearization based on the lower part of the bilinear curve with $m_s = 5$ has been considered, which resulted in a conservatism of ~3% on average across the sites. A summary of this analysis is presented in Table 5. This show that the linearization with $m_s = 4$ is most optimal to combine effective turbulence and the bilinear SN -curve without compromising structural safety (ΔW_b just above 1.0). Meanwhile, $m_s = 5$ is preferred if the linearized SN-curve is considered throughout the entire design process (ΔW_{sect} closest to 1.0). The reason for the latter is that most fatigue damage accumulates on the lower part of the bilinear SN-curve, with an average of 58% across all sites[e].

Table 5. Consequence of three different conservative linearizations of the SN-curve.

Wöhler exponent used in linearized SN-curve	Average moment of resistance ratio across all sites		
	ΔW_{sect}	ΔW_{eff}	$\Delta W_b = W_{b,eff}/W_{b,sect}$
3	0.79	0.78	0.99
4	0.92	0.93	1.01
5	0.95	0.98	1.03

The consequence of assumption IV (ΔW_{pmax}) is shown in Figure 7 where the proposed directional approach leads to an additional average reduction of ~12%, thereby confirming the rule of thumb mentioned by Veldkamp[4]. The pronounced site-to-site variation is explained by the varying wind roses. Generally, sites where the wind is concentrated in one direction show much smaller reductions than sites where the wind is less unidirectional.

[e] For offshore wind turbines importance is shifted towards the upper part of the SN-curve if wave loads are dominating.

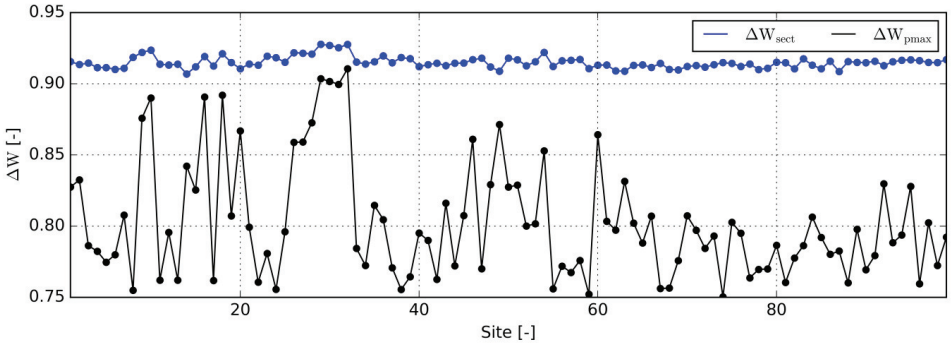

Figure 7: Consequence of neglecting directional dependence of fatigue damage accumulation in the tower, seen as the difference between ΔWsect and ΔWpmax.

5. Summary and discussion of the implications of the effective turbulence approximation

A comparison of the five presented methods to quantify the implications of using effective turbulence in wind turbine fatigue assessment is presented in Table 6. Partial safety factors are considered for the tower as it is important in the reliability analysis presented in Section 6, but for the consequence assessments they cancel out.

Table 6. Comparison of fatigue assessment methods.

Fatigue damage assessment	Characteristic turbulence model	Non-turbulence parameters	Partial safety factors	*SN*-curve	Components considered	Relative no. simulations	Accuracy/ Consequence assessment
$F_{\mathrm{DEL},m10}$	Highest effective turbulence ($m = 10$)	$\bar{C}_c$	No	Linear	All in Table 2	1/3	$\Delta\mathrm{DEL}_{\mathrm{m10}}$
$F_{\mathrm{DEL,eff}}$	Component-specific effective turbulence	$\bar{C}_c$	No	Linear	All in Table 2	1	$\Delta\mathrm{DEL}_{\mathrm{comp}}$
$W_{\mathrm{b,eff}}$	Component-specific effective turbulence	$\bar{C}_c$	Yes	Bilinear	Tower	1	ΔW_{eff}
$W_{\mathrm{b,sect}}$	Sector-wise turbulence	$\bar{C}_c$	Yes	Bilinear	Tower	12	ΔW_{sect}
$W_{\mathrm{b,pmax}}$	Sector-wise turbulence	$\bar{C}_c$	Yes	Bilinear	Tower (fixed points)	12	ΔW_{pmax}
The accuracy/consequence of all methods is obtained using the same fatigue damage reference of $F_{\mathrm{DEL,sect}} \equiv W_{\mathrm{l,sect}}$							

In all methods the reference value is assessed by a linear SN-curve using sector-wise simulations. This consistency makes the consequence assessments (ΔW) and accuracy assessments (ΔDEL) directly comparable. This is demonstrated by considering two arbitrary DELs defined at the same equivalent number of cycles (N_{eq}) in Eq. (26).

$$\frac{\mathrm{DEL}_1}{W_1} = \frac{\mathrm{DEL}_2}{W_2} = \Delta\sigma\left(N_{\mathrm{eq}}\right) \tag{26}$$

The results of each method across all 99 sites are summarized in Table 7, documenting that the effective turbulence is an accurate approximation within 4% on average. This increased understanding is important in site-specific fatigue assessment. Based on prior knowledge of the component-specific Wöhler exponent, wind shear sensitivity and load effect response bandwidth the results presented in Section 3 indicate the margin that can be expected by investing in sector-wise simulations. Alternatively, it can be checked visually if DEL $\propto \sigma_U$ at fixed wind speeds, where clear curvature indicates that the effective turbulence is less accurate (more conservative). This enhanced decision support may relieve designing engineers of doing excessive simulations, or it may reverse the choice of using a stronger turbine at a given site and farm layout.

Table 7. Comparison of accuracy/consequence of the fatigue assessment methods listed in Table 6.

Accuracy/Consequence assessment	Mean value across all sites			
	TwrBsMyt	**YawBrMyp**	**LSSGagMxa**	**RootMyb1**
$\Delta\mathrm{DEL}_{\mathrm{m10}}$	1.12	1.12	1.09	1.03
$\Delta\mathrm{DEL}_{\mathrm{comp}}$	1.01	1.01	1.04	1.03
ΔW_{eff}	0.93	-	-	-
ΔW_{sect}	0.92	-	-	-
ΔW_{pmax}	0.80	-	-	-

The typical intermediate linearization of the SN-curve with Wöhler exponent 4 for the steel tower leads to an increase of ~8% of the required moment of resistance. This consequence may be almost removed by combining omnidirectional simulations and bilinear SN-curves. However, it requires fatigue damage to be estimated directly from stress-ranges. It is therefore important to assess whether the increased engineering effort can be compensated by the expected reduction of the design parameter. In case this is not feasible the supplementary results in section 4 provide designing engineers another option to re-evaluate the design margin within the DEL framework. Simply by linearizing the lower part of the bilinear SN-curve with Wöhler exponent 5 a small margin of ~3% was obtained in this paper compared to the typical intermediate choice. It is important to note though, that this result is turbine-specific and depends on the fatigue damage distribution on the bilinear SN-curve.

The final consequence of the effective turbulence implying unidirectional wind leads to over-predictions of the tower moment of resistances by 12% on average. This observation shows that steel towers may be significantly optimized at certain sites, thereby lowering the cost of wind energy.

Overall, the potential of improving wind turbine designs by doing detailed fatigue assessments is promising, although the reductions presented in Table 7 might not be realized. In practice, other limit states or frequency requirements [f] will influence the material consumption, hence, the presented results should be considered as “upper bounds”.

Finally, it is observed that the fastest fatigue assessment method of the tower ($F_{\mathrm{DEL},m10}$) leads to an average relative increase of 40% of the required moment of resistance compared to

[f] The mass and stiffness of the tower may be governed by frequency requirements to avoid resonance of the tower at the rotor frequency (1P) and the blade passing frequency (2P or 3P).

point-wise damage accumulation with bilinear SN-curves ($W_{\mathrm{b,pmax}}$). This very high discrepancy raises the question whether the proposed directional method of point-wise fatigue accumulation violates the structural integrity of the wind turbine. This is addressed in the following section.

6. Validation of the structural integrity of the proposed steel tower design

The structural integrity of the proposed steel tower design is confirmed by a reliability assessment based on a first order reliability method (FORM). First a representative limit state equation (LSE) is formulated. This is followed by a quantification of the structural reliability in terms of the reliability index (β) which relates to the probability of failure (P_f) as shown in Eq. (27), where Φ is the standardized normal distribution function.

$$P_\mathrm{f} = \Phi(-\beta) \tag{27}$$

6.1. Limit state equation and uncertainty models

The LSE (g) is based on design Eq. (16) as outlined in Eq. (28) where bold font indicates if a variable is stochastic.

$$\begin{aligned} g(W) = \boldsymbol{\Delta} - \int_0^{2\pi} f_\theta(\theta) \int_{U_\mathrm{in}}^{U_\mathrm{out}} f_U(U|\theta) \cdot \nu \cdot t \int_0^{\infty} f_{\sigma_U}\left(\sigma_{U,\mathrm{amb}}\middle|\theta, U\right) \\ \cdot D_{\mathrm{b,lse}}\left(m_1, m_2, \mathrm{S_D}, W, \sigma_{U,\mathrm{exp}}\right) d\sigma_U dU d\theta = 0 \end{aligned} \tag{28}$$

The model uncertainty $\boldsymbol{\Delta}$ describes the fatigue strength (Miner's rule), t is time in years, f_{σ_U} is the distribution of the ambient turbulence ($\sigma_{U,\mathrm{amb}}$ assumed lognormal distributed[g]), and $D_{\mathrm{b,lse}}$ is defined by Eq. (29).

$$\begin{aligned} &D_{\mathrm{b,lse}}\left(m_1, m_2, S_\mathrm{D}, W, \sigma_{U,\mathrm{exp}}\right) \\ &= \int_0^{S_\mathrm{D}} \frac{1}{\boldsymbol{K_1}} \left(\frac{\boldsymbol{X_w X_{SCF}} \cdot S}{W}\right)^{m_1} f_{S,\mathrm{lse}}\left(S\middle|U, \sigma_{U,\mathrm{exp}}(U,\theta), \alpha = 0.2, \rho_\mathrm{c}, \varphi_\mathrm{c}\right) dS \\ &+ \int_{S_\mathrm{D}}^{\infty} \frac{1}{\boldsymbol{K_2}} \left(\frac{\boldsymbol{X_w X_{SCF}} \cdot S}{W}\right)^{m_2} f_{S,\mathrm{lse}}\left(S\middle|U, \sigma_{U,\mathrm{exp}}(U,\theta), \alpha = 0.2, \rho_\mathrm{c}, \varphi_\mathrm{c}\right) dS \end{aligned} \tag{29}$$

The model uncertainties $\boldsymbol{X_w}$ and $\boldsymbol{X_{SCF}}$ in the LSE are related to wind load effects and local stress analysis, respectively, and the point where the slope changes in the SN-curve is determined by $\Delta\sigma_\mathrm{D}$. The turbulence experienced by the turbine ($\sigma_{U,\mathrm{exp}}$) is assessed by Eq. (30) where $\boldsymbol{X_{wake}}$ models uncertainty related to Frandsen's 'wake added turbulence model'.

[g] This assumption follows the recommendation in the IEC standard,[1] where the inconsistency with Eq. (1) is also present.

$$\sigma_{U,\mathrm{exp}}(U,\theta) = \sqrt{\boldsymbol{X}_{\mathbf{wake}} \frac{U^2}{\left(1.5 + \frac{0.8\mathrm{RD}}{\sqrt{\mathrm{C_T}(U)}}\right)^2} + \sigma_{U,\mathrm{amb}}(U,\theta)^2} \tag{30}$$

All uncertainties are modelled in accordance with Table 8.[5]

Table 8. Stochastic models used for reliability assessment taken from Sørensen et al.[5]

Variable	Distribution	Expected value	Standard deviation
$\boldsymbol{\Delta}$	Normal	1	0.30
$\boldsymbol{X_{\mathrm{w}}}$	Lognormal	1	0.15
$\boldsymbol{X_{\mathrm{SCF}}}$	Lognormal	1	0.10
$\boldsymbol{\log K_1}$	Normal	Determined from $\Delta\sigma_{\mathrm{D}}$	0.20
$\boldsymbol{\log K_2}$	Normal	Determined from $\Delta\sigma_{\mathrm{D}}$	0.25
$\boldsymbol{X_{\mathrm{wake}}}$	Lognormal	1	0.15
$\boldsymbol{\log K_1}$ and $\boldsymbol{\log K_2}$ are fully correlated*			

*The characteristic values are assumed defined by the mean of $\boldsymbol{\log K}$ minus two standard deviations of $\boldsymbol{\log K}$.

To determine the load effect range distribution ($f_{S,\mathrm{lse}}$) across all sites a comprehensive model has been established by simulating a grid of windspeed and turbulence values discretized by 1m/s and 0.05m/s, respectively. For each combination 32 turbulent seeds have been used resulting in a total of 81,696 simulations. In all simulations wind shear, air density and flow inclination were set to the design recommendations in the IEC standard of 0.2, 1.225kg/m^3, and 0.0°, respectively. This is expected to have very limited influence on the results as wind shear has almost no impact on tower fatigue loads compared to turbulence.[8,13] To emphasize this the variation of tower bottom fatigue loads with respect to each wind climate parameter is shown in Figure 8.

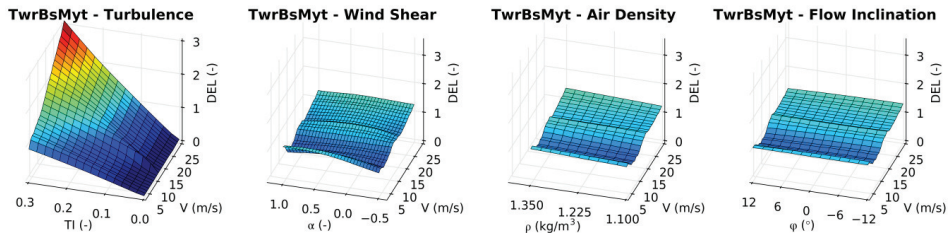

Figure 8: Tower bottom fore-aft fatigue load variation with turbulence, wind shear, air density, and flow inclination. The DELs are estimated using 100 seeds and normalized with design class IIB loads.

6.2. Structural reliability of the steel tower

To validate the proposed directional design a reference reliability index (β_{ref}) is defined. For this, $W_{\mathrm{b,sect}}$ is considered as the design value while the load effect range distribution at each windspeed and turbulence pair is based on the fore-aft moment independent of direction. This corresponds directly to the method described in the IEC background document for partial

safety factors[31]. The reliability is presented in terms of the lifetime reliability ($\beta_{\mathrm{ref},20}$) and the annual reliability in the last year of service ($\Delta\beta_{\mathrm{ref},20}$), which is approximated by Eq. (31), where $\beta_{\mathrm{ref},19}$ is the reliability index corresponding to the accumulated probability of failure at year 19.

$$\Delta\beta_{\mathrm{ref},20} = -\Phi^{-1}\left(\Phi\left(-\beta_{\mathrm{ref},20}\right) - \Phi\left(-\beta_{\mathrm{ref},19}\right)\right) \tag{31}$$

The resulting reliability indices across all available sites are shown in Figure 9.

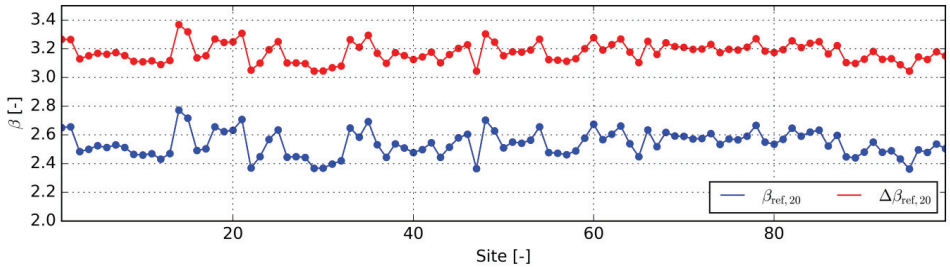

Figure 9: Reliability indices for the steel tower based on a traditional fatigue assessment method using tower fore-aft moments independent of direction.

The importance of the uncertainties is evaluated by their sensitivity factors (α_s), defined as the partial derivative of the reliability index with respect to each uncertainty in the normalized space. This is shown in Eq. (32), where u_i represent a normalized stochastic variable i and u^* is the design point corresponding to $\beta_{\mathrm{ref},20}$.

$$\left.\frac{\partial\beta_{\mathrm{ref},20}}{\partial u_i}\right|_{u=u^*} = \alpha_{s,i} \tag{32}$$

The results are summarized as average values across all sites in Table 9, showing that the load effect uncertainties $\boldsymbol{X_{\mathrm{w}}}$ and $\boldsymbol{X_{\mathrm{SCF}}}$ are the most important followed by the strength related uncertainties, $\boldsymbol{\log K}$ and $\boldsymbol{\Delta}$.

Table 9. Relative importance of the considered uncertainties.

Uncertainty	$\boldsymbol{\Delta}$	$\boldsymbol{X_{\mathrm{w}}}$	$\boldsymbol{X_{\mathrm{SCF}}}$	$\boldsymbol{\log K}$	$\boldsymbol{X_{\mathrm{wake}}}$
Average sensitivity	-0.31	0.54	0.64	-0.43	0.16

The proposed directional design approach for the tower is validated by checking if it results in approximately the same reliability level as the traditional approach. The same LSE is utilized where the moment of resistance is taken as $W_{\mathrm{b,pmax}}$ and the moment range distribution is considering the directional variation (i.e. the distribution is taken at the critical point along the circumference).

None of the uncertainties change but the damage distribution on the two parts of the SN-curve is shifted. Compared to the traditional approach where 58% of the damage is accumulated at the lower part of the SN-curve on average, this is reduced to 48% for the directional approach. Considering the high importance of $\boldsymbol{\log K}$ this may affect the reliability index considerably

since a higher uncertainty is assumed for the lower part of the SN-curve where experimental data is most expensive. Additionally, the directional model accounts for both the tower fore-aft and side-side moments. This may influence the significant conservative bias by assessing fatigue loads using the characteristic turbulence. This conservatism was quantified in Slot et. al.[13] using the same measurements as considered in this paper.

In Figure 10 the lifetime reliability (β_{20}) and the reliability at the last year of service ($\Delta\beta_{20}$) for the directional approach are shown across all sites and compared to the reference values.

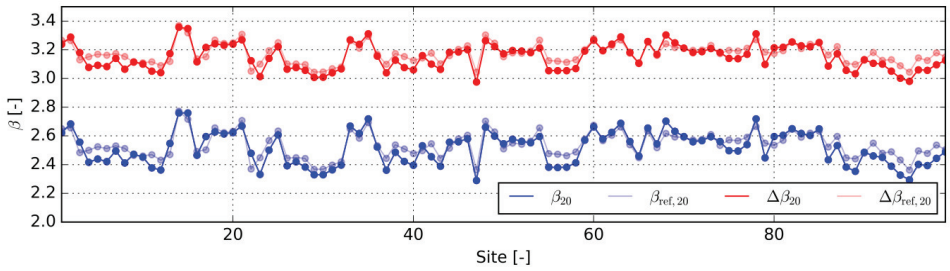

Figure 10: Reliability indices for the steel tower based on the directional fatigue assessment method with point-wise fatigue accumulation.

In Table 10 the results of the reliability analysis are summarized, confirming that both methods provide similar average reliability indices across all sites of $\Delta\beta_{\text{ave}}$~3.2 and $\beta_{20,\text{ave}}$~2.5. The minimum annual reliability index across the sites ($\Delta\beta_{20,\text{min}}$) is ~3.0 for both methods, which is slightly lower than the recommended annual reliability index of $\Delta\beta_{\text{min}} = 3.3$,[31] thereby indicating that larger partial safety factors should be applied for this specific turbine.

Table 10. Summary of reliability analysis of the steel tower.

Fatigue assessment method	$\Delta\beta_{20,\text{ave}}$	$\Delta\beta_{20,\text{min}}$	$\beta_{20,\text{ave}}$
Traditional	3.18	3.04	2.54
Directional	3.15	2.98	2.52

7. Conclusions

The implications of using the effective turbulence in site-specific fatigue assessment have been quantified by simulating a multi-megawatt wind turbine using wind data from 99 international meteorological masts. Five different methods have been developed, each designed to quantify the accuracy or consequence of the four key assumptions of the effective turbulence listed in Section 2.

The results in Section 3 document that component-specific effective turbulence leads to accurate and only slightly conservative fatigue assessments when linear SN-curves are

assumed, ranging from an average overprediction of 1% for the tower and yaw bearing to an average overprediction of 3% for the blades and 4% for the low speed shaft.

With focus on a steel tower, the consequence of assuming a linear SN-curve was quantified in Section 4. By performing sector-wise calculations it was found that using a bilinear SN-curve leads to an average reduction in the required moment of resistance of approximately 8%. A similar reduction was obtained by combining the effective turbulence simulations with bilinear SN-curves. This resulted in very accurate but slightly conservative predictions of the required moment of resistance within 1% on average compared to full sector-wise simulations.

The consequence of assuming unidirectional wind was quantified by accumulating fatigue damage point-wise along the tower circumference. This yielded an average reduction of ~12% of the required moment of resistance, but the reductions were very site-specific and only relevant when the wind is not concentrated in one direction.

In Section 6 the proposed directional approach for the tower design was shown not to compromise the structural integrity of the wind turbine compared to the traditional unidirectional approach. By a first order reliability method, similar annual reliability indices of ~3.2 were obtained for both methods.

Overall, the work presented provides a sound basis for decision making in fatigue assessment of wind turbines when it is uncertain whether sector-wise simulations are feasible at a given site-specific wind climate and farm layout. This may support the wind industry to move towards a more optimal balance between engineering effort, computational investment, and material consumption, thereby reducing the cost and environmental impact of wind energy when the entire lifecycle of wind turbines is taken into consideration.

Acknowledgement

The authors wish to thank the data providers: KNMI, ICDC, CliSAP/KlimaCampus, University of Hamburg, DTU, Vattenfall and VENTUS INGENIERÍA. The work presented is part of the project “From wind climate to wind turbine loads – efficient and accurate decision support and risk analysis” co-funded by EMD International A/S, Aalborg University, and the Innovationfund Denmark case number 5189-00022B. Their financial support is greatly appreciated.

References

1. IEC. International Standard IEC 61400-1 ed. 3, “Wind Turbines - Part 1 Design Requirements”. 2010.

2. Frandsen ST. *Turbulence and Turbulence- Generated Structural Loading in Wind Turbine Clusters.* Vol R-1188. Technical University of Denmark; 2007.

3. Henriksen SS, Malcolm DJ, Thomson J. Effective Turbulence in Wind Turbine Site Suitability Assessment. In: *European Wind Energy Conference and Exhibition 2012, EWEC 2012. 2.* ; 2012:959-966.

4. Veldkamp D. Chances in Wind Energy. PhD Thesis. 2006.

5. Sørensen JD, Frandsen S, Tarp-Johansen NJ. Effective turbulence models and fatigue reliability in wind farms. *Probabilistic Eng Mech*. 2008;23(4):531-538. doi:10.1016/j.probengmech.2008.01.009

6. Thomsen K, Sørensen P. Fatigue loads for wind turbines operating in wakes. *J Wind Eng Ind Aerodyn*. 1999;80(1-2):121-136. doi:10.1016/S0167-6105(98)00194-9

7. Mann J. Spectral velocity tensor in moderately complex terrain. *J Wind Eng Ind Aerodyn*. 2000;88(2-3):153-169. doi:10.1016/S0167-6105(00)00046-5

8. Dimitrov N, Natarajan A, Kelly M. Model of wind shear conditional on turbulence and its impact on wind turbine loads. *Wind Energy*. 2015;18(11):1917-1931. doi:10.1002/we.1797

9. Kelly M, Larsen G, Dimitrov NK, Natarajan A. Probabilistic Meteorological Characterization for Turbine Loads. *J Phys Conf Ser*. 2014;524:012076. doi:10.1088/1742-6596/524/1/012076

10. Sathe A, Mann J, Barlas T, Bierbooms WAAM, van Bussel GJW. Influence of atmospheric stability on wind turbine loads. *Wind Energy*. 2013;16(7):1013-1032. doi:10.1002/we.1528

11. Holtslag MC, Bierbooms WAAM, van Bussel GJW. Definition of the equivalent atmospheric stability for wind turbine fatigue load assessment. *J Phys Conf Ser*. 2014;524:1-10. doi:10.1088/1742-6596/524/1/012110

12. Svenningsen L, Slot RMM, Thøgersen ML. A novel method to quantify atmospheric stability. *J Phys Conf Ser*. 2018;1102. doi:10.1088/1742-6596/1102/1/012009

13. Slot RMM, Svenningsen L, Sørensen JD, Thøgersen ML. Importance of Shear in Site Assessment of Wind Turbine Fatigue Loads. *J Sol Energ*. 2018;140(4):041012. doi:10.1115/1.4039748

14. Stensgaard Toft H, Svenningsen L, Moser W, Dalsgaard Sørensen J, Lybech Thøgersen M. Wind Climate Parameters for Wind Turbine Fatigue Load Assessment. *J Sol Energ*. 2016;138(3). doi:10.1115/1.4033111

15. Argyle P, Watson S, Mantovon C, Jones I, Smith M. Modelling turbulence intensity within a large offshore wind farm. *Wind Energy*. 2018;21:1329-1343. doi:10.1002/we.2257

16. Reinwardt I, Gerke N, Dalhoff P, Steudel D, Moser W. Validation of wind turbine wake models with focus on the dynamic wake meandering model. *J Phys Conf Ser*. 2018;1037:1-11. doi:10.1088/1742-6596/1037/7/072028

17. Rychlik I. On the 'narrow-band' approximation for expected fatigue damage. *Probabilistic Eng Mech*. 1993;8(1):1-4. doi:10.1016/0266-8920(93)90024-P

18. Benasciutti D, Tovo R. Spectral methods for lifetime prediction under wide-band stationary random processes. *Int J Fatigue*. 2005;27(8):867-877. doi:10.1016/j.ijfatigue.2004.10.007

19. Jonkman JM, Butterfield S, Musial W, Scott G. *Definition of a 5-MW Reference Wind Turbine for Offshore System Development*. National Renewable Energy Laboratory; 2009.

20. Jonkman J. FAST An aeroelastic computer-aided engineering (CAE) tool for horizontal axis wind turbines. https://nwtc.nrel.gov/FAST [Accessed 2019-06-18]. Published 2015. Accessed April 3, 2017.

21. B. Jonkman NK. TurbSim A stochastic, full-field, turbulence simulator primarialy for use with InflowWind/AeroDyn-based simulation tools. https://nwtc.nrel.gov/TurbSim. Published 2016. Accessed April 3, 2017.

22. ASTM. ASTM No. E1049-85, "Standard Practice for Cycle Counting in Fatigue Analysis". 2011.

23. Murcia JP, Réthoré P, Dimitrov N, et al. Uncertainty propagation through an aeroelastic wind turbine model using polynomial surrogates. *Renew Energy*. 2017;119:910-922. doi:10.1016/j.renene.2017.07.070

24. Graf PA, Stewart G, Lackner M, Dykes K, Veers P. High-throughput computation and the applicability of Monte Carlo integration in fatigue load estimation of floating offshore wind turbines. *Wind Energy*. 2016;19:861-872. doi:110.1002/we.1870

25. Toft HS, Svenningsen L, Sørensen JD, Moser W, Thøgersen ML. Uncertainty in wind climate parameters and their influence on wind turbine fatigue loads. *Renew Energy*. 2016;90:352-361. doi:10.1016/j.renene.2016.01.010

26. Müller K, Cheng PW. Application of a Monte Carlo procedure for probabilistic fatigue design of floating offshore wind turbines. *Wind Energy Sci*. 2018;3(1):149-162. doi:10.5194/wes-3-149-2018

27. Tovo R. Cycle distribution and fatigue damage under broad-band random loading. *Int J Fatigue*. 2002;24(11):1137-1147. doi:10.1016/S0142-1123(02)00032-4

28. Dowling NE. *Fatigue Failure Predictions for Complicated Stress-Strain Histories*. Urbana, Illinois; 1971.

29. Welch P. The use of fast Fourier transform for the estimation of power spectra: A method based on time averaging over short, modified periodograms. *IEEE Trans Audio Electroacoust*. 1967;15(2):70-73. doi:10.1109/TAU.1967.1161901

30. Standard E. EUROPEAN STANDARD EUROPÄISCHE NORM Eurocode 3 : Design of steel structures - Part 1-9 : Fatigue. 2005:1-34.

31. IEC 61400-1. Safety Factors - IEC 61400-1 ed. 4 - background document. 2014.

Directional fatigue accumulation in wind turbine steel towers

RMM Slot[1,2], J Schwarte[3], L Svenningsen[1], JD Sørensen[2], and ML Thøgersen[1]

[1]EMD International A/S, Niels Jernes Vej 10, 9220 Aalborg, Denmark
[2]Dep. Of Civil Engineering, Thomas Manns Vej 23, 9220 Aalborg, Denmark
[3]Nordex Energy GmbH, Turbine Engineering, Am Vögensteich 23, 18057 Rostock, Germany

E-mail: rmms@civil.aau.dk

Abstract. Wind turbines are subject to fatigue loads during their entire lifetime of 20-25 years. A main source of the fatigue loads is the turbulence, which varies with direction due to the surrounding terrain and wake effects inside wind farms. A common approach to assess wind turbine fatigue loads is to simulate the structural response based on a site-specific wind climate, described in the IEC 61400-1 standard. To reduce the amount of needed simulations the standard introduces an "effective turbulence" approximation that integrates directional variation of turbulence, resulting in an omnidirectional value. This method implicitly assumes that all wind turbine components face the wind directly, which is a conservative simplification for components below the yaw bearing.

Using wind measurements from almost one hundred international sites, we show how this simplification leads to over-predictions of tower fatigue loads of up to 23% compared to directional fatigue accumulation. Three simplified models are developed to approximate the directional fatigue damage using various levels of information ranging from only the wind rose to full sector wise simulations. The first two recommended models may be used as proxies to decide if sector wise simulations are feasible, and the last model accurately predicts the full directional fatigue damage. The simplified models can contribute to a reduced material consumption of wind turbine towers, thereby reducing the cost of wind energy.

1. Introduction

Wind turbines experience fatigue loads during their lifetime of 20-25 years due to the fluctuating excitation from the turbulent wind field. An important task for engineers is therefore to verify that a given wind turbine design can withstand the site-specific fatigue loads in the entire design lifetime. For this purpose the design standard IEC 61400-1 ed. 3 [1] describes how a site-specific wind climate can be evaluated in terms of the windspeed distribution, windspeed standard deviation (turbulence), vertical windspeed variation (wind shear), air density, and flow inclination. Together, these parameters form the basis for simulating structural loads using aero-elastic codes, to check whether the site-specific fatigue loads are within the design loads of the considered wind turbine.

It is computationally expensive to simulate wind turbine loads, which makes it important to ensure that a site-specific wind climate is specified such that no excessive simulations are required. In the IEC standard[1] [1] this is addressed by adopting the "effective turbulence" approximation, first introduced by

[1] The design standard IEC 61400-1 ed. 3 is referred to as "IEC standard" in the remainder of the paper.

Frandsen [2], which integrates out the directional variation of the turbulence. The accuracy of the effective turbulence is beyond the scope of this paper but has been investigated in e.g. [3] using wind data from two existing wind farms, which showed good agreement between fatigue loads obtained by sector-wise and omnidirectional simulations. This was further confirmed in [4] where it was shown that combining the effective turbulence with bi-linear material fatigue strength models leads to accurate predictions of fatigue loads. However, neither [3] nor [4] investigated the consequence of neglecting directional variation of turbulence, which directly implies that fatigue damage is accumulated at the same point on a given component, regardless of the varying wind direction. This was shortly discussed in [5] stating that the rule of thumb in the industry was that neglecting directions overpredicted tower fatigue damage with 10%. As potential consequence wind turbine towers may have been over-designed for more than a decade, thereby increasing the cost of wind energy.

The aim of this work is to quantify the consequence of not taking wind direction into account when accumulating fatigue damage in a steel wind turbine tower. A modern multi-megawatt turbine is considered and wind measurements from 99 international sites are used to define real characteristic site-specific wind climates. The large number of sites is subsequently used to develop three simple models that approximate the directional fatigue damage based on different levels of information ranging from only the wind rose to full directional simulations. Together, these models form the basis for improved decision support when it is unclear if sector-wise simulations are worth the increased investment, compared to the expected material reduction by doing directional fatigue accumulation in the tower.

2. Wind measurements and site-specific wind climates

The site-specific wind climates used in this study are based on high quality 10 min. measurements of mean windspeed, mean wind direction, turbulence, and wind shear from 99 international sites. At all sites the measurements span exactly one year to account for seasonal variation and the surrounding terrain represent varying types of orography with and without nearby forest. Neither air density nor flow inclination has been measured and for consistency these parameters are fixed at all sites as $1.225\mathrm{kg/m^3}$ and 0.0°, respectively. This is a simplification but these two parameters have insignificant influence on wind turbine tower fatigue loads [6,7]. This setup was also used in [6] where a more detailed description of the sites and the measurements is presented.

To determine the characteristic site-specific wind climates according to the IEC standard [1], the wind measurements are grouped into windspeed bins of 1 m/s and 12 sectors (θ) covering 30° each. The characteristic turbulence ($\sigma_{U,c}$) is determined as the 90% quantile according to Eq. (1) using the windspeed and sector-wise turbulence mean value ($\sigma_{U,\mu}$) and standard deviation ($\sigma_{U,\sigma}$).

$$\sigma_{U,c}(U,\theta) = \sigma_{U,\mu}(U,\theta) + 1.28\sigma_{U,\sigma}(U,\theta) \tag{1}$$

The characteristic wind shear (α_c) is derived from the wind measurements as the mean value, and the windspeed distribution and sector frequencies are taken directly from the measurements.

To reflect that most modern turbines are installed in wind farms, artificial wake added turbulence has been considered. Neighbouring wind turbines are assumed located 5 rotor diameters (RD) up and downwind in the main wind direction, and 3 RD perpendicular to that. The wake added turbulence is modelled by Eq. (2) according to [1], where C_T is the thrust coefficient. Note that the wakes are assumed to cover an entire sector independent of the distance to the assumed neighbouring turbine. This simplification is not unrealistic as the main purpose of introducing the wakes is to have a directional variation of the turbulence that reflects modern utility turbines.

$$\sigma_{U,\mathrm{T}}(U,\theta) = \sqrt{\frac{U^2}{\left(1.5 + \frac{0.8RD}{\sqrt{C_\mathrm{T}(U)}}\right)} + \sigma_{U,c}(U,\theta)^2} \tag{2}$$

Finally, the characteristic turbulence values including wake contributions are used to calculate the damage equivalent effective turbulence according to Eq. (3), taken from [1], where m is the "Wöhler exponent" related to material fatigue strength.

$$\sigma_{U,\mathrm{eff}}(U,m) = \left(\int_0^{2\pi} \sigma_U^m(U,\theta) f_\theta(\theta|U) d\theta \right)^{1/m} \tag{3}$$

In table 1 the characteristic wind climate parameters are summarized.

Table 1. Characteristic wind climate parameters used for site-specific fatigue assessment.

Description	Measured	Characteristic value	Notation
Wind direction	Yes	Sector-wise frequency in 30° bins	f_θ
Windspeed	Yes	Windspeed frequency in 1m/s bins	f_U
Turbulence	Yes*	Windspeed and sector dependent 90% quantile including wake contribution	$\sigma_{U,\mathrm{T}}$
Wind shear	Yes	Mean value	α_c
Air density	No	Fixed value ($1.225\ \mathrm{kg/m^3}$)	ρ_c
Flow inclination	No	Fixed value (0.0°)	φ_c

**only the ambient turbulence is measured.*

3. Wind turbine simulation and fatigue assessment method

Fatigue damage is assessed by aero-elastic simulations of the 5MW reference wind turbine by NREL [8] during normal operation (design load case 1.2 in [1]). The turbine is simulated using FAST [9] and the turbulent wind fields are generated by TurbSIM [10], using 20 seeds for each combination of characteristic wind climate parameters.

The material fatigue strength of the steel tower is modelled by a linear SN-curve with a Wöhler exponent of 4, which relates a given stress range to the number of cycles to failure. To accumulate fatigue damage from varying stress ranges, linear summation by Miner's rule [1] is performed based on Rainflow counting [11] of the output response from the simulations. This allows the fatigue damage to be expressed in terms of a "damage equivalent load" (DEL) as defined in Eq. (4), where N_eq is an equivalent number of cycles set to 10^7 and n_i is the number of cycles with moment range ΔM_i.

$$\mathrm{DEL} = \left(\frac{1}{N_\mathrm{eq}} \sum_i n_i \Delta M_i^m \right)^{1/m} \tag{4}$$

The combined equivalent fatigue load of the tower (F_eq) from different windspeeds and directions can be combined according to Eq. (5), where U_in and U_out represent the cut-in and cut-out windspeed of the turbine, respectively.

$$F_\mathrm{eq}(f_\theta, f_U, U, \sigma_U, \alpha, \rho, \varphi, m) = \left(\int_0^{2\pi} f_\theta(\theta) \int_{U_\mathrm{in}}^{U_\mathrm{out}} f_U(U|\theta) \mathrm{DEL}(U, \sigma_U, \alpha, \rho, \varphi)^m \, d\theta dU \right)^{1/m} \tag{5}$$

4. Quantification of the consequence of neglecting direction

This section quantifies the consequence of not explicitly accounting for wind direction in fatigue accumulation of wind turbine towers. First, the method used to fully account for direction directly in the time domain is presented followed by a short discussion of the results.

To assess the directional fatigue damage the tower cross-section is divided into 36 equidistant points as shown in figure 1. For the sake of simplicity, the cross-section is assumed to be circular symmetric, hence, no door is considered. This is not expected to influence the conclusion of this paper, as the effect of the door is handled by local re-enforcements whereas the scope of this paper is the entire tower.

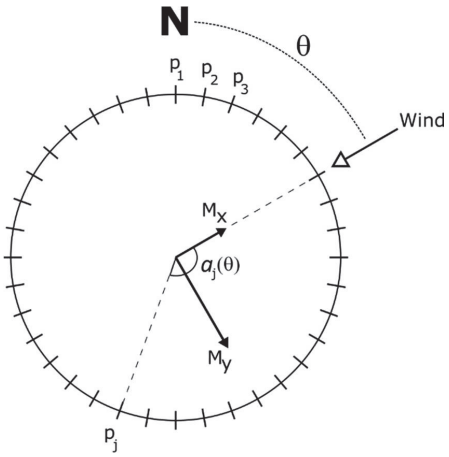

Figure 1: Sketch of the tower bottom cross-section (no door is considered).

For each simulated time step (t_s) the projected moment at each of the 36 points is evaluated by Eq. (6) where M_x is the tower side-side moment, M_y is the tower fore-aft moment, M_{p_j} is the projected moment at point p_j, and a_j is the angle between the wind direction and point p_j.

$$M_{p_j}(t_s, \theta) = M_x(t_s)\sin\left(a_j(\theta)\right) + M_y(t_s)\cos\left(a_j(\theta)\right) \tag{6}$$

Based on the projected moment time series the fatigue damage in the tower is evaluated at each point (F_{eq,p_j}) as outlined in Eq. (7).

$$F_{eq,p_j}\left(f_\theta, f_U, U, \sigma_{U,T}, \alpha_c, \rho_c, \varphi_c, m, \theta\right) = \left(\int_0^{2\pi} f_\theta(\theta) \int_{U_{in}}^{U_{out}} f_U(U|\theta)\mathrm{DEL}_{p_j}\left(U, \sigma_{U,T}, \alpha_c, \rho_c, \varphi_c, \theta\right)^m dU d\theta\right)^{1/m} \tag{7}$$

The point-wise damage equivalent load for each wind climate combination (DEL_{p_j}) is given by Eq. (8) where $\Delta M_{p_j,i}$ are the projected point-wise moment ranges.

$$\mathrm{DEL}_{p_j}(U, \sigma_{U,T}, \alpha_c, \rho_c, \varphi_c, \theta) = \left(\frac{1}{N_{eq}}\sum_i n_i \Delta M_{p_j,i}^m\right)^{1/m} \tag{8}$$

The critical point with the maximum combined fatigue damage ($F_{eq,p_{max}}$) is then assumed representative for the tower design, and the consequence of not taking direction into account is quantified as the fatigue damage ratio defined by Eq. (9).

$$\Delta F_{\mathrm{eq,eff}} = \frac{F_{\mathrm{eq,eff},y}(f_U, U, \sigma_{U,\mathrm{eff}}, \alpha_c, \rho_c, \varphi_c, m)}{F_{\mathrm{eq,p_{max}}}(f_\theta, f_U, U, \sigma_{U,\mathrm{T}}, \alpha_c, \rho_c, \varphi_c, m, \theta)} \tag{9}$$

Where $F_{\mathrm{eq,eff},y}$ is the site-specific tower fore-aft fatigue damage found by omnidirectional simulations, see Eq. (10).

$$\mathrm{F}_{\mathrm{eq,eff},y}(f_U, U, \sigma_{U,\mathrm{eff}}, \alpha_c, \rho_c, \varphi_c, m) = \left(\int_{U_{\mathrm{in}}}^{U_{\mathrm{out}}} f_U(U) \mathrm{DEL}_{\mathrm{eff},y}(U, \sigma_{U,\mathrm{eff}}, \alpha_c, \rho_c, \varphi_c)^m \, d\theta dU \right)^{1/m} \tag{10}$$

The damage equivalent load from the effective turbulence simulations at a given windspeed, $\mathrm{DEL}_{\mathrm{eff},y}$, is defined by Eq. (11) where $\Delta M_{\mathrm{eff},y,i}$ is found by Rainflow counting the fore-aft moment response.

$$\mathrm{DEL}_{\mathrm{eff},y}(U, \sigma_{U,\mathrm{eff}}, \alpha_c, \rho_c, \varphi_c) = \left(\frac{1}{N_{\mathrm{eq}}} \sum_i n_i \Delta M_{\mathrm{eff},y,i}^m \right)^{1/m} \tag{11}$$

Figure 2 shows the results of Eq. (9) across all 99 sites, where the average overprediction across the sites is 14% with a maximum of up to 23%. This documents that neglecting directional fatigue accumulation leads to unnecessary steel consumption at most real sites, but there is a significant variation from site to site. Since full sector-wise calculations require at least 12 times more simulations this motivates the need for simple approximate methods to assess the site specific overprediction, to provide decision support whether this increased computational cost is justified. Furthermore, the full method presented here requires postprocessing of the results from the aero-elastic simulations directly in the time domain (besides cycle counting), thereby introducing an extra step in the workflow from wind climate to wind turbine loads. To alleviate this effort, an accurate method is proposed that use traditional fore-aft and side-side fatigue loads from the sector-wise simulations, without losing any significant accuracy compared to the full method presented in this section.

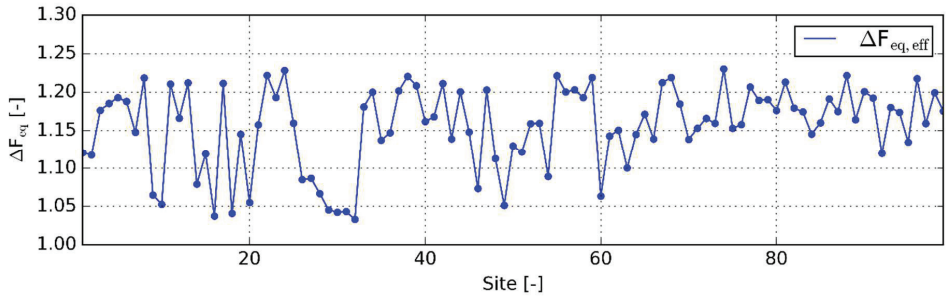

Figure 2: Overestimation of damage equivalent loads across all sites by doing omnidirectional fatigue assessment compared to explicitly accounting for direction.

5. Simplified framework to account for directional dependence of tower loads

In this section three models are developed to approximate the results of the full directional approach described in the previous section. Each model from one to three requires increased information and computational investment ranging from using the wind rose only to using sector-wise simulations.

5.1. Model 1: Spread of wind rose

A straightforward explanation for the large deviation of the overprediction of fatigue loads seen in figure 2 is the site-specific wind roses. When the wind is more unidirectional the overprediction is less

significant. This is illustrated in figure 3 where $F_{\mathrm{eq,eff}}$ is plotted as function of the site-specific max frequency of the wind across the 12 sectors ($f_{\theta,\max}$) for all 99 sites. Note that $f_{\theta,\max}$ is a very simple metric to describe the spread of the wind rose and it contains no information of the windspeed or turbulence distribution in the sectors which are both governing factors for the fatigue damage. This results in significant scatter in the datapoints, but the tendency that lower overpredictions follow with higher $f_{\theta,\max}$ is clear.

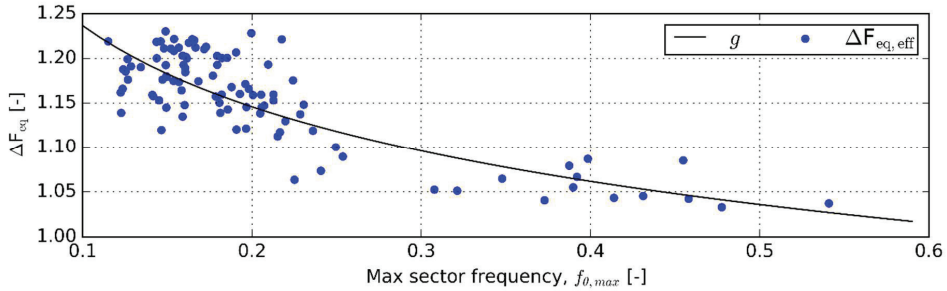

Figure 3: Overprediction of fatigue damage by not accounting for direction shown as function of the frequency of wind in the main direction.

By fitting a power function, g, to the observations a very simple tool for decision support is provided to predict if sector-wise simulations are feasible. The accuracy of this method is quantified by comparison to the full method as defined in Eq. (12), where the fitted function is given by Eq. (13).

$$\Delta F_{\mathrm{eq,M1}} = \frac{g^{-1}\left(f_{\theta,\max}\right) \cdot F_{\mathrm{eq,eff},y}(f_U, U, \sigma_{U,\mathrm{eff}}, \alpha_c, \rho_c, \varphi_c)}{F_{\mathrm{eq,p_{max}}}(f_\theta, f_U, U, \sigma_{U,\mathrm{T}}, \alpha_c, \rho_c, \varphi_c, \theta)} \tag{12}$$

$$g\left(f_{\theta,\max}\right) = 0.96 \cdot f_{\theta,\max}^{0.11} \tag{13}$$

5.2. Model 2: Omnidirectional simulations

To approximate $F_{\mathrm{eq,p_{max}}}$ directly based on fatigue load estimates from omnidirectional simulations, the simplified method described by Eq. (14) is proposed, where $f_\theta(\theta_k)$ is the frequency of wind measurements in sector k, a_j is the angle between sector k and point p_j, and $F_{\mathrm{eq,eff},x}$ describes the side-side bending fatigue damage from the omnidirectional simulations (estimated by the same procedure as $F_{\mathrm{eq,eff},y}$).

$$F_{\mathrm{eq,M2}}(f_\theta, f_U, U, \sigma_{U,\mathrm{eff}}, \alpha_c, \rho_c, \varphi_c, \theta) = \max_{\mathrm{p}_j}\left(\sqrt[m]{\sum_{k=1}^{12} f_\theta(\theta_k) \cdot \left|\sin\left(a_j(\theta_k)\right) F_{\mathrm{eq,eff},x} + \cos\left(a_j(\theta_k)\right) F_{\mathrm{eq,eff},y}\right|^m}\right) \tag{14}$$

To quantify the accuracy of this method the predictions are compared to the full method as defined in Eq. (15).

$$\Delta F_{\mathrm{eq,M2}} = \frac{F_{\mathrm{eq,M2}}(f_\theta, f_U, U, \sigma_{U,\mathrm{eff}}, \alpha_c, \rho_c, \varphi_c, \theta)}{F_{\mathrm{eq,p_{max}}}(f_\theta, f_U, U, \sigma_{U,\mathrm{T}}, \alpha_c, \rho_c, \varphi_c, \theta)} \tag{15}$$

5.3. Model 3: Sector-wise simulations

This last method is intended to accurately approximate the fatigue loads of the full method without explicitly accounting for the fore-aft and side-side moment interaction in the time domain. It is initially based on the assumption that the tower fore-aft and side-side moment accumulate fatigue damage fully independent, in which case the full method of assessing the fatigue damage boils down to the fatigue damage combination in Eq. (16).

$$F_{\mathrm{eq,indep}}(f_\theta, f_U, U, \sigma_{U,\mathrm{T}}, \alpha_\mathrm{c}, \rho_\mathrm{c}, \varphi_\mathrm{c}, \theta) = \max_{\mathrm{p_j}} \left(\sqrt[m]{\sum_{k=1}^{12} f_\theta(\theta_k) \cdot \left(\sqrt[m]{\left|\sin\left(a_j(\theta_k)\right) F_{\mathrm{eq},x,k}\right|^m + \left|\cos\left(a_j(\theta_k)\right) F_{\mathrm{eq},y,k}\right|^m} \right)^m} \right) \tag{16}$$

Where $F_{\mathrm{eq},x,k}$ represent the combined sector specific side-side fatigue damage as outlined in Eq. (17), with the side-side damage equivalent load ($\mathrm{DEL}_{x,k}$) defined by Eq. (18), where $\Delta M_{x,k,i}^m$ is found by counting the side-side moment response.

$$F_{\mathrm{eq},x,k}(f_U, U, \sigma_{U,\mathrm{T}}, \alpha_\mathrm{c}, \rho_\mathrm{c}, \varphi_\mathrm{c}, \theta_k) = \left(\int_{U_\mathrm{in}}^{U_\mathrm{out}} f_U(U|\theta_k) \mathrm{DEL}_{x,k}\left(U, \sigma_{U,\mathrm{T}}, \alpha_\mathrm{c}, \rho_\mathrm{c}, \varphi_\mathrm{c}\right)^m d\theta dU \right)^{1/m} \tag{17}$$

$$\mathrm{DEL}_{x,k}(U, \sigma_{U,\mathrm{T}}, \alpha_\mathrm{c}, \rho_\mathrm{c}, \varphi_\mathrm{c}) = \left(\frac{1}{N_\mathrm{eq}} \sum_i n_i \Delta M_{x,k,i}^m \right)^{1/m} \tag{18}$$

Equations (17) and (18) describe the sector-wise side-side fatigue damage, but the procedure is the same for the fore-aft fatigue damage ($F_{\mathrm{eq},y,k}$).

By checking the accuracy of Eq. (16) it was found that the assumption of independence leads to a slight non-conservative bias compared to the full method of ~1%. To calibrate the final version of model 3 a site-specific offset is therefore introduced by weighting the side-side loads slightly higher in the load combination by using a power of 2 instead of m as shown in Eq. (19).

$$F_{\mathrm{eq,M3}}(f_\theta, f_U, U, \sigma_{U,\mathrm{T}}, \alpha_\mathrm{c}, \rho_\mathrm{c}, \varphi_\mathrm{c}, \theta) = \max_{\mathrm{p}_j} \left(\sqrt[m]{\sum_{k=1}^{12} f_\theta(\theta_k) \cdot \left(\sqrt[2]{\left|\sin\left(a_j(\theta_k)\right) F_{\mathrm{eq},x,k}\right|^2 + \left|\cos\left(a_j(\theta_k)\right) F_{\mathrm{eq},y,k}\right|^2} \right)^m} \right) \tag{19}$$

The accuracy of the calibrated model 3 is quantified by comparison to the full method as defined in Eq. (20)

$$\Delta F_{\mathrm{eq,M3}} = \frac{F_{\mathrm{eq,M3}}(f_\theta, f_U, U, \sigma_{U,\mathrm{T}}, \alpha_\mathrm{c}, \rho_\mathrm{c}, \varphi_\mathrm{c}, \theta)}{F_{\mathrm{eq,p_{max}}}(f_\theta, f_U, U, \sigma_{U,\mathrm{T}}, \alpha_\mathrm{c}, \rho_\mathrm{c}, \varphi_\mathrm{c}, \theta)} \tag{20}$$

5.4. Summary of the developed models

In Table 2 an overview of the three simplified methods is presented. For comparison the computational time is specified in a relative sense (Relative cost), as the actual computational time is highly dependent on the aero-elastic code and specific turbine that is considered.

Table 2. Simplified methods to account for directional fatigue damage variation.

Simplified approach	Accuracy assessment*	Relative cost	Short description
Model 1 - Eq. (12)	$\Delta F_{\mathrm{eq,M1}}$	0	Proxy to assess the overprediction with no information of actual loads.
Model 2 - Eq. (15)	$\Delta F_{\mathrm{eq,M2}}$	1/12	Proxy to predict the fatigue damage of the full model by omnidirectional simulations.
Model 3 - Eq. (19)	$\Delta F_{\mathrm{eq,M3}}$	1	Accurate model to evaluate the fatigue damage of the full model without projecting moment time series.

**The accuracy of all methods is evaluated with respect to the same fatigue damage obtained by the full model for comparison.*

Note that model 3 requires the same amount of simulations as the full method making it very suitable for e.g. response surface methods to predict the fatigue loads based on pre-run simulations [12,13].

6. Results and recommendations

The results of applying the three developed models across all 99 sites are shown in figure 5 and summarized in Table 3. For comparison the results of using the omnidirectional effective turbulence are also presented, which show that the developed model results are more accurate at all sites. Care should be taken though, as both model 1 and 2 result in non-conservative fatigue assessments at some of the sites. Based on the observations the following recommendations are considered by the authors:

Model 1 *– Spread of wind rose*:
Using information of the wind rose only, this model provides an initial estimate of the consequence of neglecting direction when accumulating fatigue damage. A core benefit of this model is that it requires no expert knowledge of wind turbine simulation. The accuracy is comparable to the second method, but it cannot be used to predict fatigue loads directly. Instead, it may be used either to decide if omnidirectional simulations should be skipped entirely, or in conjunction with the results from the second method to assess whether directional simulations are feasible at the specific turbine location.

Model 2 *– Omnidirectional simulations:*
Using omnidirectional fatigue loads an estimate of the actual directional fatigue damage is obtained, but since the method may lead to non-conservative assessments it is only recommended as a proxy to decide if sector-wise simulations are justifiable. In contrast to the first approach, a clear benefit of this method is that it allows the designing engineer to compare the expected material savings in the fatigue limit state with the margins from other design load cases. The importance of this is illustrated by the following simple example: The initial simulations show that the ultimate limit state governs the tower design, hence, any expected reduction in material consumption in the fatigue limit state is irrelevant.

Model 3 *– Sector-wise simulations:*
This last model may be used directly to predict fatigue loads within 1% of the full method across all analysed sites. The computational cost is the same as for the full method, but it alleviates the designing engineers for the extra step in the workflow from wind climate to wind turbine loads of computing projected moments.

Table 3. Summarized results of all simplified methods.

Simplified approach	ΔF_{eq} minimum [-]	ΔF_{eq} Maximum [-]	ΔF_{eq} Average [-]	ΔF_{eq} Std.dev. [-]
Effective turbulence	1.033	1.230	1.156	0.053
Model 1	0.940	1.076	1.004	0.027
Model 2	0.938	1.097	1.013	0.029
Model 3	0.995	1.001	0.999	0.001

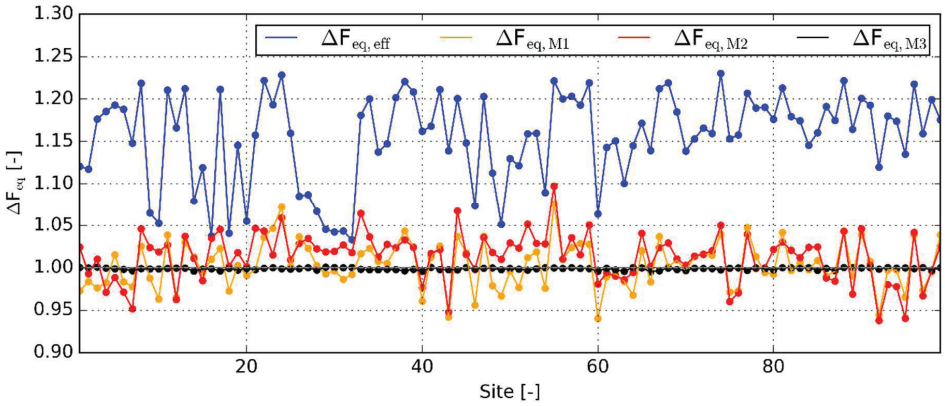

Figure 4: Results of analysing all 99 sites using the effective turbulence approximation (blue) and the three simplified models (yellow, red, and black) compared to the full directional approach.

7. Conclusions

Fatigue assessment of wind turbine components is commonly based on simulations using omnidirectional effective turbulence to limit computational time. This approach implicitly assumes that fatigue damage accumulates independently of the wind direction, which is a simplification for all components below the yaw bearing. Using wind measurements from 99 real sites this assumption has been shown to overestimate DELs by an average of 14% for wind turbine steel towers, compared to explicitly accounting for direction in the fatigue accumulation.

Utilizing the large number of available sites three simplified models have been developed to approximate the full sector-wise model. Model 1 is based only on wind measurements which makes it accessible to wind and site engineers without expert knowledge of wind turbine simulation. The method can predict the actual overprediction within 8% of the full model. Model 2 is based on results of omnidirectional simulations, making it possible to predict the actual fatigue loads of the full model within 10%. Both models 1 and 2 show promising results, but for some sites they are non-conservative, hence, they should only be used as proxies to decide if full sector-wise simulation are justified at the considered site and turbine location. The third method accurately predicts the directional fatigue damage using sector wise simulations, but without explicitly accounting for tower fore-aft and side-side bending in the time domain. This method captures the fatigue loads of the full model within 1% without any bias and is regarded as accurate as the time-based calculation.

The models and results that have been presented in this work may contribute to an overall reduction in the steel consumption of wind turbine towers, thereby reducing the cost of wind energy and the environmental impact of wind turbines when the entire life-cycle is considered.

Acknowledgement
The authors wish to thank the data providers; KNMI, ICDC, CliSAP/Klima-Campus, University of Hamburg, DTU, Vattenfall, and VENTUS INGENIERÍA. The presented work is part of the project "From wind climate to wind turbine loads – Efficient and accurate decision support and risk analysis" cofounded between Innovation Fund Denmark, EMD International A/S, and Aalborg University. Their financial support is greatly appreciated.

References

[1] IEC. 2010 International Standard IEC 61400-1 ed. 3, "Wind Turbines - Part 1 Design Requirements".
[2] Frandsen S T 2007 *Turbulence and turbulence- generated structural loading in wind turbine clusters* (Technical University of Denmark)
[3] Henriksen S S, Malcolm D J and Thomson J 2012 Effective Turbulence in Wind Turbine Site Suitability Assessment *European Wind Energy Conference and Exhibition 2012, EWEC 2012. 2.* pp 959–66
[4] Sørensen J D, Frandsen S and Tarp-Johansen N J 2008 Effective turbulence models and fatigue reliability in wind farms *Probabilistic Eng. Mech.* **23** 531–8
[5] Veldkamp D 2006 *Chances in Wind Energy* (Delft University)
[6] Slot R M M, Svenningsen L, Sørensen J D and Thøgersen M L 2018 Importance of Shear in Site Assessment of Wind Turbine Fatigue Loads *J Sol Energ* **140** 041012
[7] Dimitrov N, Natarajan A and Kelly M 2015 Model of wind shear conditional on turbulence and its impact on wind turbine loads *Wind Energy* **18** 1917–31
[8] Jonkman J, Butterfield S, Musial W and Scott G 2009 *Definition of a 5-MW reference wind turbine for offshore system development* (NREL/TP-500-38060)
[9] Jonkman J 2015 FAST An aeroelastic computer-aided engineering (CAE) tool for horizontal axis wind turbines
[10] B. Jonkman N K 2016 TurbSim A stochastic, full-field, turbulence simulator primarialy for use with InflowWind/AeroDyn-based simulation tools
[11] ASTM 2011 ASTM No. E1049-85, "Standard Practice for Cycle Counting in Fatigue Analysis".
[12] Toft H S, Svenningsen L, Moser W, Sørensen J D and Thøgersen M L 2016 Assessment of wind turbine structural integrity using response surface methodology *Eng. Struct.* **106** 471–83
[13] Murcia J P, Réthoré P-E, Dimitrov N, Natarajan A, Sørensen J D, Graf P and Kim T 2017 Uncertainty propagation through an aeroelastic wind turbine model using polynomial surrogates *Renew. Energy* **119** 910–22

Surrogate Model Uncertainty in Wind Turbine Reliability Assessment

René M. M. Slot[1,3], John D. Sørensen[1], Bruno Sudret[2], Lasse Svenningsen[3], and Morten L. Thøgersen[3]

[1]Department of Civil Engineering, University of Aalborg, Aalborg, 9220, Denmark
[2]Chair of Risk, Safety and Uncertainty quantification, ETH, Zürich, Switzerland
[3]EMD International A/S, Aalborg, 9220, Denmark

Correspondence to: René M. M. Slot (rmms@civil.aau.dk)

Abstract. Lowering the cost of wind energy entails an optimization of material consumption of wind turbine components without compromising structural safety. Typically, wind turbines are designed by the partial safety factor method which is calibrated by full probabilistic models and presented in the IEC 61400-1 design standard. This approach significantly reduces the amount of aero-elastic simulations required to assess the fatigue limit state of wind turbines, but it may lead to inconsistent reliability levels across wind farm projects. To avoid this, wind turbines may be designed by full probabilistic methods using surrogate models to approximate fatigue load effects. Doing so, it is important to quantify and model all relevant uncertainties including that of the surrogate model itself. Here we quantify this uncertainty according to Eurocode 1990 for polynomial chaos expansion (PCE) and Kriging using wind data from 99 real sites and the 5MW reference turbine by NREL. We investigate a wide range of simulation efforts used to train the surrogates and our results show that Kriging yields a higher accuracy per invested simulation compared to PCE. This improved understanding of using PCE and Kriging in fatigue reliability assessment may significantly benefit decision support in full probabilistic design of wind turbines.

Key words: Wind turbine, Fatigue loads, Structural reliability, Surrogate models, Model uncertainty

1. Introduction

To lower the cost of wind energy it is important to utilize wind turbines to their full load bearing capacity but without compromising structural safety. A typical design approach is to follow the partial safety factor method, calibrated by full probabilistic models and presented in standardized codes as the IEC 61400-1 design standard for wind turbines[1]. This semi-probabilistic approach accounts for variability and uncertainty in strength and load parameters by using characteristic values defined by quantiles. A final design equation is then adjusted by partial safety factors to meet a target structural reliability level which is defined with consideration of economic loss and risk of human lives to optimize material consumption from a societal point of view.[2] This simplified framework provides a direct advantage in computational requirements to assess whether a given wind turbine class is suited for a particular site and park layout; However, it may lead to inconsistent reliability levels as the simple characteristic input cannot fully explain the variation of the load response.[3,4] To cover

all relevant structural components partial safety factors are therefore typically calibrated based on conservative assumptions. As a result, it can be expected that wind turbines in general are over-designed thereby leading to a higher cost of wind energy than necessary. To avoid this excess use of materials site-specific assessment of wind turbines may be directly based on a full probabilistic analysis as described in the recent 4th edition of the IEC 61400-1 design standard[1].

The main challenge in full probabilistic analysis of wind turbines is the need for significantly more load evaluations than the safety factor approach. In particular, fatigue analysis during normal operation (Design load case 1.2[1]) involves an infeasible amount of load simulations as fatigue damage accumulates during the whole lifetime of the turbine. It is therefore necessary to assess the integrated fatigue load across the entire joint wind climate distribution. For onshore wind turbines this includes at least wind direction (θ), wind speed (U), turbulence (σ_U), vertical wind shear exponent (α), air density (ρ), and flow inclination (φ).[5] Consequently, the sheer amount of aero-elastic simulations that needs to be carried out to fully evaluate the lifetime fatigue load imposes a computational barrier to probabilistic design.[6] To circumvent this barrier a shortcut from wind climate to wind turbine fatigue loads is required.

Various methods have been proposed to simplify wind turbine fatigue load assessment using surrogate models, also referred to as meta-models, response surfaces or proxies. This motivated Dimitrov et al.[7] to benchmark the accuracy of several surrogate techniques against each other. Their emphasis was prediction of lifetime fatigue loads by importance sampling, quadratic regression, nearest-neighbour interpolation, polynomial chaos expansion (PCE) and Kriging. Overall, they found Kriging and PCE to be superior, with Kriging having the highest accuracy overall, but also an increased computational time compared to PCE when predicting new samples.

Surrogate models make it feasible to carry out full probabilistic design of wind turbines. In Toft et al.[8] a quadratic response surface was used for reliability analysis of onshore wind turbines with focus on modelling wind climate uncertainties. Morató et al.[9] established a Kriging surrogate model to capture Von Mises stresses in a reliability analysis of offshore wind turbines in the ultimate limit state. In addition, they investigated the influence of the number of samples and seeds that were used to calibrate the model. With focus on offshore wind turbine fatigue loads Teixeira et al.[10] used a Kriging model to analyse the importance of different wind and wave climate parameters. In Murcia et al.[11] the uncertainty propagation properties of PCE was used to analyse the sensitivity of the wind climate on the power output and structural response of an onshore turbine. Focussing on blade design Hu et al.[12] proposed a reliability based design optimization which relied on multiple Kriging surrogate models to predict fatigue loads in critical structural hotspots. They included wind climate uncertainty, both spatial and temporal, while also considering manufacturing uncertainties of the composite laminate.

A common goal of the previous literature on wind turbine fatigue reliability is to establish novel reliability models and quantify the long chain of uncertainties from wind climate to wind turbine load effects. In this context, an important uncertainty is still missing in the literature; namely that of using a surrogate model to approximate fatigue loads instead of performing direct aero-elastic simulations. The scope of this paper is to study this uncertainty using wind measurements from 99 real wind turbine sites. This provides a solid basis to quantify a general uncertainty model for future applications. In this work PCE and Kriging are considered due to

their very promising capability in terms of capturing fatigue loads, propagating uncertainty and carrying out sensitivity analyses. The two techniques also represent two main approaches to predict a model output, namely regression (PCE) and interpolation (Kriging).

2. Wind Measurements

High quality measurements of wind direction, windspeed, turbulence, and wind shear from 99 real wind turbine sites are used in this study. All measurements are from meteorological masts or from wind power projects and represent a wide spread in geographical location and terrain complexity with and without nearby forestry. The measurements were also used by Slot et. al.[3] where a detailed description of the data may be found.

2.1. Ambient joint wind climate

The site-specific joint distribution of wind direction, windspeed, turbulence, and wind shear is described in terms of conditional distributions as summarized in Table 1. Measurements leading to air density and flow inclination were unavailable at most sites. Instead air density time series have been estimated from a meso-scale model while flow inclination is modelled as a fixed value dependent on the site-specific orography, see Table 2. These simplifications are not expected to have a significant effect given the low importance of both air density and flow inclination on site-specific fatigue loads compared to wind speed, turbulence and wind shear.[3,4,13]

Table 1: Joint wind climate distribution

Wind climate parameter	Notation	Description
Wind direction	$P_\theta(\theta)$	Discrete distribution[5]
Wind speed	$f_U(U\|\theta)$	Weibull distribution[5]
Turbulence[a]	$f_{\sigma_U}(\sigma_U\|U,\theta)$	Lognormal distribution[5]
Wind shear	$f_\alpha(\alpha\|\sigma_U,U,\theta)$	Normal distribution[4,13]
Air density	$f_\rho(\rho)$	Normal distribution[4]
Flow inclination	φ	Fixed value

To define the conditional distributions of wind speed the wind direction is binned into 12 sectors covering 30° each as recommended in the IEC 61400-1 standard[5]. The conditional distributions of turbulence are determined by further binning wind speed by 1 m/s. To model wind shear dependent on direction, wind speed and turbulence the procedure described in Dimitrov et al.[13]

[a] A Weibull distribution may also be considered as recommended in the IEC 61400-1 ed. 4 design standard.

is adopted. In each wind speed and direction bin all turbulence samples are ranked and divided into five equally sized bins, each assumed to represent a width of 0.2 of the turbulence cumulative distribution function. Subsequently a wind shear distribution is fitted to the shear values in each of the turbulence bins.

To define the turbulence and wind shear distributions the first and second moments of the available data are required. To obtain robust estimates only direction and wind speed bins with 50 or more samples are considered. For bins with less than 50 samples the distribution parameters are extrapolated in order to get a full description of the joint wind climate. Following the IEC 61400-1 standard[1] the mean value (μ_{σ_U}) and standard deviation (σ_{σ_U}) of the turbulence distribution are extrapolated by linear models as described by Eqs. (1) and (2).

$$\mu_{\sigma_U}(U|\theta) = a_{\mu_\sigma}(\theta) \cdot U + b_{\mu_\sigma}(\theta) \tag{1}$$

$$\sigma_{\sigma_U}(U|\theta) = a_{\sigma_\sigma}(\theta) \cdot U + b_{\sigma_\sigma}(\theta) \tag{2}$$

The mean value of the wind shear distribution (μ_α) is approximated as the median of μ_α at the three highest accepted wind speed bins given direction and turbulence. This imitates that atmospheric stability typically turn towards neutral conditions at medium to high wind speeds where the mean wind shear becomes constant.[14] Finally, the standard deviation of the wind shear distribution is extrapolated inversely proportional to wind speed as shown in Eq. (3).[15] All model parameters a, b, and c in are fitted based on the available data in accepted bins.

$$\sigma_\alpha(U|\theta, \sigma_U) = \frac{c_\alpha(\theta, \sigma_U)}{U} \tag{3}$$

Table 2: Flow inclination model

Site-specific orography	Flat terrain	Hilly terrain	Steep terrain
Fixed flow inclination	0°	6°	12°
Number of sites	62	27	10

2.2. Wake added turbulence

All the included measurements represent ambient climates. This does not reflect the reality of most turbines, where wakes are present in some directions. Wake added turbulence is therefore considered by assuming a rectangular grid layout where a neighbouring turbine is placed 5 rotor diameters (RD) up- and downwind in the main wind direction, and 3 RD perpendicular to that. The wake added turbulence ($\sigma_{U,wake}$) is modelled according to the IEC 61400-1 standard[1] as outlined in Eq. (4), where C_T is the thrust coefficient.

$$\sigma_{U,wake}(U,\theta) = \frac{U}{1.5 + \frac{0.8\,RD(\theta)}{\sqrt{C_T(U)}}} \tag{4}$$

To significantly limit the required computations in this paper without loss of generality the wakes are assumed to perfectly align with the defined sectors regardless of the distance between the two turbines. This is a simplification but the main purpose of introducing the wakes is to reflect a real case representative range of turbulence values. The ambient and wake added turbulence may be combined to the total turbulence that is experienced by the turbine ($\sigma_{U,T}$) by Eq. (5).

$$\sigma_{U,T}(U,\theta) = \sqrt{\sigma_U(U,\theta)^2 + \sigma_{U,wake}(U,\theta)^2} \tag{5}$$

3. Probabilistic Model for Fatigue Failure

The main objective of a probabilistic design approach is to assess the structural reliability of a given failure mode and check if it meets the target reliability level. This requires a representative limit state equation (LSE) to calculate the failure probability which cover relevant uncertainties on strengths and loads. In this section a simple yet representative LSE for wind turbine fatigue failure is presented.

3.1. Wind turbine simulation and fatigue loads

To define a representative LSE it is relevant to discuss how fatigue loads are calculated. In this paper the framework of "damage equivalent loads" (DEL) is adopted. It is therefore implicitly assumed that fatigue strength of materials is modelled by a linear SN-curve and that Miner's rule[16] may be used to accumulate fatigue damage from varying load effect amplitudes.

All fatigue loads are based on 10 min effective[b] simulations of the 5MW reference wind turbine by NREL[17] using its baseline controller. The turbine is simulated in the aero-servo-elastic software FAST[18] and each realized wind field is computed in TurbSIM[19] using the Kaimal spectrum[20]. The output of the simulations are timeseries of load effects for various sensors on the main components of the turbine, which are reduced to a spectrum of load effect amplitudes (ΔF_i) and a corresponding number of cycles (n_i) by Rainflow counting.[21] This is then further condensed to a single scalar, the DEL, which represents the load effect range that produces the same fatigue damage as the entire spectrum. The DEL is outlined in Eq. (6) where the wind climate parameters except turbulence are gathered in the vector $\boldsymbol{C} = [U, \alpha, \rho, \varphi]$ to ease notation. The equivalent number of cycles, N_{eq}, is used as a reference value and may be selected arbitrarily if it is kept the same when comparing different DELs.

[b] The term "effective" is used to indicate that transient start-up behaviour is removed.

$$DEL(\boldsymbol{C}, \sigma_{U,T}) = \left(\frac{1}{N_{eq}} \sum_i n_i \Delta F_i^m \right)^{1/m} \quad (6)$$

The combined site-specific equivalent fatigue load (F_{eq}) with a one year reference period may be assessed by Eq. (7) where f_{Site} models the joint wind climate distribution and $c_{sim} = \frac{1year}{T_{sim}}$ is a correction factor accounting for the simulation time (T_{sim}).

$$F_{eq,direct} = \left(c_{sim} \sum_\theta P_\theta(\theta) \int_{\sigma_U} \int_{\boldsymbol{C} \in \mathbb{R}^4} f_{Site}(\boldsymbol{C}, \sigma_U | \theta) DEL\left(\boldsymbol{C}, \sigma_{U,T}\right)^m d\boldsymbol{C} d\sigma_U \right)^{1/m} \quad (7)$$

To limit the amount of results that are shown in this paper only the six main sensors listed in Table 3 are considered. The sensors represent varying sensitivities to the wind climate parameters and controller actions and reflect the overall path of the wind loads from acting on the blades until being reacted by the soil. The fatigue strength of each component is modelled by typical Wöhler exponents used in the literature.[4,11,13,22]

Table 3: Wind turbine sensors

Component	Sensor description	Notation	Unit	Wöhler exponent
Blade	Blade root flap-wise bending	RootMyb1	kNm	10
Blade	Blade root edge-wise bending	RootMxb1	kNm	10
Main shaft	Low speed shaft torque	LSSGagMxa	kNm	6
Tower (top)	Yaw bearing tilt	YawBrMyp	kNm	4
Tower (top)	Yaw bearing yaw	YawBrMzp	kNm	4
Tower (bottom)	Tower bottom fore-aft bending	TwrBsMyt	kNm	4

3.2. Limit state equation

Following the described approach of evaluating fatigue loads directly by aero-elastic simulations a LSE for fatigue failure (g_{direct}) is defined as shown in Eq. (8).[22,23]

$$g_{direct}(z, t) = \Delta - \frac{N_{eq} t}{K} \left(X_{Load} X_{SCF} \frac{F_{eq,direct}}{z} \right)^m \quad (8)$$

Here z is the design parameter relating load effects to stresses and t is time in years. The model uncertainties Δ and K account for Miner's rule and the SN-approach respectively, and X_{Load}

and X_{SCF} models the uncertainty on wind load effects and stress concentration factors[c]. Typical examples of the model uncertainties are presented in Table 4.[8,22,23]

Table 4. Stochastic models

Variable	Distribution	Expected value	Standard deviation		
			m=4	m=6	m=10
Δ	Normal	1	0.30	0.40	0.50
X_{Load}	Lognormal	1	0.15	0.15	0.15
X_{SCF}	Lognormal	1	0.10	0.15	0.15
$\log K$	Normal	-	0.20	0.15	0.25

Based on the LSE the accumulated failure probability (P_f) and associated reliability index (β) of the considered component may be estimated by Eq. (9), where Φ is the cumulative standard normal distribution.

$$P_f = \Phi(-\beta) = P(\mathrm{g}_{direct}(z,t) \leq 0) \tag{9}$$

To evaluate the failure probability the accumulated fatigue damage across the entire joint wind climate has to be estimated. Direct aero-elastic simulation for this application is extremely computationally demanding, and in most cases unfeasible. This barrier may be overcome by accurate surrogate models to predict DELs as discussed in the introduction. Surrogates makes it possible to evaluate the site-specific fatigue loads but with a reduced accuracy compared to direct simulation ($F_{eq,proxy}$). This should be properly accounted for in the LSE by introducing an additional model uncertainty related to the surrogate model itself (X_{Proxy}). The model uncertainty is related to the load effect, similar to X_{Load} and X_{SCF}, and is applied alongside these as shown in Eq. (10).

$$\mathrm{g}_{Proxy}(\mathrm{z},\mathrm{t}) = \Delta - \frac{N_{\mathrm{eq}} t}{K}\left(X_{Load} X_{SCF} X_{Proxy} \frac{F_{eq,proxy}}{z}\right)^m \tag{10}$$

4. Surrogate Models for Fatigue Load Prediction

The surrogate model uncertainty will depend on the surrogate model type and how many simulations that have been invested in training it.[7] Two surrogate techniques are included in this work namely Kriging and PCE, and both are implemented in the general purpose uncertainty quantification framework UQLab[24]. This section outlines the input domain and the experimental design that is used for training the models followed by a brief summary of each surrogate technique with emphasis on how they are configured in this specific work. For a more general explanation of the details and theory behind Kriging we refer to Santner et al.[25] and for PCE we refer to Sudret[26].

[c] The linear relationship between load effects and stresses is based on simple beam theory. To account for non-linear effects a "stress concentration factor" is typically applied.

4.1. Input domain and experimental design

Regardless of the choice of surrogate model it is necessary to sample an experimental design. This requires an input domain that covers the joint wind climate distributions across all 99 sites as to avoid extrapolation by the surrogates which may lead to very unpredictable results. Meanwhile, the input domain should also encompass "physically realistic" wind climate combinations to ensure validity of the aero-elastic simulations used to estimate the output DELs. An input domain that meets these two objectives was defined by Dimitrov et al.[7] partly based on theoretical considerations of atmospheric stability. In this work it is chosen to tailor the input domain specifically to the 99 available sites by using all data including wake added turbulence. This is illustrated in Figure 1 for turbulence intensity[d] (i.e. 10min wind speed coefficient of variation) and wind shear as function of wind speed. The bounds (blue lines) are based on approximations to the extreme quantiles of all data (red lines) with a slight conservative offset.

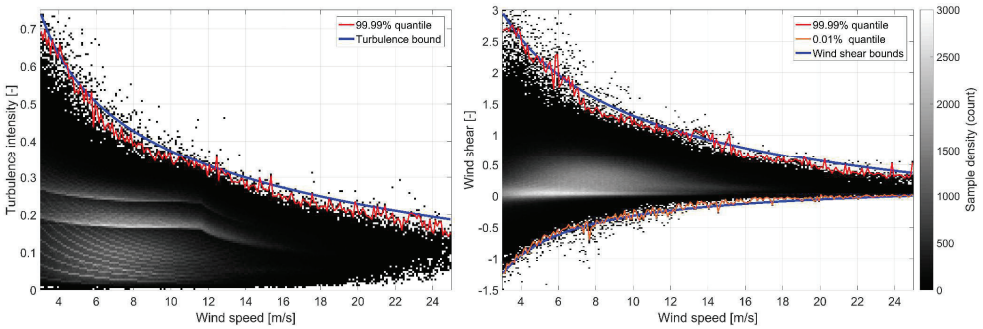

Figure 1: Turbulence bound (left) and wind shear bounds (right) as function of wind speed based on all available measurements. The pronounced clear lines inside the turbulence samples at 0.2 and 0.3 correspond to the wake added turbulence at 3 RD and 5 RD. The smaller clear lines are a product of the decimal truncation when the wind measurements are logged.

The bounds on air density are based on the meso-scale modelled data as shown in Figure 2, and the bounds on flow inclination are based on engineering judgement in the interval from -16° to 16°.

[d] Turbulence intensity is used such that the slight offset of the bound account for the increasing scale of turbulence with increasing wind speed.

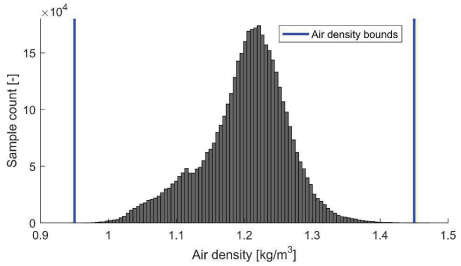

Figure 2: Air density bounds based on all available measurements.

Together, the defined bounds enclose a hyper-volume in the 5-dimensional space of the considered wind climate parameters. An experimental design consisting of 625 is sampled uniformly inside this hyper-volume using a quasi-random Halton sequence. This ensure a good space-filling both for the entire experimental design but also when only a subset of the experimental design is considered. To avoid any clear patterns in the Halton sequence, which may compromise the accuracy of the surrogates, a reverse-radix scrambling is performed as described by Kocis and Whiten[27]. The experimental design is shown in Figure 3. Each of the corresponding *DEL*s are estimated using 100 seeds, resulting in a total of 62,500 aero-elastic simulations.

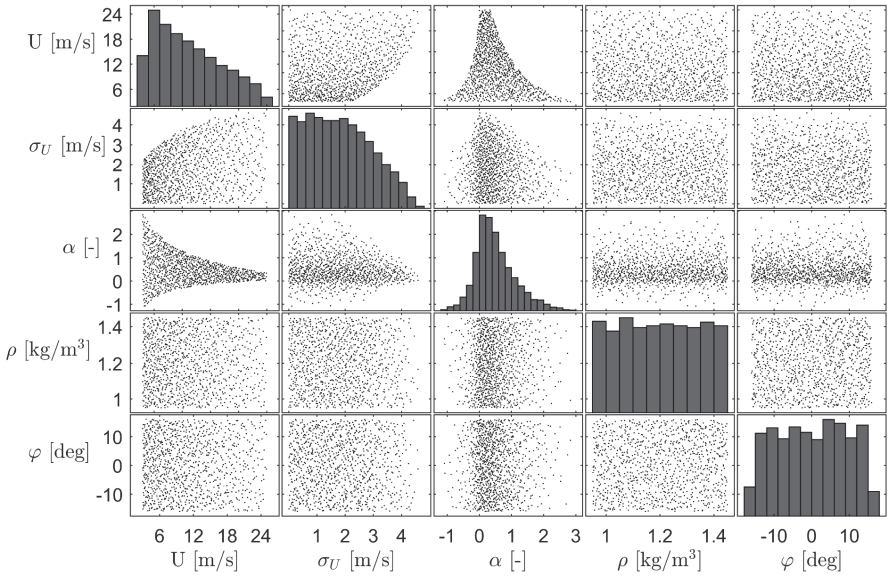

Figure 3: Experimental design with 625 samples drawn uniformly inside the bounded hyper-volume of the wind climate parameters.

4.2. Polynomial chaos expansion

In this work the Wiener-Askey generalized PCE is considered.[28] Generally, it may be used to approximate a function (Y) of a random vector ($\boldsymbol{X}$) in dimension D ($\boldsymbol{X} \in \mathbb{R}^D$) by an infinite expansion of a multivariate orthonormal polynomial basis (Ψ) with respect to the joint probability density function of the input. This is outlined in Eq. (11) where j is a multi-index of the components of the multivariate polynomials.

$$\mathrm{Y}(\boldsymbol{X}) = \sum_{j \in \mathbb{N}^D} c_j \Psi_j(\boldsymbol{X}) \tag{11}$$

The polynomial basis is built from a set (family) of univariate orthonormal polynomials with respect to each input variable, and classical families have been developed which cover common input distributions.[28] For simplicity, the experimental design is therefore transformed into the standard uniform space by Rosenblatt transformation[29]. Consequently, only the Legendre family of orthonormal polynomials is required to build the PCE.

For practical application the infinite sum of polynomials in Eq. (11) is truncated using a hybrid least angle regression algorithm to penalize higher order terms together with a hyperbolic truncation scheme to disregard insignificant interactive terms, see details in Blatman and Sudret[30]. By considering polynomial degrees up to 20 the PCE which minimize the leave one out cross-validation error (ϵ_{LOO}) is selected following the implementation in UQLab[31]. The ϵ_{LOO} is chosen as optimization metric to increase robustness towards over-fitting of the PCE when high order polynomials are considered.

4.3. Kriging

Kriging is a stochastic interpolation technique which assumes the model output (Y) to be a realization of a deterministic mean defined by a regression model ($\boldsymbol{\beta}_{KRG}\boldsymbol{f}_{KRG}^{\mathrm{T}}$) and a correlated stochastic process (Z), see Eq. (12).[25]

$$\mathrm{Y}(\boldsymbol{X}) = \boldsymbol{\beta}_{KRG}\boldsymbol{f}_{KRG}^{\mathrm{T}}(\boldsymbol{X}) + Z(\boldsymbol{X}) \tag{12}$$

The first term models the trend (mean) of the output by a set of basis functions $\boldsymbol{f}_{KRG}(\boldsymbol{X}) = [f_1(\boldsymbol{X}), \dots, f_n(\boldsymbol{X})]$ and associated regression coefficients $\boldsymbol{\beta}_{KRG} = [\beta_1, \dots, \beta_n]$. The second term is interpolating the known residuals at the experimental design by a stationary zero mean Gaussian process (Z) fully described by its covariance (cov):

$$cov(\boldsymbol{X}, \boldsymbol{X}') = \sigma_{KRG}^2 R(\boldsymbol{X}, \boldsymbol{X}', \boldsymbol{\theta}_{\boldsymbol{R}}) \tag{13}$$

Here σ_{KRG}^2 is the overall process variance (assumed constant) and R models the correlation between $Z(\boldsymbol{X})$ and $Z(\boldsymbol{X}')$ by their inter-distance and a correlation function defined by the hyper parameters $\boldsymbol{\theta}_{\boldsymbol{R}}$. Once a suitable basis of functions and a correlation model is chosen $\boldsymbol{\beta}_{KRG}$, σ_{KRG}^2, and $\boldsymbol{\theta}_{\boldsymbol{R}}$ may be estimated by maximizing the likelihood of observing the output at the experimental design.[32]

A priori it is known that the sensitivity between fatigue loads and the different wind climate parameters vary significantly. Therefore, an anisotropic separable correlation formulation is considered as shown in Eq. (14).

$$R(\boldsymbol{X}, \boldsymbol{X'}, \boldsymbol{\theta_R}) = \prod_{i=1}^{D} R(X_i, X_i', \theta_{R,i}) \tag{14}$$

A main challenge when calibrating an accurate Kriging model is to select an appropriate trend and correlation function. By a combinatorial approach similar to Morató et al.[9] we found universal Kriging with a quadratic trend and the Matérn 3/2 correlation function to yield the best results overall.

5. Method for Assessment of Surrogate Model Uncertainty

The surrogate model uncertainties of PCE and Kriging are estimated according to EN 1990[33]. In this section the method is briefly outlined followed by a description of the numerical integration scheme that is used to assess the site-specific fatigue loads.

5.1. EN 1990 method

The model uncertainty X_{proxy} is estimated by rewriting it in terms of a unit mean lognormal error term ($X_{proxy,EN}$) and a mean value correction factor to account for the model bias (b_{proxy}), see Eq. (15).

$$F_{eq,direct} = b_{proxy} X_{proxy,EN} F_{eq,proxy} \tag{15}$$

Given the available set of 99 statistically independent[e] joint wind climates the bias may be estimated using a least squares approach as shown in Eq. (16).

$$b_{proxy} = \frac{\sum_{i=1}^{99} F_{eq,direct,i} \, F_{eq,proxy,i}}{\sum_{i=1}^{99} F_{eq,proxy,i}^2} \tag{16}$$

Next, the logarithm of the residuals at each site is estimated by Eq. (17).

$$\delta_{EN,i} = \ln\left(\frac{F_{eq,direct,i}}{b_{proxy,EN} F_{eq,direct,i}}\right) \tag{17}$$

An estimate of the standard deviation of the residuals ($\sigma_{\delta,EN}$) is then assessed by Eq. (18) where $\delta_{EN,\mu}$ is the mean value of all error realizations.

[e] The diversity of the included sites in terms of complexity and geographical spread validate the assumption of independence.

$$\sigma_{\delta,EN} = \sqrt{\frac{1}{99-1}\sum_{i=1}^{99}\left(\delta_{EN,i} - \delta_{EN,\mu}\right)^2} \tag{18}$$

The coefficient of variation of the lognormal surrogate model uncertainty (V_{proxy}) is then obtained by Eq. (19).

$$V_{proxy} = \sqrt{e^{\sigma^2_{\delta,EN}} - 1} \tag{19}$$

5.2. Numerical fatigue load integration

To estimate the surrogate model uncertainty, it is required to assess F_{eq} by direct simulation. This is not trivial and involves hundreds of thousands of aero-elastic simulations. It is therefore relevant to discuss the applied method for integrating the fatigue load in detail in the following.

With flow inclination being fixed (φ_{fix}) the dimension of the integration problem in Eq. (7) is reduced as shown in Eq. (20). Here the 12 discrete directions are directly introduced and $\boldsymbol{C}_R = [U, \alpha, \rho]$ contain the reduced set of wind climate parameters of wind speed, wind shear and air density.

$$F_{eq}(\varphi_{fix}) = \left(c_{sim} \sum_{k=1}^{12} p_\theta(\theta_k) \underbrace{\int_{\sigma_U} \int_{\boldsymbol{C}_R \in R^3} f_{Site}(\boldsymbol{C}_R, \sigma_U | \, \theta_k) DEL\left(\boldsymbol{C}_R, \sigma_{U,T}, \varphi_{fix}, m\right)^m d\boldsymbol{C}_R \, d\sigma_U}_{F^m_{eq,sect,k}} \right)^{\frac{1}{m}} \tag{20}$$

To find an optimal numerical integration scheme it is sufficient to consider the sector wise fatigue loads ($F_{eq,sect,k}$), which mathematically is the m'th order weighted Hölder mean of DEL with respect to f_{Site}. In turn, $F^m_{eq,sect,k}$ is the expected value of DEL^m and may be estimated approximatively by Monte-Carlo (MC) sampling, which avoids the "curse of dimensionality" associated to traditional grid-based integration.[6] The MC-integration is outlined in Eq. (21) where N is the number of samples and p models the probability of generating sample i in terms of ambient turbulence.

$$F^m_{eq,sect,k}(\varphi_{fix}) \approx \frac{1}{N}\sum_{i=1}^{N} \frac{f_{Site}\left(\boldsymbol{C}_{R,i}, \sigma_{U,i} | \, \theta_k\right) DEL\left(\boldsymbol{C}_{R,i}, \sigma_{U,T,i}, \varphi_{fix}, m\right)^m}{p(\boldsymbol{C}_{R,i}, \sigma_{U,i})} \tag{21}$$

The convergence behaviour depends on the choice of the MC-sampling distribution (h_{MC}). In principle convergence is obtained faster if it resembles the product of DEL^m and f_{Site} to concentrate samples in the region which contributes most to the integral (i.e. importance sampling). This leads to the following main considerations for h_{MC}:

1. Since DELs are raised to the power of m it is important to sample high fatigue load events with a low probability of occurrence.
2. Wind climate combinations with a high probability of occurrence have to be sampled to capture the majority of the wind turbines lifetime.

The importance of point 1 was clearly shown by Graf et al.[6] where MC-integration was benchmarked by sampling from the joint wind climate distribution (i.e. $h_{MC} = f_{Site}$) which lead to very slow convergence rates for components with high Wöhler exponents.

Optimizing h_{MC} with respect to point 1 is sensor-specific but in general it requires unlikely wind climates to be sampled (e.g. very high turbulence or wind shear). On the other hand, optimization of h_{MC} with respect to point 2 is site-specific and requires likely wind climates to be sampled. To cover all 99 sites and all considered sensors a straight-forward compromise is then to sample equally dense across the entire input domain defined in Section 4 (i.e. h_{MC} uniformly distributed).

Several techniques can be used to sample from h_{MC} but in low dimensions (lower than 6) it was shown by Morokoff and Catflisch[34] that quasi-random numbers from low-discrepancy sequences provide fast convergence. Instead of a convergence ratio $\propto N^{-0.5}$ for crude MC a Halton sequence obtain a convergence ratio $\propto N^{-\lambda}$ where $0.5 \leq \lambda \leq 1$ with $\lambda \to 1$ for low dimensions.

A main question to answer is how many samples that are needed to assess F_{eq}. Based on the results of Graf et al.[6] and a preliminary convergence study using a surrogate it was found reasonable to evaluate the integral by 25,000 DELs. This results in an accuracy within approximately 1% of the converged value obtained at one million samples for all considered sensors. Given that the surrogate model uncertainty is obtained by a relative comparison of $F_{eq,direct}$ and $F_{eq,proxy}$, both estimated by the same MC-samples, the small error is assumed to be insignificant.

Finally, it is noted that each sample in the MC-integration correspond to one specific flow inclination so three databases of fatigue loads were simulated to cover all 99 sites. Using 100 seeds to estimate each DEL this resulted in a total of 7.5 million simulations to accurately assess $F_{eq,direct}$.

6. Quantification of the Surrogate Model Uncertainty

Using the presented methods, the surrogate model uncertainty across all considered sensors is quantified. First an example is shown for the blade root flap-wise bending moment to clearly outline how the results are obtained step-by-step. Then the surrogate model uncertainty is

quantified for all considered sensors and presented as the worst case across the sensors as it is impractical to differentiate the surrogate model uncertainty for each sensor[f].

6.1. Blade root bending moment example

Using the full experimental design, a Kriging and PCE model is trained to capture fatigue loads of the blades. Both surrogates are then used to estimate the site-specific fatigue loads across all 99 sites by Eq. (20) which is compared to direct simulation as shown in Figure 4.

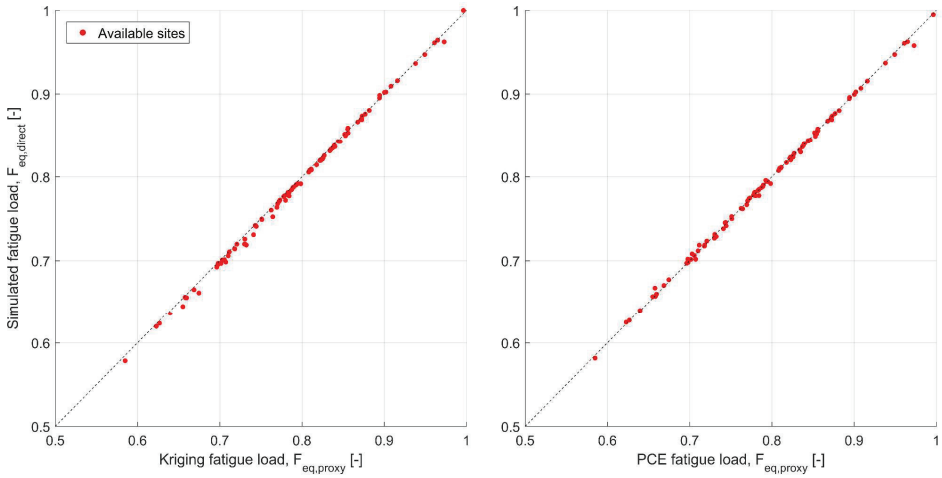

Figure 4: Normalized site-specific fatigue loads on the blades predicted by Kriging and PCE and compared to direct simulation. The dashed lines indicate the perfect model where $F_{eq,proxy} = F_{eq,direct}$

Based on this comparison the surrogate model uncertainty is estimated by Eqs. (16) and (19). The results are presented in Table 5.

Table 5: Surrogate model uncertainty for blade flap-wise bending.

Surrogate model	Bias [-]	Coefficient of variation [-]
PCE	1.001	0.004
Kriging	1.004	0.004

Given the typical scale of the other uncertainties in the LSE listed in Table 4 the resulting surrogate model uncertainties of both PCE and Kriging are insignificant and may be neglected.

[f] This representation of the surrogate model uncertainty is in line with the model uncertainty for wind load effects being identical across all considered sensors.

Next, it is investigated how the results change with the amount of simulations that are invested in training the surrogate models. This is illustrated in Figure 5 where the coefficient of variation is plotted as function of the number of samples in the experimental design and how many seeds that are used to evaluate the DELs. Similarly, the model bias is shown as function of invested simulations in Figure 6. The number of samples starts at 100 as both models become significantly inaccurate for smaller experimental designs. The noise in the PCE results is explained by the adaptive scheme to select the optimal polynomial degree which may change for each combination of samples/seeds in order to minimize ϵ_{LOO}.

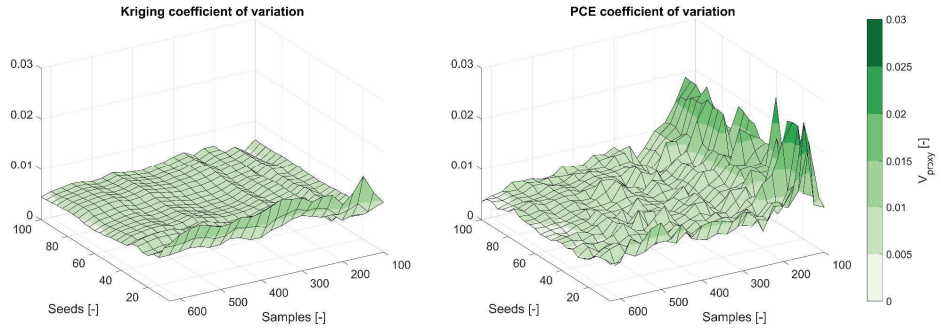

Figure 5: Coefficient of variation of the surrogate model uncertainty for blades using Kriging and PCE shown as function of the number of samples used for training and number of seeds used to evaluate DELs at each sample.

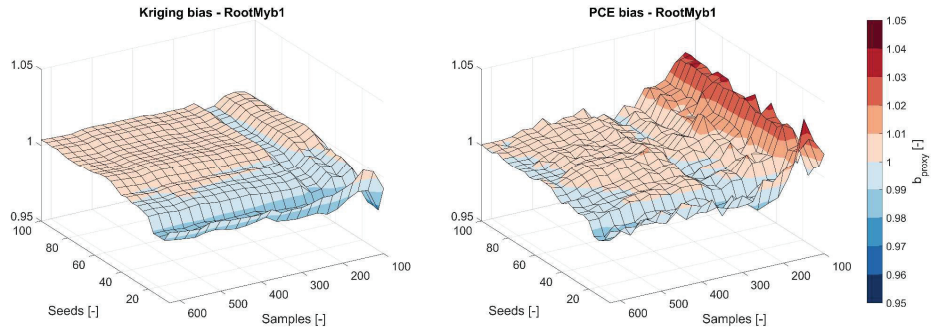

Figure 6: Surrogate model bias for blades using Kriging and PCE shown as function of the number of samples used for training and number of seeds used to evaluate DELs at each sample. The apparent "valley" in the Kriging results at approximately 200 samples is due to the oscillating convergence behaviour of the bias across samples. This is clearly seen when less than 100 samples are considered, but to keep the figures consistent and clean this is not included here.

6.2. Surrogate model uncertainty across all sensors

Following the described procedure for the blade flap-wise bending the surrogate model uncertainty has been computed for all sensors in Table 3. The maximum model uncertainty across the sensors is plotted in Figure 7 for both surrogates.

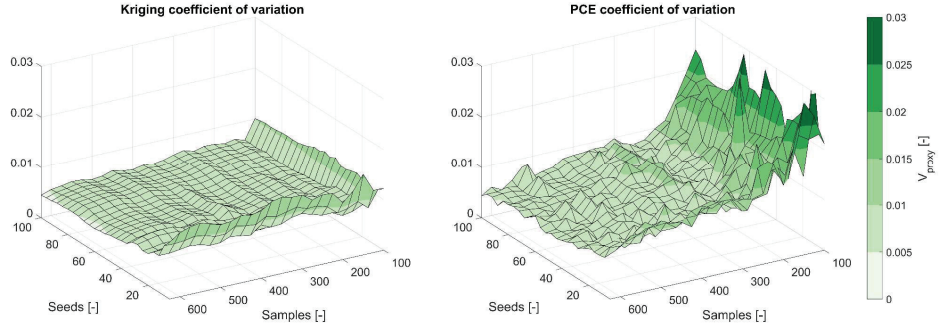

Figure 7: Surrogate model uncertainty coefficient of variations across all considered sensors shown as function of the number of samples used for training and number of seeds used to evaluate DELs at each sample.

Relatively few samples and seeds are required for the surrogate models to obtain a converged model uncertainty of ~0.5%.

To analyse the surrogate model bias it is necessary to consider both the minimum and maximum across all sensors as illustrated in Figure 8 and Figure 9, respectively. This show that for sparse designs (low number of samples) PCE tends to be non-conservative while Kriging seems to be almost exclusively conservative across all sensors.

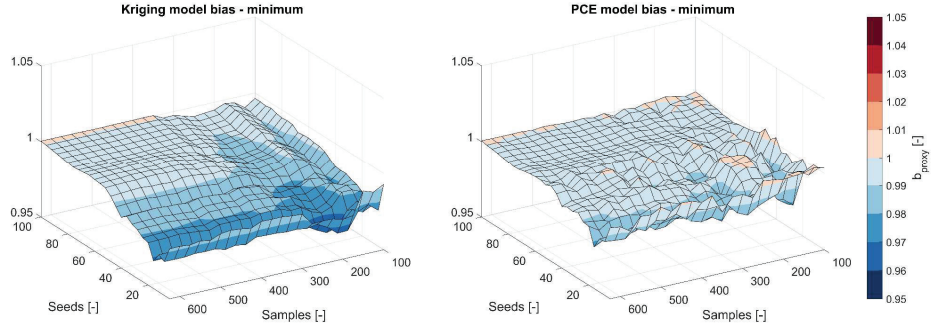

Figure 8: Minimum surrogate model bias across all considered sensors shown as function of the number of samples used for training and number of seeds used to evaluate DELs at each sample.

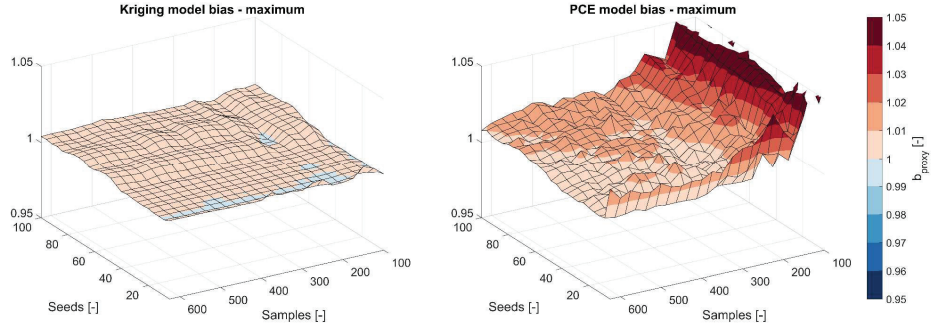

Figure 9: Maximum surrogate model bias across all considered sensors shown as function of the number of samples used for training and number of seeds used to evaluate DELs at each sample. The PCE model bias at 100-150 samples is missing due to a sharp increase to 1.10 which would otherwise distort the figure.

7. Sensitivity Analysis and General Recommendations

Both Kriging and PCE can be trained to accurately predict fatigue loads with a relatively small computational investment. In this section a sensitivity analysis is conducted to assess how the surrogate model uncertainty affects the reliability level of the considered components. This is used to define three levels of accuracy followed by a set of recommendations by the authors on training PCE and Kriging for fatigue reliability analysis of wind turbines.

7.1. Reliability sensitivity analysis

To estimate the sensitivity of the surrogate model uncertainty a reference design is established by assuming that each component is designed to the limit using direct aero-elastic simulation. This implies that the reliability index at the last year of service is exactly the target of $\Delta\beta_t = 3.3$ [1], where a lifetime of 20 years is assumed. Here the yearly probability of failure is approximated as $\Delta P_{f,20} \cong P_{f,20} - P_{f,19}$ where $P_{f,20}$ and $P_{f,19}$ represent the failure probability at years 19 and 20, respectively. The failure probabilities are estimated by the LSE presented in Eq. (8) where the uncertainties are modelled according to Table 4.

Using the reference design of each component the reliability index at the last year of service ($\Delta\beta$) is calculated by the LSE in Eq. (10) where b_{proxy} and V_{proxy} are varied individually. The sensitivity of the surrogate model uncertainty is then quantified as the ratio of the reliability index with respect to the target reliability ($\Delta\beta/\Delta\beta_t$). In Figure 10 this is shown for a representative range of V_{proxy} for both PCE and Kriging where the relative change of the reliability is less than 0.5%. Figure 11 shows the results of varying b_{proxy} within a representative range, demonstrating that $\Delta\beta/\Delta\beta_t \cong b_{proxy}$ for all components considered.

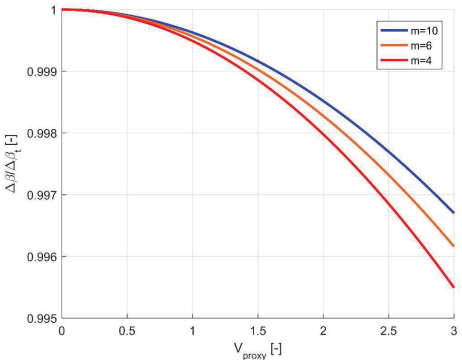

Figure 10: Reliability index sensitivity to the surrogate model uncertainty coefficient of variation.

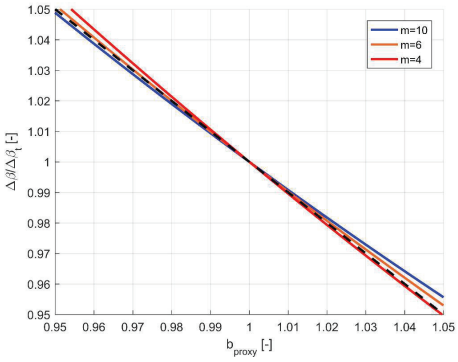

Figure 11: Reliability index sensitivity to surrogate model bias. The dashed line indicates $\Delta\beta/\Delta\beta_t = b_{proxy}$.

7.2. Surrogate model accuracy

Typically, the target reliability index is specified with one decimal suggesting that a change of less than 1% of the reliability index at the limit is negligible. V_{proxy} may therefore be ignored in reliability analysis of wind turbines for both Kriging and PCE when at least 100 samples are considered in the experimental design.

The change in reliability is roughly proportional to b_{proxy} which makes the bias significant when it is outside the range of 0.99 to 1.01. This is made clear by Table 6, which leads to the definition of three accuracy classes.

Table 6: Absolute reliability for varying surrogate model bias.

b_{proxy}	0.95	0.96	0.97	0.98	0.99	1.00	1.01	1.02	1.03	1.04	1.05
$\Delta\beta$	3.1	3.2	3.2	3.2	3.3	3.3	3.3	3.4	3.4	3.4	3.5

High accuracy is obtained when $0.99 \leq b_{proxy} \leq 1.01$ where the estimated reliability index is unchanged on the first decimal. Medium accuracy is obtained when $0.96 \leq b_{proxy,EN} \leq 1.04$ leading to a slight change of ±0.1 of the estimated reliability index. If $0.96 > b_{proxy,EN} > 1.04$ low accuracy is obtained which potentially changes the estimated reliability index significantly with more than ±0.2. The accuracy classes are illustrated for both PCE and Kriging in Figure 12.

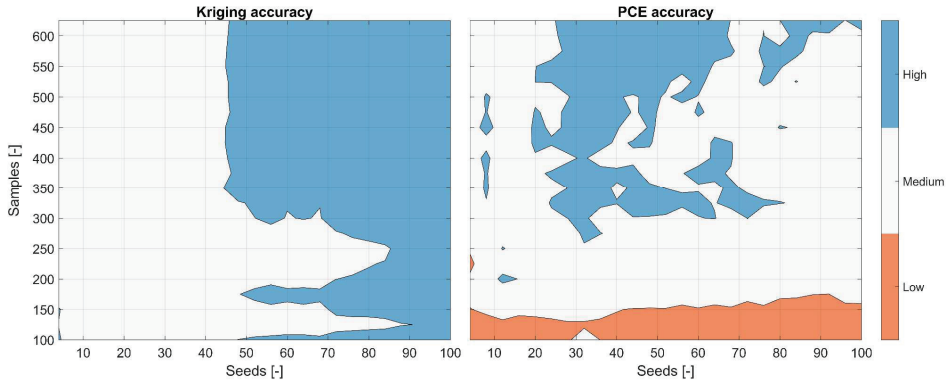

Figure 12: Surrogate model bias divided by three accuracy classes. Notice the clear pattern of increasing accuracy with the number of seeds for Kriging and the increased accuracy with number of samples for PCE.

For Kriging it is seen that the accuracy depends mostly on the number of seeds that are used. The upper right corner confirms a converged plateau of high accuracy which require an experimental design with more than 350 samples using at least 50 seeds to assess each DEL. If a medium accuracy is acceptable it is only required to use more than 100 samples and at least 4 seeds.

For PCE the accuracy depends on the density of the experimental design. A high accuracy may be obtained, but even when the full design is used the accuracy is not fully consistent with an increase in seeds. This indicates that the PCE coefficients may not have converged in the investigated range of samples and seeds. If more than 175 samples are considered the PCE model reach a medium accuracy, and a low accuracy is obtained for experimental designs with less than ~175 samples.

7.3. Recommendations

The results of the optimization analysis are summarized in Tables 7 and 8 as a set of recommendations towards training Kriging and PCE for fatigue reliability analysis. Since only a subset of load-bearing wind turbine components are considered the recommendations are slightly conservative compared to the results shown in Figure 12.

It is important to note that the recommendations are tied to the current setup of using the 5MW reference turbine by NREL together with the experimental design described in section 4. The minimum samples and seeds are also dependent on the size of the input domain which directly relates to the sample density. If a similar experimental design is used together with a smaller or larger input domain emphasis should therefore be put on the recommended maximum leave one out error. Because the proposed experimental design is uniformly distributed without any emphasis on the specific turbine response it is also expected that the recommended maximum leave one out error can be used as tentative guidance for other (similar) turbines.

Table 7: Kriging recommendations

Accuracy	Minimum samples in DoE [-]	Minimum seeds to assess DEL [-]	Total amount of 10-min simulations [-]	Maximum ϵ_{LOO} [%]
High	400	75	30.000	0.60
Medium	100	10	1.000	2.00
Low	100	4	400	3.25

Table 8: PCE recommendations

Accuracy	Minimum samples in DoE [-]	Minimum seeds to assess DEL [-]	Total amount of 10-min simulations [-]	Maximum ϵ_{LOO} [%]
High	>625	50	>31.250	0.35
Medium	200	10	2.000	1.35
Low	100	4	400	2.20

8. Comparison and Discussion of PCE and Kriging

Overall Kriging obtains a better accuracy than PCE per simulation, but it also requires more computational power to predict new samples compared to PCE.[7] However, it is noted that h_{MC} in the presented numerical integration is completely independent of the sector-wise joint wind climate distributions. A direct advantage of this is that the DEL of each MC-sample has to be evaluated only once per fixed flow inclination to cover all 99 sites. This neglects the difference in computational time between PCE and Kriging when predicting DELs compared to the simulations invested in training the surrogates.

To increase the accuracy of PCE it requires more samples while Kriging requires more seeds. This observation is in line with the fundamentals of the surrogates of regression and interpolation, respectively. If few seeds are used to evaluate the DELs it can be interpreted as noise which Kriging is forced to capture when interpolating the residuals. On the other hand, PCE levels out the noise in a mean sense, but a relatively large number of samples are needed to reliably fit the coefficients of the expansion.

While not shown in this paper, this encouraged an analysis of using Polynomial Chaos Kriging[35] (PCK) as implemented in UQLab[36]. This method combines the two surrogate models by using the PCE as basis functions (trend) for the universal Kriging model. In a best-case scenario this could lead to a surrogate model which is accurate for a small experimental design (as Kriging) using just a few seeds to estimate DELs (as PCE). However, the results of using PCK mostly resembles that of using PCE, and it is therefore not preferred over universal Kriging. The reason is probably that the residuals used to estimate σ^2_{KRG} and $\boldsymbol{\theta_R}$ appear without any significant

correlation as they mostly just represent the noise from using few seeds. In turn, the interpolation only influences predictions at the very vicinity of the experimental design, which was also observed by Dimitrov et al.[7]

Another possibility to increase the accuracy of Kriging is to introduce a so-called "nugget". The nugget models a set of values that are added to the diagonal of $R(\boldsymbol{X}, \boldsymbol{X}', \theta_R)$, thereby allowing a non-zero uncertainty bound around the experimental design. A well optimized nugget could therefore potentially make the Kriging model more robust to the noise from using a small number of seeds.[37] To the best of the authors knowledge a general framework to include and optimize a nugget in universal Kriging is not yet developed, and therefore this approach was not pursued further.

9. Summary and Conclusions

Using wind data from 99 international sites the model uncertainty related to approximating lifetime fatigue loads by Kriging and PCE has been quantified based on aero-elastic simulations of the 5MW reference turbine by NREL. The main components of the turbine were considered namely; blades, low speed shaft, yaw bearing, and tower.

All available data was used to define an experimental design to train the surrogates in terms of wind speed, turbulence, wind shear exponent, air density and flow inclination. Using up to 625 samples, with up to 100 seeds to evaluate fatigue loads at each sample, both surrogate models were calibrated using UQLab. For Kriging, a combinatorial approach was used to conclude that universal Kriging with a second order trend and the Matérn 3/2 correlation is optimal to predict fatigue loads.

The model uncertainty of both surrogates across all sensors was estimated by the recommended approach in Eurocode 1990, Annex D. This showed that the model uncertainty coefficient of variation is less than 2.5%. In contrast, the model bias varied significantly for the two surrogate models between 0.95 to 1.05.

Based on a sensitivity study it was shown that the model uncertainty coefficient of variation changes the structural reliability index less than 0.5% which is negligible compared to the target reliability of 3.3. In addition, the sensitivity study showed that the relative change in reliability index is approximately equal to the model bias across all considered components.

Three accuracy classes were introduced based on the bias of the surrogate models namely high, medium, and low accuracy. Compared to direct simulation a surrogate model with a high accuracy estimate reliability indices within ±0.05, for medium accuracy the error is within ±0.15 and for low accuracy the error on the first decimal is ≥0.15.

It was documented that Kriging obtains a high accuracy for the 5MW turbine when more than 30.000 aero-elastic simulations are performed. In comparison, PCE did not consistently obtain a high accuracy in the investigated range of 625 samples and 100 seeds. However, using more than 200 samples and 10 seeds PCE obtain a medium accuracy.

Overall, Kriging obtains a higher accuracy per invested simulation compared to PCE. Kriging is therefore the preferred method over PCE for reliability analysis of onshore wind turbines, when using the methods described in this paper.

Acknowledgements

The authors wish to thank the data providers: KNMI, ICDC, CliSAP/KlimaCampus, University of Hamburg, DTU, Vattenfall and VENTUS INGENIERÍA. The work presented in this paper is part of the PhD project "From wind climate to wind turbine loads – efficient and accurate decision support and risk analysis" co-funded by EMD International A/S, Aalborg University and the Innovationfund Denmark case number 5189-00022B. Their financial support is highly appreciated.

References

1. IEC. International Standard IEC 61400-1 ed. 4, "Wind Turbines - Part 1 Design Requirements". 2019.
2. ISO. International Standard ISO 2394:2015, "General principles on reliability for structures." 2015.
3. Slot RMM, Svenningsen L, Sørensen JD, Thøgersen ML. Importance of Shear in Site Assessment of Wind Turbine Fatigue Loads. *J Sol Energ*. 2018;140(4):041012. doi:10.1115/1.4039748
4. Stensgaard Toft H, Svenningsen L, Moser W, Dalsgaard Sørensen J, Lybech Thøgersen M. Wind Climate Parameters for Wind Turbine Fatigue Load Assessment. *J Sol Energ*. 2016;138(3). doi:10.1115/1.4033111
5. IEC. International Standard IEC 61400-1 ed. 3, "Wind Turbines - Part 1 Design Requirements". 2010.
6. Graf PA, Stewart G, Lackner M, Dykes K, Veers P. High-throughput computation and the applicability of Monte Carlo integration in fatigue load estimation of floating offshore wind turbines. *Wind Energy*. 2016;19:861-872. doi:110.1002/we.1870
7. Dimitrov N, Kelly M, Vignaroli A, Berg J. From wind to loads: wind turbine site-specific load estimation using databases with high-fidelity load simulations. *Wind Energy Sci*. 2018;3:767-790. doi:10.5194/wes-2018-18
8. Toft HS, Svenningsen L, Sørensen JD, Moser W, Thøgersen ML. Uncertainty in wind climate parameters and their influence on wind turbine fatigue loads. *Renew Energy*. 2016;90:352-361. doi:10.1016/j.renene.2016.01.010
9. Morató A, Sriramula S, Krishnan N. Kriging models for aero-elastic simulations and reliability analysis of offshore wind turbine support structures. *Ships Offshore Struct*. 2018;0(0):1-14. doi:10.1080/17445302.2018.1522738
10. Teixeira R, O'Connor A, Nogal M, Krishnan N, Nichols J. Analysis of the design of experiments of offshore wind turbine fatigue reliability design with Kriging surfaces. *Procedia Struct Integr*. 2017;5:951-958. doi:10.1016/j.prostr.2017.07.132
11. Murcia JP, Réthoré P, Dimitrov N, et al. Uncertainty propagation through an aeroelastic wind turbine model using polynomial surrogates. *Renew Energy*. 2017;119:910-922. doi:10.1016/j.renene.2017.07.070

12. Hu W, Choi KK, Cho H. Reliability-based design optimization of wind turbine blades for fatigue life under dynamic wind load uncertainty. *Struct Multidiscip Optim*. 2016;54(4):953-970. doi:10.1007/s00158-016-1462-x

13. Dimitrov N, Natarajan A, Kelly M. Model of wind shear conditional on turbulence and its impact on wind turbine loads. *Wind Energy*. 2015;18(11):1917-1931. doi:10.1002/we.1797

14. Svenningsen L, Slot RMM, Thøgersen ML. A novel method to quantify atmospheric stability. *J Phys Conf Ser*. 2018;1102. doi:10.1088/1742-6596/1102/1/012009

15. Kelly M, Larsen G, Dimitrov NK, Natarajan A. Probabilistic Meteorological Characterization for Turbine Loads. *J Phys Conf Ser*. 2014;524:012076. doi:10.1088/1742-6596/524/1/012076

16. Miner MA. Cumulative damage in fatigue. *J Appl Mech*. 1945;12:159-164.

17. Jonkman JM, Butterfield S, Musial W, Scott G. *Definition of a 5-MW Reference Wind Turbine for Offshore System Development*. National Renewable Energy Laboratory; 2009.

18. Jonkman J. FAST An aeroelastic computer-aided engineering (CAE) tool for horizontal axis wind turbines. https://nwtc.nrel.gov/FAST [Accessed 2019-06-18]. Published 2015. Accessed April 3, 2017.

19. B. Jonkman NK. TurbSim A stochastic, full-field, turbulence simulator primarialy for use with InflowWind/AeroDyn-based simulation tools. https://nwtc.nrel.gov/TurbSim. Published 2016. Accessed April 3, 2017.

20. Standard. IEC 61400-1 ed. 3, 2005, International Electrotechnical Commission, Wind turbines, Part 1: Design requirements, Edition 3 (2005) incl. Amendment 1 (2010). 2010.

21. ASTM. ASTM No. E1049-85, "Standard Practice for Cycle Counting in Fatigue Analysis". 2011.

22. Sørensen JD, Frandsen S, Tarp-Johansen NJ. Effective turbulence models and fatigue reliability in wind farms. *Probabilistic Eng Mech*. 2008;23(4):531-538. doi:10.1016/j.probengmech.2008.01.009

23. IEC 61400-1. Safety Factors - IEC 61400-1 ed. 4 - background document. 2014.

24. Marelli S, Sudret B. UQLab: A Framework for Uncertainty Quantification in Matlab. In: *Vulnerability, Uncertainty, and Risk*. Reston, VA: American Society of Civil Engineers; 2014:2554-2563. doi:10.1061/9780784413609.257

25. Santner TJ, Williams BJ, Notz WI. *The Design and Analysis of Computer Experiments*. New York, NY: Springer New York; 2018. doi:10.1007/978-1-4939-8847-1

26. Sudret B. Polynomial chaos expansions and stochastic finite element methods. In: Phoon KK, Ching J, eds. *Risk and Reliability in Geotechnical Engineering*. Taylor and Francis; 2015:265-300.

27. Kocis L, Whiten WJ. Computational investigations of low-discrepancy sequences. *ACM Trans Math Softw*. 1997;23(2):266-294. doi:10.1145/264029.264064

28. Xiu D, Karniadakis GE. The Wiener--Askey Polynomial Chaos for Stochastic Differential Equations. *SIAM J Sci Comput*. 2002;24(2):619-644. doi:10.1137/S1064827501387826

29. Rosenblatt M. Remarks on a Multivariate Transformation. *Ann Math Stat*. 1952;23(3):470-472.

30. Blatman G, Sudret B. Adaptive sparse polynomial chaos expansion based on least angle regression. *J Comput Phys*. 2011;230:2345-2367. doi:10.1016/j.jcp.2010.12.021

31. Marelli S, Sudret B. *UQLab User Manual - Polynomial Chaos Expansions*. ETH Zurich: Report UQLab-V1.0-105; 2017.

32. Lataniotis C, Marelli S, Sudret B. The Gaussian process modelling module in UQLab. September 2017.

33. CEN. EN 1990, Eurocode - Basis of structural design. 2002.

34. Morokoff WJ, Caflisch RE. Quasi-Monte Carlo Integration. *J Comput Phys*. 1995:218-230.

35. Schöbi R, Sudret B, Wiart J. Polynomial-chaos-based Kriging. *Int J Uncertain Quantif*. 2015;5(2):171-193.

36. Marelli S, Sudret B. *UQLab User Manual - PC-Kriging*. ETH Zurich: Report UQLab-V1.0-105; 2017.

37. Andrianakis I, Challenor PG. The effect of the nugget on Gaussian process emulators of computer models. *Comput Stat Data Anal*. 2012;56(12):4215-4228. doi:10.1016/j.csda.2012.04.020

Consistent direct-drive version of the NREL 5MW turbine

R M M Slot[1,2], L Svenningsen[1], J D Sørensen[2], and M L Thøgersen[1]

[1]EMD International A/S, 9220 Aalborg, Denmark
[2]Department of Civil Engineering, Aalborg University, 9220 Aalborg, Denmark

E-mail: rmms@civil.aau.dk

Abstract. Access to relevant reference wind turbine models is important to the wind energy community to advance turbine technology and lower the cost of wind energy. Multiple reference turbines are available, which can be used to simulate their structural response using aero-elastic codes. A common feature of current reference turbines is the utilization of a gearbox, and at present no direct-drive reference model is publicly available. This does not reflect the trend in the industry with direct-drive turbines becoming increasingly popular.

In this work we develop an onshore direct-drive version of the geared 5MW reference wind turbine by NREL. The presented direct-drive model is a fully consistent conversion of the geared design, intended to analyse the differences in structural loads between the two concepts.

By simulating the developed direct-drive turbine model we show that fatigue loads on the drivetrain differ significantly for the gearless design, with approximately 10% lower loads for design class IIB from the IEC 61400-1 design standard. The developed direct-drive turbine model can be used in the wind energy community to improve the understanding of differences in structural loads between geared and direct-drive designs of modern multi-megawatt wind turbines.

1. Introduction

Multiple reference wind turbines are available for the scientific community to simulate the response of modern utility turbines. Some relevant examples are the 1.5MW windPACT turbine [1], the 5MW turbine by NREL [2], and the 10MW turbine by DTU [3]. Recently an 8MW reference turbine was also developed in the LEANWIND project to fill the gap between the 5MW turbine by NREL and the 10MW turbine by DTU [4]. A common feature for all currently available reference turbines is the utilization of a gearbox to increase the rotational speed of the rotor to match the demand of a high-speed electrical generator. However, for utility wind turbines in the megawatt range the concept of "direct-drive" design, where the generator is connected directly to the shaft of the turbine rotor, has become widely used.

As the direct-drive concept becomes increasingly popular, it is important to study how it differs from its geared counterpart. This is also reflected by the "IEA Wind Task 37 - Systems Engineering" [5] where a direct-drive version of the 10MW turbine by DTU for offshore application is under development. In [6] a 5MW direct-drive turbine was also developed for the aero-elastic code HAWC2 with focus on showing its application for floating spar-buoy wind turbines. However, although the model was described in detail, it was not made publicly available.

The aim of the present work is to develop a consistent direct-drive version of the 5MW reference turbine by NREL. The model is developed for onshore applications using the freely available aero-elastic code FAST [7]. The goal is to establish a one-to-one conversion of the existing reference turbine, which makes the developed model suitable for comparing structural loads for the two design concepts

even though the 5MW reference turbine may not necessarily reflect the design of modern utility turbines. The developed direct-drive model is intended as an open access reference turbine for the wind energy community.

2. Direct-drive specifications and assumptions

The transition from gearbox to direct-drive is based on the following two key assumptions:

- The control strategy used for the geared design is applicable for the direct-drive design.
- The total mass of the entire nacelle is the same for both designs.

The former assumption implies that the baseline controller for the geared 5MW turbine can be redesigned by scaling the control parameters related to the speed of the high-speed shaft (HSS) and the torque. The latter assumption implies that the same structural properties of the tower may be used for both designs. It is noted though, that there will likely be a difference in the weight of the nacelle between the two concepts for real turbines but depending on the manufacturer it may be either lighter or heavier. A simple approach for a generic model is therefore to assume the same weight which in turn also makes it possible to compare loads in the tower without influence of changes in its design.

The drivetrain of the original 5MW reference turbine consists of a high-speed multiple-stage gearbox system with a ratio of 1:97. It is modelled as a single torsional degree of freedom system with a structural damping ratio of 5% relative to the critical damping. In the developed direct-drive design the gearbox is "removed" by changing the ratio to 1:1, while assuming that the drive-shaft torsional stiffness and damping constant is the same as for the geared design. Note that this approach does not actually remove the HSS in the structural model; However, this has no influence on the results as the "fictional" HSS can be considered equivalent to the low speed shaft (LSS) that is attached directly to the rotor when appropriate scaling is applied to the control parameters.

Another important difference between the geared and direct-drive design concepts is the size and type of generator. The generator inertia around the "fictional" HSS in the model must be specified in accordance to a direct-drive low speed generator, which is larger than traditional high-speed generators. Furthermore, the change of generator and removal of the gearbox may influence the location of the nacelle center of mass (NacCM). In the developed direct-drive design NacCM is assumed unchanged compared to the geared turbine (1.9m "downwind" compared to the yaw axis). The influence of this assumption on fatigue loads is analysed in a sensitivity study in section 3.

In the following the changes made to successfully convert the geared design to a direct-drive-design are quantified, first focusing on the controller specifications and next the drivetrain specifications.

2.1. Controller specifications

The baseline controller for the geared 5MW turbine consists of a generator-torque controller and a full-span rotor-collective blade-pitch controller both described in detail in [2]. The controller operates in five regions; 1, 1½, 2, 2½ and 3 which is shown schematically in Figure 1.

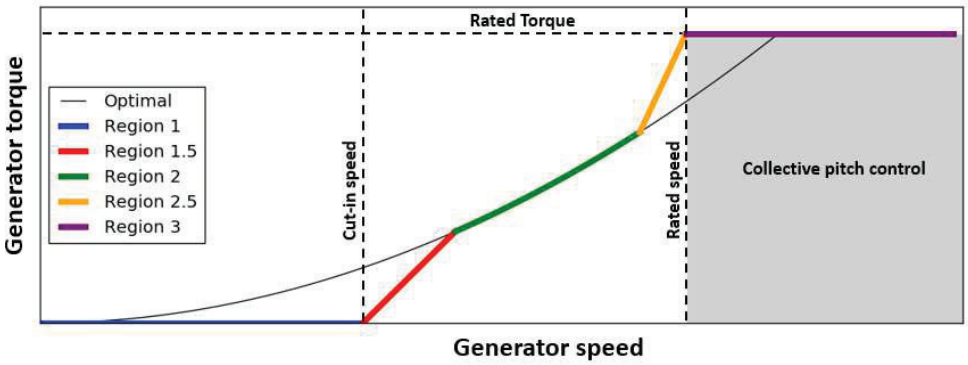

Figure 1: Schematic overview of the 5MW reference turbine baseline controller by NREL.

Region 1 is before cut-in windspeed where the torque is zero and the wind is used to accelerate the rotor for start-up. Region 2 is the control region for optimized power capture, where the torque is controlled to maintain an optimal tip speed ratio. In region 3 the rated generator power is reached, and the control system is designed to keep this constant by collective pitch of the blades. Region 1½ is a linear transition between regions 1 and 2 used for start-up and region 2½ is a linear transition between regions 2 and 3 used to limit tip speed and thus noise emissions near rated power [2].

To adapt the generator-torque controller to the direct-drive version all HSS speed parameters are scaled down with respect to the change in gearbox ratio (GBRatio) and all torque parameters are scaled up (factor of 97). All changes are listed in Table 1 using the same parameter descriptions as in the source code for the controller [2].

Table 1. Generator torque control parameters.

Parameter	Description	Gearbox design	Direct-drive design	Scaling
Rated rotor speed [RPM]	-	12.1	12.1	-
GBRatio [-]	Gearbox ratio	1:97	1:1	-
VS_CtInSp [rad/s]	Transitional generator speed (HSS side) between regions 1 and 1 1/2	70.16224	0.72332	GBRatio
VS_MaxRat [Nm/s]	Maximum torque rate (in absolute value) in torque controller	15,000.0	1,455,000.0	GBRatio
VS_MaxTq [Nm]	Maximum torque in region 3 (HSS side)	47,402.91	4,598,082.27	GBRatio
VS_Rgn2K [Nm/(rad/s)^2]	Generator torque constant in Region 2 (HSS side)	2.332287	2,128,615.373	GBRatio^3
VS_Rgn2Sp [rad/s]	Transitional generator speed (HSS side) between regions 1 1/2 and 2	91.21091	0.940319	GBRatio
VS_RtGnSp [rad/s]	Rated generator speed (HSS side)	121.6805	1.254438	GBRatio
VS_RtPwr [W]	Rated generator power in Region 3	5,296,610.0	5,296,610.0	-

The blade-pitch controller operates in region 3 using gain-scheduled proportional integral control on the speed error between the filtered generator speed and the desired generator speed. The pitch control is adapted to the direct-drive design by scaling the pitch gains and desired HSS speed according to the change in gearbox ratio as described in Table 2. The parameter descriptions are taken from the source code for the controller [2].

Table 2. Full-span rotor-collective pitch control parameters.

Parameter	Description	Gearbox design	Direct-drive design	Scaling
PC_KI [-]	Integral gain for pitch controller at rated pitch	0.008068634	0.782657498	GBRatio
PC_KP [s]	Proportional gain for pitch controller at rated pitch	0.01882681	1.82620057	GBRatio
PC_RefSpd [rad/s]	Desired (reference) HSS speed for pitch controller	122.9096	1.2671	GBRatio

2.2. Drivetrain specifications

The direct-drive generator inertia is set to 250,000kgm^2, assuming that the generator has a diameter of approximately 6m, with a mass of the generator yoke including magnets and a brake disc of approximately 25,000 kg. These parameters are based on engineering judgement and may deviate for real designs and therefore a sensitivity study of the influence of the generator inertia on fatigue loads is conducted in section 3. In Table 3 some selected structural properties related to the drivetrain of the direct-drive and geared design are compared. Note that the generator inertia is specified around the HSS which is artificial in the direct-drive design and equal to the LSS. For comparison, the reflected load inertia of the generator around the LSS in the gearbox design should be scaled with the gearbox ratio squared (~5,000,000 kgm^2), which results in a factor or ~20 between the two inertias.

Table 3. Drivetrain comparison.

Parameter	Description	Gearbox design	Direct-drive design	Scaling
DrTrDOF [-]	Drivetrain rotational degree of freedom	Enabled	Enabled	-
GenIner [kgm^2]	Generator inertia about HSS	534.12	250,000.0	Engineering judgement
DTTorSpr [Nm/rad]	Drivetrain torsional spring	867,637,000	867,637,000	-
DTTorDmp [Nm/(rad/s)]	Drivetrain torsional damper	6,215,000	6,215,000	-

3. Results

In this section the performance of the developed 5MW direct-drive turbine is compared to the original gearbox design. To verify the scaling of the controller, both turbines are simulated in FAST when exposed to a linearly increasing windspeed event and a turbulent wind field above rated windspeed, respectively.

The results of the simulations are shown in figures 2 and 3 in terms of wind speed, generator power and blade pitch. Coloured lines represent the direct-drive design (DD) and the black lines represent the original gearbox design (GB). Overall, the output from the two turbines is very similar indicating a successful conversion of the controller.

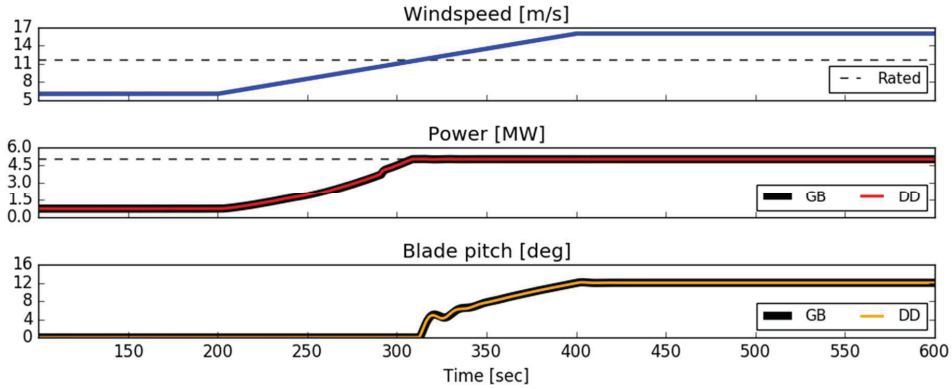

Figure 2: Comparison of the original and scaled controller during a linear increase in windspeed from 6m/s to 16m/s. GB is the original geared turbine and DD is the direct-drive version.

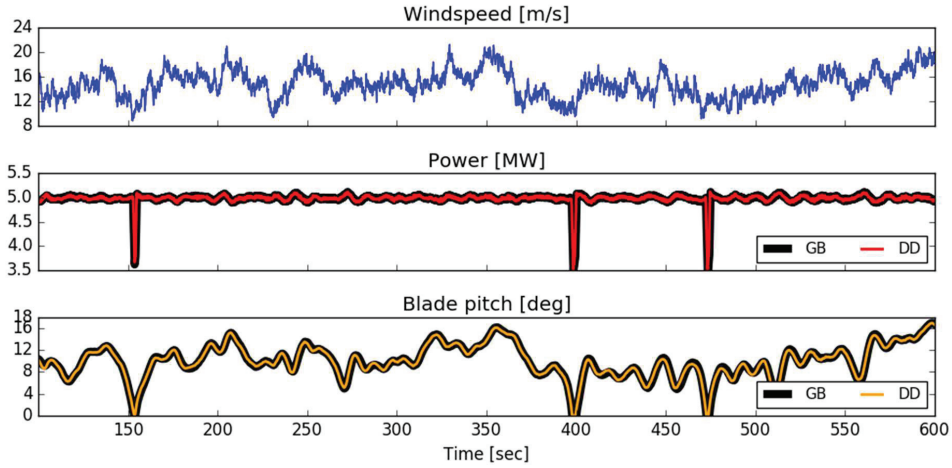

Figure 3: Comparison of the original and scaled controller at a mean windspeed of 17m/s and turbulence intensity of 0.15. GB is the original geared turbine and DD is the direct-drive version.

3.1. Fatigue loads

Based on wind turbine class IIB defined in the Design Standard IEC 61400-1 3rd ed. [8], fatigue loads during normal operation have been computed for both designs, assuming a lifetime of 20 years. The results are summarized in Table 4 in terms of "damage equivalent loads" (DEL) for four selected main components. For all components a slight reduction in fatigue loads is achieved by the direct-drive design concept; However, the only significant reduction is obtained for the LSS, with a reduction of approximately 10%.

Table 4. Design class IIB fatigue loads for both designs and the relative difference.

Component	DEL Gearbox [kNm]	DEL Direct-drive [kNm]	Relative Difference
Blade root flapwise moment	9,504	9,418	-0.9%
Yaw bearing tilt moment	7,848	7,837	-0.1%
Tower bottom for-aft moment	44,690	44,531	-0.4%
Low speed shaft torque	1,733	1,554	-10.3%

The reduction in the LSS torque fatigue load is directly related to the reduction in the reflected load inertia. This is shown in Figure 6 where the shaft torque and blade root flap moment timeseries are compared when both the geared and direct-drive turbine are exposed to a turbulent wind field. For the blades almost no difference is observed whereas the LSS torque is significantly "smoothed" by the lower inertia, thus leading to fewer load cycles.

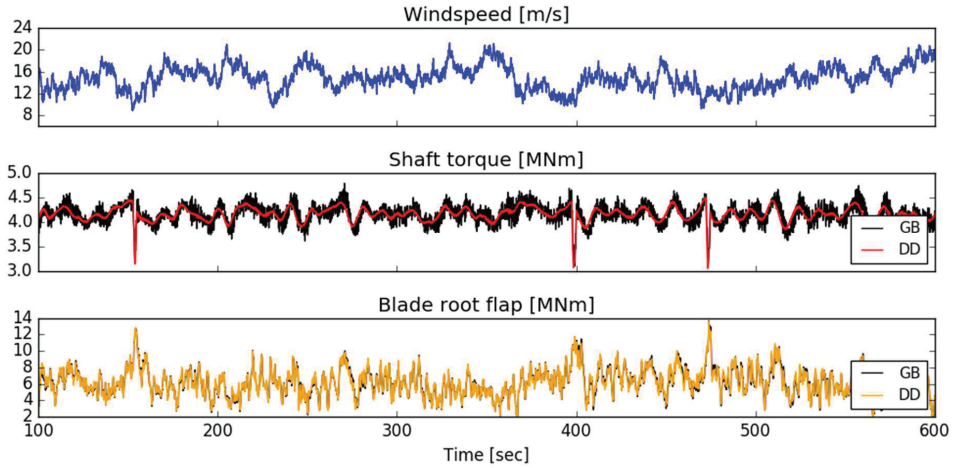

Figure 4: Response time series of LSS torque and blade root flap moment. GB is the original geared turbine and DD is the direct-drive version.

3.2. Sensitivity study, generator inertia

The chosen generator inertia (250,000kgm^2) is based on engineering judgement, hence it is subject to uncertainty. Therefore, a sensitivity study has been conducted where the generator inertia has been changed between 200,000kgm^2 and 500,000kgm^2 and the sensitivity of DELs for the selected main sensors has been evaluated. The turbine is simulated using a highly turbulent wind field with a mean wind speed of 15m/s. The results of the sensitivity analysis are shown in figure 5 normalized with the chosen design.

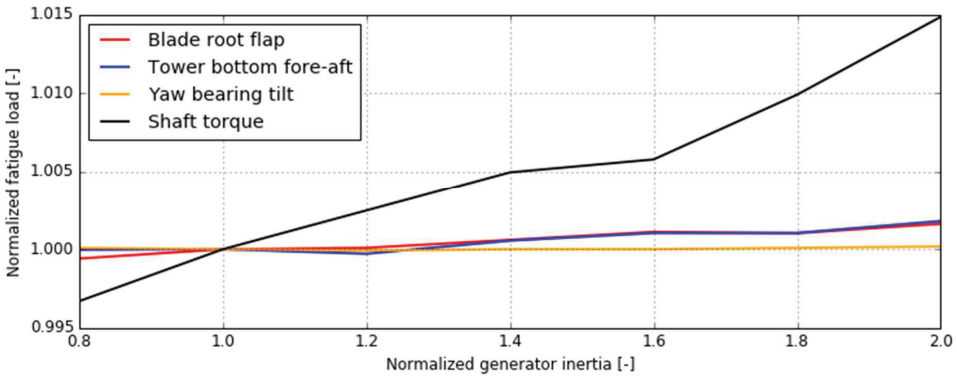

Figure 5: Fatigue load sensitivity to generator inertia normalized with respect to the default inertia of 250.000 kgm^2 for easy comparison.

In the range from 200,000kgm^2 to 500,000kgm^2 the relative difference is 0.2% for the blades and tower, 0.0% for the yaw bearing and 1.8% for the shaft. Therefore, the chosen inertia of 250,000kgm^2 seems appropriate and a specific generator should differ significantly from this to have a noticeable effect on the fatigue loads.

3.3. Sensitivity study, Nacelle center of mass

The NacCM is located 1.9m "downwind" compared to the yaw axis in the original geared design, and the same position is assumed for the direct-drive design. In this section it is investigated if the DELs on the main components are sensitive to moving the center of mass for the direct-drive design. Note that when the center of mass is moved the nacelle inertia (NacIner) around the yaw axis is changed using the parallel axis theorem where the mass of the nacelle is 240,000kg and its base inertia is 1,741,493kgm^2 [2]. The possible change in the eigen-frequency related to the torsion mode shape of the tower is not accounted for, as it is assumed that the mass and position of the rotor hub and blades are by far the most important contributions to this frequency. The result of the sensitivity study is shown in figure 6 normalized with the chosen NacCM position.

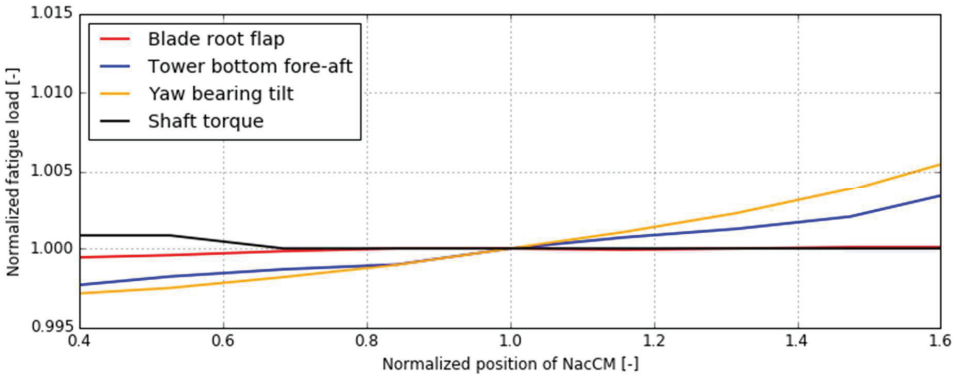

Figure 6: Fatigue load sensitivity towards the downwind position of NacCM normalized with respect to the default position of 1.9m downwind for easy comparison.

It is seen that in the investigated range between 0.7m downwind and 3.1m downwind the relative fatigue load difference is 0.1% for the blades, 0.6% for the tower, 0.9% for the yaw bearing tilt and 0.1% for the shaft. Results have also been computed (but not shown here) for the yaw bearing yaw and the tower torsion, as they are expected to see the highest sensitivity, but both are within 2%.

4. Conclusion

A fully consistent direct-drive version of the onshore 5MW reference wind turbine by NREL has been developed. By assuming the same control strategy for both designs, the baseline controller for the 5MW geared turbine has been scaled to apply to the direct-drive version. To achieve a consistent one-to-one conversion the weight of the nacelle is assumed the same both designs. Using typical values for the dimensions and mass of a low speed generator its inertia around the low speed shaft of the direct-drive turbine has been established. The position of the nacelle center of mass is assumed unchanged compared to the geared design.

By simulating design class IIB fatigue loads during normal operation for both the original geared and the developed direct turbine turbines, it is shown that only the fatigue loads on the low speed shaft change significantly between the two design concepts. Compared to the geared turbine, the direct-drive design obtained approximately a 10% lower DEL in the main shaft, while the blade root flapwise moment, tower base for-aft moment, and yaw bearing tilt moment were all within 1%.

Sensitivity studies with respect to fatigue loads were performed for the generator inertia and nacelle center of mass position. This showed that both design parameters should deviate significantly from the chosen values to have a significant impact on the results. By doubling the generator inertia none of the investigated components showed a relative difference in fatigue loads larger than 2%. Similarly, the position of the nacelle center of mass was moved more than 1m both upwind and downwind without any changes in fatigue loads greater than 2%.

The developed direct-drive turbine is intended as an open access reference turbine, which can be used by the wind energy community to analyse the difference in structural loads between a geared turbine and a fully consistent direct-drive version. It is noted that even though the 5MW reference turbine may not represent modern utility wind turbines perfectly, the developed direct-drive turbine together with the original geared turbine may still provide a solid basis for comparative analyses of the two design concepts.

Acknowledgements

The authors of this paper wish to thank Jason Jonkman (NREL) and Torben Knudsen (AAU) for their help with adapting the original controller for the geared 5MW turbine to apply to a consistent direct-drive design. We also wish to thank Henrik Stiesdal for his great help on understanding the most important differences between geared and direct-drive wind turbine design concepts.

The work leading to this paper has been conducted as part of the PhD project “From wind climate to wind turbine loads – Efficient and accurate decision support and risk analysis” co-funded between EMD International A/S, Aalborg University and the Danish innovation fund. The financial support is greatly appreciated.

References

[1] Malcolm D J 2006 WindPACT Turbine Rotor Design Study WindPACT Turbine Rotor Design Study

[2] Jonkman J, Butterfield S, Musial W and Scott G 2009 *Definition of a 5-MW reference wind turbine for offshore system development* (NREL/TP-500-38060)

[3] Bak C, Zahle F, Bitsche R, Yde A, Henriksen L C, Nata- A and Hansen M H 2013 Description of the DTU 10 MW Reference Wind Turbine *Report-I-0092* 1–138

[4] Desmond C, Murphy J, Blonk L and Haans W 2016 Description of an 8 MW reference wind turbine *J. Phys. Conf. Ser.* **753** 092013

[5] IEA Wind Task 37 Systems Engineering, https://windbench.net/iea37, Accessed 2018-08-28

[6] Sethuraman L, Xing Y, Gao Z, Venugopal V, Mueller M and Moan T 2014 A 5MW direct-drive generator for floating spar-buoy wind turbine: Development and analysis of a fully coupled Mechanical model *Proc. Inst. Mech. Eng. Part A J. Power Energy* **228** 718–41
[7] Jonkman J 2015 FAST An aeroelastic computer-aided engineering (CAE) tool for horizontal axis wind turbines
[8] Standard 2010 IEC 61400-1 ed. 3, 2005, International Electrotechnical Commission, Wind turbines, Part 1: Design requirements, Edition 3 (2005) incl. Amendment 1 (2010).

ISSN (online): 2446-1636
ISBN (online): 978-87-7210-483-6

AALBORG UNIVERSITY PRESS